

**Visual Field Analysis Using Digital Signal Processing  
Of Visual Evoked Potentials**

**by**

**Michael Stephen Bradnam MA CEng MIEE MIPS M**

**Thesis submitted to the University of Glasgow  
for the degree of Doctor of Philosophy.**

This research was conducted in the

West of Scotland Health Boards

Department of Clinical Physics and Bio-Engineering,

Glasgow and the Tennent Institute of Ophthalmology,

University of Glasgow, Western Infirmary, Glasgow.

**January 1994**

ProQuest Number: 11007929

All rights reserved

INFORMATION TO ALL USERS

The quality of this reproduction is dependent upon the quality of the copy submitted.

In the unlikely event that the author did not send a complete manuscript and there are missing pages, these will be noted. Also, if material had to be removed, a note will indicate the deletion.



ProQuest 11007929

Published by ProQuest LLC (2018). Copyright of the Dissertation is held by the Author.

All rights reserved.

This work is protected against unauthorized copying under Title 17, United States Code  
Microform Edition © ProQuest LLC.

ProQuest LLC.  
789 East Eisenhower Parkway  
P.O. Box 1346  
Ann Arbor, MI 48106 – 1346

Thesis  
9808  
copy 1

GLASGOW  
UNIVERSITY  
LIBRARY

To Fiona, Craig and Stuart.

## ABSTRACT

Perimetry is the measurement of the visual field and has important clinical applications in the diagnosis and management of many conditions causing visual impairment. Current clinical methods of perimetry are subjective and are difficult or impossible to perform in some groups of patients such as the young, the elderly and those with severe learning difficulties. This thesis describes the development of an alternative objective form of perimetry, called electroperimetry, which records the cortical potentials evoked by visual stimuli in different parts of the visual field.

No commercial electrophysiology system was suitable for the research, so a completely new system based on a personal computer was developed. The system described has two novel features: it uses a Digital Signal Processing (DSP) card to enable real-time signal processing and it provides a wide range of software generated stimuli.

Hitherto, a major limitation of electroperimetry had been the time taken to recover visual evoked cortical potential (VECP) signals from electroencephalographic activity and muscle noise. In order to minimise the recording time, the signal-to-noise ratio (SNR) had to be increased. This was achieved by using steady-state stimuli, by analysing the VECP in the frequency domain and by using four recording electrodes. A new DSP method based on adaptive noise cancelling was developed which has a number of advantages over conventional Fourier analysis for real-time signal measurement.

Visual stimuli were created using computer graphics and presented to the subject on a computer monitor screen. Work concentrated on optimising pattern-reversal checkerboard stimuli for testing visual field quadrants, and the optimum check-size for testing different size fields was determined. As a result, a dartboard pattern-reversal stimulus was developed in which the most effective check-size was presented at each location in the visual field. The increased SNR enabled the testing of smaller areas within each visual field quadrant. It has been proposed that motion stimuli may be useful for testing the extramacular area of the visual field, so motion-onset stimuli were developed and compared with pattern-reversal stimuli. It was concluded that pattern-reversal stimuli were superior for electroperimetry because the motion-onset VECP is reduced by adaptation to moving stimuli.

Accurate positioning of the stimulus on the retina is essential for electroperimetry. A new method of fixation monitoring was introduced which also helped patients to concentrate and reduced fatigue. In addition, a novel system employing a miniature LCD display and an indirect ophthalmoscope has been developed to enable VECPs to be recorded whilst the stimulus pattern is simultaneously positioned on the retina under direct view of the operator. VECPs from transient dark pattern-onset stimuli were investigated for this system.

The steady-state stimulus and signal analysis techniques developed were clinically evaluated using a large number of subjects including 17 patients with complete and absolute hemifield and quadrantic field defects. Quadrant field stimuli were used and were presented on a computer monitor screen. A unique aspect of this study was the use of objective signal detection techniques. The results confirmed patterns of subjective visual field loss. The system currently has a sensitivity and specificity of at least 85% and 80% respectively for detecting non-seeing areas of the visual field. The results have demonstrated that when subjective perimetry is not possible the developed system is of potential clinical value to the ophthalmologist. Current developments are aimed at further improving the sensitivity and specificity of the system whilst keeping the recording time to a minimum.

## LIST OF CONTENTS

	Page
Title	1
Abstract	3
List of contents	4
List of illustrations	7
List of tables	12
Preface	13
Acknowledgement	14
Author's declaration	16
Definitions	20
<b>Chapter 1 INTRODUCTION</b>	<b>21</b>
1.1 Visual system	22
1.2 The visual field	29
1.3 Perimetry	40
1.4 Clinical electrophysiology of the visual system	44
1.5 Electroperimetry	53
1.6 Conclusion and aims	59
<b>Chapter 2 INSTRUMENTATION AND RECORDING METHODS</b>	<b>62</b>
2.1 Introduction	62
2.2 System design specification	63
2.3 System hardware	64
2.4 Software	71
2.5 Monitor interference	74
2.6 Monitor luminance calibration	77
2.7 Monitor luminance and contrast uniformity	77
2.8 System duplication	80
2.9 Recording methods	80
2.10 Signal labelling and measurement	91
2.11 System validation	92
2.12 Conclusion	108

**List of contents (continued)**

	Page
<b>Chapter 3    DIGITAL SIGNAL PROCESSING OF VECPS</b>	110
3.1    Introduction	110
3.2    Review of the application of digital signal processing to VECPs	111
3.3    Transient signal processing development	125
3.4    Steady-state signal processing development	129
3.5    Conclusion	151
 <b>Chapter 4    STIMULUS DEVELOPMENT</b>	 153
4.1    Introduction	153
4.2    Steady-state VECPs from checkerboard pattern-reversal stimulation of visual field quadrants	154
4.3    Steady-state VECPs from dartboard pattern-reversal stimulation of the visual field	169
4.4    Transient VECPs from motion-onset stimuli	181
4.5    Transient VECPs from dark and bright pattern-onset stimuli	197
4.6    Conclusion	205
 <b>Chapter 5    NEW STIMULUS DELIVERY SYSTEM</b>	 207
5.1    Introduction	207
5.2    Review of stimulus methods	208
5.3    Stimulus delivery using an indirect ophthalmoscope	208
5.4    Preliminary studies	216
5.5    Blue light hazard assessment	221
5.6    Ophthalmoscopic study	237
5.7    Instrument housing	243
 <b>Chapter 6    CLINICAL EVALUATION</b>	 246
6.1    Introduction	246
6.2    Preliminary study	247
6.3    Main study	255

**List of contents (continued)**

	Page
<b>Chapter 7 CONCLUSION</b>	291
7.1 Recording system	292
7.2 Signal processing developments	293
7.3 Stimulus development	294
7.4 Subject fixation	296
7.5 Stimulus projection	297
7.6 Clinical evaluation	298
7.7 Future work	299
Glossary	300
List of references	303

## LIST OF ILLUSTRATIONS

		Page
1.1	Enlarged retina showing relative positions of the photoreceptors, bipolar cells and ganglion cells.	23
1.2	The visual pathway from the eyes to the primary visual cortex.	25
1.3	The left striate cortex and the right half of the visual field.	30
1.4	An example of a normal visual field from a right eye.	32
1.5	The 'hill of vision'. A three dimensional representation of the visual field, showing retinal sensitivity at each point in the field.	33
1.6	Central visual field chart from a left eye showing typical glaucomatous field defects.	37
1.7	Peripheral visual field charts from a Tubingen perimeter showing a complete homonymous hemianopia with some central sparing.	39
1.8	Normal pattern-reversal VECF.	48
1.9	Pattern-reversal VECF from a patient with right optic neuritis.	49
1.10	Normal transient VECF for monocular pattern-reversal stimulation of the right hemi-field.	51
2.1	Block diagram of system hardware.	65
2.2	Photograph showing head box preamplifier, amplifier, stimulus monitor and earthed steel cabinet.	68
2.3	Mumetal screening cone.	76
2.4	Central screen luminance versus grey level for two contrast settings; with a uniform image filling the screen.	78
2.5	Luminance versus image size for arbitrary luminance settings.	79
2.6	Luminance values measured from stimulus monitor for pattern of white discs on grey background.	81
2.7	Ten-twenty system for electrode placements.	83
2.8	'Queens Square' system for electrode placements.	85
2.9	Patient connections to differential amplifier.	86
2.10	Subject during recording showing how electrode leads are positioned to reduce the risk of induced interference from magnetic fields.	88
2.11	Variation of P100 latency with age.	98
2.12	Normal flash VECF.	101
2.13	Variation of P100 latency with age for hemi-field stimuli.	107

**List of illustrations (continued)**

		Page
3.1	The effect of stimulus frequency on the pattern-reversal VECP.	116
3.2	Build-up of the pattern-reversal steady-state VECP from onset of the first stimulus.	117
3.3	Example of a frequency spectrum from a steady-state VECP.	118
3.4	Effect of truncation in the time domain on the frequency response of the Butterworth filter.	127
3.5	Basic structure of an adaptive noise canceller.	131
3.6	Structure of modified adaptive noise canceller.	132
3.7	Response of the adaptive noise canceller to a 5 $\mu\text{V}$ signal, using various time constants.	140
3.8	Response of the adaptive noise canceller to a 5 $\mu\text{V}$ signal in simulated EEG activity.	142
3.9	Response of ANC to a time varying signal in simulated EEG activity.	143
3.10	Response of ANC to a time varying signal in simulated EEG activity.	144
3.11	Accuracy and precision of signal measurement using various methods of signal analysis.	145
3.12	Response of the adaptive noise canceller to a steady-state VECP recording.	147
3.13	Response of the ANC to a time varying steady-state VECP. The amplitude varied with stimulus contrast.	148
3.14	Response of the ANC to a time varying steady-state VECP, due to a variation in the stimulus phase.	149
4.1	The relationship between maximum VECP amplitude and check-size for different stimulus field-sizes in the inferior nasal field quadrant.	158
4.2	The relationship between maximum VECP amplitude and check-size for different stimulus field-sizes in the superior nasal field quadrant.	159
4.3	VECP amplitude for different stimulus field-sizes and check-sizes in the inferior nasal quadrant.	160
4.4	Optimum check-sizes versus retinal eccentricity for the inferior nasal field quadrant.	164
4.5	VECP amplitude for different stimulus field-sizes and check-sizes in the superior nasal quadrant.	166

### List of illustrations (continued)

	Page	
4.6	VECP amplitude for different numbers of pattern elements in the inferior nasal quadrant.	167
4.7	Example of a dartboard pattern stimulus.	171
4.8	Check-size versus retinal eccentricity for the dartboard stimulus, compared with optimal check-sizes.	172
4.9	The twelve areas of the visual field tested with the dartboard stimulus.	173
4.10	Spectrum of VECP recording.	176
4.11	Novel motion stimulus.	184
4.12	Vertical bar stimulus.	185
4.13	Typical pattern-reversal VECP from bar stimulus pattern.	188
4.14	Typical motion-onset VECP.	190
4.15	Typical VECP waveform following stimulus onset and offset.	200
5.1	Optics of the indirect ophthalmoscope.	209
5.2	LCD stimulation of the retina during indirect ophthalmoscopy.	211
5.3	Kyocera KL6448E-STP-FFW LCD.	212
5.4	Magnification of the indirect ophthalmoscope.	213
5.5	Optics of the indirect ophthalmoscope to show the effect of the position of the condensing lens on the retinal magnification.	214
5.6	Pattern-onset VECPs recorded from the LCD stimulus.	220
5.7	Blue light hazard function.	222
5.8	Indirect ophthalmoscope radiometry.	226
5.9	Spectral irradiance from indirect ophthalmoscope for two bulb voltage settings.	228
5.10	Transmission of yellow lens coating.	229
5.11	Transmission of liquid crystal display in clear transmissive state for two contrast settings.	230
5.12	Blue light hazard weighted spectral irradiance using 6 Volt bulb setting, clear lens and LCD.	231
5.13	Blue light hazard weighted spectral irradiance using 7.5 Volt bulb setting, clear lens and LCD.	232
5.14	Blue light hazard weighted spectral irradiance using 6 Volt bulb setting, yellow coated lens and LCD.	233

### List of illustrations (continued)

	Page
5.15 Blue light hazard weighted spectral irradiance using 7.5 Volt bulb setting, yellow coated lens and LCD.	234
5.16 Full-field VECP recorded during indirect ophthalmoscopy from a checkerboard pattern-onset stimulus.	239
5.17 VECP signals recorded during indirect ophthalmoscopy from a quadrant field stimulus.	240
5.18 Photographs of the indirect ophthalmoscope stimulus delivery system showing the LCD housing, adapter circuit housing and lens assembly.	244
5.19 Photograph of the indirect ophthalmoscope delivery system mounted on a slit-lamp table in front of a test subject.	245
6.1 Quadrant field stimulus.	248
6.2 Electrode montage.	250
6.3 Frequency spectrum of recording showing VECP signal at 7.711 Hz and estimate of EEG noise.	251
6.4 A summary of the visual fields tested.	252
6.5 Subject 1 - field chart and result of electroperimetry for right eye.	258
6.6 Subject 1 - field chart and result of electroperimetry for left eye.	259
6.7 Subject 2 - field chart and result of electroperimetry for right eye.	261
6.8 Subject 2 - field chart and result of electroperimetry for left eye.	262
6.9 Subject 3 - field chart and result of electroperimetry for right eye.	264
6.10 Subject 4 - field chart and result of electroperimetry for right eye.	266
6.11 Subject 4 - field chart and result of electroperimetry for left eye.	267
6.12 Subject 5 - field chart and result of electroperimetry for right eye.	269
6.13 Subject 5 - field chart and result of electroperimetry for left eye.	270
6.14 Subject 6 - field chart and result of electroperimetry for right eye.	272
6.15 Subject 6 - field chart and result of electroperimetry for left eye.	273
6.16 Subject 7 - field chart and result of electroperimetry for right eye.	275
6.17 Subject 7 - field chart and result of electroperimetry for left eye.	276
6.18 Subject 8 - field chart and result of electroperimetry for right eye.	278
6.19 Subject 8 - field chart and result of electroperimetry for left eye.	279
6.20 Subject 9 - field chart and result of electroperimetry for right eye.	281

**List of illustrations (continued)**

	<b>Page</b>
6.20 Subject 9 - field chart and result of electroperimetry for left eye.	282
6.21 Subject 10 - field chart and result of electroperimetry for right eye.	284
6.22 Subject 10 - field chart and result of electroperimetry for left eye.	285
6.23 Receiver operating characteristic (ROC) curve for various probabilities of signal detection.	287

## LIST OF TABLES

		Page
1.1	Terms used to describe visual field loss.	35
2.1	Biodata PA400 physiological amplifier specification.	69
2.2	Results from pattern-reversal stimulus.	95
2.3	Results from flash stimulus.	102
2.4	Results from hemi-field pattern-reversal stimulus.	105
4.1	Optimum check-size for assessing visual field quadrants of varying angular subtense.	162
4.2	Optimum check-size for VECF recording from varying retinal eccentricities.	163
4.3	Frequency of largest VECF amplitude occurring on each recording channel.	177
4.4	VECF amplitude from dartboard stimulation.	178
4.5	VECF signal-to-noise ratio from dartboard stimulation.	179
4.6	Results using pattern-reversal stimulus.	189
4.7	Results using motion-onset stimulus.	191
4.8	Cross-correlation values for pairs of recordings.	201
4.9	Peak latencies.	203
4.10	Peak-to-peak amplitudes.	204
5.1	Summary of VECF results obtained using pattern-onset stimulation on the Kyocera KL6448E-STP-FFW LCD screen.	219
5.2	Effective blue light retinal irradiance and duration for maximum permissible exposure for various measurement conditions.	235

## PREFACE

Perimetry has important clinical applications in the field of ophthalmology but current methods are subjective and are difficult or impossible to perform in some groups of patients. Dr D M I Montgomery, an ophthalmologist working in the Tennent Institute of Ophthalmology, recognised that the measurement of visual evoked cortical potentials could be used to develop an objective form of perimetry that would overcome the limitations of subjective techniques. In collaboration with Dr D Allan, a Senior Physicist working with the West of Scotland Health Boards Department of Clinical Physics and Bio-Engineering, Dr Montgomery made some preliminary measurements in 1988. This work was further developed in collaboration with Dr A L Evans and the author, both working for the West of Scotland Health Boards Department of Clinical Physics and Bio-Engineering. Together they sought grant funding in 1989 for the developments described in this thesis.

## ACKNOWLEDGEMENT

The author gratefully acknowledges the financial assistance of the Disability Research Committee of the Chief Scientist Office, Home and Health Department, The Scottish Office, grant number K/RED/E/4/1.

The author wishes to thank the following people:

Professor A T Elliott, West of Scotland Health Boards Department of Clinical Physics and Bio-Engineering, and Professor C M Kirkness, Tennent Institute of Ophthalmology, for providing the facilities of their departments for the research.

Dr J O Rowan, supervisor and Deputy Director of the West of Scotland Health Boards Department of Clinical Physics and Bio-Engineering; Dr A L Evans, grant holder and Head of Instrumentation, West of Scotland Health Boards Department of Clinical Physics and Bio-Engineering; Dr D M I Montgomery, grant holder and Senior Registrar, Tennent Institute of Ophthalmology; Dr D Keating, grant holder and Principal Physicist, West of Scotland Health Boards Department of Clinical Physics and Bio-Engineering; Dr D Allan, grant holder and formerly a Senior Physicist with the West of Scotland Health Boards Department of Clinical Physics and Bio-Engineering; and Dr B E Damato, a grant holder and formerly a Senior Lecturer and Honorary Consultant, Tennent Institute of Ophthalmology; for guidance and assistance.

Dr R McFadzean, Consultant Neuro-Ophthalmologist, Institute of Neurological Sciences, Glasgow and Dr G N Dutton, Consultant Ophthalmologist, Tennent Institute of Ophthalmology, for helpful advice and the referral of patients.

Dr D L Davies, Dr D Barr, Dr E Mutlukan, Dr J Ainsworth, Dr M Briggs, Dr V Ferguson and Dr D Grosset for referring patients for evaluation.

The following members of the West of Scotland Health Boards Department of Clinical Physics and Bio-Engineering also provided advice or assistance: Dr H Moseley, Mr W Richardson, Miss A Cluckie, Mr M Glegg, Mr D Smith, Mr R Laing, Mr S Dunn, Mr S MacCalman, Mr I McLeod, Mr J Ferguson, Mr R Thompson, Mr J MacFarlane and Mr I Irving.

IBM United Kingdom Ltd supplied and fitted the mumetal cone to the stimulus monitor; including Mr M McCreery and Mr R Small, Greenock, and Mr I Drummond, Glasgow.

Dr J Morrison, Department of Physiology, University of Glasgow, for the opportunity to attend his senior honours course on vision and for helpful discussions on the visual system.

Dr J Richter, Department of Electrical Engineering, University of Glasgow, gave helpful advice on electromagnetic screening.

Miss E McClure, Principal Optometrist, and her staff performed subjective perimetry at the Tennent Institute of Ophthalmology.

Mr J McCormick, Tennent Institute of Ophthalmology, and Miss M Finlayson of the West of Scotland Health Boards Department of Clinical Physics and Bio-Engineering provided photographic services.

Finally, but certainly not least, the author wishes to thank the many patients, colleagues, friends and members of his family who acted as volunteer test subjects.

## AUTHOR'S DECLARATION

The material presented in this thesis is the author's own work with the following exceptions:

Dr A L Evans and Miss A Cluckie contributed to the development of computer software and assisted with development and evaluation of the adaptive noise canceller, presented in Chapter 3. Miss Cluckie worked under the supervision of Dr A L Evans and the author.

Mr M Glegg contributed to the development of computer software for the duplicate system constructed for use at the Royal Hospital for Sick Children in Glasgow (Section 2.8).

Dr E Mutlukan was responsible for proposing the hypothesis that dark stimuli have advantages over bright stimuli for perimetry because of differences in the 'on' and 'off-pathways' of the visual system. This work is discussed in Section 4.5.

Under the guidance of the author, Mr S MacCalman provided technical assistance with the radiometric measurements presented in Sections 5.5.4 and 5.5.5.

Mr I McLeod assisted in the design and construction of the LCD housing presented in Section 5.7. The author produced the specification and preliminary design for this instrument.

## PUBLICATIONS

Material contained in this thesis has been published in the following three papers:

Bradnam MS, Keating D, Montgomery DMI, Evans AL, Damato BE and Cluckie A (1992).

Steady-state visual evoked cortical potentials from stimulation of visual field quadrants: optimizing pattern variables for the size of the field to be investigated.

Docum Ophthalmol 79, 151-160.

Mutlukan E, Bradnam MS, Keating D and Damato BE (1992).

Visual evoked cortical potentials from transient dark and bright stimuli: selective 'on' and 'off-pathway' testing?

Docum Ophthalmol 80, 171-181.

Bradnam MS, Evans AL, Montgomery DMI, Keating D, Damato BE, Cluckie A and Allan D (1993).

A personal computer based visual evoked potential stimulus and recording system.

Docum Ophthalmol (in press).

## **PRESENTATIONS**

Material contained in the thesis has also been disseminated at local, national and international meetings including the following presentations:

Keating D, Bradnam MS, Montgomery DMI, Evans AL and Damato BE.

Steady-state visual evoked cortical potentials from stimulation of visual field quadrants: optimising the pattern variables for the size of the field to be investigated.

XXIX Symposium of the International Society for Clinical Electrophysiology of Vision, July 1991, Oxford, England.

Bradnam MS, Evans AL, Keating D, Montgomery DMI and Damato BE.

A visual evoked potential stimulus and recording system based on a digital signal processing card.

Annual Conference of the Institute of Physical Sciences in Medicine, September 1991, Exeter, England.

Mutlukan E, Bradnam MS, Keating D and Damato BE.

Differences between evoked potential responses from on and off pathways.

British Conference for Basic Eye Research, March 1992, Manchester, England.

Mutlukan E, Bradnam MS, Keating D and Damato BE.

Differences between visual evoked cortical potentials from on and off pathways in the human visual system.

Association for Research in Vision and Ophthalmology, May 1992, Sarasota, Florida, USA.

Bradnam MS, Cluckie A, Damato BE, Evans AL, Keating D and Montgomery DMI.  
A visual evoked potential recording system incorporating a digital signal processing card.

XXX Symposium of the International Society for Clinical Electrophysiology of Vision., May 1992, Vienna, Austria.

Bradnam MS, Cluckie A, Damato BE, Evans AL, Keating D and Montgomery DMI.  
Adaptive filtering of steady-state visual evoked cortical potentials.

XXX Symposium of the International Society for Clinical Electrophysiology of Vision., May 1992, Vienna, Austria.

Mutlukan E, Bradnam MS, Keating D and Damato BE.

Visual evoked cortical potential recording from parallel pathways.

IX Congress of the European Society of Ophthalmology, May 1992, Brussels, Belgium.

Bradnam MS, Montgomery DMI, Keating D, Evans AL and Damato BE.

Motion visual evoked cortical potentials.

Annual Conference of the Institute of Physical Sciences in Medicine, September 1992, Lincoln, England.

Cluckie A, Bradnam MS and Evans AL.

Adaptive filtering of steady-state visual evoked cortical potentials.

Annual Conference of the Institute of Physical Sciences in Medicine, September 1992, Lincoln, England.

Montgomery DMI, Bradnam MS, Evans AL, Keating D and Moseley H.

A new method of recording visual evoked potentials during ophthalmoscopy.

European Meeting of the International Society for Clinical Electrophysiology of Vision, April 1993, Nottingham, England.

Bradnam MS, Evans Al, Conway R, Glegg M, McCulloch DL, Saunders KJ and Dutton GN.

A computerised system for the assessment of visual acuity in multiply handicapped children.

Annual Conference of the Institute of Physical Sciences in Medicine, September 1993, Bristol, England.

Bradnam MS, Dutton GN, Saunders KJ, McCulloch DL, Conway R, Evans AL and Glegg M.

Computerised visual assessment of multi-handicapped children: what can your child see?

Annual Conference of the Institute of Physical Sciences in Medicine, September 1993, Bristol, England.

Bradnam MS, Montgomery DMI, McFadzean R, Keating D, Evans AL, Damato BE.  
Electroperimetry.

First Meeting of the European Neuro-ophthalmological Society, October 1993, Zurich, Switzerland.

## DEFINITIONS

- ANC - Adaptive noise canceller (Sections 3.2.2 and 3.4). A method for estimating a signal corrupted with uncorrelated noise. In this laboratory, a novel implementation of the ANC has been developed to estimate visual evoked cortical potentials (VECPs) corrupted with electroencephalographic activity and muscle noise. An adaptive filter is used to cancel the noise and provide an estimate of the VECP signal.
- DSP - Digital signal processing. The mathematical processing of digital signals (Chapter 3).
- Electroperimetry - An objective form of perimetry in which the visual field is assessed by recording the cortical potentials evoked in response to visual stimuli (Section 1.5).

For further definitions and explanations of abbreviations please refer to the glossary.

# 1. INTRODUCTION

This chapter describes the visual system. The concept of the visual field is introduced and it is explained how different forms of visual impairment cause characteristic defects in the visual field.

Measurement of the visual field is called perimetry. Perimetry has a number of important clinical uses which are explained. The current clinical methods of perimetry are subjective and are difficult or impossible to perform in some groups of patients. There is therefore a need for an alternative objective form of perimetry. A way of achieving this is to use electrophysiology to measure the electrical responses produced by the visual system in response to stimulation.

The main methods for clinical electrophysiology are introduced and their application to visual field analysis is discussed. Measurement of visual evoked cortical potentials can be used to assess visual fields but current methods have a number of major limitations:

1. The traditional method for signal recovery is signal averaging and it is very slow.
2. When small parts of the visual field are tested the signal-to-noise ratio is reduced and the test is even slower.
3. Objective signal detection methods have not been applied to determine the significance of the recorded signals.
4. Patient studies have been published using quadrant field stimuli but these have not employed smaller stimulus areas.
5. A reliable method for patient fixation needs to be developed.

An explanation is given of how the current work is aimed at overcoming each one of these limitations.

## 1.1 VISUAL SYSTEM

Sensory input to the visual system is received through the photoreceptors in the retina and is transmitted to the visual cortex via the visual pathway. Hubel (1988) provides a useful review of the visual system.

### 1.1.1 Retina

The retina can be considered to be an extension of the brain. In the retina there are two types of photoreceptor cells, cones and rods. There are about five to seven million cones and about 100 million rods (Osterberg 1935, Curcio et al 1990). The rods are not colour specific whilst there are three types of cone with maximum sensitivity to violet ( $\sim 430$  nm), blue-green ( $\sim 530$  nm) or yellow-green ( $\sim 560$  nm) wavelengths of light (Hubel 1988). The distribution of the photoreceptors has been mapped (Osterberg 1935, Curcio et al 1990) and the peak cone density was found to be at the centre of the retina with 50% of cones within  $18^\circ$  of the centre. In contrast, there are no rods present in the central  $1.25^\circ$  of the retina and the peak rod density is about  $15^\circ$  from the centre (Curcio et al 1990).

The photoreceptors hyperpolarise in response to light and their outputs project to bipolar cells (Figure 1.1). There are two groups of bipolar cells; one group hyperpolarises in response to light whilst the other group provide signal inversion by depolarising in response to light (Hubel 1988).

The bipolar cells in turn project to ganglion cells from which axons travel in the optic nerve (Figure 1.1). There are about one million ganglion cells (Curcio and Allen 1990, Jonas et al 1992) and the highest densities are found in the central  $15^\circ$  of the retina (Curcio and Allen 1990). Ganglion cells discharge impulses and are classed as either on-centre cells or off-centre cells (Hubel 1988) according to their response to light. The discharge rate of on-centre ganglion cells increases in response to light whilst the discharge rate of off-centre cells decreases.

Ganglion cells usually have an antagonistic surround; on-centre cells have an off-surround and off-centre cells have an on-surround (Hubel 1988). The surround mechanism requires the convergence of inputs from a number of bipolar cells. In the central retina the convergence is small and the photoreceptor density is high, so the receptive field of each ganglion cell is small. In the peripheral retina the convergence

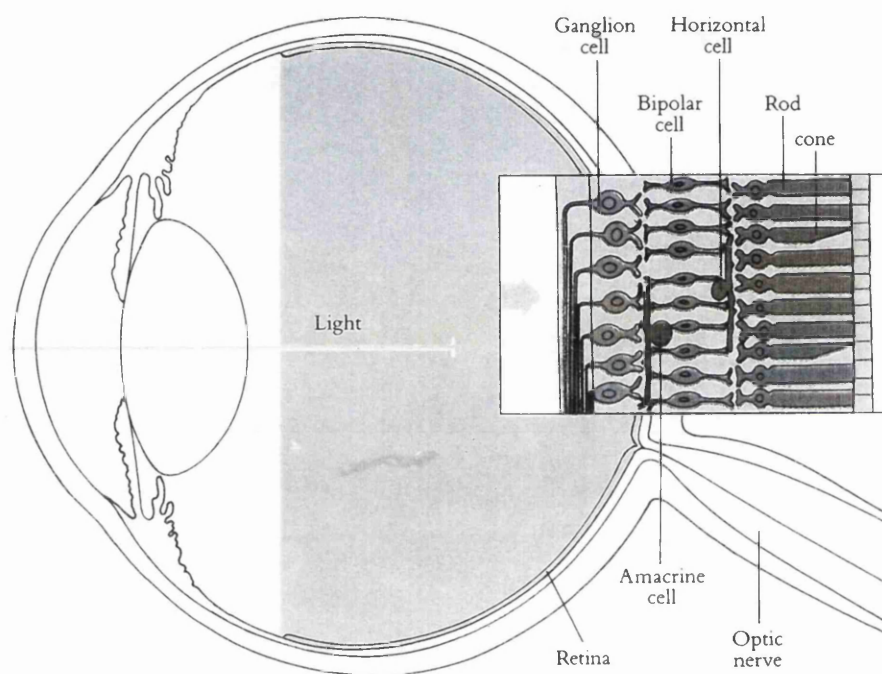


Figure 1.1 Enlarged retina showing relative positions of the photoreceptors, bipolar cells and ganglion cells. (From Hubel DH (1988). *Eye, brain and vision*. Scientific American, New York. Reproduced with permission of the publisher).

is greater and the photoreceptor density is less, so the receptive field of each ganglion cell is consequently larger. The surround mechanism provides spatial tuning and is therefore an elementary part of visual processing. Taking an on-centre / off-surround ganglion cell as an example, a maximal response is obtained only when a light stimulus totally covers the central receptive field. If the stimulus is too small excitation is sub-maximal; whilst if it is too large the inhibitory surround is recruited and the response is inhibited. The optimum stimulus increases in size with eccentricity due to the increasing receptive field sizes (Hubel 1988).

The anatomy of the retina is reviewed by Duke-Elder and Wybar (1961) and Marshall (1991). The central area of the retina is known as the macula and is defined as the area of the retina in which the number of layers of nuclei in the ganglion cell layer exceeds two. The diameter of the macula is 5 to 6 mm, which corresponds to an angle of  $20^\circ$  assuming a retinal magnification of  $276 \mu\text{m}/\text{degree}$  (Holden and Fitzke 1988).

At the centre of the macula is a shallow rounded pit known as the fovea which is  $5^\circ$  in diameter and is formed by the radial displacement of the inner retinal layers. The foveal margin is in fact the thickest part of the retina ( $300 \mu\text{m}$ ) due to the large number of displaced intermediary neurones and ganglion cells.

In the centre of the floor of the fovea, exactly on the optic axis of the eye, is a slight dip referred to as the foveola. The foveola is about  $1^\circ$  in diameter and contains closely packed cones which facilitate a high level of visual acuity. This area of the retina is rod-free and is also avascular. The absence of blood vessels, together with the absence of cells overlying the photoreceptors, contribute to the high level of visual acuity.

The axons of the retinal ganglion cells avoid the fovea and take arcuate paths through the surface of the retina to the optic disc from where they leave the retina and form the optic nerve (Figure 1.2). There are no photoreceptors over the optic disc and so the image forming on it cannot be seen. The optic disc is located about 4 mm ( $15^\circ$ ) to the nasal side and 0.8 mm ( $3^\circ$ ) to the superior side of the fovea. There is a large interindividual variation in the size of the optic disc but the average horizontal disc diameter is 1.8 mm (Jonas et al 1988) which corresponds to an angle of  $6.5^\circ$ .

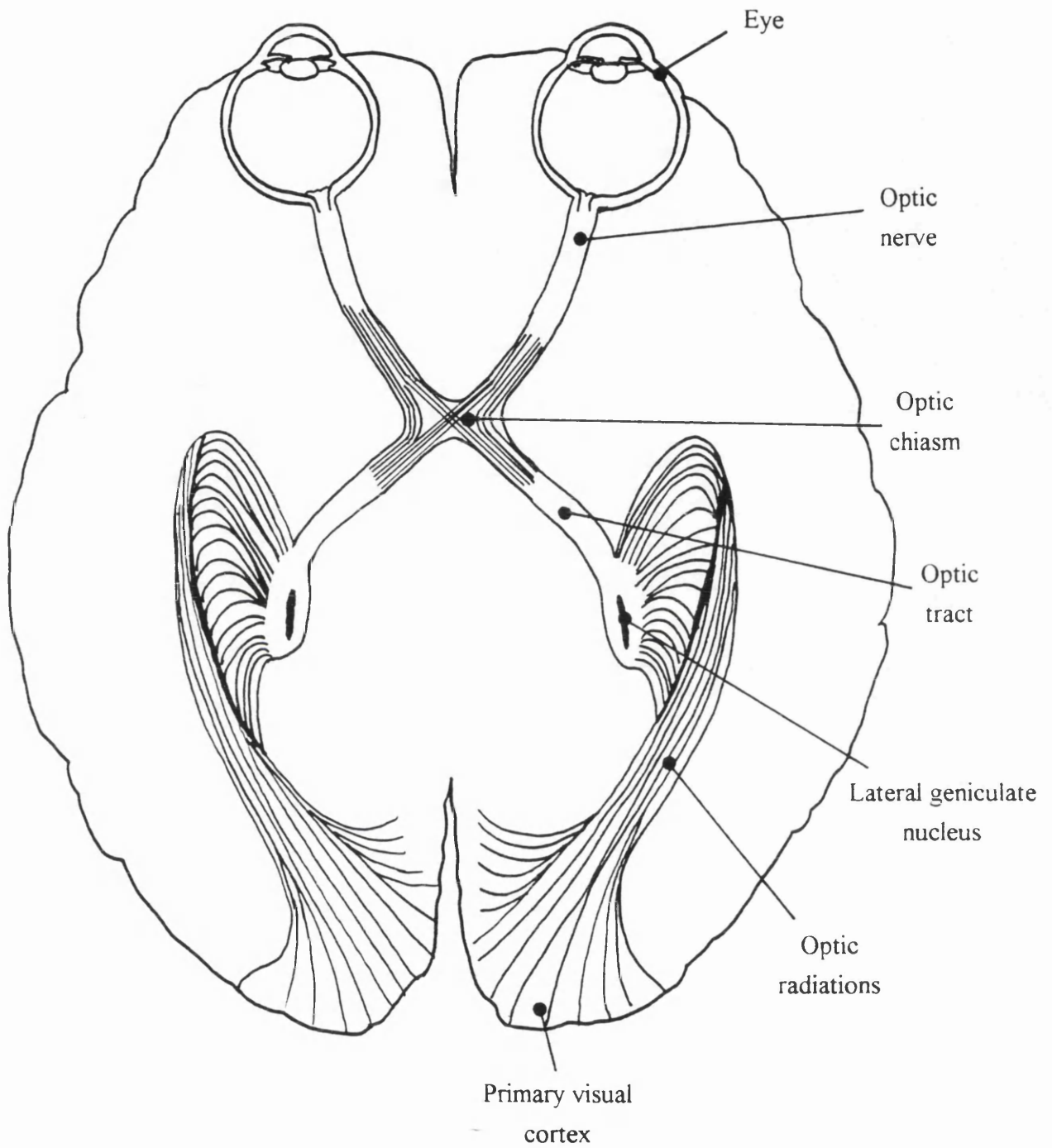


Figure 1.2 The visual pathway from the eyes to the primary visual cortex.

### **1.1.2 Visual Pathways**

The visual pathway from the retina to the visual cortex can be segregated into on and off pathways dependent on whether the input is from on-centre ganglion cells or off-centre ganglion cells.

The visual pathway can also be classified as magnocellular and parvocellular according to the classification of neurones in the lateral geniculate nucleus (LGN) (Section 1.1.4). The cells are histologically and physiologically different. The small parvocellular cells are mainly spectrally sensitive whilst the large magnocellular cells exhibit broadband sensitivity. The parvo and magnocellular pathways form separate distinct layers in the LGN and also project to separate layers of the primary visual cortex (Hubel 1988, Zeki 1992).

### **1.1.3 Optic Nerves, optic chiasm and optic tracts**

The nerve axons in the optic nerves are at first simply bundled together in the same arrangement as in the optic disc, with the nerve fibres from the macula occupying a sector shaped area in the temporal portion of the nerve (Hoyt and Tudor 1963). As the optic chiasm is approached the macular fibres move centrally into the nerve and become more diffusely dispersed (Hoyt and Luis 1963).

The optic chiasm (Figure 1.2) is formed by the junction and partial decussation of the optic nerves. The route of the axons through the chiasm is determined by their retinal origin (Hoyt and Luis 1963). Axons from the temporal retina pass into the ipsilateral optic tract whilst those from the nasal retina pass into the contralateral optic tract. As a result of this crossover each optic tract carries information on the contralateral hemi-field of vision. There is also a rearrangement of the nerve fibres in the chiasm according to their size. Small diameter fibres, which are principally from the macular area of the retina, rise to the superior areas of the chiasm and optic tract whilst large diameter fibres, which are principally from the extramacular area, descend during their passage through the chiasm to the inferior area of the optic tract.

It is possible that the division of the two hemi-fields in the chiasm is not exactly along the vertical meridian of the visual field. There is evidence from work with monkeys that there is an overlap of about 1° due to the overlap of ganglion receptive fields (Talbot and Marshall 1941, Stone et al 1973, Bunt and Minckler 1977, Fukuda et al

1989) although this finding has recently been contradicted by Tootell et al (1988) who found no evidence for an overlap. Some studies have also provided evidence for bilateral representation of the foveola (Bunt and Minckler 1977, Leventhal et al 1988, Fukuda et al 1989) although again this finding has been contradicted by Tootell et al (1988) and was not proven by Stone et al (1973). The apparent contradictions in these experimental findings could be explained by the fact that different workers used different species of monkey and also used a variety of measurement techniques, including various staining methods (Stone et al 1973, Bunt and Minckler 1977, Tootell et al 1988, Fukuda et al 1989) and microelectrode recordings (Talbot and Marshall 1941).

Most of the optic tract fibres pass to the lateral geniculate nuclei but a few fibres go to other structures that produce eye movements and control the pupillary light reflex (Hubel 1988).

#### **1.1.4 Lateral Geniculate Nucleus**

There are two lateral geniculate nuclei situated in the forebrain (Figure 1.2). Almost all of the LGN cells receive input directly from the optic tract fibres and act as a relay sending axons on to the primary visual cortex located at the occipital pole of the visual cortex (Hubel 1988). Some LGN cells, however, synapse locally on other geniculate cells, others receive input back from the visual cortex and others receive input from the brainstem reticular formation, which has a role in attention or arousal (Hubel 1988).

The terminations of the optic tract fibres with the cells in the LGN are topographically organised as are the corresponding terminations with the primary visual cortex. (Topographic organisation means that the cells are arranged next to each other according to their relative positions on the retina and hence the visual field.)

#### **1.1.5 Optic Radiation**

The fibres extend from the LGN to the primary visual cortex in a broad band known as the optic radiation (Figure 1.2). The anatomy of the optic radiation has been reviewed by Harrington and Drake (1990).

The fibres fan out so that the upper and lower field quadrants are separated by the macular fibres. The dorsal fibres, which correspond to the inferior field quadrant, pass backward in a fairly direct course to terminate in the dorsal portion of the primary visual cortex. The ventral fibres, which correspond to the superior field quadrant, initially travel anterior and slightly inferior, looping around the inferior horn of the lateral ventricle (Meyer's loop) before continuing to the ventral portion of the primary visual cortex. The macular fibres terminate in the posterior pole of the primary visual cortex.

### **1.1.6 Visual Cortex**

The primary visual cortex is also known as the striate cortex or area V1 and corresponds to area 17 on the Brodmann architectonic map of the brain (Brodmann 1909). Area V1 is found in both the right and left hemispheres of the brain and contains a precise topographical map of the contralateral visual field (Hubel 1988, Harrington and Drake 1990). Area V1 is surrounded by the prestriate cortex which extends to the posterior bank of the superior temporal sulcus and correspond to areas 18 and 19 on the Brodmann map. This area contains at least four separate visual processing areas, V2, V3, V4 and V5.

Most of the output from V1 is sent to V2. V1 and V2 perform parallel processing with cells whose function it is to detect colour, orientation, end-stopping, direction and stereopsis. Each of the other visual areas has a specialised visual function and receives its input from projections of V1 and V2 from either the magno or parvocellular pathway (Hubel 1988, Zeki 1992).

Area V3 is concerned with dynamic form, the shape of objects in motion. It receives its input from the magnocellular pathway.

Area V4 receives its input from the parvocellular pathway, mostly from the central retina. V4 has two functions, to process colour and colour with form.

Area V5 is also known as area MT (for medial temporal) and processes motion. It receives its input from the magnocellular pathway with hardly any representation of the central retina.

The function of these specialised visual areas was originally determined using microelectrode studies in monkeys such as the owl monkey (Zeki 1980) and the macaque (Maunsell and Van Essen 1983). More recently it has been possible to confirm this organisation in the human visual cortex using positron emission tomography (PET). PET can be used to measure increases in regional cerebral blood flow when people perform certain tasks. Zeki et al (1991) showed that areas V1, V2 and V4 were functional during colour vision whilst V1, V2 and V5 were functional during motion stimulation. V4 is located in the lingual and fusiform gyri of the prestriate cortex and V5 is located in the region of the temporo-parieto-occipital junction.

Each area of the visual cortex projects forward to other structures in the brain as well as back to those areas from which they received their input. It has been proposed that the specialised areas V3, V4 and V5 send information back to V1 and V2 so that the results can be mapped back onto the visual field (Zeki 1992).

## **1.2 THE VISUAL FIELD**

The visual field can be defined as the part of space in which objects are simultaneously visible to the steadily fixating eye (Harrington and Drake 1990). The visual field of each eye extends approximately 60° superiorly, 75° inferiorly, 60° to the nasal side and 100° to the temporal side (Werner 1991). There is a blind spot in the visual field that corresponds to the position of the optic disc (Section 1.1.1) and is located 15° to the temporal side of the fovea and 3° inferior of the horizontal meridian.

### **1.2.1 Representation of the Visual Field in the Striate Cortex**

Much of the knowledge of the cortical representation of the visual field has come from the study of war wounded (Inouye 1909, Holmes and Lister 1916, Holmes 1918). Visual field deficits were correlated with the position of missiles penetrating the occipital cortex and used to construct a map. The most well known map was produced by Holmes (1945) and is shown in Figure 1.3.

The map shows an ordered topographic representation of the contralateral hemi-field of vision. The vertical meridian is represented along the periphery of the

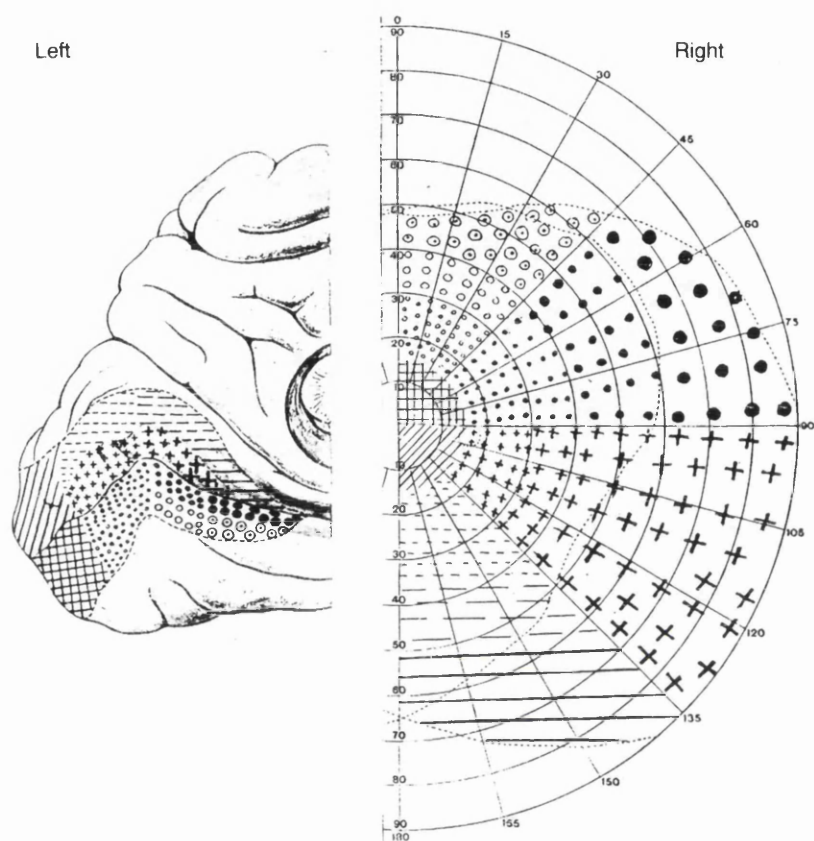


Figure 1.3 The left striate cortex and the right half of the visual field. The different patterns indicate the corresponding segments of the visual field on the cortex. (From Holmes G (1945). The organisation of the visual cortex in man. *Proc R Soc Lond Series B (Biol)* 132, 348-361. Reproduced with permission of the publisher).

striate cortex. The superior visual field is represented in the inferior striate cortex and *vice versa*. The central field is represented in the occipital pole and is 'magnified' relative to the peripheral field which is mapped anteriorly. According to this map, approximately 25% of the surface of the striate cortex processes the central 15° of vision.

This map has been confirmed by studies using x-ray computed tomography (Spector et al 1981) and PET (Fox et al 1987). However, recent work correlating the visual field deficits of patients with occipital lobe lesions with magnetic resonance images (Horton and Hoyt 1991, McFadzean et al 1993) have suggested a revision of the map. The revised map shows a greater representation of the central visual field, with the central 30° covering approximately 83% of the striate cortex.

The distance in the cortex, in millimetres, concerned with 1° of the visual field has been termed cortical magnification (Daniel and Whitteridge 1961). The cortical magnification in man has been found to be inversely proportional to retinal eccentricity (Rovamo and Virsu 1979, Horton and Hoyt 1991) and is proportional to the density of ganglion cells in the retina (Rovamo and Virsu 1979, Curcio and Allen 1990).

### **1.2.2 Sensitivity of the Visual Field**

The sensitivity of the visual field varies across its surface in accordance with its cortical representation. Consequently the visual field is most sensitive in the centre and least sensitive in the periphery. Small objects are seen distinctly within the visual field when they are near the visual axis whilst larger or brighter stimuli are required if they are to be seen in the peripheral field.

The visual field can be represented as a map showing the retinal sensitivity at different locations. The most familiar clinical representation is an isoptre plot in which isoptres are drawn, connecting visual field test locations of equal threshold (Figure 1.4). If the visual field were to be plotted in three dimensions, as sensitivity against retinal location, it would appear as a 'hill of vision' (Traquair 1927) with a pit at the blind spot (Figure 1.5).

HAAG STREIT AG  
BERN-SCHWEIZ

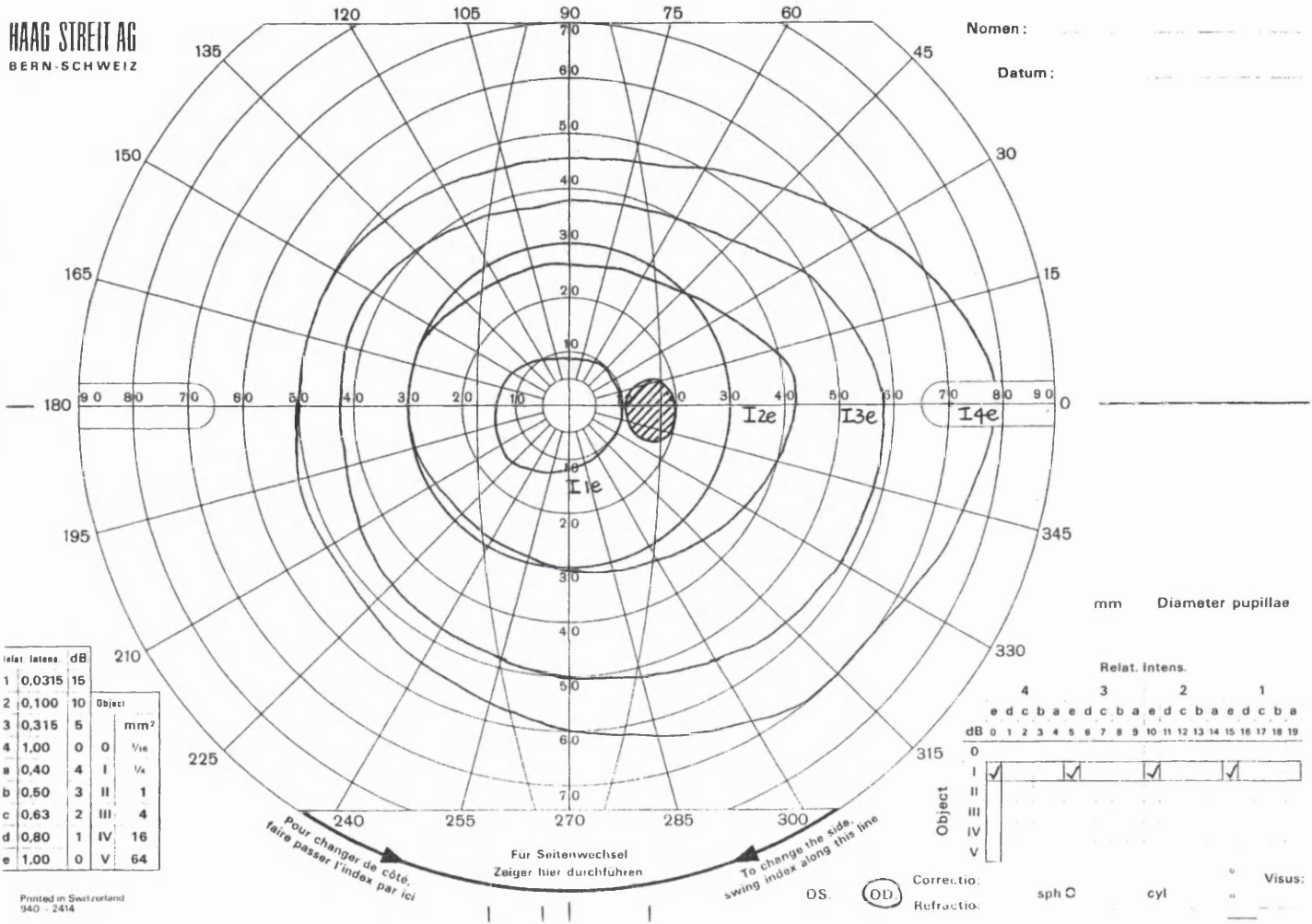


Figure 1.4 An example of a normal visual field from a right eye. This field was plotted by means of a Goldmann perimeter and the isoptres show sensitivity thresholds determined using stimulus targets of different brightness.

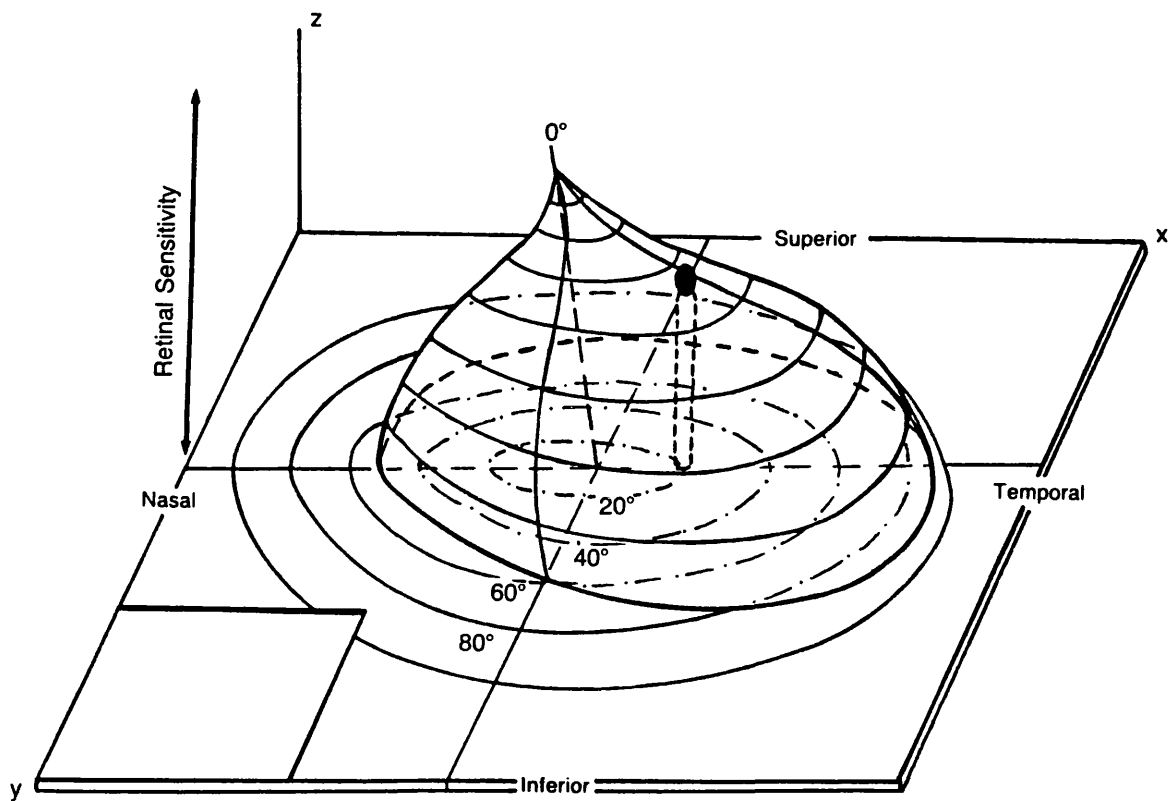


Figure 1.5 The 'hill of vision'. A three dimensional representation of the visual field, showing retinal sensitivity at each point in the field, as described by Traquair (1927). This example shows the retinal sensitivity of a right eye. (From Werner EB (1991).

Manual of visual fields. Churchill Livingstone, New York. Reproduced by permission of the publisher).

The measurement of visual fields is clinically important because it can show characteristic variations and abnormalities in sensitivity when the visual system is affected by disease or damage. Therefore by careful interpretation of variations in the visual field map it is possible to anatomically locate the lesion which produced the variation.

Visual field measurement has a number of uses:

1. To establish a diagnosis, such as glaucoma.
2. To estimate the anatomical location of pathology within the visual pathways.
3. To provide a prognosis, such as in glaucoma.
4. To assess visual function, such as in stroke patients.
5. To monitor the progress of disease, such as in glaucoma, and to guide clinical intervention where possible.

The terms used to describe visual field loss are described in Table 1.1.

### **1.2.3 Types of Visual Field Loss**

Types of visual field loss are reviewed in Harrington and Drake (1990), Townsend et al (1991) and Werner (1991). Some of the most common types of field loss are described below.

#### **Pre-chiasmal pathology**

Pre-chiasmal field loss is caused by intraocular disease or disease of the optic nerve and is often characterised by scotomatous defects.

Glaucoma is a common cause of visual field loss. Defects in the visual field are caused by loss of optic nerve fibres and are usually associated with raised intraocular pressure. The overall prevalence of primary open angle glaucoma is about 0.4 % in western countries, rising to 1 % around the age of 70 and to 3 % over the age of 75

**Table 1.1 Terms used to describe visual field loss**

Scotoma	Localised defect
Constriction	Defect limiting the peripheral extent of the visual field.
Absolute	Defect so dense that the patient does not respond to the maximum stimulus used.
Relative	Defect disappears or becomes smaller using a brighter or larger stimulus.
Hemianopia	Defect involving only left or right half of the visual field.
Quadrantanopia	Hemianopic defect involving only a superior or inferior quadrant.
Homonymous	Defect affects the same part of the field of both eyes.
Complete	Entire right or left hemi-field is lost.
Incomplete	At least a part of involved hemi-field in one eye is partially or totally spared.
Congruous	Defects are the same size, shape and location for the two eyes and are superimposable. Lesions in the visual cortex are congruous.
Incongruous	Defects for the two eyes are different. Lesions just posterior to the chiasm in the optic tracts tend to be incongruous.

(Leske 1983). In the early stages of glaucoma the large nerve fibres from the magnocellular pathway (Section 1.1.2) are most at risk of damage and 20% may be lost before a visual field defect is detectable (Quigley et al 1989). In glaucoma the frequency of scotomata is approximately the same in the upper and lower halves of the visual field, but the locations of the scotomata vary widely (Aulhorn and Karmeyer 1977). In the upper half of the visual field, arcuate scotomata are found corresponding to the route of axons from the retinal ganglion cells (Section 1.1.1), whilst in the inferior half of the field the scotomata lie predominantly in the nasal quadrant. An example of a glaucomatous visual field is shown in Figure 1.6. Effective control of glaucoma can only be achieved using frequent, regular and detailed examination of the visual field.

Lesions such as tumours, scars and retinal haemorrhages produce dense, localised scotomata.

Retinal detachments produce visual field defects which correspond exactly with the area of the detached retina and in the early stages have a characteristic sloping border. In contrast, retinoschisis produces an absolute visual field defect with a very sharp border.

Field defects due to retinitis pigmentosa are highly variable. The defect commonly starts in the mid peripheral retina at an eccentricity of 20° to 25° from fixation and in the late stages the fields are often characterised by a small residual central island of vision.

### **Chiasmal pathology**

Compression of the optic chiasm causes field defects which are dependent on the course of the nerve fibres through the chiasm (Section 1.1.3).

Compression of the optic nerve as it enters the optic chiasm produces a junctional scotoma, a combination of an optic nerve defect in one eye and a temporal superior quadrantanopia in the other eye.

Compression of the chiasm from below, such as from a pituitary tumour, causes a superior quadrantic bitemporal hemianopia. Superior quadrantic bitemporal hemianopia may also be caused by a decelerating head trauma resulting in shearing of

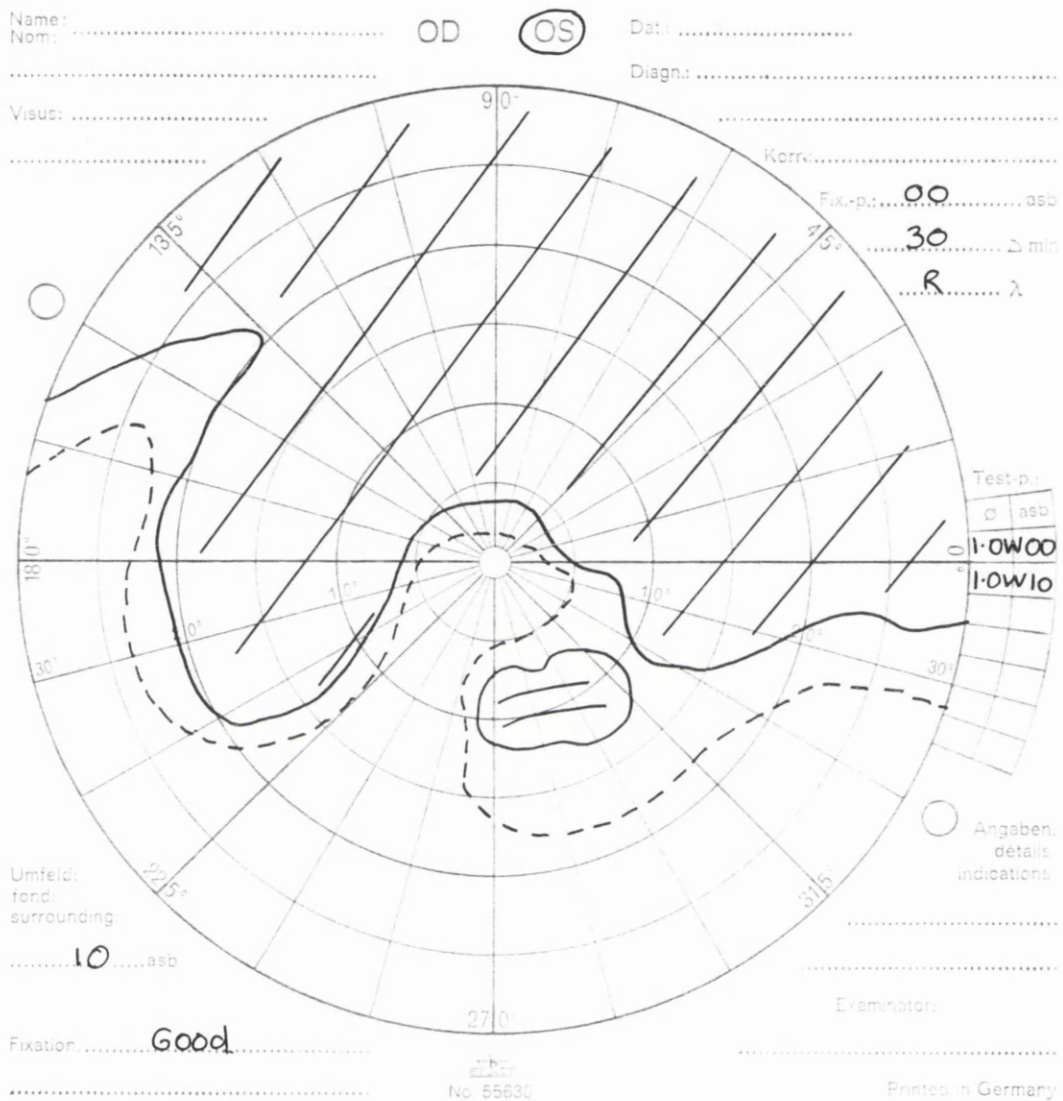


Figure 1.6 Central visual field chart from a left eye showing typical glaucomatous field defects. The field was recorded by means of a Tubingen perimeter. The subject was a 58 year old lady with bilateral open angle glaucoma. The upper field shows baring of the blindspot.

the blood supply from below. Compression of the chiasm from above, such as from a craniopharyngioma, causes an inferior quadrantic bitemporal hemianopia. An aneurysm of one internal carotid artery can displace the chiasm, compressing it against a normal artery, and can produce a binasal hemianopia.

### **Post chiasmal pathology**

Compression of the optic tract (Section 1.1.3) produces homonymous visual field defects which are incongruous.

The nerve fibres in the optic radiations are not in a compact bundle but a wide fan (Section 1.1.5) and are vulnerable to a wide range of insults. For example, damage to the nerve fibres in Meyer's loop (Section 1.1.5) causes homonymous superior quadrantanopia whilst lesions in the parietal lobe tend to produce homonymous hemianopia. The optic radiations are supplied by the middle cerebral artery and patients who develop hemiparesis due to disease of this artery often have an homonymous hemianopia on the same side.

In normal brains the blood supply to V1 is often supplied entirely by the calcarine branch of the posterior cerebral artery (Smith and Richardson 1966). In this situation a calcarine artery infarct would result in a complete homonymous hemianopia. Such a defect is often referred to as a 'macular splitting' homonymous hemianopia. In some subjects, however, V1 is also supplied by the posterior temporal or parieto-occipital branch of the posterior cerebral artery or an occipital branch of the middle cerebral artery (Smith and Richardson 1966). In these cases, an infarct of the calcarine artery would result in a homonymous hemianopia with sparing of the central visual field. As the central field corresponds to the macular area of the retina, such a field defect is often referred to as a 'macular sparing' homonymous hemianopia. The extent of the sparing is dependent on the extent of the dual blood supply. Figure 1.7 shows an example of a complete homonymous hemianopia with some central sparing.

Occasionally glioma, metastases and meningioma cause visual dysfunction in the optic radiations and occipital cortex.

Due to the functional specialisation of the visual processing, damage to the prestriate cortex can impair the recognition of objects causing visual agnosia (Zeki 1992). Such agnosias include the inability to recognise faces and familiar surroundings. A lesion in

A

OD

Test-p.:	
Ø	asb
	0.4 W00
	1.0 W00

Dat.: .....

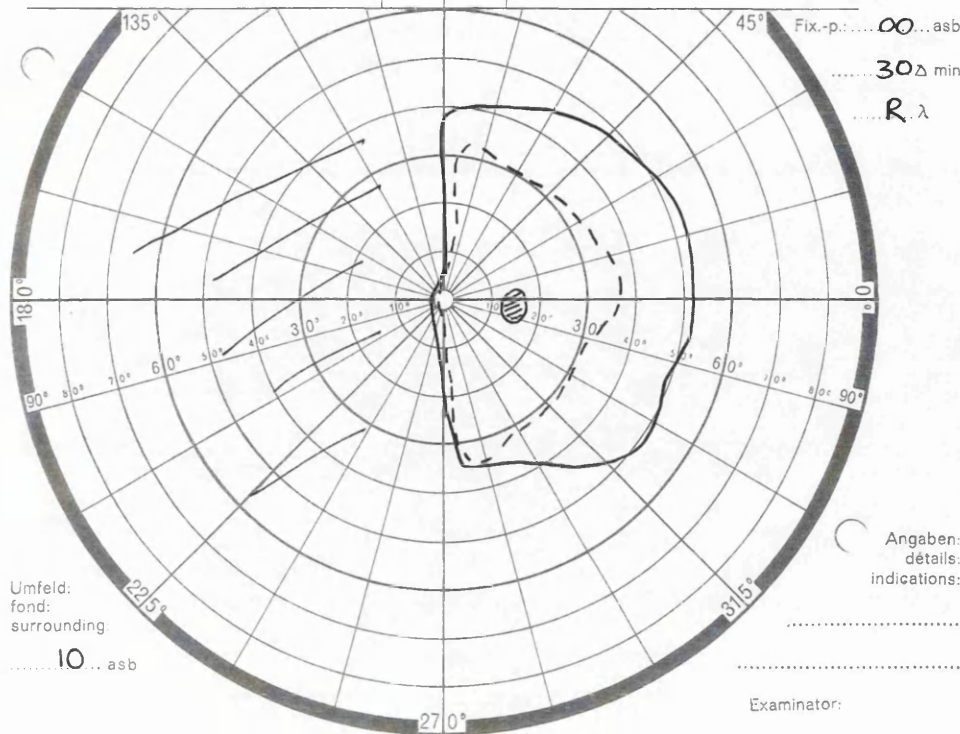
Diagn.: .....

Korr.: .....

Name: .....

Nom: .....

Visus: .....



B

OS

Test-p.:	
Ø	asb
	0.4 W00
	1.0 W00

Dat.: .....

Diagn.: .....

Korr.: .....

Name: .....

Nom: .....

Visus: .....

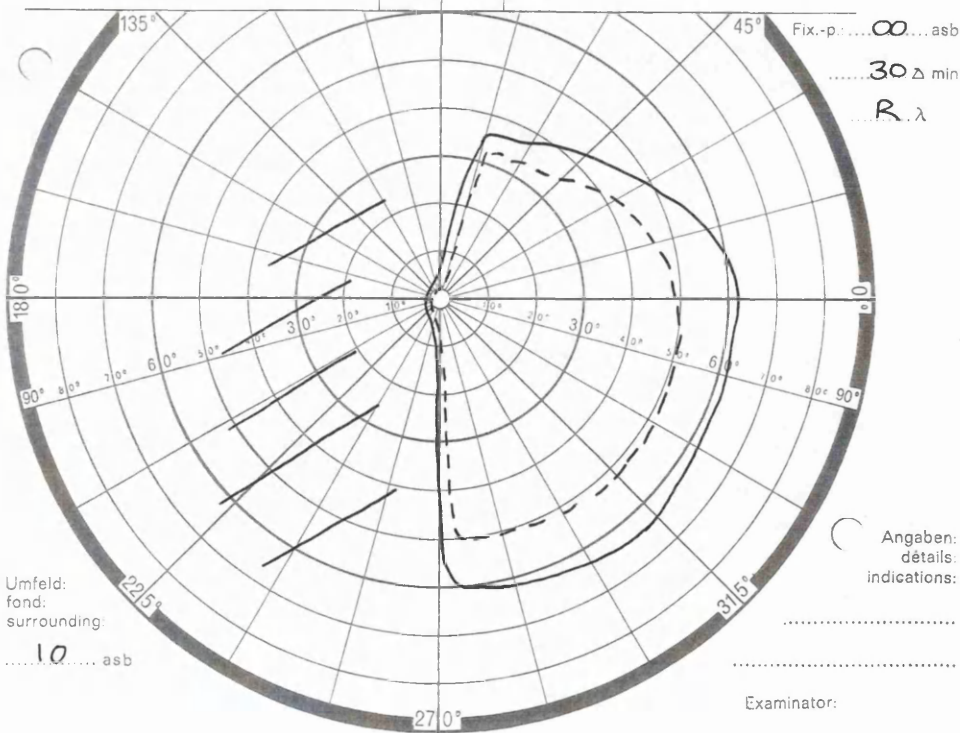


Figure 1.7 Peripheral visual field charts from a Tübingen perimeter showing a complete homonymous hemianopia with some central sparing, a) right eye and b) left eye. The subject was a 69 year old lady who had developed an occipital infarct.

area V5 produces akinetopsia, in which the patient cannot see or interpret objects in motion. Some patients with homonymous hemianopia due to cortical pathology are unaware of their visual field loss because the part of the cortex responsible for recognising the significance of the loss is also destroyed.

#### **1.2.4 Clinical Visual Field Testing**

In clinical practice it is essential to test the visual field of each eye independently for many pathological conditions to be detected.

It is also essential to test the visual field out to an eccentricity of about 25° to 30° but not necessarily beyond (Bedwell 1982, Weber and Dobek 1986, Werner 1991). In glaucoma early visual field defects usually occur at an eccentricity of approximately 15° (Aulhorn and Karmeyer 1977). Most of the nerve fibres in the visual pathway serve central vision and therefore almost all significant neurological visual field defects are found to affect the central 30° (Werner 1991). In addition, due to the high cortical magnification of the central visual field (Section 1.2.1) a 30° visual field examination tests 83% of V1 and a 24° examination tests 80% of V1 (Horton and Hoyt 1991).

### **1.3 PERIMETRY**

The measurement of visual fields is called perimetry and is reviewed in a number of texts including Bedwell (1982), Harrington and Drake (1990), Townsend et al (1991), Werner (1991).

#### **1.3.1 Principles of Perimetry**

The simplest and crudest form of examination is confrontation in which the examiner tests the visual field using simple objects such as his moving finger. A large range of commercially available measurement devices is now available to the ophthalmologist which facilitate clinical testing under controlled conditions. These devices are sensitive to even subtle field defects. They can be either manual or automated with some degree of computer control.

The visual field can be measured using a curved surface or bowl, with the eye positioned at the focus of the bowl. The central visual field can be measured using a flat surface and this is often referred to as campimetry.

There are two ways of performing perimetry. Kinetic perimetry uses moving stimulus targets whilst static perimetry uses stationary targets. In kinetic perimetry a target of constant intensity and size is repeatedly moved towards central fixation from the peripheral visual field. The test subject responds when he first sees the stimulus. Isoptres are then drawn on a chart linking points of equal sensitivity. In static perimetry the stimulus is presented in the same place at various sizes or intensity until it is seen by the test subject. The advantages of kinetic perimetry over static perimetry are that it is relatively fast and that it is useful for plotting the borders of field defects with steeply sloping sides. The drawbacks of using kinetic perimetry are that it is difficult to detect small or shallow scotomata and to plot the borders of field defects with gradually sloping sides (Townsend et al 1991, Werner 1991).

The brightness of the stimulus target and the background are carefully controlled to ensure test reproducibility. The brightness is measured in apostilbs (asb), where  $1 \text{ asb} = 0.31831 \text{ cd/m}^2$ . The retinal sensitivity can be expressed in decibels (dB) by a formula which generates high numbers where the visual field is sensitive and low numbers where it is insensitive. The exact formula varies between different perimeters. This demonstrates the lack of standardisation between instruments and makes the comparison of results from different perimeters difficult (Keltner et al 1986).

It is very time consuming to find the sensitivity threshold across the whole visual field. A quicker alternative is to make measurements with suprathreshold stimuli which are about 0.5 dB brighter than the normal sensitivity threshold (Harrington and Drake 1990). The disadvantage of this technique however, is that no information is produced on the depth of the field defect.

### **1.3.2 Manual Perimeters**

The Goldmann perimeter of 1945 (Bedwell 1982, Harrington and Drake 1990, Townsend et al 1991, Werner 1991) is probably the most widely used perimeter in the world. Stimuli are projected onto the inside surface of a bowl and it can be used to perform quantitative kinetic and static perimetry. The Tübingen perimeter (Bedwell

1982, Harrington and Drake 1990, Townsend et al 1991, Werner 1991) is similar in design to the Goldmann perimeter but was designed to perform static profile perimetry more easily. Both these perimeters can test the central and the peripheral visual fields.

The Friedmann Visual Field Analyser was introduced in 1966 (Bedwell 1982, Townsend et al 1991) and is very popular in Europe and Japan. It is used to perform static quantitative measurement of the central visual field out to an eccentricity of 25°. Multiple stimuli are presented simultaneously from behind holes in a flat plate and the operator records the number and location of the stimuli seen by the test subject. In this way it is possible to test the visual field more quickly, than is possible with the Goldmann perimeter (Bedwell 1982).

Peripheral fields are sometimes measured using the Aimark, light projection arc perimeter, introduced in the 1930s (Bedwell 1982, Werner 1991).

### **1.3.3 Automated Perimeters**

Automated perimeters were developed to make perimetry more widely available by dispensing with the need for extensively trained and experienced operators.

The two most popular automated perimeters are the Octopus perimeter (Bedwell 1982, Harrington and Drake 1990, Werner 1991) and the Humphrey field analyser (Townsend et al 1991, Werner 1991). Both systems use projection stimuli and provide an extensive range of programmed test protocols. These systems have the advantages that the test procedure is exactly repeatable and they can also store the results, provide statistical analysis, display results in a variety of formats and provide hardcopy.

### **1.3.4 Current developments in perimetry**

The availability of low-cost personal computers with computer graphics capability is enabling the development of a new generation of perimeters tailored for specific needs.

A computerised visual field test has been specially developed for use with children (Johnston et al 1989). Conventional perimetric tests cannot usually be performed with children because the tests are long, tedious and require steady fixation. This new test uses a game format to hold the child's attention and unlike conventional tests, the child is allowed to move his eye.

Fitzke et al (New Scientist 1991) have developed a test for screening for glaucoma. The test uses moving stimuli and is designed to test the nerve fibres of the magnocellular pathway which subserve movement detection and which are preferentially damaged in the early stages of glaucoma (Section 1.2.3).

Keating and Mutlukan (1993) have developed an automated multistimulus perimeter. Upon seeing a stimulus, the patient responds to the computer via a touch screen and this makes the test faster than conventional multistimulus perimetry.

The use of computer graphics in these perimeters enables the use of novel stimuli. For example, dark stimuli can be used, which may have a useful clinical role in testing the off-pathway of the visual system (Mutlukan and Damato 1992).

These low-cost computerised perimeters will make perimetry more accessible and enable wider screening for diseases such as glaucoma.

### **1.3.5 Limitations of Clinical Perimetry**

Despite the latest achievements in perimetry the technique remains subjective and relies on the co-operation and concentration of the patient. Mapping the visual field can be very time consuming and even the most co-operative patient's concentration varies over the duration of the test. Tests typically take 15 to 30 minutes per eye. The tests are particularly difficult or impossible to perform in the young, the elderly, those with severe learning difficulties and stroke victims. Testing these groups can also be complicated by difficulties in communication, because the tests require a verbal or motor response.

The reliability of perimetric tests can be checked by monitoring fixation on a television monitor and by testing with stimuli placed in the blindspot. Nevertheless, it is still possible for co-operative subjects to give variable results (Katz and Sommer 1991).

There is therefore a clinical need for an objective form of perimetry. One way of achieving this is to use electrophysiology techniques to detect the evoked signals produced in the visual system in response to stimulation.

## **1.4 CLINICAL ELECTROPHYSIOLOGY OF THE VISUAL SYSTEM**

### **1.4.1 Introduction**

Clinical electrophysiology offers non-invasive measurement techniques to objectively test the function of the visual system. These techniques record evoked potentials which are electrical signals generated by the nervous system in response to sensory stimulation. The electroretinogram (ERG) records the evoked response from the retina and the visual evoked cortical potential (VECP) records the evoked response from the visual cortex.

### **1.4.2 A Review of the Electroretinogram**

#### **The flash ERG**

The flash ERG provides a measure of the function of the outer retinal layer, containing the photoreceptors, and the mid retinal layer, containing the bipolar cells (Figure 1.1).

A diffuse light flash stimulus is used. The ERG is recorded using an electrode placed on the cornea and amplified using a physiological amplifier. The ERG has two principal components, a negative 'a' wave followed by a positive 'b' wave. The 'a' wave occurs about 12 ms after the light stimulus and is generated by the photoreceptors. The 'b' wave occurs after about 30 ms and is related to the activity of the bipolar and Mueller cells (Carr and Siegel 1990).

The ERG amplitude depends on the stimulus intensity. A normal photopic response to a single flash stimulus is about 50  $\mu\text{V}$  in amplitude and is dominated by the response from the cones. If the stimulus is presented in excess of 15 times per second (flicker stimulus) the rods do not have time to respond and a pure cone response is

obtained. A normal scotopic response, obtained after a period of dark adaptation, is about 300  $\mu\text{V}$  in amplitude and is dominated by the response from the rods.

In retinitis pigmentosa, the ERG amplitude is reduced or absent. Congenital stationary night blindness causes a reduced or absent scotopic 'b' wave and sometimes a reduced scotopic 'a' wave. Disorders of the cone system lead to an absent flicker ERG (Carr and Siegel 1990).

### **The pattern electroretinogram**

The pattern ERG (PERG) is a relatively new test and not widely used but it provides further information on retinal function. The PERG provides functional information on the mid and inner retinal layers and has been reviewed by Berninger and Arden (1988). The measurement technique differs from the standard ERG in that a pattern stimulus is used. The response is only 2  $\mu\text{V}$  in amplitude and therefore requires careful recording techniques and the use of signal averaging.

The PERG has two main components, a positive peak 50 ms from stimulus onset,  $\overline{\text{P50}}$ , and a negative peak 95 ms from stimulus onset,  $\overline{\text{N95}}$ . (Conventions for labelling electrophysiological waveforms are explained in Section 2.10.3). The  $\overline{\text{P50}}$  component is a luminance response originating in the mid retinal layer. The  $\overline{\text{N95}}$  component originates from the ganglion cells in the inner retinal layer (Maffei and Fiorentini 1981) and shows spatial tuning due to the receptive fields of the ganglion cells (Section 1.1.1).

The  $\overline{\text{P50}}$  and  $\overline{\text{N95}}$  are usually affected separately in disease.  $\overline{\text{P50}}$  is reduced in macular disorders while  $\overline{\text{N95}}$  may be selectively affected in conditions where the optic nerve is damaged (Holder 1987). In glaucoma the PERG is often significantly reduced in amplitude before it is possible to detect a visual field defect and may therefore provide a useful prognostic indicator for patients with ocular hypertension (Berninger and Arden 1988). In diabetic retinopathy the PERG can be used to demonstrate retinal ischaemia. PERG measurements are usefully combined with VECF measurements. Both tests can confirm damage to the optic nerve, whilst an abnormal VECF in the presence of a normal PERG implies damage posterior to the optic nerve.

### 1.4.3 A Review of the Visual Evoked Cortical Potential

There have been a number of reviews of the VECP including Galloway (1981), Drasdo (1983), Galloway (1986), Regan and Spekreijse (1986) and Celesia (1991). The VECP is also described in recent texts by Spehlmann (1985), Regan (1989), Carr and Siegel (1990) and Heckenlively and Arden (1991).

The VECP measures electrical activity from the striate cortex, V1, and the prestriate cortex (Spekreijse 1980, Maier et al 1987, Beers et al 1992). When the visual cortex is stimulated it can be thought of as a voltage dipole causing currents to flow over the surface of the scalp. By placing electrodes on the scalp it is possible to measure a potential difference due to the currents. The VECP is dominated by the response from the central visual field due to cortical magnification and the orientation of the striate cortex (Halliday et al 1977). Similarly due to orientation of the relevant parts of the cortex, the inferior visual field contributes a greater proportion of the total VECP than does the superior visual field.

The recorded potentials are of the order 1 to 20  $\mu\text{V}$  in amplitude and are buried in ongoing electroencephalographic (EEG) activity which is commonly up to 60  $\mu\text{V}$  in amplitude. The signal recorded from the electrodes is first filtered and amplified using a physiological amplifier. The VECP is then usually recovered from the background noise by means of signal averaging. The principle of signal averaging is based on the assumption that EEG noise occurs in a random fashion and cancels out when successive recordings are averaged (Regan 1989). In clinical practice it is usually necessary to average 100 recordings in order to obtain a sufficiently clear and reproducible VECP waveform.

The technique of signal averaging was pioneered by George Dawson in the 1950s (Regan and Spekreijse 1986). Dawson's first averager was an electromechanical device (Dawson 1954) and this was succeeded by an electronic version in 1958 (Regan and Spekreijse 1986). It was not, however, until 1960 (Cobb and Dawson 1960) that the first averaged VECP was published. The number of VECP studies then rapidly increased as signal averagers became commercially available.

Workers initially experimented with simple flash stimuli and Ciganek (1961) produced a key paper in which he described the characteristics of the flash VECP waveform. The response to flash stimuli is very dependent on the luminance of the stimulus and unfortunately its amplitude and latency are very variable (Spehlmann 1985). Through

time the flash stimulus has been largely superseded by patterned stimuli such as the pattern-reversal checkerboard. The pattern-reversal response is more related to the stimulus pattern size, contrast and frequency of reversal and is less dependent on luminance because the stimulus is isoluminant. Pattern stimuli are the most clinically useful stimuli because they have a smaller intra- and interindividual variation than flash stimuli and are generally more sensitive to disease processes (Spehlmann 1985).

Despite the disadvantages highlighted above, the flash VECP still has clinical uses. When the optic media are opaque or the visual acuity is very poor the pattern stimulus is of no use but a flash stimulus can give useful information about central visual function (Galloway 1986, Galloway 1988) due to cortical magnification of the central retina (Section 1.2.1). The flash VECP can therefore be used, for example, to provide prognostic information before cataract surgery or vitrectomy (Galloway 1986, Galloway 1988).

In the late 1960s research interest switched from the flash VECP to the pattern VECP in order to test different functions of the visual system (Regan and Spekreijse 1986). A significant clinical breakthrough came in 1972 when it was discovered that the pattern-reversal VECP was delayed in optic neuritis (Halliday et al 1972). This event heralded the widespread clinical introduction of the pattern VECP. The diagnosis of optic neuritis and multiple sclerosis using the pattern-reversal VECP remains one of the most widely used applications of visual electrophysiology.

Figure 1.8 illustrates a typical recording from a checkerboard pattern-reversal stimulus. The recordings were made from an electrode positioned 5 cm superior to theinion so that the recording site was directly over the visual cortex. The recordings were made relative to a reference electrode positioned 12 cm superior to the nasion. The waveforms have three characteristic features: a negative peak at approximately 75 ms, labelled  $\overline{N75}$ , a positive peak at approximately 100 ms, labelled  $\overline{P100}$ , and a negative peak at 145 ms, labelled  $\overline{N145}$ . Most patients fit this characteristic pattern but some recordings are more difficult to label and interpret, with  $\overline{N75}$  not easily seen. In contrast to Figure 1.8, Figure 1.9 illustrates typical recordings from a patient with optic neuritis. The signal from the right eye is characteristically delayed.

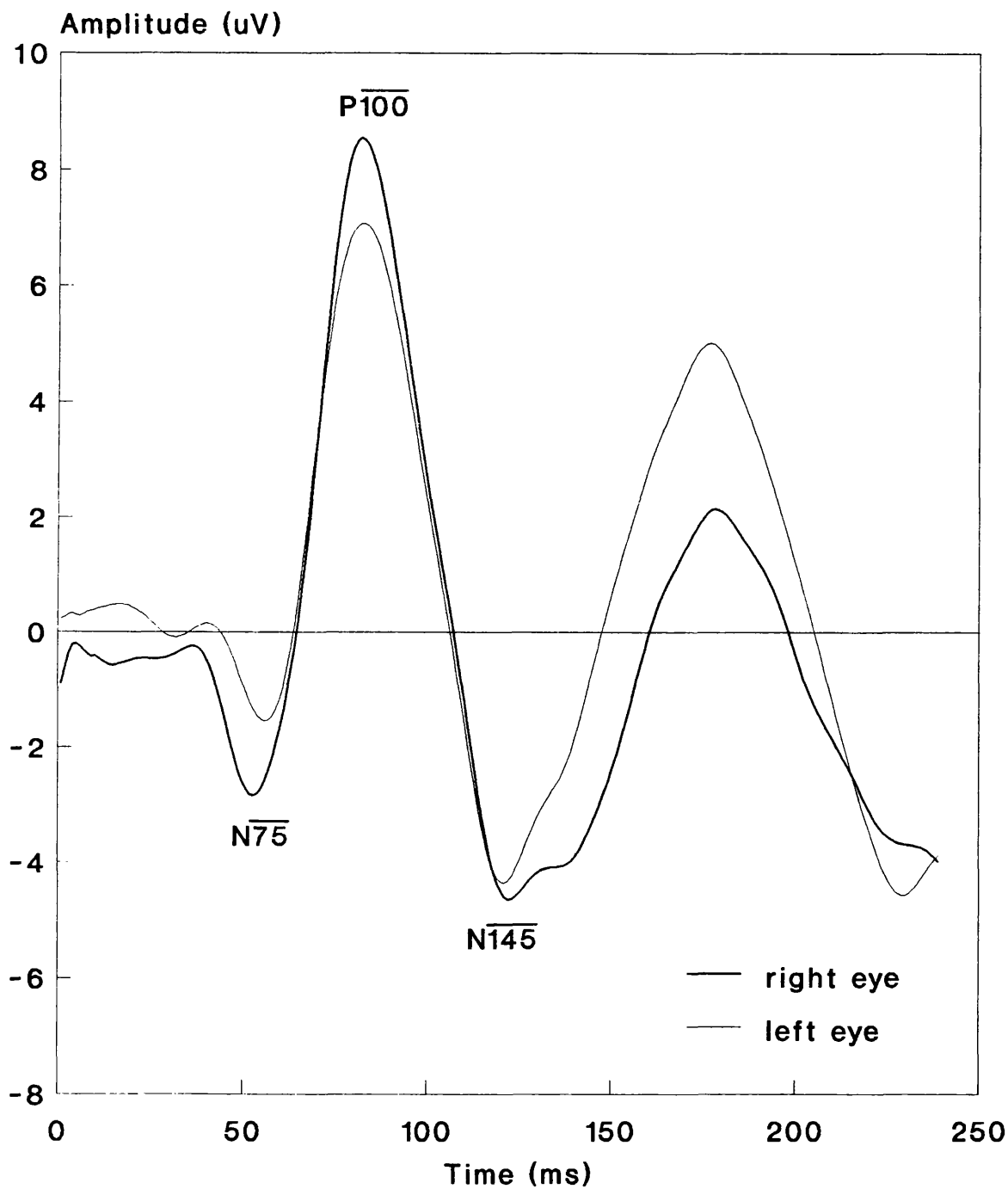
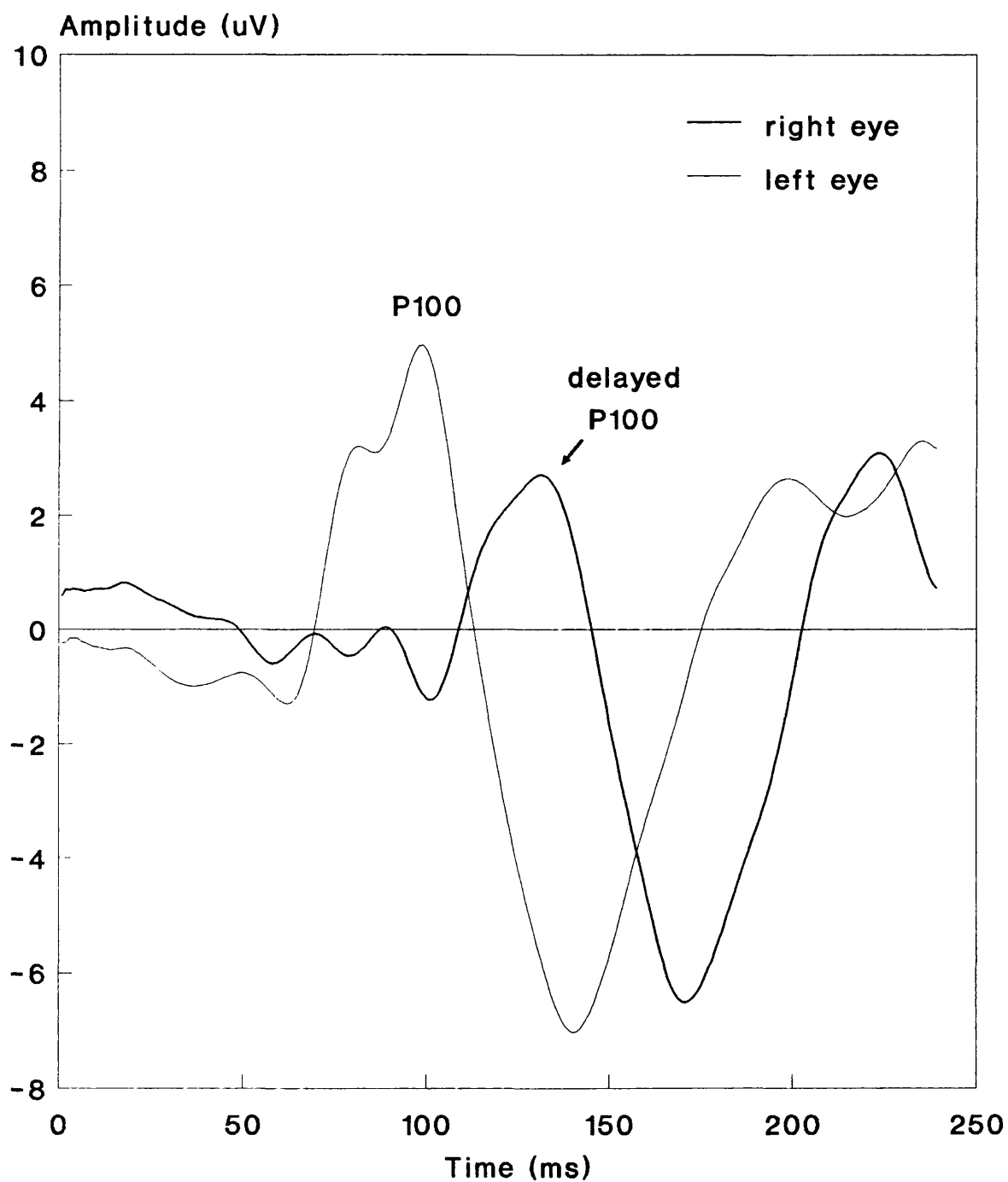


Figure 1.8 Normal pattern-reversal VECP  
the characteristic positive and negative  
peaks are labelled.



**Figure 1.9** Pattern-reversal VEP from a patient with right optic neuritis. The signal from the right eye is delayed.

The pattern VECP exhibits spatial tuning properties and in normal subjects the largest response is obtained with 15' checks. The VECP recorded from small checks is dominated by the central field whilst the VECP recorded from large checks is dominated by more peripheral areas of the visual field (Harter 1970).

The finest stimulus pattern which yields a detectable signal can be used to infer the visual acuity, or resolving power, of the visual system (Hyvarinen 1991). This threshold can also be determined by extrapolating from the amplitude of suprathreshold VECP measurements (Tyler 1991). For infants and multiply handicapped children the VECP provides a method of assessing visual acuity which cannot be obtained by subjective techniques (Sokol et al 1983, Hyvarinen 1991, Taylor and McCulloch 1992). This objective test is also useful for testing patients who claim to have poor visual acuity and are suspected of hysteria or malingering (Galloway 1986).

A combination of full-field and hemi-field stimuli can be used to localise lesions in the visual pathway and objectively detect visual field defects (Blumhardt et al 1977, Galloway 1981, Spehlmann 1985, Galloway 1986).

Monocular full-field stimuli are used to detect visual field defects due to retinal or prechiasmal pathology, whilst monocular patterned hemi-field stimuli are used to detect hemianopia from chiasmal or postchiasmal pathology.

A gross monocular visual field defect will result in a reduced or absent VECP.

A pattern-reversal stimulus is usually used for hemi-field investigations (Spehlmann 1985). Blumhardt et al (1977) wrote a key paper in this field and they described how the normal VECP from a hemi-field pattern-reversal stimulus has a characteristic asymmetric voltage distribution about the midline of the occipital scalp and requires the use of additional recording electrodes positioned equidistant from the midline. Due to the orientation of the visual cortex, the maximum response is detected on the midline and contralateral to the stimulated side of the cortex and has peaks similar to those of the full-field VECP, that is  $\overline{N75}$ ,  $\overline{P100}$  and  $\overline{N145}$ . The signals recorded over the excited hemisphere usually have a lower amplitude and may show  $\overline{P75}$ ,  $\overline{N105}$  and  $\overline{P135}$  peaks. An example is illustrated in Figure 1.10. The mid-occipital electrode was placed 5 cm superior to the inion and the right and left occipital electrodes were placed 5 cm either side. The left temporal electrode was

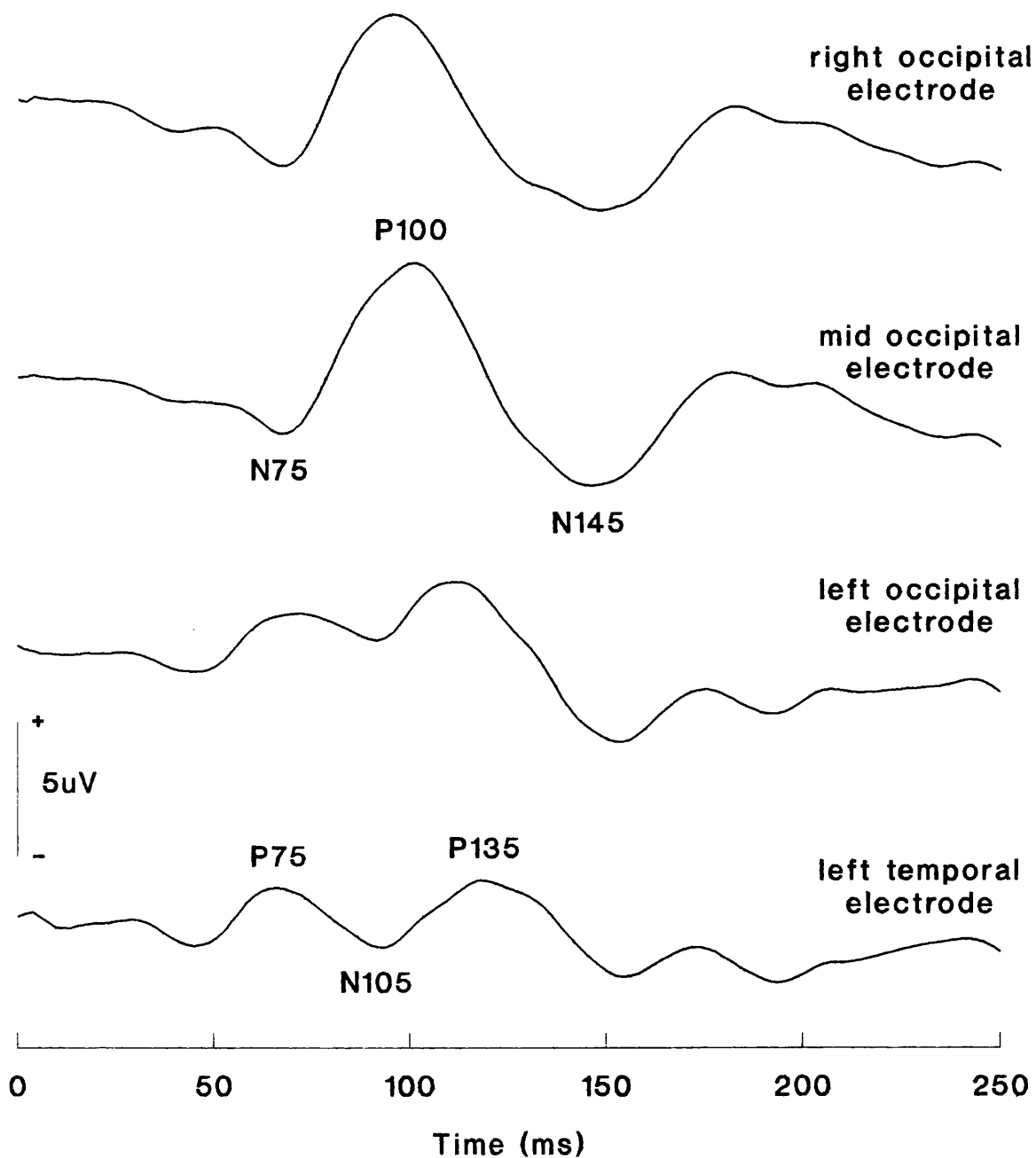


Figure 1.10 Normal transient VEP for monocular pattern-reversal stimulation of the right hemi-field. Characteristic peaks are labelled.

placed 10 cm left of the midline. All recordings were made relative to an electrode placed 12 cm superior to the nasion. Stimulation of a hemi-field with a complete hemianopia will result in an absent VECF. Lesions which are incomplete may reduce the amplitude, distort the shape and occasionally increase the latency of the involved VECFs (Spehlmann 1985). Whilst hemi-field stimuli are suitable for detecting large visual field abnormalities (Blumhardt 1977), smaller stimulus fields are required to detect smaller visual field defects (Cappin and Nissim 1975, Howe and Mitchell 1980, Yanashima 1982).

Since the introduction of hemi-field VECF studies, x-ray computed tomography (CT) and magnetic resonance imaging (MRI) have become available for imaging the visual system and accurately localising lesions. Nevertheless, evoked potential studies may reveal functional abnormalities of the visual system when imaging tests are normal. Evoked potential recording and imaging techniques are therefore complementary to one other (Chiappa 1991).

As explained earlier in this section, the VECF measures cortical activity. By means of multi-channel recordings it is now possible to map the distribution of the evoked potential on the scalp and to estimate the location and orientation of the cortical generators (Celesia 1991). This technique is enabling researchers to determine the cortical origin of different components in the VECF but it is uncertain whether the technique will become a routine clinical tool (Nunez et al 1991).

#### **1.4.4 Conclusion**

The ERG, PERG and the VECF can all detect lesions in the visual system and therefore offer the potential of providing objective information on the visual field. The most appropriate recording technique depends on the type of pathology suspected. If a problem is suspected at the retinal level then an ERG or PERG is likely to be most sensitive although the VECF will be sensitive to pathology involving the macula. If a problem exists posterior to the optic nerve a VECF is the only test modality available. In this sense the ERG, PERG and VECF are complementary techniques.

The advantage of using the VECF for visual field testing, however, is that it measures the whole visual system: optics, neural stimulation, conduction and processing. A limitation of any objective technique using the VECF, however, will be the fact that it

is less sensitive to the peripheral visual field due to cortical magnification and orientation. Nevertheless, the development of VECP techniques can still be justified on the grounds that the central visual field is the most important part to test (Section 1.2.4)

## **1.5 ELECTROPERIMETRY**

### **1.5.1 Introduction**

The concept of using VECPs for detailed visual field analysis has been pursued for about 30 years, the first experiments being made by Copenhaver and Beinhocker (1963). They introduced the term electroperimetry (Beinhocker et al 1966) to describe objective analysis using the VECP, although subsequently the term has also been used to describe measurements made using the ERG (Henkes and Van Lith 1973).

As yet there is no commercially available instrument for performing electroperimetry. The following sections review the problems that have to be addressed before electroperimetry can become a practical clinical tool. Electroperimetry by means of the VECP is considered for the reasons given in Section 1.4.4.

### **1.5.2 Stimulus Types**

There is no consensus as to which is the best stimulus for electroperimetry. As with conventional clinical visual electrophysiology, unstructured and patterned stimuli have been used.

For simple flash stimuli the source most often used has been a Xenon flash tube (Copenhaver and Beinhocker 1963, Beinhocker et al 1966, Schreinemachers and Henkes 1968, Henkes and Van Lith 1973, Adachi-Usami et al 1978, Kojima and Zrenner 1980). Other sources have been an LED (Elberger and Spydell 1985) and a monitor (Regan and Milner 1978, Howe and Mitchell 1980, Yanashima 1982).

Patterned stimuli have usually been produced on a monitor screen which could obviously be very flexible if the pattern were software generated. Patterns have included a checkerboard (Howe and Mitchell 1980, Yanashima 1982) and a circularly

symmetric difference of two Gaussian functions with the geometric centres superimposed (Sandini et al 1983). A checkerboard stimulus has also been produced using a rotating polaroid screen (Cappin and Nissim 1975).

### 1.5.3 Clinical Studies

As yet there have been very few clinical studies with patients.

Copenhaver and Beinhocker (1963) demonstrated visual field defects in two patients: one with a right homonymous hemianopia and one with a scotoma due to a retinal tumour. They used a 3.9 Hz flash stimulus subtending  $2.5^\circ$  and tested various points in the visual field out to an eccentricity of  $30^\circ$ . The signal was recovered using signal averaging which was very time consuming. Furthermore, only one recording channel was used so it is unlikely that the maximum signal-to-noise ratio (SNR) was obtained.

The remaining studies have all used quadrant checkerboard stimuli.

Cappin and Nissim (1975) studied 21 patients with glaucoma, 11 patients with ocular hypertension and 10 normals. They studied homonymous visual field quadrants using a pattern which subtended  $22^\circ \times 22^\circ$ . The checks each subtended  $50'$  and the pattern reversed 12 times per second. The VECPs corresponding to small visual field defects showed a phase shift relative to normal homonymous quadrants. No signal was recordable if the field defect filled more than three quarters of the quadrant. Like Copenhaver and Beinhocker (1963), only one recording channel was used and the signal was recovered using slow signal averaging.

In a study of 12 patients, Howe and Mitchell (1980) found that quadrantic field stimulation made a substantial improvement in the detection of homonymous field defects due to cerebrovascular accident and migraine. The stimulus pattern reversed 12 times per second. The test stimulus was only eight degrees wide and six degrees high. Twenty minute checks were used to maximise the response from the central segment of the quadrant. The quadrant was subsequently retested using  $50'$  checks to maximise the response from the peripheral part. As before, only one recording channel was used and the signal recovery was limited by signal averaging.

Yanashima (1982) demonstrated homonymous hemianopia and quadrantanopia in a small group of patients. He used a specially developed electrophysiology system which had a number of advantages over the systems used in previous studies. The SNR was maximised by recording from five electrodes placed over the visual cortex and by analysing the recordings in the frequency domain. The recording time was reduced by testing four quadrants simultaneously, each quadrant was tested with a slightly different frequency. A limitation of the study was that the stimulus only extended to an eccentricity of  $10^\circ$ . The study could have been further improved by extending the signal processing to include the use of objective signal detection methods.

In conclusion, quadrant field stimulation as described above has proved clinically useful but only provides crude information on the visual field. There is little clinical literature on more detailed examination of the visual field. This is probably due to the difficulty in recording a measurable signal from the peripheral areas of the visual field, the time consuming nature of the test and the technical limitations of the available electrophysiology systems.

In order to record the VEP from small areas of the peripheral retina the stimulus should be optimised so that the SNR is maximised. In order to complete the test in a reasonably short time the method of signal recovery should be optimised so that signals can be detected rapidly.

#### **1.5.4 Optimisation of Stimuli for Electroperimetry**

A number of strategies have been developed to maximise the VEP amplitude from stimulation of the peripheral visual field.

##### **Patterned stimuli**

In quadrant field studies the check-size can be varied in order to measure the response from the central or peripheral parts of the visual field (Section 1.4.3 and Section 1.5.3) because the most effective check-size increases with retinal eccentricity.

Sandini et al (1983) increased the size of their pattern stimulus with retinal eccentricity according to the reciprocal of the cortical magnification factor.

## Flash stimuli

Workers using flash stimuli have also varied the stimulus size according to retinal eccentricity to increase the size of the VECP amplitude from the peripheral field (Beinhocker et al 1966, Henkes and Van Lith 1973).

Kojima and Zrenner (1980) demonstrated that the VECP is related to the number of rods and cones stimulated and so varies under scotopic and photopic conditions. The advantage of performing electroperimetry under photopic conditions is that these are the same conditions used for psychophysical clinical perimetry (Henkes and Van Lith 1973). The advantage of recording VECPs under scotopic conditions however is that the peripheral visual field is relatively more sensitive. Under scotopic conditions, using a 5° diameter stimulus, Adachi-Usami et al (1978) could record the VECP up to 25° eccentricity but found a high interindividual variability. They were pessimistic that the scotopic VECP would enable measurement of retinal sensitivity with an adequate resolution for clinical use. Kojima and Zrenner (1980) however showed good reproducible results for 4 subjects along one meridian under scotopic conditions. A disadvantage of performing electrophysiology under scotopic conditions is that a long adaptation period of 20 to 40 minutes is required and slow stimulation rates have to be used to prevent light adaptation. Despite these problems scotopic VECPs have been shown to be useful in discriminating between normal subjects and subjects with night blindness (Airas and Peterson 1985) and in identifying cases of concentric field restriction (Peterson and Airas 1985).

The colour of the stimulus and the background also affect the relative contributions of cones and rods to the VECP. A white stimulus has the advantage of exciting all photoreceptors whilst red light (Schreinemachers and Henkes 1968, Henkes and Van Lith 1973) leaves the green and blue cones relatively undisturbed. Other colours used in electroperimetry experiments have included yellow (Copenhaver and Beinhocker 1963), green (Copenhaver and Beinhocker 1963, Elberger and Spydell 1985), orange (for photopic stimulation) and blue (for scotopic stimulation) (Kojima and Zrenner 1980).

The VECP signal amplitude is an integral of the flash luminance and duration (Wicke et al 1964, Beinhocker et al 1966). There have been similar findings with ERG measurements and it has been found that there is a stimulus duration at which the response saturates (Henkes and Van Lith 1973). These observations have parallels in

Bloch's law which describes temporal influences on the psychophysical threshold of vision.

### **New stimuli**

An alternative way of improving the relative sensitivity of the peripheral retina may be to use moving stimuli. The parts of the visual cortex which process motion receive their input from the magnocellular pathway (Section 1.1) in which the peripheral retina is well represented. This hypothesis is supported by recent reports in the literature which showed that the amplitude of the motion-onset VECF is significantly larger for extramacular than for macular stimulation (Kubova and Kuba 1992, Kuba and Kubova 1992). Muller et al (1990) were able to record VECFs from motion-onset stimuli at an eccentricity of 23°.

### **1.5.5 Scattered Light**

When recording VECFs due to localised stimuli it must be ensured that the measured signals are not due to light scattered to other parts of the retina. The retinal distribution of stray light has been thoroughly investigated by de Mott and Boynton (1958a,b) mostly using eyes excised from steers. Their measurements showed that about 70% of scattered light comes from the cornea, whilst the remainder comes from the lens. They were also able to measure the distribution of scattered light as a function of angle from the incident light direction. These results show, for example, that at an angle of 5° the illuminance of the scattered light is about 2.5 log units less than the source. Consequently, if the source illuminance is more than 2.5 log units above the VECF threshold, the light scattered 5° from the stimulus will contribute to the recording.

The effect of scattered light can be minimised in photopic test conditions by the addition of a light adapting surround to the stimulus (Copenhaver and Beinhocker 1963, Beinhocker et al 1966, Schreinemachers and Henkes 1968, Henkes and Van Lith 1973, Adachi-Usami et al 1978, Kojima and Zrenner 1980, Sandini et al 1983). In scotopic test conditions the effect of scattered light is minimised because the stimulus luminance is very close to the minimum threshold of stimulation (Adachi-Usami et al 1978, Kojima and Zrenner 1980, Airas and Peterson 1985, Peterson and Airas 1985).

### 1.5.6 Fixation Monitoring

Reliable fixation is essential for electroperimetry (Beinbocker et al 1966). A number of methods for monitoring fixation have been tried but none is ideal. Fixation can be checked using an infrared camera (Fujimoto and Adachi-Usami 1988), but this can be difficult to assess. Fixation can also be checked by using a reference VECP signal which is recorded from small checks positioned at fixation (Spekreijse 1980). This technique enables fixation to be checked to within 30' of arc, but the patient must have normal visual acuity which is not always the case if extensive field defects are present. A third method is to place additional recording electrodes on either sides of the eyes and record the electrooculogram. The problem with this technique is that in addition to the time and discomfort of placing an additional two electrodes on the patient, an additional amplifier channel is also required.

### 1.5.7 Signal Recording

The distribution of the VECP over the surface of the scalp varies according to the location of the stimulus in the visual field. Therefore the number and position of recording electrodes is critically important. Blumhardt et al (1977) found that four or five recording sites were necessary for hemi-field stimulation. Regan and Milner (1978) concluded that at least two channels are required for electroperimetry. Yanashima (1982) detected quadrant field defects using quadrant field stimulation and four recording channels, he concluded that more than two channels should be used. Surprisingly, many experiments with electroperimetry have only used one channel and it is therefore highly likely that the measured SNR was sub-optimal for many of the stimuli investigated.

Most electroperimetry studies have used transient stimuli occurring at a rate of about once per second and have recovered the signal from background noise by signal averaging. When higher stimulus frequencies have been used the signal has also been measured using a frequency analyser (Regan and Milner 1978) or a Fast Fourier Transform (FFT) (Yanashima 1982).

In electroperimetry no advanced method of digital signal processing (DSP) has been used to improve the SNR. Potential methods of improving the SNR include Wiener filtering (Cerutti et al 1987a, de Weerd 1981), parametric filtering (Cerutti et al 1987b) and adaptive filtering (Widrow et al 1975, Widrow and Stearns 1985).

The processed signals need to be characterised by a number of key parameters. This is usually achieved by quoting the amplitude or latency of various key features. For high frequency stimulation the latency is quoted as a phase. In general the amplitude of the VECP increases and the latency decreases with stimulus intensity (Regan 1972, Adachi-Usami 1978, Kojima and Zrenner 1980). Kojima and Zrenner (1980) argued that latency was a more reliable measurement criterion than amplitude because the amplitude measurements were variable and influenced by the distance between the stimulated part of the visual cortex and the recording electrode.

Some attempts have been made to automatically analyse the signal. Beinhocker et al (1966) integrated the VECP response and empirically determined whether a signal was present or not. Kleinschmidt et al (1992) decided that amplitudes and latencies were too variable to use and tested the significance of differences in variance of the EEG for 512 ms before and after stimulation.

## **1.6 CONCLUSION AND AIMS**

An objective technique for performing perimetry would be a useful clinical tool especially for testing those patients who are unable to co-operate adequately with conventional subjective methods. For such a technique to be clinically useful it should record VECPs and enable testing of the visual field out to a retinal eccentricity of 25° to 30° (Section 1.2.4). In order to make the test practical it should take no longer than 15 minutes per eye to complete.

To date most clinical electroperimetry data has been recorded using visual field quadrant stimuli. To enable finer resolution of the visual field, the stimuli need to be further optimised for stimulation of the extramacular visual field and faster recording methods need to be developed. Many commercial systems are now available to perform visual electrophysiology but the variety of stimuli offered is limited, in general because the stimuli are produced by dedicated hardware.

The current availability of low-cost personal computers with high resolution graphics allows the development of new stimuli for optimal stimulation of the peripheral retina.

A further limitation of commercial electrophysiology equipment is that signal averaging is the only method of signal recovery. Recent developments in DSP may

facilitate rapid signal detection and measurement through methods such as adaptive filtering. High-speed signal processors which are specialised microprocessors designed to perform computationally intensive DSP algorithms in real-time are now commercially available on low-cost processor cards for use in a PC, complete with memory and interface circuits.

Reliable fixation is essential for electroperimetry but there is currently no ideal method for monitoring fixation. An alternative approach would be for the test subject to undertake a simple task that could be completed only if they were fixating properly. Such a task would have the added advantage of helping the subject to concentrate on fixating. Johnston et al (1989) found this approach very successful in their computerised subjective perimeter (Section 1.3.4). For those patients who are unable to reliably perform a simple task, the only satisfactory method of fixation would be for the clinician to project the stimulus under direct view onto the appropriate part of the retina.

The aims of the current research are:

1. To develop a visual electrophysiology system based on a PC with two novel features: a DSP card to enable real-time signal processing and a wide range of software generated stimuli.
2. To develop DSP techniques for fast objective signal detection and measurement.
3. To optimise stimuli for testing different parts of the visual field using a computer monitor. In particular, to optimise quadrant field stimuli with a view to recording from smaller areas of the visual field and to investigate the use of motion stimuli for electroperimetry.
4. For those patients able to fixate on a monitor screen, to develop a method of monitoring fixation which involves a simple task and also helps the patient to concentrate.
5. For those subjects unable to fixate reliably on a monitor screen, to develop an instrument which enables VECPs to be recorded whilst pattern stimuli are positioned on the retina by the examiner under direct vision.

6. To clinically validate the use of quadrant field stimuli by assessing patients with complete and absolute hemi-field and quadrant field defects, and implement methods for objective signal detection.

## **2. INSTRUMENTATION AND RECORDING METHODS**

### **2.1 INTRODUCTION**

This chapter describes the instrumentation and recording techniques used to develop methods for objective visual field analysis using digital signal processing of visual evoked cortical potentials. No commercial electrophysiology system was suitable for the research and a new system based on a personal computer has been developed. This development is described together with the clinical validation.

A number of commercial systems are also now based on PCs which have the advantages of being able to archive data in a standard format, use various hardcopy facilities and perform administrative tasks. Several microcomputer based systems are also described in the literature (de Waal et al 1983, Epstein et al 1983, Stanziano et al 1988, Torok 1990). The reasons for their construction include the need for compact portable systems (de Waal et al 1983) and the search for alternatives to the high cost, limited flexibility and limited performance of commercial systems. Nevertheless, these systems all have a restricted range of stimuli and are limited to slow averaging or off-line spectral analysis.

The system described in this chapter has two novel features; it uses a DSP card to enable real-time signal processing and it provides a wide range of software generated stimuli.

## 2.2 SYSTEM DESIGN SPECIFICATION

The system was designed to be capable of performing routine electrophysiology as well as allowing the development of novel visual stimuli and signal detection techniques.

The basic specification of the system was as follows:

1. The system should be able to record VECPs or ERGs.
2. The system should be based on widely available commercial hardware and include a PC and a DSP card.
3. The visual stimuli should be software generated and displayed on a monitor.
4. The system should enable stimuli to be presented at slow transient rates (once per second or less) as well as fast steady-state rates (four to twenty times per second).
5. A range of patterned stimuli should be available and the range of presentation modes should include pattern-reversal, pattern-onset, pattern-offset and motion.
6. The DSP card should enable real-time signal processing including signal averaging and facilitate the development of on-line adaptive filtering techniques for the detection of steady-state VECPs.
7. The system should provide four recording channels.
8. The system should comply with the British Standard BS 5724 part 1 for patient connected electromedical equipment (British Standards Institution 1989). BS 5724 part 1 is equivalent to the standard IEC 601 part 1 (International Electrotechnical Commission 1988).
9. In order to be consistent with other centres the system should enable the recording of flash ERGs to agreed international standards (Marmor et al 1989).

## 2.3 SYSTEM HARDWARE

### 2.3.1 System overview

The system hardware is based on an IBM personal computer PS/2 30-286 with an 80287 co-processor. The computer has a 16 bit, AT compatible, bus with three expansion slots (Figures 2.1). One slot is used for the DSP card, a second slot is used for an analogue input/output card and the third slot is used for a card to drive two computer monitors. Patterned stimuli are presented on a computer monitor and flash stimuli are presented using a Ganzfeld bowl or a Xenon strobe. A four channel physiological amplifier is used to amplify and filter signals before they are digitised in the analogue input/output card.

### 2.3.2 Physiological amplifier

The physiological amplifier has two purposes:

1. To amplify the difference in potential between two electrodes so that the output voltage is within the operating range of the analogue input/output card in the computer (Figure 2.1).
2. To filter the recording and improve the SNR. The filter is set to attenuate frequencies outside the range of frequencies contained in the VECF under study.

A differential amplifier must be used to reduce the effect of common mode interference, such as that due to mains electricity. One recording electrode is connected to the positive input of the amplifier  $V_+$  and the other is connected to the negative input  $V_-$ . The electrode connected to  $V_-$  is often referred to as the 'reference' electrode. The amplifier output is equal to the difference between the two inputs multiplied by the amplifier gain.

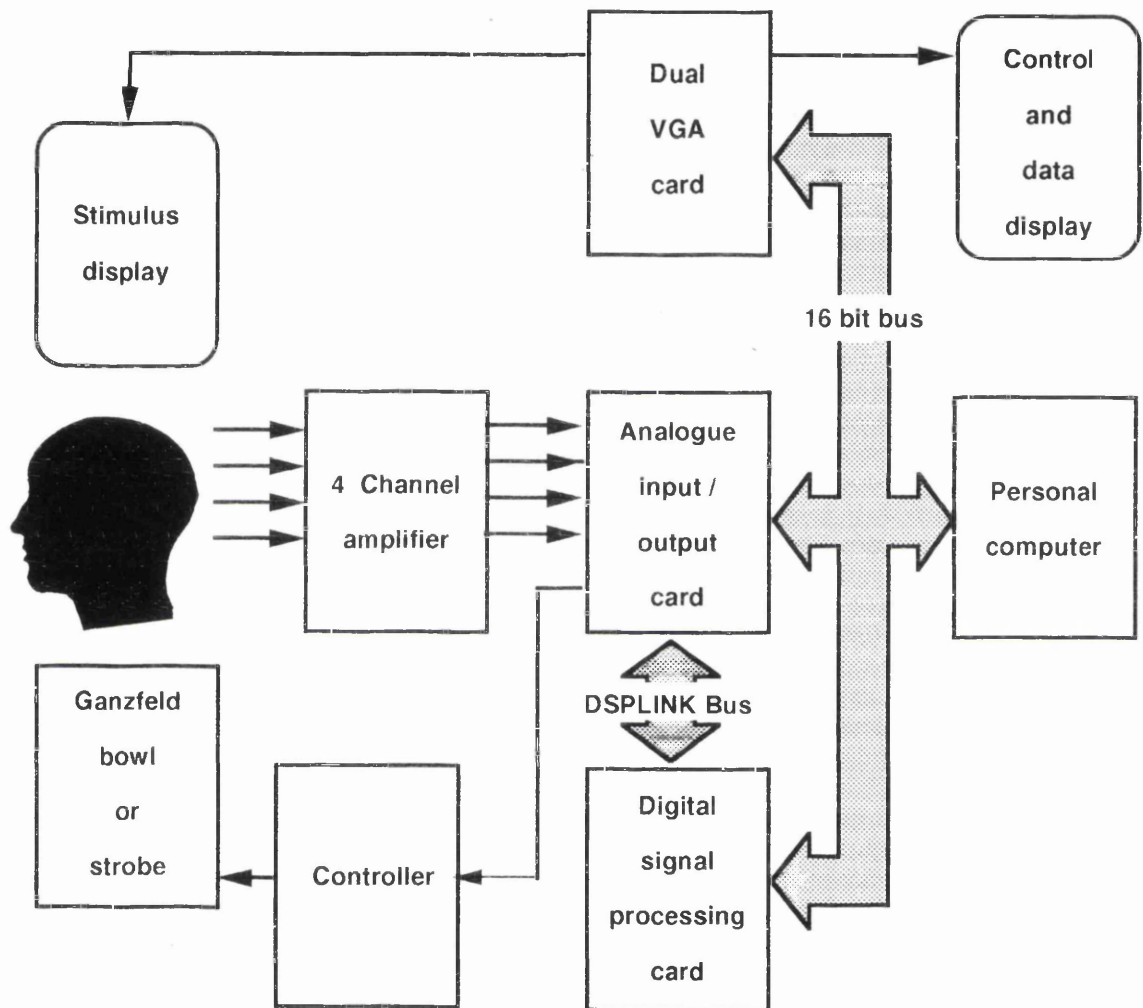


Figure 2.1 Block diagram of system hardware.

Differential amplifiers require a third 'reference' input and this is obtained by using a third electrode, usually placed anywhere on the head. To avoid confusion with the 'reference' connected to  $V_-$ , the third input is often referred to as the 'indifferent', 'guard' or 'ground' electrode. The use of the term 'ground' is itself misleading because the amplifier input should be opto-isolated for the electrical safety of the patient and the term 'guard' is therefore used in the following text.

The difference in potential between  $V_+$  and  $V_-$  is mainly due to cerebral potentials which have different voltages and timings at the two recording sites. Extracerebral potentials or artefact such as mains interference often have the same voltage and timing at the two sites and cancel at the amplifier input.

In typical recording conditions, the maximum differential voltage is  $100 \mu\text{V}$  and the amplifier gain is 100,000. This gain is very large so the amplifier must have a very low input noise specification in order to prevent adding significant noise to the signal.

The input impedance of the amplifier must be high in order to avoid loss of signal amplitude. A typical electrode impedance is in the range one to five kilo-ohms, so the input impedance should be ten mega-ohms or more (Spehlmann 1985).

As described above, amplifiers should ideally reject common mode signals at their inputs. However, amplifiers are not perfect and in practice they amplify a small fraction of the common signal. The ability of the amplifier to reject common mode signals is called the common mode rejection ratio (CMRR). The CMRR of an amplifier is measured as the differential gain divided by the common mode gain. Due to the high gain used in evoked potential recordings the amplifier CMRR should be at least 10,000:1 or 80 dB (Spehlmann 1985).

The amplifier should have a range of filter settings. The low frequency high-pass cut-off is normally set to 1 Hz. The high frequency low-pass cut-off is typically 100 Hz, some workers use 300 Hz while others use a cut-off as low as 30 Hz. The cut-off frequencies should not be too close to the signal frequency components because otherwise the filter can distort the phase of the signal. The low-pass filter roll-off slope should not exceed 40 dB per decade and the high-pass filter roll-off should not exceed 20 dB per decade because steeper slopes may cause signal distortion.

The specifications and costs of seven commercially available amplifiers were evaluated and a Biodata PA400 (Biodata, Manchester, UK) four channel physiological amplifier

was chosen for evoked potential studies (Figure 2.2). The specification of the amplifier is summarised in Table 2.1. The amplifier input is opto-isolated and was designed to comply with BS 5724 for BF class I equipment. In order to prevent noise pick-up in long leads, the amplifier has a head box preamplifier (Figure 2.2) which is placed close to the patient.

It was necessary to make one modification to the standard amplifier. The voltage output was limited to  $\pm 2$  V so as not to damage the input of the analogue card (Section 2.3.3). Note that this modification had no effect on the performance of the amplifier, two volts is twice its linear output range.

A disadvantage of the Biodata amplifier was that it was not suitable for ERG studies. The Biodata amplifier saturates if the input offset voltage exceeds 80 mV. In ERG studies the offset voltage between the recording electrodes can be 100 mV or more. Two single channel physiological amplifiers were therefore designed for ERG recordings and constructed in the Department of Clinical Physics and Bio-Engineering. These amplifiers incorporated Intronic isolation instrumentation amplifiers and had a CMRR of 135 dB.

### **2.3.3 Analogue Input/Output Card**

The output signals from the physiological amplifier are digitised using a four channel analogue input/output card (Loughborough Sound Images). The card has a 12 bit resolution analogue-to-digital converter (ADC) that can sample at rates of up to 50 kHz. The sampling rate is controlled by means of a programmable timer. The timer generates interrupts that are serviced by the software running on the DSP card. In order to prevent aliasing of the frequency components in the input signal, the sampling rate must be at least two times greater than the maximum frequency component in the input. A typical sampling frequency for VECG recording is 500 Hz. The maximum operating range of the ADC is  $\pm 2.5$  V and the maximum input range is  $\pm 3$  V.

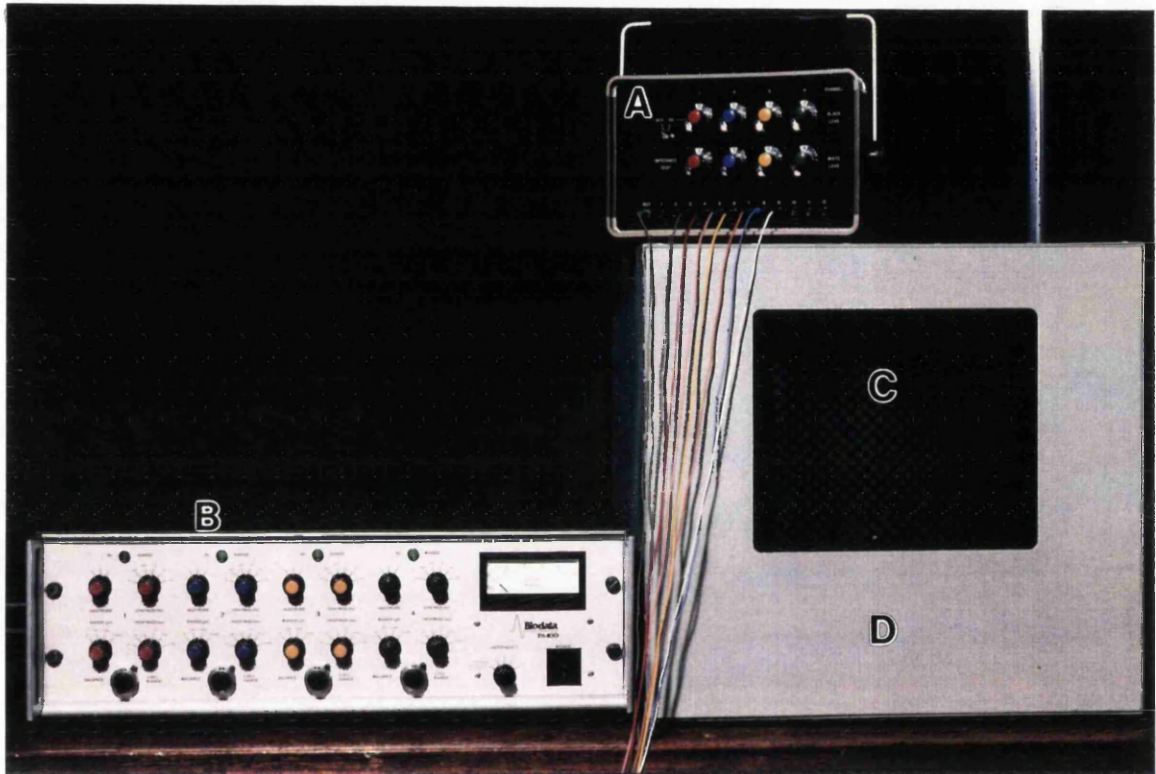


Figure 2.2 Photograph showing head box preamplifier (A), amplifier (B), stimulus monitor (C) and earthed steel cabinet (D).

**Table 2.1 Biodata PA400 Physiological Amplifier Specification**

Full scale deflection	10, 100 $\mu\text{V}$ and 1, 10 mV with a multiplier of 1, 2 or 5.
Frequency response	DC to 10 kHz
Output	DC or AC, linear within $\pm 0.5$ V range.
Input impedance	100 M $\Omega$
Bandwidth High-pass	DC or time constant of 10, 1, 0.2, 0.02, or 0.002 s.
Low-pass	30, 100, or 300 Hz, or 1, 3, or 10 kHz.
Common mode rejection ratio	100 dB (measured)
Noise (referred to input)	0.95 $\mu\text{V}$ (0.8 -300 Hz, measured tangentially with inputs shorted together).

### 2.3.4 DSP Card

The DSP card is a TMS320C25 Processor Board (Loughborough Sound Images, Loughborough, UK) which is based on a Texas Instruments TMS320C25 processor that operates at 40 MHz. This card is used to process the digitised signals from the analogue input/output card.

Specific advantages of using the DSP to process the data in preference to the PC are as follows:

1. The processor is optimised for performing DSP, for example, one integer multiplication and addition can be performed in one machine cycle.
2. The PC is free to perform other tasks such as controlling graphics and accessing storage discs.
3. The DSP card has its own 16 bit bi-directional parallel interface, 'DSPLINK', which facilitates the rapid transfer of data between the analogue card and the PC. Data would otherwise have to be transferred on the main PC bus.
4. The interrupts from the timer on the analogue card can be serviced immediately by the DSP card. In contrast, the PC has to handle interrupts from a number of sources and has to queue them in order of priority.

The DSP card has 32 kilobytes of memory which are used to store acquired and processed data. This memory can also be accessed by the PC whilst the DSP card is operating.

### 2.3.5 Stimulus Monitor

A wide range of luminance values and good luminance uniformity are the principal requirements of an appropriate stimulus monitor (Barber 1981). Unfortunately no information was available from manufacturers on the luminance uniformity of their monitors or even the range of luminances available. One dozen commercially available colour monitors with screen sizes of 12 or 14 inches were surveyed. The monitor with the best image uniformity was the IBM model 8512, a 14 inch monitor (Figure 2.2).

This monitor could also provide a wide range of luminance values through the adjustment of its brightness and contrast controls.

Two monitors are used in the system, one for the stimulus and the other for the operator's control screen. The displays are driven by a dual Video Graphics Adapter (VGA) card (VGA<sup>2</sup>, Cebra Communications, Bournemouth, UK) which is compatible with the standard IBM VGA. A Polaroid CP-Universal 1 computer filter (Infotrieve, Clydebank, UK) is fitted over the monitor screen to reduce glare and improve contrast. The filter is also earthed thus eliminating static and reducing electromagnetic radiation from the monitor.

### **2.3.6 Flash Stimuli**

Flash stimuli are routinely used for ERG measurements and are also used for VECF studies. The stimulus is produced externally to the system using standard commercial equipment, either a Ganzfeld bowl or a Xenon strobe (Medelec, Old Woking, UK). ERG measurements must be made using a Ganzfeld bowl to comply with the international ERG standard (Marmor et al 1989). A one bit digital output on the analogue input/output card is used to trigger these devices.

## **2.4 SOFTWARE**

Much effort has been expended in software development. The basic system software alone took six months to develop.

### **2.4.1 Software Languages**

Texas Instruments TMS320C25 assembly language is used to control the DSP card, and so provide fast signal acquisition and processing. 80286 assembly language is used to control the VGA<sup>2</sup> card and the data transfer between the PC and the DSP card. The rest of the software is written in Pascal and provides the overall system control.

### **2.4.2 System Operation**

To facilitate ease of use, the system is either controlled via menus or pre-prepared protocols. The user is prompted to select various screens such as stimulus set-up, data acquisition and data analysis. During data acquisition and analysis the system is operated using function keys.

### **2.4.3 Stimulus Generation and Control**

Stimuli are generated using computer graphics (with the exception of flash stimuli) and can be of any shape. Various types of stimulus presentation mode are available including pattern-reversal, pattern-onset, pattern-offset and motion-onset.

The system is very flexible, for example, the pattern parameters that can be selected include meridian and eccentricity, number of elements, shape of elements, element size, shade of background, shade of elements and stimulus rate.

The patterns are typically drawn in 640 x 350 pixel resolution using a palette of 16 colours. Each colour is produced using three analogue colour outputs; red, green and blue. Although, in theory, analogue signals are infinitely variable, in practice, each colour output is limited to 64 levels due to the finite resolution of the digital-to-analogue converters (DACs) producing the signal. Nevertheless, 256,000 individual colour hues are possible. By adding the colours in equal amounts a 64 point grey scale can be generated. Grey level zero corresponds to the colour black and grey level 63 corresponds to white.

The stimulus is usually changed by manipulating the VGA<sup>2</sup> colour palette registers (Wilton 1987). As with the standard IBM VGA, the VGA<sup>2</sup> card generates an interrupt at the start of the monitor vertical retrace. In order to synchronise changes in the colour palette to the vertical retrace, the system interrupt service routine has been revectorred (Wilton 1987) and a new routine written. A number of discrete stimulus frequencies are therefore possible. When transient stimulus frequencies are used, consecutive stimulus periods are varied by 56 ms to reduce the risk of EEG alpha wave activity becoming time-locked to the VECF.

Pattern-reversal stimuli are drawn in two colours, usually black and white. The stimulus is created by reversing or swapping the colour palette attributes of the two colours in the pattern.

Pattern-onset stimuli are drawn in two colours also. Prior to stimulus presentation, the colour palette attributes of the two colours are usually grey. The stimulus is produced by changing one colour palette attribute to white at the same time as the other is changed to black. A pattern-offset stimulus is produced when the colour attributes are redefined as grey.

Motion-onset stimuli are produced by one of two methods. In one method the stimulus pattern consists of black and white bars, made up of 6 lines. Each line is drawn in a separate colour from the colour palette. Colour palette animation creates an illusion of motion in a direction orthogonal to the bars. The second method for producing motion is to scroll the screen and hence the bars. Horizontal scrolling is achieved in VGA graphics by continually modifying the horizontal start address in the video memory.

The distance from the patient to the screen is typically 40 cm in order that the screen subtends  $30^\circ \times 24^\circ$  on the retina. Patients maintain fixation by looking at a letter. The letter is usually coloured red so that the patient can easily identify it. Commercial stimulus systems usually use a black spot as a fixation mark. The use of a fixation letter rather than a spot helps the patient to maintain the correct optical accommodation and so keep the pattern in focus. If the patient has poor visual acuity, less than 6/18, the fixation letter is replaced by a spot.

Stimulation due to scattered light from the pattern is minimised by generating a grey pattern surround on the screen.

Flash stimuli are usually triggered by a TTL pulse which can be generated by toggling the one bit digital output on the analogue input/output card (Section 2.3.3). One complication is that some commercial equipment use an active high trigger pulse whilst others use an active low pulse. The timing of the flash is under software control. Transient flash stimuli are used for VECP and ERG recordings and a flash rate of 30 Hz is used to record flicker ERGs (Section 1.4.2).

#### **2.4.4 Data Acquisition and Analysis**

The signal processing software running on the DSP card initially sets the sample rate clock on the analogue card and calibrates the ADC. The sample rate clock then generates hardware interrupts which are serviced by the DSP card and are used to acquire and process data. In this way the DSP card has been used to implement real-time signal averaging, fast Fourier transforms and adaptive filtering.

When performing signal averaging the programme rejects artefacts such as blinks by ignoring epochs of data which exceed predetermined amplitude thresholds. The threshold usually employed is  $\pm 50 \mu\text{V}$  but if the input is too noisy, too much data is rejected and the threshold has to be increased.

Both the acquired and processed data are saved in the external memory of the DSP card from where they are read by the PC. When signal averaging, the raw data and the running average are displayed on the operator's monitor at the end of every sweep. The user can thus observe the progress of the data processing and the quality of the raw input signal.

Acquired data can be processed using various options. Two cursors are available for each channel to measure amplitude and latencies. Other features available include low-pass digital filters, cross-correlation and automatic peak detection.

#### **2.4.5 Hardcopy**

Hardcopy to a Hewlett Packard ColorPro pen plotter is achieved using ASCII codes. Other output devices are accessed via commercial graphics packages such as Harvard Graphics.

### **2.5 MONITOR INTERFERENCE**

As described in Section 2.4.3, the pattern stimulus is synchronised to the vertical retrace of the monitor, as in some other systems (de Waal et al 1983, Epstein et al 1983). The advantage of the synchronisation is that the timing of the stimulus is consistent and larger evoked potentials are produced (Hayward and Mills 1980).

There are however, two disadvantages, the effects of which must be minimised:

1. The recorded signal is synchronised to electromagnetic interference from the vertical deflection coils of the monitor.
2. In some subjects an additional luminance flicker response is obtained at the screen refresh rate (Hayward and Mills 1980, van Lith et al 1978, van Lith et al 1979). The screen refresh rate of VGA displays is approximately 70 Hz in graphics mode.

The system was first tested with no electromagnetic screening of the monitor and the VECP recordings were found to include 70 Hz interference. Various screening methods were then implemented and investigated using test phantoms. One phantom was designed to mimic recording from a patient's head and consisted of a plastic container of tap water which was placed 40 cm in front of the monitor screen. Recordings were then made from electrodes placed in the water. The electrodes were not allowed to touch and the impedance between them was approximately 10 k $\Omega$ . Electric fields were successfully screened by fitting an earthed polaroid filter to the front of the monitor and by placing the monitor in an earthed steel cabinet (Figure 2.2).

The recordings were still susceptible to magnetic interference and this was investigated using a test phantom consisting of a 20 turn coil of wire, approximately 15 cm in diameter. The direction of the magnetic flux lines was determined by making recordings along three orthogonal axes from a number of locations. Forty centimetres in front of the monitor, where the patient would be situated, the flux lines were horizontal and parallel to the monitor screen. Magnetic interference at this location was reduced by 75 % by fitting a mumetal cone over the vertical deflection coils of the monitor. The earthed steel cabinet reduced the interference by 30 %. Mumetal is a nickel alloy with high magnetic permeability and low saturation and is often used to screen electronic circuits from magnetic interference. The cone is illustrated in Figure 2.3, it was approximately 15 cm in diameter and 15 cm in length. The cone was placed inside the monitor case and positioned so that it totally covered the coil assembly on the rear of the tube. It was held in position with silicone rubber adhesive.

The amplitude of the flicker response is luminance dependent (Van Lith et al 1979) and frequency dependent. The response was avoided in most subjects by using a maximum screen luminance of 60 cd / m<sup>2</sup>.

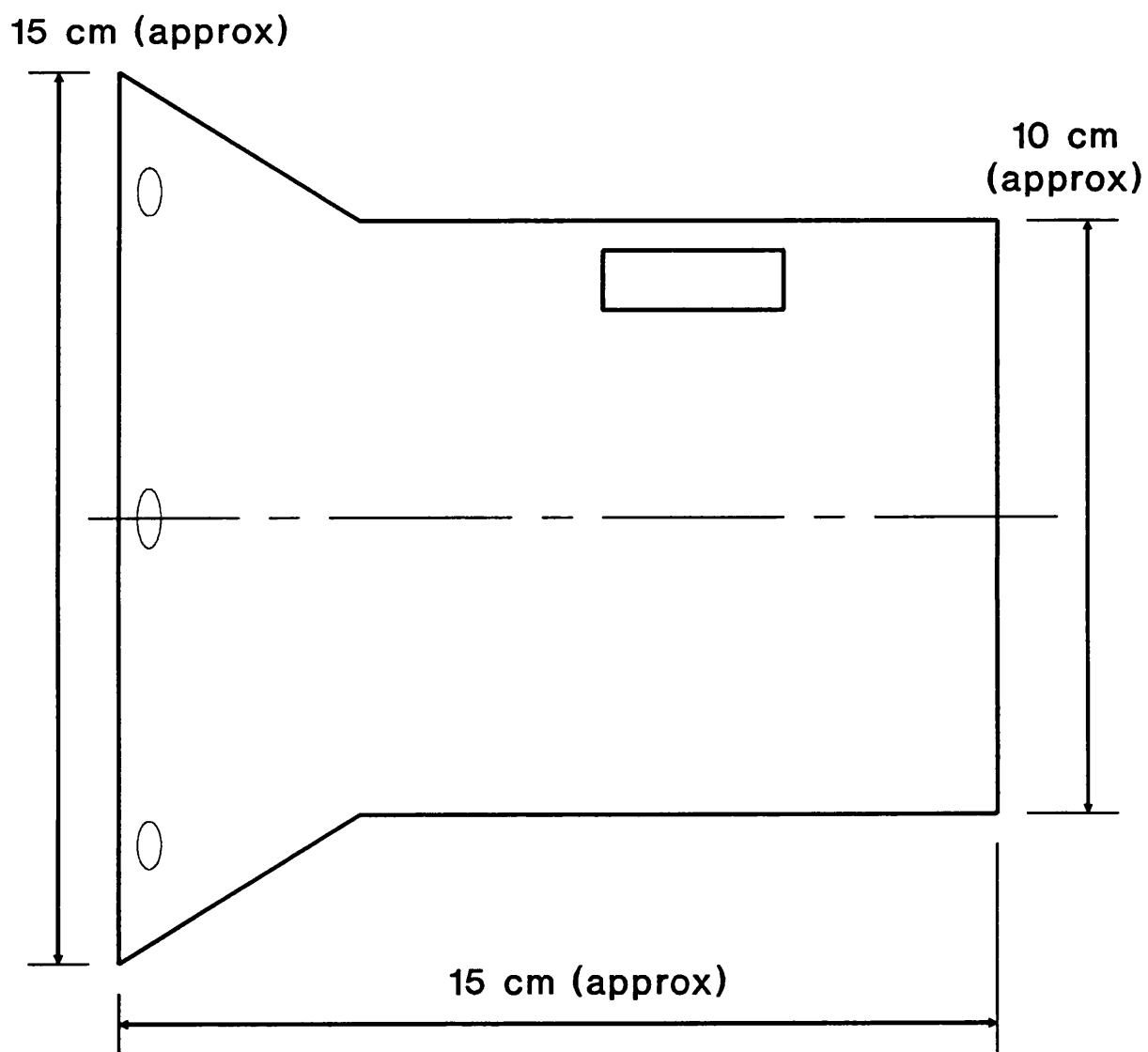


Figure 2.3 Mumetal screening cone.

All sources of interference were further reduced by 90 % by filtering the recordings with a low-pass digital filter (Section 3.3.3).

## 2.6 MONITOR LUMINANCE CALIBRATION

The monitor luminance was calibrated using a photocell with a photometric filter, either an International Light IL1700 (International Light, Newburyport, Mass, USA) or a Minolta nt-1 spot photometer. The luminance was always measured in the centre of the screen to avoid measurement errors due to screen non uniformity. When calibrating the luminance of the grey levels, the luminance was found to saturate (Figure 2.4) and the luminance at which saturation occurred was found to be dependent on image size (Figure 2.5). This phenomenon was also found with other types of monitor tested. In practice, the monitor was operated at a maximum luminance of  $60 \text{ cd/m}^2$  so that the image luminance was independent of image size and did not saturate (Figure 2.5). The maximum luminance was set using the brightness and contrast controls on the monitor. For this setting a look-up table of luminance versus grey level was created by measuring the screen luminance at each grey level. The grey levels were set according to the calibration, so that the screen remained isoluminant during pattern-onset and pattern-offset presentation. This ensured that VECPs from pattern-onset and pattern-offset were truly pattern specific due to a contrast change and were not contaminated by a luminance response. A practical advantage of using pattern-reversal stimuli is that no grey scale calibration is required, the pattern simply reverses (Section 2.4.3) and the total screen luminance remains constant.

## 2.7 MONITOR LUMINANCE AND CONTRAST UNIFORMITY

The luminance of the IBM 8512 monitor is relatively uniform but is not perfectly flat. VECPs recorded from pattern stimuli are most sensitive to contrast (Spehlmann 1985) and it was therefore necessary to check that the image contrast remained uniform across the screen surface.

A test pattern was devised to measure the luminance and contrast variations across the screen. The pattern consisted of 36 white discs presented on a grey background. Each disc subtended a visual angle of two degrees and was separated from its neighbours by a distance equal to their diameter. The monitor grey scale was calibrated (Section 2.6)

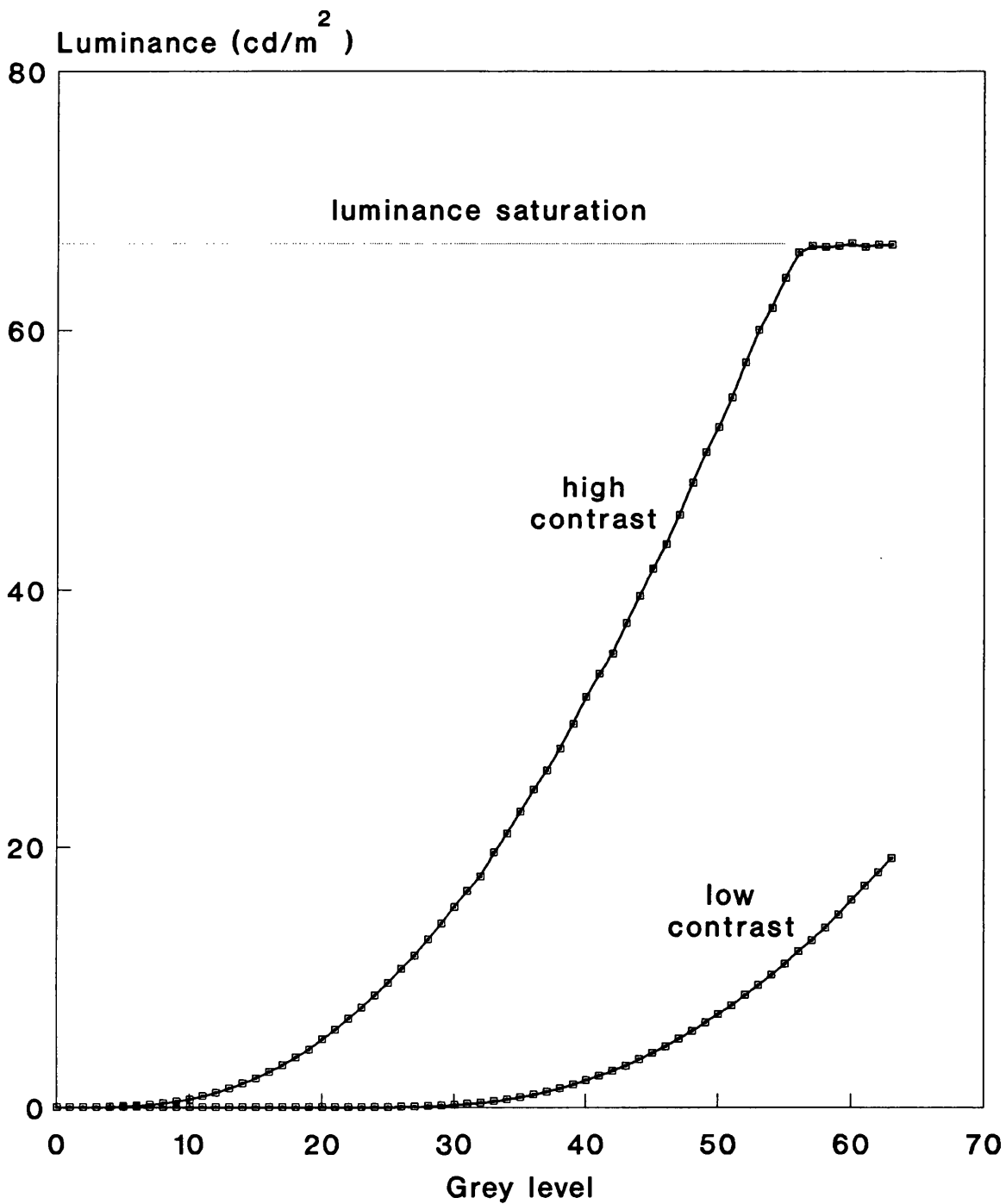


Figure 2.4 Central screen luminance versus grey level for two contrast settings with a uniform image filling the screen. (Grey level defined in Section 2.4.3.)

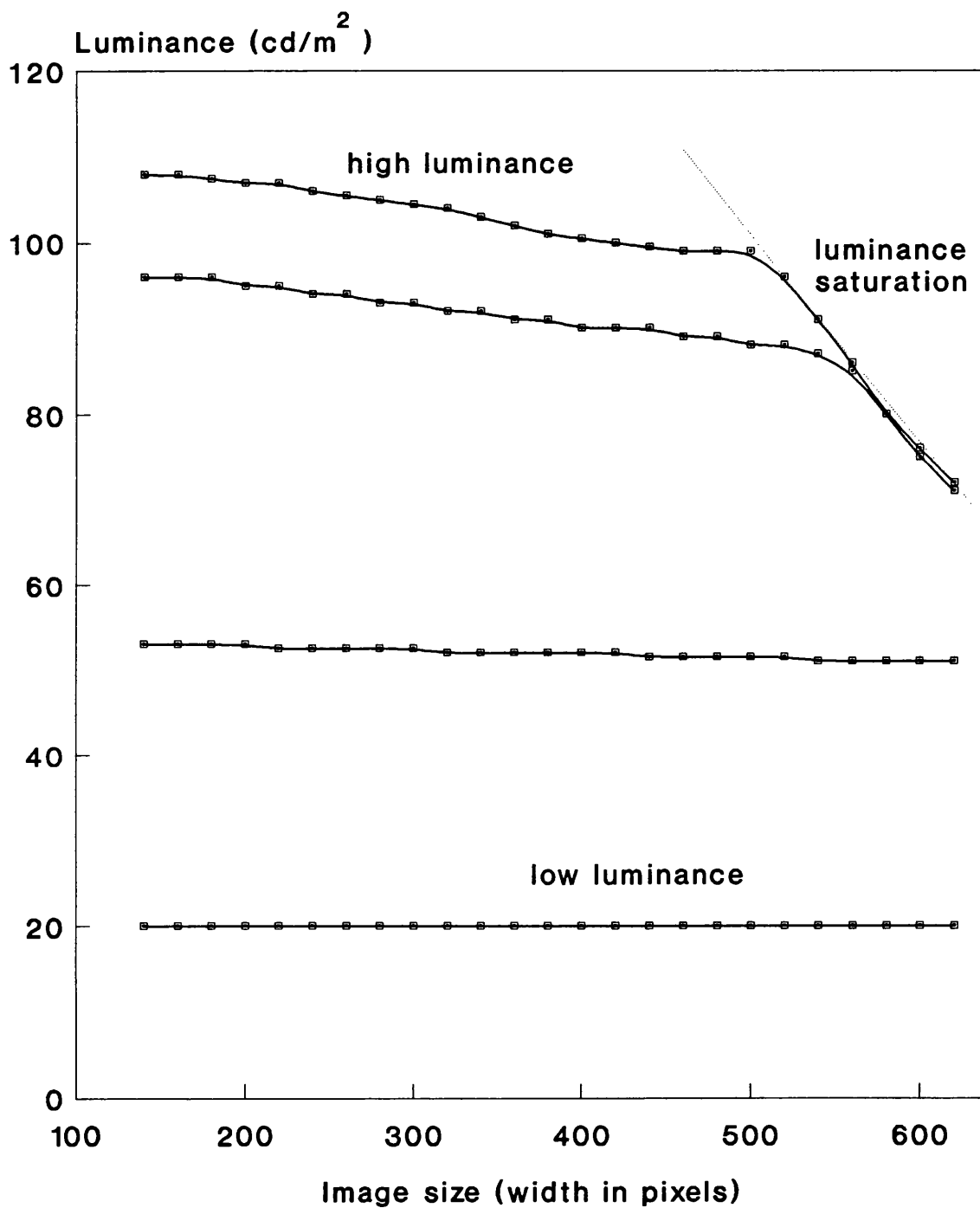


Figure 2.5 Luminance versus image size for four arbitrary luminance settings; image has same aspect ratio as screen.

so that the discs had a nominal luminance of  $20 \text{ cd/m}^2$  at the centre of the screen and the background had a nominal luminance of  $10 \text{ cd/m}^2$  also at the centre of the screen.

A spot photometer was used to measure the luminance at the centre of each disc and inter disc space. The Michaelson contrast of each disc was then calculated using the formula:  $\text{contrast} = (L_{\text{max}} - L_{\text{min}}) / (L_{\text{max}} + L_{\text{min}})$  where  $L_{\text{max}}$  is the disc luminance and  $L_{\text{min}}$  is the background luminance.

The luminance measurements are presented in Figure 2.6. The luminance of the discs and the background was found to be within 90 % of their central values over much of the screen surface but dropped to 75 % in the corners. The Michaelson contrast remained constant at 30 % across the screen surface.

In conclusion, non uniformities in the screen luminance are unlikely to significantly affect the results of pattern VECPs because the image contrast remained constant.

## **2.8 SYSTEM DUPLICATION**

A duplicate system has now been constructed to objectively assess vision in multiply handicapped children and is in use at the Fraser of Allander Assessment Unit, Royal Hospital for Sick Children, Glasgow. In this system a dual super VGA card (Cebra Communications) has been used which offers an increased colour resolution of 256 colours at a screen resolution of  $800 \times 600$  pixels. Rather than write custom software for administration, patient details are automatically appended to an ASCII file which is then accessed by a commercial database and word-processing package. Although this method is simple it has proved to be very effective.

## **2.9 RECORDING METHODS**

### **2.9.1 Recording Electrodes**

The best electrodes for recording VECPs are EEG silver-silver chloride skin electrodes, typically 6 mm in diameter.

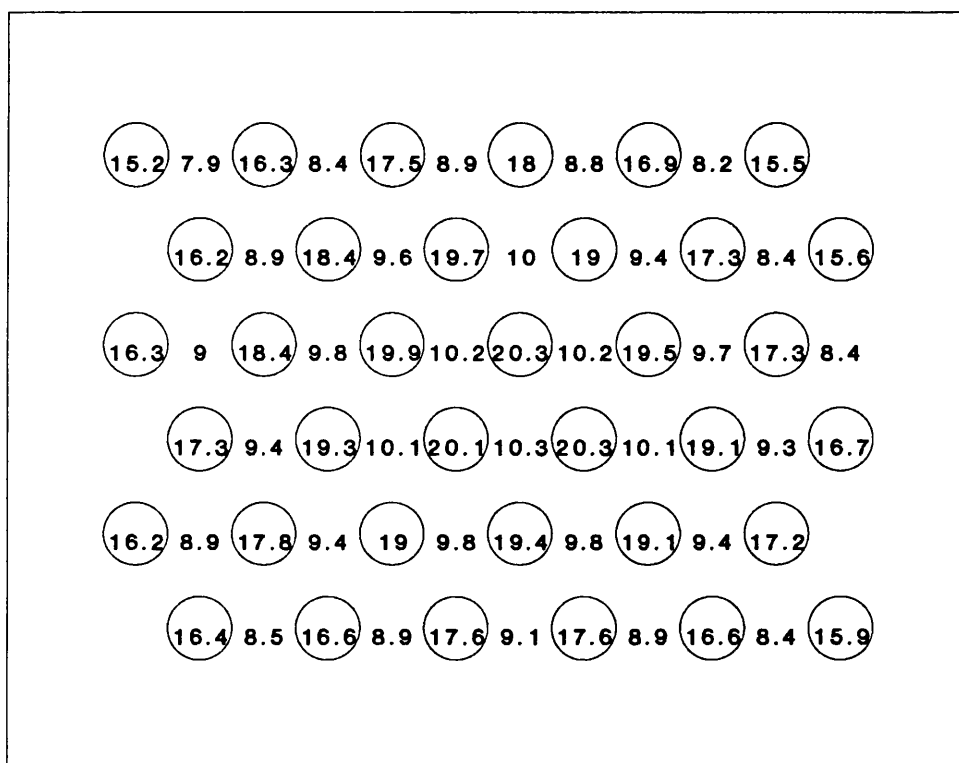


Figure 2.6 Luminance values measured from stimulus monitor for pattern of white discs (nominal  $20 \text{ cd/m}^2$ ) on grey background (nominal  $10 \text{ cd/m}^2$ )

A chemical reaction occurs at the electrode surface. If pure metal electrodes such as platinum are used, electrolysis occurs and gas bubbles form producing an unstable, high resistance interface. The electrode instability can produce electrical noise and drift which may be larger than the signal being measured.

Silver-silver chloride electrodes work differently. They are composed of silver with a chloride coating and during recording the coating depletes on one electrode and builds up on another. The chemical reaction at the anode is  $\text{Ag} + \text{Cl}^- \rightarrow \text{AgCl} + \text{e}^-$  and the chemical reaction at the cathode is  $\text{AgCl} + \text{e}^- \rightarrow \text{Ag} + \text{Cl}^-$ . No gas bubbles are produced at the interface during these reactions, the resistance of the interface remains low, it does not polarise and there is no electrical noise (Cameron and Skofronick 1978). Silver-silver chloride electrodes therefore provide the electrode of choice for patient monitoring.

In practice, the electrodes are recessed from the skin and the gap filled with a conductive paste. This is because a complex layer of positive and negative charge forms at the surface of the electrode which can cause artefacts if disturbed.

Silver-silver chloride electrodes can be prepared from pure silver electrodes by using electrolysis or by chemical reaction using sodium hypochlorite. The author found that sodium hypochlorite produced the most durable chloride coating. The coating produced by electrolysis sometimes peeled away from the silver substrate.

### 2.9.2 Electrode Montage

The position of recording electrodes on the scalp is critical due to variations in the topography of the visual evoked response. The aim of the placement is to obtain the largest VECP with the clearest definition of its components. In practice the largest VECP signals are recorded from the scalp directly over the visual cortex.

In most laboratories the electrode montage conforms to one of two systems: the ten-twenty electrode system (Jasper 1958) or the 'Queen Square' system (Blumhardt et al 1977).

The ten-twenty electrode system (Figure 2.7) was originally devised to standardise EEG recordings, it places particular electrodes over particular areas of the brain and it is independent of skull size. Five points are marked along the midline and are

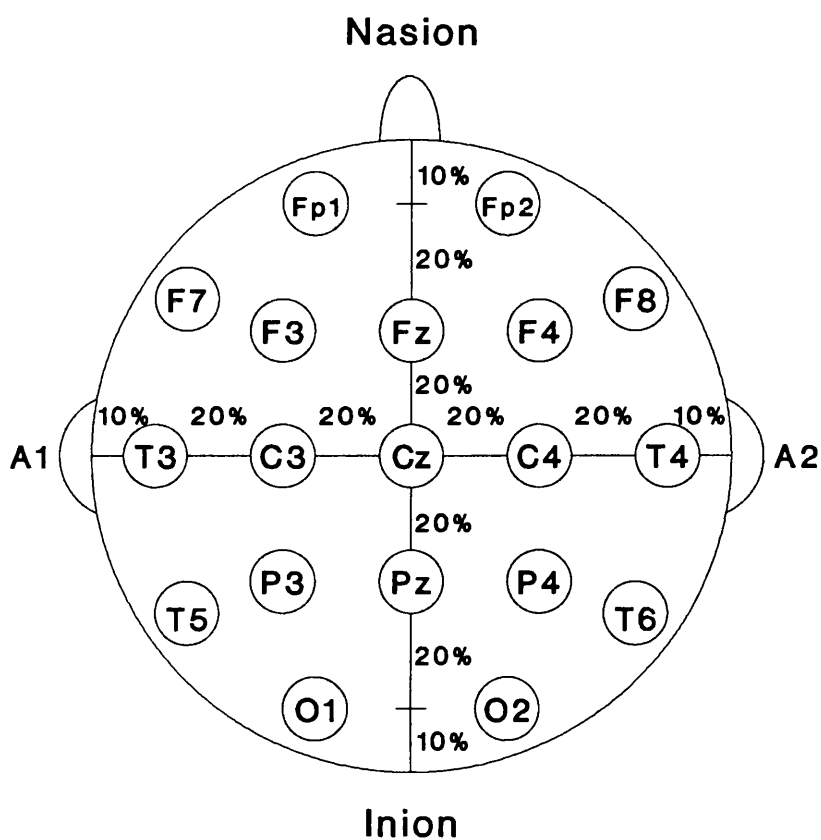


**Figure 2.7 Ten-twenty system for electrode placements:**  
 Fp, frontal pole position; F, frontal line of electrodes;  
 C, central line of electrodes; P, parietal line of  
 electrodes; O, occipital line.

designated frontal pole (Fp), frontal (F), central (C), parietal (P) and occipital (O). Fp is 10 % of the nasion-inion distance above the nasion and F, C and O are positioned in 20 % steps back from Fp. Lateral measurements are made from a line running between the left and right preauricular points via the vertex, C. The temporal points T are 10 % of the distance from the preauricular points. The central points  $C_3$ ,  $C_z$  and  $C_4$  are separated by 20 %. VECP recordings are often made from  $O_z$  relative to  $P_z$ ,  $C_z$ ,  $F_z$ ,  $A_1$ ,  $A_2$  or  $A_1$  and  $A_2$  linked. The advantage of using a distant reference point such as  $F_z$  is that it is relatively unaffected by the VECP. A disadvantage, however, is that there is a greater variation in the EEG between the electrodes which causes additional noise in the recording. A further disadvantage of using  $F_z$  is that it is susceptible to muscle noise from eye movements.

The 'Queen Square' system was proposed for pattern VECP measurements with more recording sites over the visual cortex (Figure 2.8). In particular, the lateral occipital electrodes are in a better position for recording responses to hemi-field stimuli than are the corresponding  $O_1$  and  $O_2$  points of the ten-twenty system. The reference electrode is the mid-frontal electrode (MF). The recording electrodes are spaced in 5 cm increments from the inion. In children increments of 3 cm are more appropriate due to the smaller skull size.

The guard electrode (Section 2.3.2) is usually placed on the head: at the vertex, on a mastoid process or on an earlobe.

### 2.9.3 Electrode Site Preparation

Each recording site is lightly abraded using a skin preparation, such as 'Omniprep' (DO Weaver and Co., Aurora, USA) or cleaned using 'Skin Pure' (Nihon Khoden, Tokyo) applied using a cotton bud. The electrodes are fixed to the scalp with a conductive paste, such as 'Elefix' (Nihon Khoden, Tokyo) (Cookman 1990) or 'Ten-20 conductive EEG paste' (DO Weaver and Co., Aurora, USA).

The electrode impedances should be in the range one to five kilo-ohms and should be balanced to reduce common mode interference. Figure 2.9 demonstrates the typical electrical connections to a patient during the recording of a VECP. The amplifier multiplies the difference in potential between  $V_+$  and  $V_-$ . A capacitively coupled current of about  $1 \mu\text{A}$  typically flows through the patient (Cameron and Skofronick 1978). If the electrode resistances  $R_+$  and  $R_-$  are balanced the amplifier output  $V_o$  is

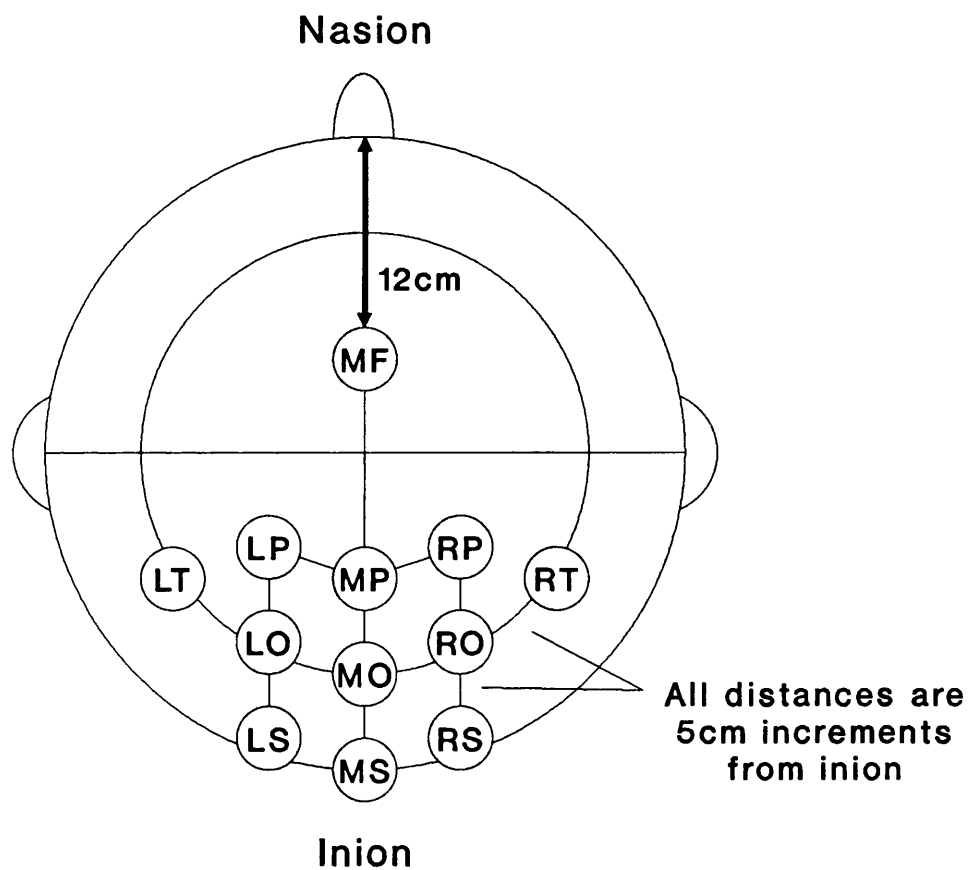


**Figure 2.8 'Queen Square' system for electrode placements:**  
 F, frontal; O, occipital; P, parietal; S, suboccipital;  
 T, temporal; M, midline; R, right; L, left.

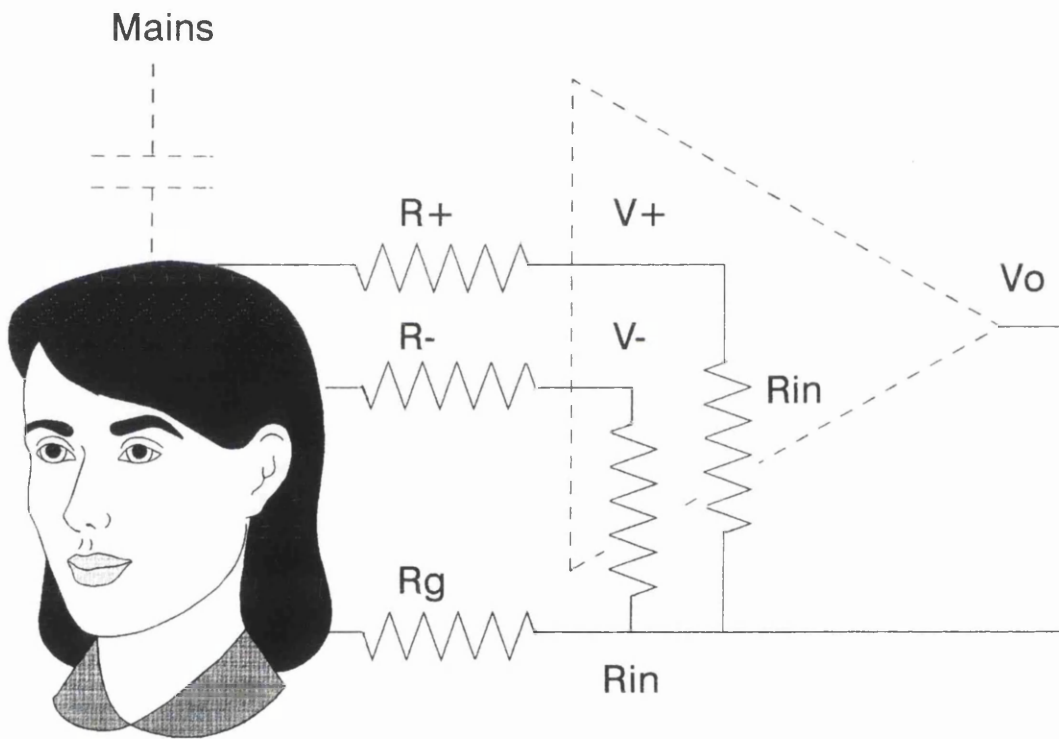


Figure 2.9 Patient connections to differential amplifier.

not contaminated with mains interference. If the electrodes are not applied well and not balanced significant noise may result. For example if  $R_+$  is  $1k\Omega$ ,  $R_-$  is  $10k\Omega$ , the guard electrode  $R_g$  is  $10k\Omega$  and the amplifier input impedance  $R_m$  is  $100M\Omega$  then the difference between  $V_+$  and  $V_-$  is  $0.9\mu V$  which is significant compared to the size of the VECP.

The electrode impedance is measured by applying a constant AC current source to a pair of electrodes and measuring the voltage between them. A DC current source could polarise the electrodes. The Biodata PA400 physiological amplifier uses a 10 Hz current source to test the impedance. The electrode impedance varies with frequency, however, and the international ERG standard (Marmor et al 1989) recommends using a test frequency in the range 30 to 200 Hz for consistency between centres.

To reduce the risk of induced interference from magnetic fields the electrode leads should not form large loops but should be twisted or bundled closely together as is illustrated in Figure 2.10.

#### **2.9.4 Subject Variables**

In any method of recording VECPs it is important to accurately log and to understand the action of subject variables (Towle 1983, Spehlmann 1985), so that the recordings can be correctly interpreted.

##### **Age**

The amplitude and latency of responses alter with age, particularly during infancy and after the age of 65 years. Therefore any comparison of responses must either be between age-matched subjects or there must be a correction for age.

##### **Sex**

The sex of the subject may affect the results and must be recorded.

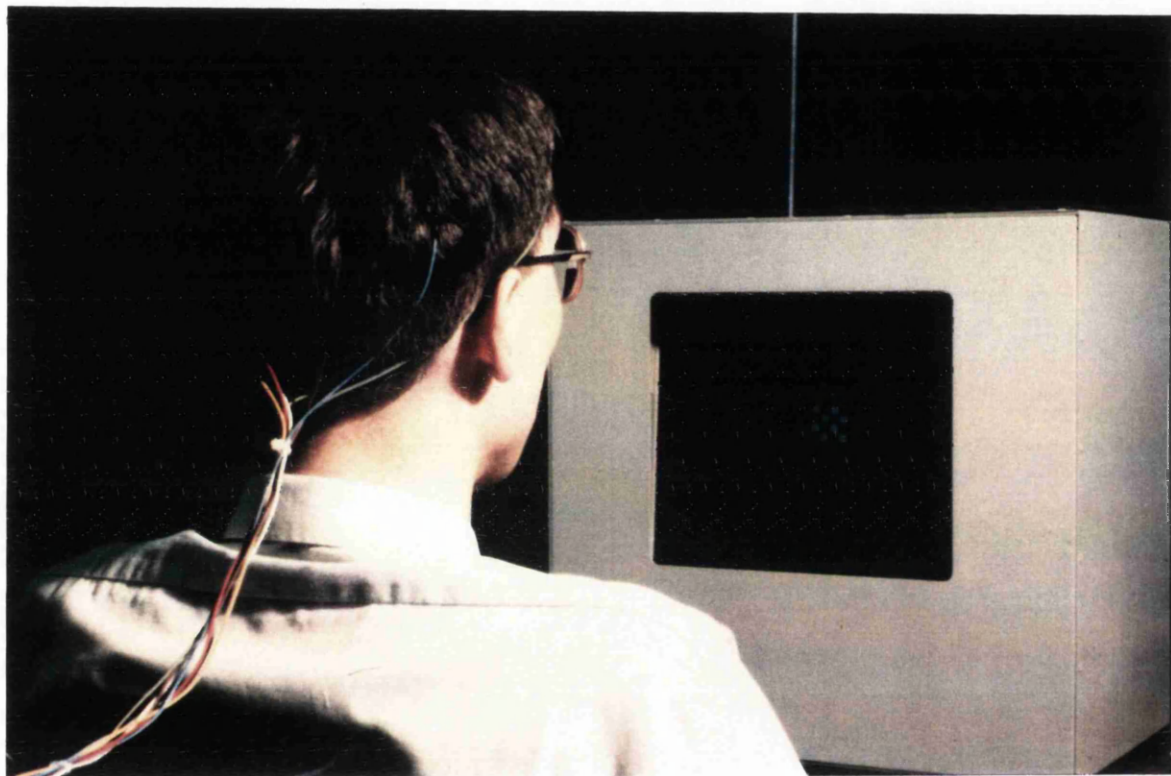


Figure 2.10 Subject during recording showing how electrode leads are positioned to reduce the risk of induced interference from magnetic fields.

## **Pupillary Size**

The pupil forms the aperture of the eye's optical system and thus affects the stimulus luminance falling on the retina. This is very relevant to patients with Glaucoma as many have very miotic pupils due to their medication. The flash VECP depends predominantly on retinal illumination and is therefore affected by the pupillary size.

Retinal illuminance can be controlled in a number of ways if required:

1. Select patients with a specific pupil size.
2. Dilate the pupil: not suitable for patients with narrow anterior chamber angles.
3. Use an artificial pupil.
4. Compensate with neutral density filter.
5. Use a Maxwellian viewing system to form an image at the level of the pupil which is independent of pupil size.
6. Make latency corrections on the measurements.

Airas and Peterson (1985) suggest using a corneal ERG electrode to keep the patient's eye open, to ensure that retinal illumination remains constant during the test. The author considers that this suggestion is unreasonable unless an ERG is also going to be recorded because the corneal lens electrode is uncomfortable and can scratch the cornea.

VECP signals due to patterned stimuli are less susceptible to luminance changes than those due to flash stimuli. Nevertheless, luminance effects must be taken into account in any measurements.

## **Refractive Error**

Refractive errors must be corrected to avoid blurring of the stimulus on the retina. This is particularly important for stimuli with small pattern elements.

## **Intraocular Opacities**

Intraocular opacities reduce stimulus luminance and blur the image on the retina.

## **Drugs and Anaesthesia**

The VECP will vary due to the action of drugs and anaesthesia.

## **Ocular Dominance**

Ocular dominance has been reported to slightly modify the VECP amplitude and latency.

### **2.9.5 Recording Artefact and Variability**

The repeatability of any VECP recording is affected by artefacts and by variations in the recording conditions.

#### **Artefact**

Movement artefact and muscle noise can be reduced by relaxing the patient and ensuring that they are comfortably restrained. Noise due to eye movements could be monitored by recording the electro-oculogram (Section 1.5.6). Artefact due to electromagnetic interference has been discussed in Sections 2.3.2, 2.3.5, 2.5, 2.9.1, 2.9.2 and 2.9.3. If any artefact causes large transients in a recorded signal, then that signal should not be included in the averaged waveform (Section 2.4.4).

#### **Attentiveness**

The mental attentiveness and fatigue of the patient can also affect VECP signals (Beinhocker et al 1966, Cerutti et al 1987b). Cerutti et al found an absence of VECP response in the presence of a dominant EEG alpha rhythm. They suggested that the alpha activity was due to a loss of attention and resulted in poor focusing of the

stimulus on the retina. Airas and Peterson (1985) found EEG alpha activity time-locked to scotopic VECs in one third of their normal subjects. In some subjects the alpha activity appeared to be linked with a lack of attention.

## **2.10 SIGNAL LABELLING AND MEASUREMENT**

Evoked potentials consist of a series of positive and negative peaks or waves. The VEC is characterised by the latency and amplitude of these features.

### **2.10.1 Peak Latency Measurement**

The transient VEC is the average response to single stimulus events. The time, or latency, of each peak is therefore usually measured relative to the stimulus onset.

The steady-state VEC is periodic in nature and its timing is usually expressed as a phase relative to the stimulus frequency. The signal is an interaction of cortical responses to successive stimuli and so peaks in the signal cannot therefore be attributed to any one stimulus. Another reason for measuring phase is that the timing of the peaks in the steady-state VECs is frequency dependent.

### **2.10.2 Peak Amplitude Measurement**

There are three standard methods for measuring the amplitude of transient VECs (Spehlmann 1985):

1. 'Peak to baseline'. The amplitude of the peak is measured relative to a baseline. The baseline can be derived from a pre stimulus period in the recording or from an average of the recording. This method is poor if the baseline is noisy.
2. 'Peak to peak'. The amplitude difference between two successive peaks is measured. This method has the advantage of not requiring a baseline.
3. 'Mean peak to peak'. The amplitude is defined as the mean of two successive peak to peak measurements.

The amplitude of steady-state VECPs can be measured by:

1. Measuring the amplitude of the frequency components in the frequency domain.
2. Measuring the peak to peak amplitude in the time domain.

### **2.10.3 Labelling of Peaks in the Transient VECP**

In clinical practice it is necessary to refer to specific peaks in the transient VECP waveform and to define normal ranges for amplitude and latency of each peak. As yet there is no agreed standard labelling system and there are three systems in widespread use:

1. 'Polarity and latency'. Positive and negative peaks are labelled P and N respectively and are followed by a number corresponding to the peak latency in milliseconds. Characteristic peaks are distinguished from the peaks measured in individual recordings by writing a horizontal line above the label. In the pattern-reversal VECP for example the main characteristic is a positive peak occurring at a latency of 100 ms and this can be labelled  $\overline{P100}$  (Figure 1.8). This labelling system is also used for the PERG (Section 1.4.2).
2. 'Number in sequence'. Peaks are labelled in the order of their occurrence using the Roman numerals I, II, III etc. The polarity of the peak corresponding to each numeral is dependent on the stimulus used and the peak from which labelling starts.
3. 'Polarity and number in sequence'. Positive and negative peaks are labelled P and N respectively and their order is indicated using Arabic numerals. A sequence of peaks may therefore be labelled P1, N1, P2 etc. (Figure 2.12).

## **2.11 SYSTEM VALIDATION**

### **2.11.1 Introduction**

The system operation was carefully validated in three stages:

1. The recording system was checked using electrical test signals.

2. The stimulus timing was then checked by recording the electrical output from a photometer placed in front of the stimulus.
3. Finally, the complete system was checked by recording VECPs from a normal range of subjects using standard stimuli (transient pattern-reversal and flash). The shape, amplitude and latency of the recorded signals were compared with data reported in the literature.

It is good practice for each laboratory to collect a normal range of clinical data for each and every system they operate because the exact amplitudes and latencies of the peaks in the VECP are critically dependent on the precise stimulus and recording conditions used (Spehlmann 1985).

### **2.11.2 Pattern-reversal VECPs**

#### **Method**

Thirty normal subjects were examined, 18 male and 12 female, ranging in age from 19 to 60 years. All subjects had a corrected visual acuity of 6/6 or better, except one with an acuity of 6/9. All had normal pupils (3 to 6 mm in diameter) and normal visual fields.

The stimulus consisted of a black and white checkerboard, the white squares had a luminance of  $55 \text{ cd/m}^2$  and the contrast was greater than 98 %. Each check subtended  $50'$  and the total stimulus subtended  $23^\circ \times 23^\circ$ . The viewing distance from the screen was 40 cm and subjects viewed a fixation letter in the centre of the stimulus. Subjects were optically corrected during the study. The pattern reversed approximately every 0.8 s. The exact interstimulus period was varied by 56 ms to avoid EEG alpha activity from becoming time-locked to the VECP. Monocular stimulation was used for each eye in turn. The unstimulated eye was covered with a gauze eye pad.

Recordings were made from the mid-occipital site MO relative to the mid-frontal position MF. A guard electrode was positioned on the scalp within the hairline. The amplifier low frequency cut-off was 0.8 Hz and the high frequency cut-off was 100 Hz. Signals were digitised at a rate of 512 Hz and recorded for 500 ms from stimulus presentation. Two averages of 100 responses were recorded from each eye. The

signal reproducibility was checked subjectively by overlaying the responses on the computer screen and objectively by using cross-correlation (Section 3.3.4). The two recordings were summed and filtered using a digital low-pass filter, cut-off frequency 40 Hz (Section 3.3.3), to attenuate residual high frequency noise.

The latencies of the characteristic peaks  $\overline{N75}$ ,  $\overline{P100}$  and  $\overline{N145}$  were measured and the signal amplitude was measured peak to peak.

## Results

Figure 1.8 shows a typical pattern-reversal VECP recorded in the study and shows the characteristic  $\overline{N75}$ ,  $\overline{P100}$  and  $\overline{N145}$  peaks. A statistical analysis of the results is shown in Table 2.2. Other than for the interocular comparison of the  $\overline{P100}$  latency, the statistical analysis was performed using data from a random eye from each subject, as recordings from two eyes in the same subject cannot be considered strictly independent. Standard deviations have not been quoted for the signal amplitude measurements as the measurements were not normally distributed.

The main component of the waveform is the  $\overline{P100}$  peak. There is a correlation of 0.47 between the latency of this peak and age. A linear regression line was fitted to the data. The equation of the line is  $\overline{P100}(\text{ms}) = 88.9 + [0.225 \times \text{Age}(\text{years})]$  and it is illustrated in Figure 2.11. The data in Table 2.2 show that there is a much smaller interocular variation in the latency of  $\overline{P100}$  compared to interindividual variation.

## Discussion

The VECP wave shape, together with the amplitudes and latencies of the characteristic peaks, showed good agreement with published data (Spehlmann 1985). The VECP may be classed as being abnormal if the amplitude is significantly reduced or absent in one eye. The latency of the  $\overline{P100}$  peak has a relatively small normal range and is the most sensitive parameter for detecting abnormal waveforms (Spehlmann 1985, Halliday et al 1977). A waveform can be classed as abnormal if the  $\overline{P100}$  peak is delayed beyond its normal range. In addition, unocular lesions can be detected if the interocular difference is outside its normal range.

**Table 2.2 Results from Pattern-reversal Stimulus**

Population	All subjects	Male subjects	Female subjects	Random eye from each subject
Number	30	18	12	29
	Age (years)	Age (years)	Age (years)	Cross-correlation
Mean	36	38	33	0.87
Median	30	32	29	0.88
Minimum	19	19	21	0.55
Maximum	60	59	60	0.98
First quartile	25.25	27.75	22.25	0.85
Third quartile	50	50.75	44	0.94

**Table 2.2 (continued) Results from Pattern-reversal Stimulus**

Population	Random eye from each subject	Random eye from each male subject	Random eye from each female subject	All subjects
Number	30	18	12	28
	$\overline{P100}(\text{ms})$	$\overline{P100}(\text{ms})$	$\overline{P100}(\text{ms})$	Interocular difference in $\overline{P100}(\text{ms})$
Mean	96.98	99.62	93.18	-0.91
Standard deviation	6.43	6.2	4.65	2.64
Median	95.7	98.65	91.8	0
Minimum	85.9	87.9	85.9	-5.9
Maximum	115.2	115.2	101.6	3.9
First quartile	91.8	95.7	89.8	-3.43
Third quartile	100.1	104	95.7	1.9

**Table 2.2 (continued) Results from Pattern-reversal Stimulus**

Population	Random eye from each subject	Random eye from each subject	Random eye from each subject	Random eye from each subject
Number	30	30	30	30
	$\overline{N75}(\text{ms})$	$\overline{N145}(\text{ms})$	$\overline{P100} - \overline{N75}$ ( $\mu\text{V}$ )	$\overline{P100} - \overline{N145}$ ( $\mu\text{V}$ )
Mean	64.38	138.67	11.69	15.71
Standard deviation	4.27	9.01	-	-
Median	64.5	138.7	9.65	14.15
Minimum	56.6	119.1	2.0	4.9
Maximum	72.3	154.3	28.7	37.9
First quartile	61.63	132.95	7.23	10.2
Third quartile	68.4	143.08	14.45	18.47

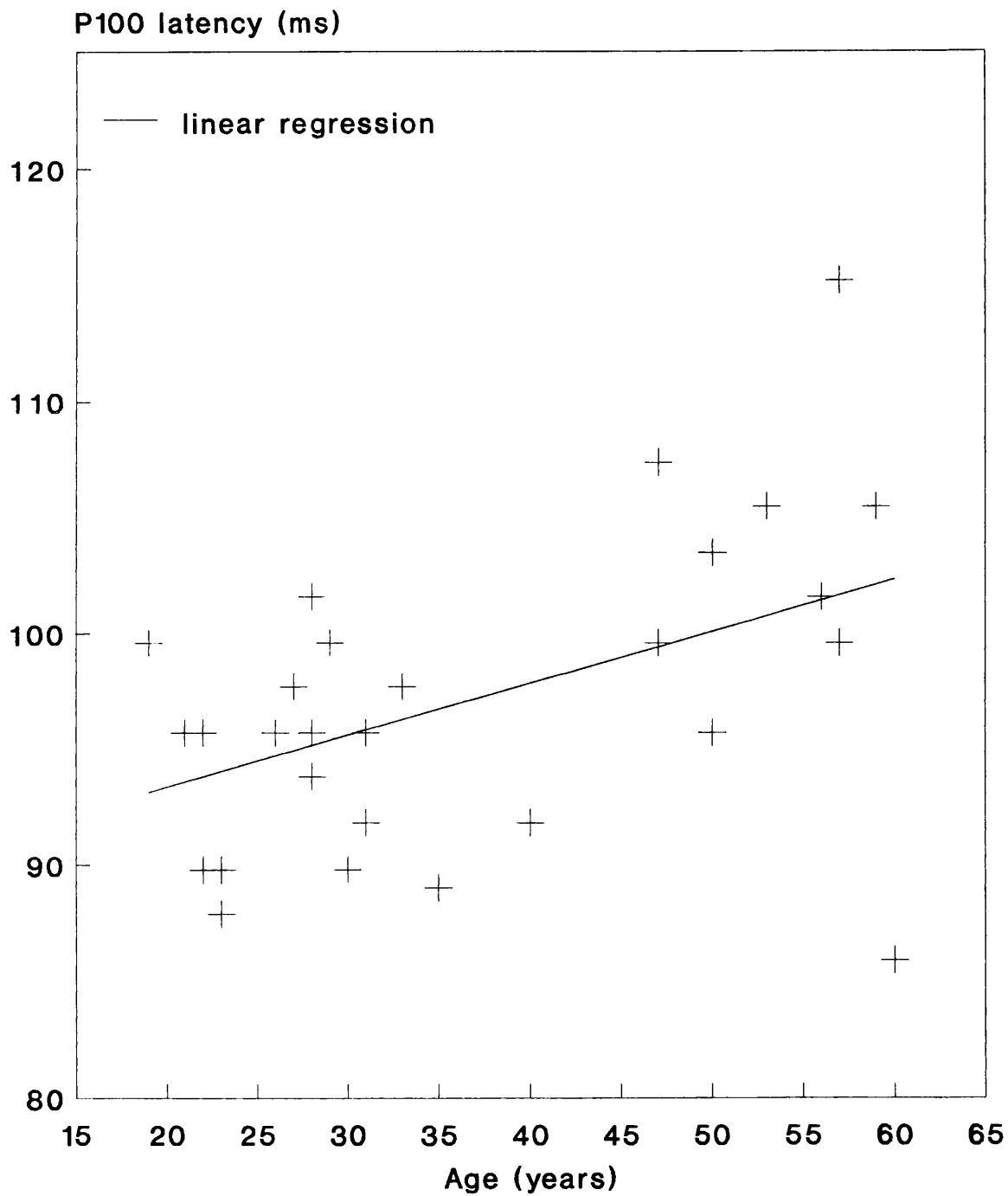


Figure 2.11 Variation of P100 latency with age for a random eye from 30 subjects.

The system should be extremely sensitive at detecting unocular lesions such as those present in multiple sclerosis and optic neuritis, because the interocular difference in the  $\overline{P100}$  latency has a very small normal range. The system has already been used to detect many such cases and Figure 1.9 shows the VECPs obtained from a patient with optic neuritis.

### 2.11.3 Flash Stimulus

#### Method

Twenty seven normal subjects were examined, 16 male and 11 female, ranging in age from 19 to 59 years. All subjects had a corrected visual acuity of 6/6 or better, except one subject with an acuity of 6/9 in both eyes and two subjects with an acuity of 6/12 in one eye. All subjects had normal pupils (3 to 6 mm in diameter) and normal visual fields.

The stimulus was a Medelec flash head powered by a Medelec OS5 power supply on intensity setting number four. The stimulus was presented 30 cm in front of the subject's face at a rate of approximately once every 0.8 s. The interstimulus period was varied by 56 ms to avoid EEG alpha activity from becoming time-locked to the VECP. Monocular stimulation was used for each eye in turn. In order that no light could be perceived from the unstimulated eye, it was covered with an eye patch and with one of the subject's hands.

Recordings were made from the mid-occipital site MO relative to the mid-frontal position MF. A guard electrode was positioned on the scalp within the hairline. The amplifier low frequency cut-off was 0.8 Hz and the high frequency cut-off was 100 Hz. Signals were digitised at a rate of 512 Hz and recorded for 500 ms from stimulus presentation. Two averages of 100 responses were recorded from each eye. The signal reproducibility was checked subjectively by overlaying the responses on the computer screen and objectively by using cross-correlation. The two recordings were summed and filtered using a digital low-pass filter, cut-off frequency 40 Hz, to attenuate residual high frequency noise.

The latencies and amplitudes of the most reproducible features were recorded and analysed.

## Results

A typical VECF recorded from the flash stimulus is shown in Figure 2.12. The most reproducible features in the flash VECFs were a major positive peak P1 occurring approximately 100 ms from stimulus onset and two negative peaks N1 and N2 occurring 50 and 130 ms from stimulus onset. In some VECFs additional negative peaks were recorded at a latency of 30 or 70 ms.

A statistical analysis of the results is shown in Table 2.3. The analysis was performed on data from a random eye from each subject. The interindividual range in the peak latencies was greater than that for the pattern-reversal VECF. The repeatability of the flash VECF, as measured by cross-correlation, was slightly less than that for the pattern-reversal VECF.

## Discussion

As reported in the literature the flash VECF was found to be more variable than the pattern-reversal VECF (Spehlmann 1985). This variability was most evident in interindividual variations in waveform and peak latency.

The flash VECF will vary according to the exact stimulus conditions used in each laboratory. N1, P1 and N2 most closely correspond to the peaks I, IV and V described by Ciganek (1961). The negative peak observed in some patients at a latency of 70 ms may correspond to Ciganek's peak III.

### 2.11.4 Hemi-field Pattern-reversal Stimulus

#### Method

Twenty two normal subjects were examined, 13 male and 9 female, ranging in age from 19 to 57 years. All subjects had a corrected visual acuity of 6/6 or better, except one with an acuity of 6/9. All had normal pupils (3 to 6 mm in diameter) and normal visual fields.

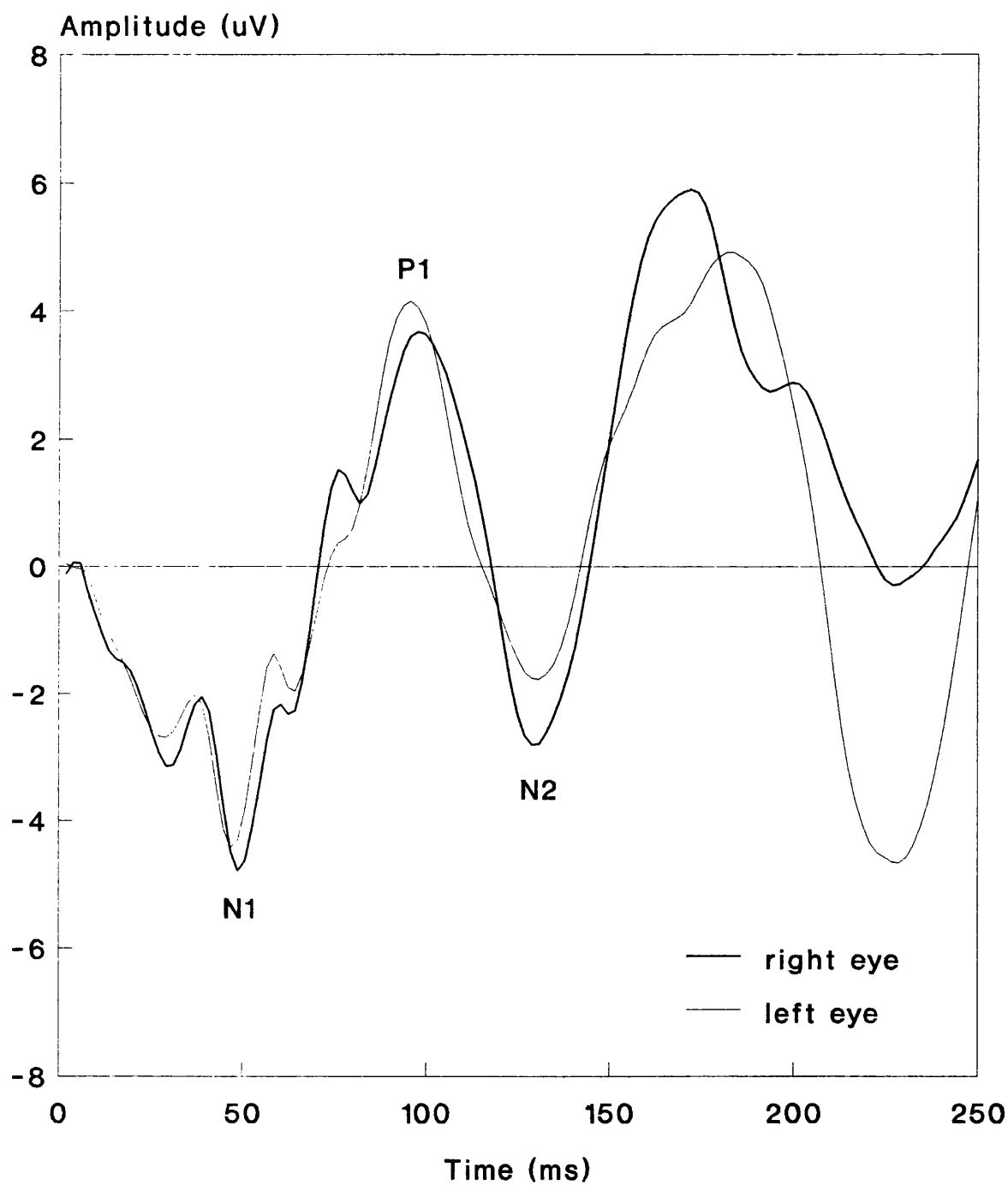


Figure 2.12 Normal flash VECP. The characteristic positive and negative peaks are labelled N1, P1 and N2.

**Table 2.3 Results from Flash Stimulus**

Population	All subjects	Male subjects	Female subjects	Random eye from each subject
Number	27	16	11	25
	Age (years)	Age (years)	Age (years)	Cross-correlation
Mean	34	36	31	0.87
Median	29	30	28	0.89
Minimum	19	19	21	0.61
Maximum	59	59	56	0.96
First quartile	23	27.25	22	0.83
Third quartile	47	49.25	35	0.93

**Table 2.3 (continued) Results from Flash Stimulus**

Population	Random eye from each subject				
Number	27	27	27	27	27
	N1 latency (ms)	P1 latency (ms)	N2 latency (ms)	P1-N1 ( $\mu$ V)	P1-N2 ( $\mu$ V)
Mean	50.0	96.1	130.6	10.93	9.75
Standard deviation	10.62	9.62	14.23	-	-
Median	48.8	97.7	130.9	10.4	10.1
Minimum	25.4	66.4	82	2.4	2.3
Maximum	74.2	107.4	154.3	24.2	18.5
First quartile	46.9	91.8	123	6.6	6.1
Third quartile	53	103.5	142.6	14.3	12.4

The stimulus consisted of a black and white checkerboard, the white squares had a luminance of  $55 \text{ cd/m}^2$  and the contrast was greater than 98 %. Each check subtended  $50'$  and the total stimulus subtended  $22^\circ \times 22^\circ$ . The viewing distance from the screen was 40 cm and subjects viewed a fixation letter one degree to the side of the pattern. Subjects were optically corrected during the study. To avoid stimulation of the fovea due to scattered light, the checkerboard was positioned on a grey background with a luminance of  $28 \text{ cd/m}^2$ . The pattern reversed approximately every 0.8 s. The exact interstimulus period was varied by 56 ms to avoid EEG alpha activity from becoming time-locked to the VECP. Monocular stimulation was used for each eye in turn. The unstimulated eye was covered with a gauze eye pad.

Recordings were made from MO, RO and LO relative to the mid-frontal position MF. In addition a fourth channel was recorded from the temporal electrode (RT or LT) ipsilateral to the stimulated hemisphere. A guard electrode was positioned on the scalp within the hairline. The amplifier low frequency cut-off was 0.8 Hz and the high frequency cut-off was 100 Hz. Signals were digitised at a rate of 512 Hz and recorded for 500 ms from stimulus presentation. Two averages of 100 responses were recorded for each hemi-field from each eye. The signal reproducibility between the same hemi-fields in opposite eyes was analysed objectively using cross-correlation. The two recordings were summed and filtered using a digital low-pass filter, cut-off frequency 40 Hz, to attenuate residual high frequency noise.

The latency of the characteristic  $\overline{\text{P100}}$  peak was measured from the mid-occipital electrode.

## Results

The typical response to the hemi-field pattern-reversal stimulus is described in Section 1.4.3. Figure 1.10 shows a typical hemi-field pattern-reversal VECP recorded using the system. The main component of the midline recording is the  $\overline{\text{P100}}$  peak and a statistical analysis is shown in Table 2.4. Taking data from a random hemi-field from a random eye from each subject, there is a correlation of 0.65 between the latency of the  $\overline{\text{P100}}$  peak and age. A linear regression line with the equation  $\overline{\text{P100}}(\text{ms}) = 85.4 + [0.384 \times \text{Age}(\text{years})]$  was fitted to the data and is illustrated in Figure 2.13.

**Table 2.4 Results from Hemi-field Pattern-reversal Stimulus**

Population	All subjects	Male subjects	Female subjects
Number	22	13	9
	Age (years)	Age (years)	Age (years)
Mean	35	37	31
Median	31	33	26
Minimum	19	19	21
Maximum	57	57	56
First quartile	22.75	28	22
Third quartile	47.75	50	39

**Table 2.4 (continued) Results from Hemi-field Pattern-reversal Stimulus**

Population	Random hemi-field from random eye of each subject	Random hemi-field from random eye of each subject	Random hemi-field from each subject
Number	22	22	22
	Cross-correlation	$\overline{P100}(\text{ms})$	Interocular difference in $\overline{P100}(\text{ms})$
Mean	0.81	98.74	-1.24
Standard deviation	-	7.52	3.83
Median	0.83	95.7	0
Minimum	0.56	89.8	-11.7
Maximum	0.96	117.2	3.9
First quartile	0.74	93.8	-3.9
Third quartile	0.88	102.1	0.5

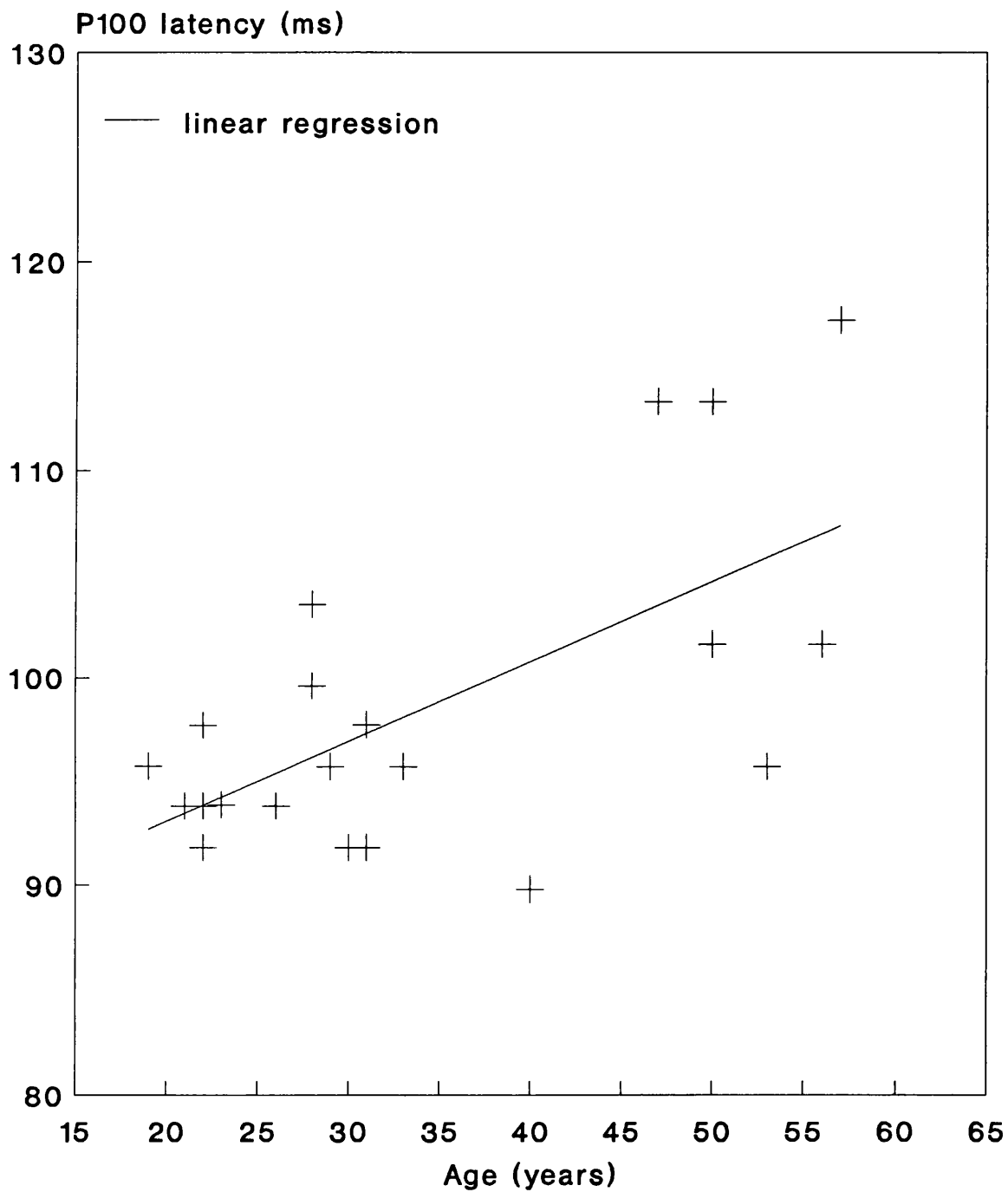


Figure 2.13 Variation of P100 latency with age for hemi-field stimuli. Data taken from a random hemi-field from a random eye from 22 subjects

## Discussion

The topography of the hemi-field pattern-reversal VECPs recorded in this study conformed to that described in the literature (Blumhardt et al 1977, Spehlmann 1985).

The hemi-field pattern stimulus is routinely used to investigate chiasmal and post chiasmal pathology. The stimulus can also be used to detect unocular lesions effecting the nasal or temporal nerve fibres by measuring interocular differences in the  $\overline{P100}$  latency (Spehlmann 1985).

## 2.12 CONCLUSION

A system has been developed for recording VECPs and ERGs which uses recent advances in technology to overcome the limitations of conventional systems and to provide a wide choice of stimuli and real-time DSP.

The system is based on a PC and the stimulus is generated in computer graphics and presented on a monitor screen. Magnetic interference from the monitor vertical deflection coils has been significantly reduced through the use of a novel mumetal screening cone.

The effect of image size on the monitor screen luminance has been studied in detail. It has therefore been possible to ensure that the monitor is used in a linear operating region and that the luminance of stimuli is independent of their size.

Real-time DSP is performed by means of a commercial DSP card installed in the computer.

The system is easy to use. Stimulus set-up and data acquisition is controlled by means of menus or more simply by pre-prepared protocols. In common with commercial systems this system has hardcopy facilities and can be used for administrative purposes.

The system was immediately adopted in the clinical environment due to the thorough commissioning, testing and optimisation procedures to which it had been subjected. As well as enabling research and development, the system is used to provide a regional clinical service performing in excess of 400 patient studies per annum. The attention

to user-friendliness in the software controlling both data acquisition and analysis has contributed to this success.

In conclusion, a development system has been constructed for visual electrophysiology, which meets the design specification of Section 2.2. Due to the versatility of the system it is suitable for the successful development of stimuli and VECP signal processing methods for objective analysis of the visual field.

### **3. DIGITAL SIGNAL PROCESSING OF VECPS**

#### **3.1 INTRODUCTION**

This chapter describes the author's development of DSP methods for rapid objective visual field analysis. The aims of these developments were:

1. To develop a technique for rapidly detecting the presence of an evoked potential when small parts of the visual field were stimulated. This would enable rapid screening of the visual field for absolute field defects.
2. To develop a technique for rapidly measuring the signal amplitude and latency (or phase) when small parts of the visual field were stimulated. This would enable signals from different parts of the visual field to be compared.

The DSP methods available for development were dependent on the stimulus mode employed (transient, steady-state or pseudo random binary stimulation). The various methods are reviewed and their suitability for electroperimetry discussed.

DSP methods based on steady-state stimulation were chosen for further development. In particular, a DSP method based on adaptive noise cancelling was developed which has a number of advantages over conventional Fourier analysis for rapid real-time signal analysis. The development of the adaptive noise canceller is described and its performance is demonstrated using a number of simulations.

Some basic DSP tools were also required for the analysis of transient VECF waveforms and these are also described.

## **3.2 REVIEW OF THE APPLICATION OF DIGITAL SIGNAL PROCESSING TO VECPS**

### **3.2.1 Transient VECPS**

#### **Introduction**

The transient VECP is the response to single stimulus events, presented at a rate of about once per second or less and is used in routine clinical practice (Section 1.4.3). The VECP is usually recovered from the background EEG by synchronised averaging of many successive responses (Section 1.4.3).

The recovered signal is strictly an estimate of the actual VECP, because it is contaminated with some residual noise. This is always true, irrespective of the stimulation mode or the signal processing method employed.

#### **Signal Averaging**

The VECP is typically recovered by averaging the responses to 100 stimulus presentations. Signal averaging is based on the hypothesis that the VECP is linearly superimposed on the EEG activity and that the following assumptions are valid (Regan 1989):

1. The response is always the same for identical stimuli.
2. The EEG is uncorrelated with the evoked potential signal.
3. EEG recordings are uncorrelated with each other.
4. The EEG is a zero mean random process.

The SNR should therefore theoretically improve by the square root of the number of averages.

In practice, the assumption that the EEG noise is a zero mean random process uncorrelated with the VECP signal does not always hold (Ungan and Basar 1976, Gevins 1984). In particular the EEG may include periods of sustained EEG alpha

activity which can become time-locked to the VECP signal. This problem can be minimised by either randomising the interstimulus interval or alternatively by varying the interstimulus interval by a period corresponding to half a cycle of the alpha activity (Section 2.4.3).

The single responses which build to form the VECP may also be considerably different from one another (Cerutti et al 1987b) and may vary with time according to the mental attentiveness and fatigue of the patient (Section 2.9.5).

Despite the fact that the theoretical assumptions for signal averaging are not fully met, signal averaging does provide a significant improvement in SNR and the residual noise continues to decrease with the number of recordings averaged. Signal averaging is in widespread clinical use because of its simplicity. However, because of its time consuming nature it is not very suitable for electroperimetry.

### **A Posteriori 'Wiener' Filtering**

Walter (1969) proposed the use of a posteriori 'Wiener filtering' (APWF) to improve the SNR of the signal estimate in time averaged VECPs. It was hoped that the increase in SNR would enable a reduction in the number of averages required to recover the VECP and the technique has subsequently been widely discussed in the literature (Doyle 1975, Hartwell and Erwin 1976, Ugan and Basar 1976, de Weerd and Martens 1978, Carlton and Katz 1980, de Weerd 1981).

If uncorrelated noise is linearly superimposed upon a signal, a Wiener filter produces a least mean square estimate of the signal based upon prior knowledge of the signal and noise spectra (Walter 1969). The filter theory assumes that the signal and noise spectra are time-invariant. However, in evoked potential studies, these spectra are not known and can only be estimated retrospectively from spectral analysis of the individual recordings and their composite average.

There are conflicting reports on the practical success of the APWF and it has never been more than a research tool. The performance of APWF is critically dependent on the filter structure (Doyle 1975) and the accuracy of the estimates of the signal and noise spectra. Hartwell and Erwin (1976) reported that the APWF gave a better estimate of the evoked signal than signal averaging. Subsequently however, Ugan

and Basar (1976) concluded that signal averaging gave the best result, whilst Carlton and Katz (1980) found no improvement in the signal estimate produced by APWF.

de Weerd (1981) reasoned that the lack of success of APWF was the fact that the signal and noise spectra overlap and vary with time. Time-varying filters have therefore been developed which take the temporal distribution of the signal and noise into account (de Weerd 1981, de Weerd and Kap 1981, Cerutti et al 1987a). Time-varying APWF can successfully filter noise components from signal components in the same frequency band as long as they share the same band at different points in time.

For the filter to be effective, good estimates of the signal and noise spectra are required. This means that the signal average used to estimate the signal spectrum must itself have a high SNR. In practice APWF can only help to reduce the number of stimulus presentations when the SNR of the signal average is in excess of 20 dB (de Weerd and Martens 1978). Stimulation of small areas of the visual field in electroperimetry produces small VECF signals and it is therefore unlikely that the SNR will be sufficiently high to reduce the number of stimulus presentations.

### **Evoked Potential Modelling**

An alternative method for measuring signal sweep VECFs has been developed based on a filter model driven by white noise (Cerutti et al 1987b, Liberati 1988, Liberati et al 1989). Like APWF, the model requires prior knowledge of the signal spectrum which can only be obtained from an initial signal average with a high SNR. Consequently it is unlikely that the model can be used to reduce the time taken for electroperimetry.

### **Signal detection of transient VECFs**

No objective technique for detection of transient VECF signals is currently available. Most laboratories simply 'detect' the presence of a signal by subjectively determining the measurement repeatability. In practice, two averaged recordings are made from the same stimulus and one recording is overlaid on top of the other. If the two waveforms have features which closely match each other in amplitude and latency, then the recording is deemed to be 'repeatable' and a signal has been 'detected'. However, if the SNR is small it is often difficult to decide whether a signal has been detected.

Cross-correlation can be used to objectively determine measurement repeatability (Regan 1989, van der Tweel and Estevez 1991) but it is not in widespread use. The author is aware of only one paper in which cross-correlation values are quoted (Collins et al 1978). The major problem with using cross-correlation as a method of signal detection is deciding what level of correlation to consider significant. In addition, the result of cross-correlation is dependent on the time window tested (Section 3.3.4).

An alternative approach for detecting transient VECPs would be to assess the residual noise level and the SNR in the signal average. Elberling and Don (1984) used this concept to assess auditory evoked potentials and it may be possible to adapt the technique for VECP analysis. The residual noise level and SNR are estimated by measuring the variance at points in the waveform. The statistical significance of the SNR is then calculated using the F-distribution.

An objective on-line measure of the SNR would be useful for minimising the time required for signal averaging in the following ways:

1. For objective signal detection, averaging would only need to continue until the SNR exceeded some criterion or the residual noise level was sufficiently small.
2. For accurate measurement of the signal amplitude, averaging would only need to continue until the residual noise level was equal to the desired level of measurement precision.

## **Discussion**

Electroperimetry based on transient VECPs is currently limited to signal averaging which is very slow. Advanced signal processing methods such as time-varying APWF could probably be applied to improve the SNR of the final signal average and so improve the final signal estimate. However, these methods are unlikely to be of practical use in reducing the number of stimulus presentations required.

If transient stimuli are to continue to be employed for electroperimetry the most profitable DSP developments would be to have an on-line measurement of the SNR, residual noise level and cross-correlation. These techniques would help standardise recording practice by ensuring that the same statistical confidence limits were applied to all recordings. Data acquisition could be stopped as soon as the necessary statistical

confidence limits for the SNR and residual noise level were reached and the cross-correlation would give a measure of the signal repeatability.

### 3.2.2 Steady-state VECPs

#### Introduction

Steady-state VECPs are obtained from stimulation rates in excess of about five per second (Spehlmann 1985). The individual responses interact and produce a periodic signal with discrete components at the stimulus frequency and its harmonics (Spehlman 1985). Regan (1966) introduced the term steady-state to describe the waveform because the amplitude and phase of each frequency component remain constant with time.

Figure 3.1 illustrates the effect of stimulus frequency on the pattern-reversal VECP for one subject. The waveforms were obtained for this illustration by synchronous averaging of 200 sweeps of data. At a stimulus frequency of 5 reversals per s the VECP is periodic in nature. In the steady-state VECP no one feature can be attributed to any particular stimulus. Nevertheless, at slow steady-state stimulus frequencies, the dominant positive peak is closely related to the dominant  $\overline{P100}$  peak in the transient waveform. As the stimulus frequency is increased the harmonic content of the VECP signal decreases and the response tends to a sine wave at the pattern-reversal rate.

Figure 3.2 shows how the steady-state VECP quickly builds up from the onset of the first stimulus.

The steady-state VECP is most appropriately analysed in the frequency domain (Regan 1977). Figure 3.3 illustrates the frequency spectrum of a typical steady-state VECP recording. The signal has discrete components at the stimulus frequency and its harmonics whilst the EEG and muscle noise are distributed over a wider frequency range. Signal analysis in the frequency domain therefore yields an increase in the SNR which in turn enables shorter recording times.

The steady-state VECP is simply described by the amplitude and phase of each frequency component. Measurement of steady-state VECPs therefore has a firm mathematical basis which is unambiguous (Regan 1989). In contrast, when transient

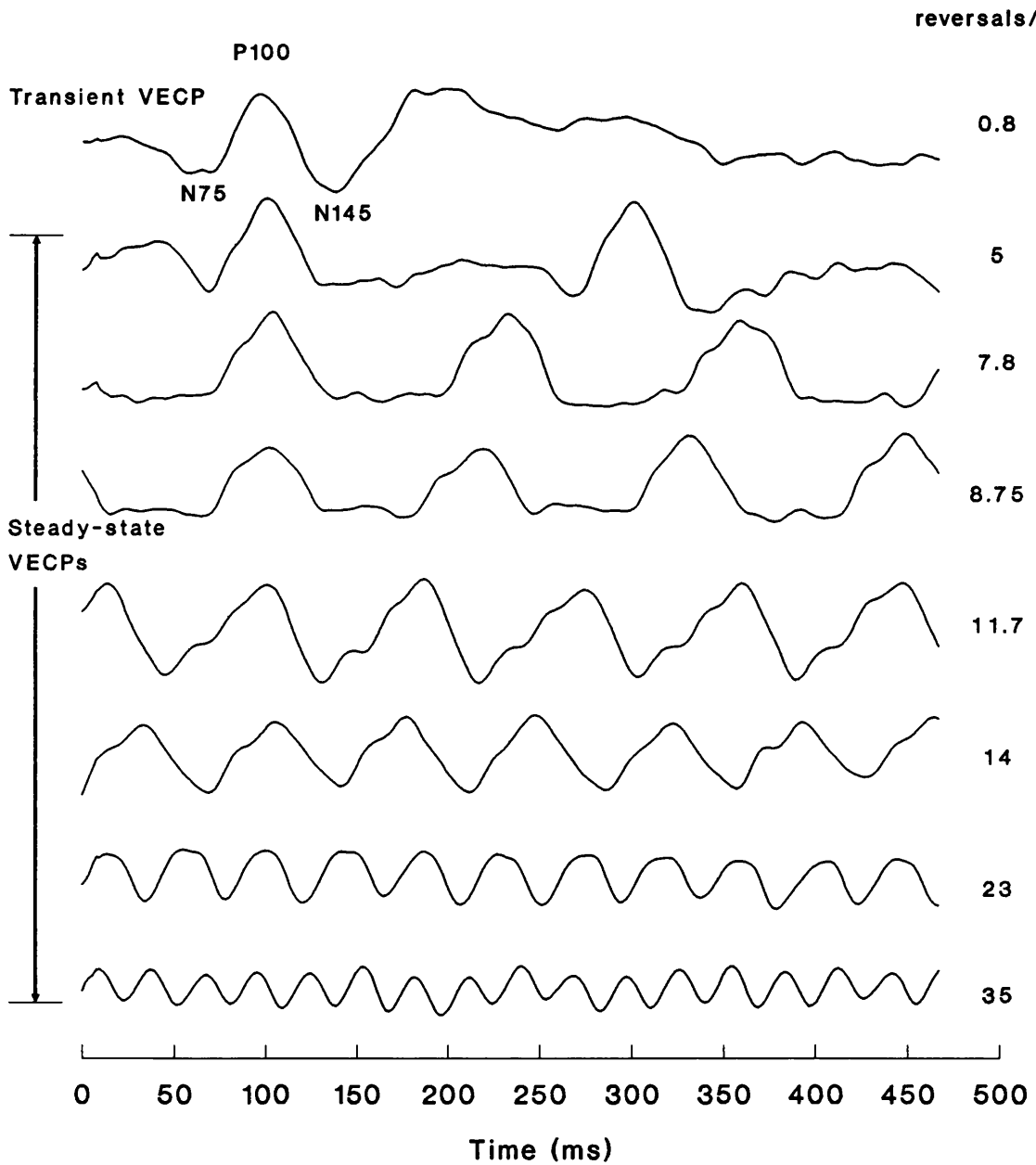


Figure 3.1 The effect of stimulus frequency on the pattern-reversal VECP.

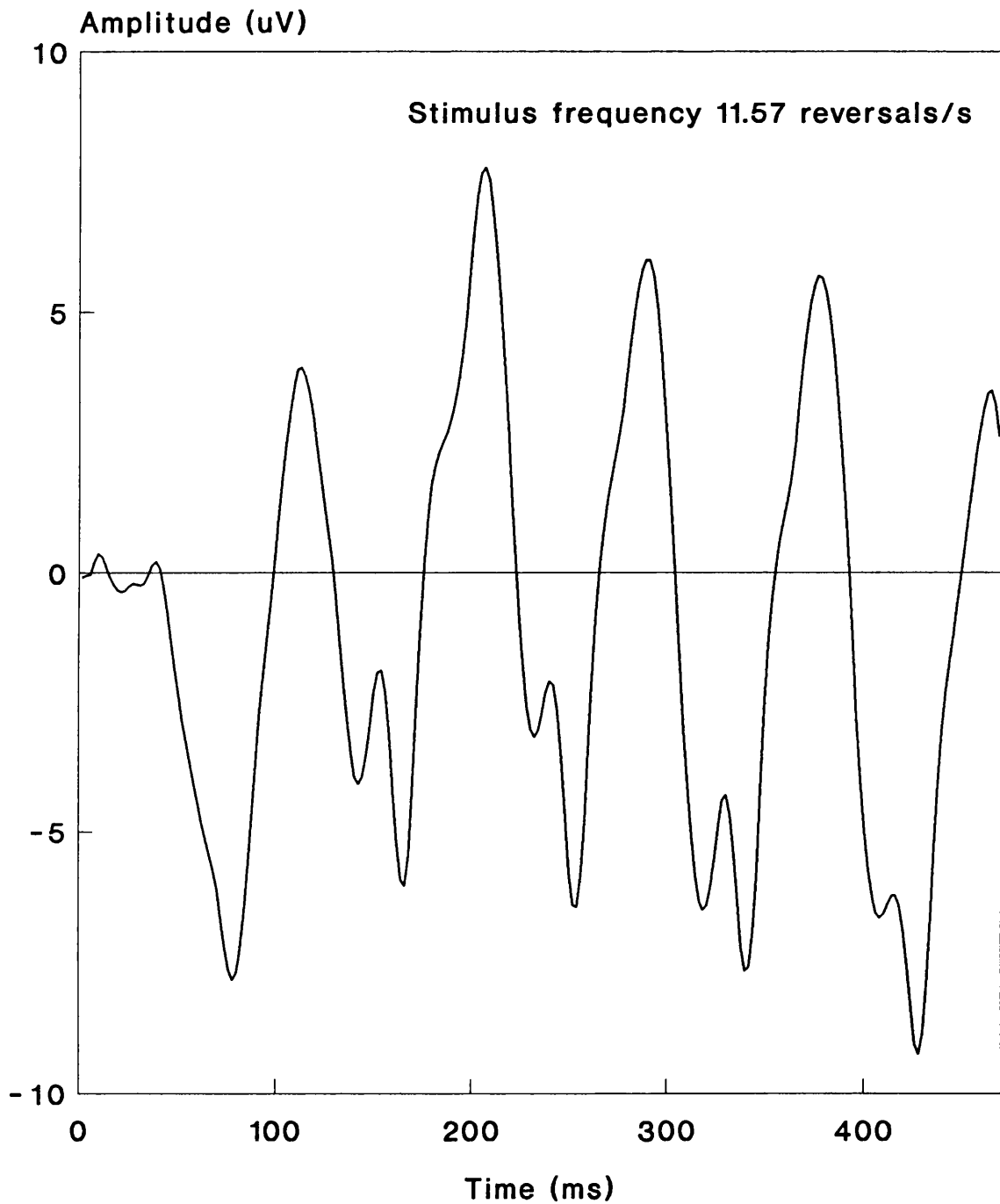


Figure 3.2 Build-up of the pattern-reversal steady-state VECP from onset of the first stimulus.

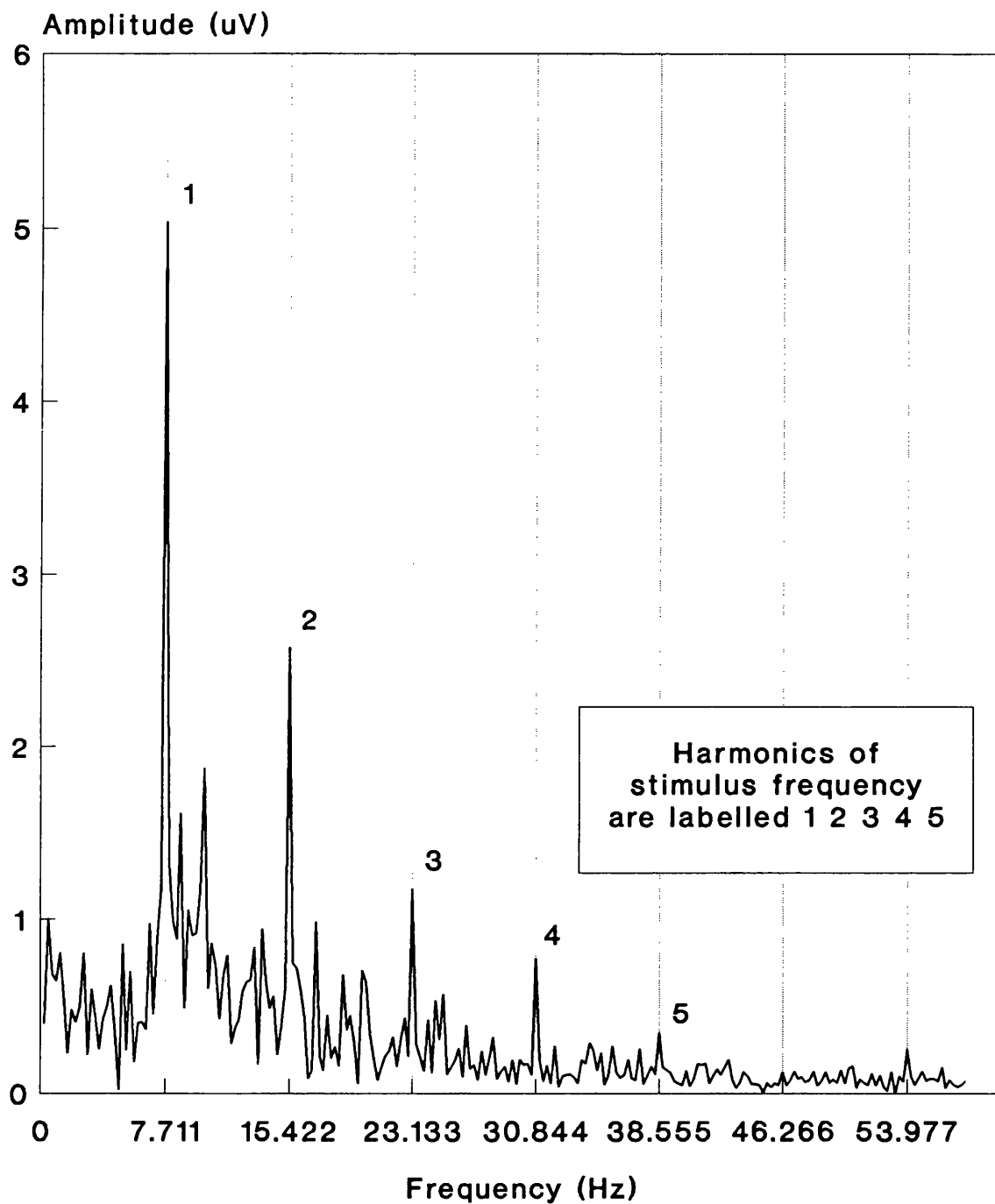


Figure 3.3 Example of a frequency spectrum from a steady-state VECF recording. Stimulus frequency 7.711 Hz.

VECPs are analysed, particularly from non standard stimuli, arbitrary decisions often have to be made to determine which features to measure (Regan 1989). These decisions are made more difficult by interindividual variations in the shape of the waveform. A further advantage of steady-state VECPS is that they are more reproducible (Cappin and Nissim 1975).

Steady-state VECPS have already been used with some success to study patients with quadrantic visual field defects (Cappin and Nissim 1975, Howe and Mitchell 1980, Yanashima 1982). However, only one study (Yanashima 1982) used frequency domain analysis to improve the SNR and none of the studies used objective signal detection techniques.

The visual system is non-linear so in a clinical sense the transient and steady-state VECPS should strictly be considered as complementary techniques. Glaucomatous field defects may for example be more detectable with the use of steady-state stimuli because glaucoma selectively damages the large optic nerve fibres and corresponding ganglion cells (Trick 1985, Quigley et al 1987, Bach and Speidel-Fiaux 1989) which preferentially respond to higher temporal frequencies. This view is supported by a well controlled full-field VECPS study (Towle et al 1983). Another study concluded that steady-state stimuli made a useful contribution as part of a multi-modal stimulus approach (Howe and Mitchell 1986).

Steady-state VECPS have also been used to study the response to stimuli with different spatial frequencies (Regan 1977, Celesia 1991) and to determine sensory thresholds for spatial frequency (Norcia et al 1985) and contrast sensitivity (Campbell and Maffei 1970, Seiple et al 1984).

Despite the many advantages and applications of the steady-state VECPS it is usually only used as a research tool. There are a number of possible reasons why the technique has not been routinely implemented:

1. The procedures necessary to record and analyse steady-state VECPS have not been widely available on commercial electrophysiology systems.
2. A long lead time is required to collect and analyse normal data before the test can be used to identify abnormal recordings.

## Measurement of steady-state VECPs

Several methods are available to measure the steady-state VECP (Norcia et al 1985, Strasburger 1987) and they can be classified into one of two groups according to whether the detection process is phase insensitive or phase sensitive. A phase insensitive detector is equally sensitive to all signal phases whilst a phase sensitive detector is optimally sensitive to one signal phase.

If the phase of a sinusoidal signal is unknown or time varying a phase insensitive technique is required (Norcia et al 1985) which measures both signal amplitude and phase. The method most widely used is the discrete Fourier transform implemented using the fast Fourier transform (FFT) algorithm (Cooley and Tukey 1965). The frequency resolution of Fourier analysis is the reciprocal of the total recording time. Signal averaging is also a phase insensitive technique and as well as being used on its own it can be combined with Fourier analysis to average spectra.

If the phase of a sinusoidal signal is known and remains constant, then the optimal measurement technique is a phase sensitive detector (Norcia et al 1985, Strasburger 1987). In this technique, noise is rejected if either its frequency or phase is different from a reference signal. Phase sensitive methods can yield a 3 dB improvement in the SNR when compared with phase insensitive methods. The most commonly used method of phase sensitive detection is an analogue synchronous-demodulation technique known as the lock-in amplifier (Nelson et al 1984, Schacham and Pratt 1985). The lock-in amplifier provides a real-time response and has been used to measure sweep VECPs in which one stimulus parameter (e.g. spatial frequency) is continuously altered during the recording period. A disadvantage of phase sensitive detectors is that if the reference phase is wrong, or if the signal phase changes during a recording, the method loses its effectiveness in filtering the noise and the signal is suppressed thus reducing the SNR (Strasburger 1987).

Recent developments in adaptive noise cancelling (Widrow et al 1975, Widrow and Stearns 1985) offer a number of potential advantages for the analysis of steady-state VECPs and should be investigated. The basic adaptive noise canceller (ANC) is phase insensitive, adapting to changes in both the signal amplitude and phase. Single frequency analysis using the ANC is less computationally intensive than the FFT; it also requires significantly less memory, enables real-time implementation and provides continuous temporal information on variations in the signal. The author recognised

that the ANC had further potential and could be modified to operate as a phase sensitive detector when the signal phase was known.

### **Objective signal detection of steady-state VECP**

A variety of methods have been implemented to objectively detect steady-state VECP signals. Surprisingly these methods are not widely used and have not been applied to electroperimetry. Objective detection of steady-state VECPs is either based on the spectral content of the recording (Norcia et al 1985, Norcia et al 1989, Eizenman et al 1993) or the temporal variation of the signal at the stimulus frequency (Strasburger 1987).

Norcia et al (1985, 1989) used a discrete Fourier transform to measure the spectrum of steady-state VECP recordings. Signal detection was based on an empirical relationship that the amplitude of the spectrum at the stimulus frequency had to exceed the amplitude of the spectrum at an adjacent EEG noise frequency by a factor of at least 3:1.

Eizenman et al (1993) also detected steady-state VECPs using the signal spectrum. The noise power was estimated from ten frequencies adjacent to the stimulus frequency. Statistical modelling and receiver operating characteristic (ROC) analysis were used to calculate the probability of detection and probability of false positive detection for different signal-to-noise ratios. For an SNR of 2.4 the probability of detection was 70 % whilst the probability of false positive detection was 5 %. If the SNR was 2.2 or 2.9, then the probabilities of false positive detection were 10 % and 1 % respectively.

Temporal information on the steady-state VECP signal can be obtained at the expense of frequency resolution by sub-dividing the recording into a number of periods and then measuring the signal in each period. A confidence interval for the mean signal amplitude and phase can then be derived from the variance of the individual measurements. A signal is detected if the confidence interval for the mean signal amplitude excludes zero. Strasburger (1987) measured the signal in terms of its sine and cosine components and used the Central Limit Theorem (Hays 1963) to calculate the confidence limits. The confidence interval generated by the Central Limit Theorem is a rectangle in the sine/cosine co-ordinate system. Alternatively, a confidence ellipse could be calculated using Hotelling's  $t^2$  statistic (Hotelling 1931, Anderson 1958,

Morrison 1976). This method has already been successfully applied to the detection of steady-state auditory evoked potentials (Picton 1987a, b).

Regan (1989) has developed a simple 'rule of thumb' for assessing the reliability of steady-state VECP recordings. The method uses temporal information on the sine and cosine components of the signal. Unfortunately the technique has no statistical basis and the author found it unreliable when used to assess simulated signals.

## **Discussion**

The steady-state VECP has a number of significant advantages over the transient VECP for developing techniques in electroperimetry:

1. The steady-state VECP can be recorded more rapidly than the transient VECP.
2. The SNR of the steady-state VECP is enhanced by analysis in the frequency domain.
3. Objective signal detection techniques have already been developed for the steady-state VECP.
4. Temporal information on the VECP can be obtained by sub-dividing the recording into a number of time periods and measuring the signal in each. These measurements can be used to calculate the confidence interval of the signal mean and can also be used to detect temporal trends in the amplitude and the phase of the signal due to reduced attention, sensory adaptation, progressive fatigue or loss of ocular accommodation.
5. The steady-state VECP is represented by discrete frequency components at the stimulus frequency and its harmonics. Therefore, if different parts of the visual field are stimulated at different frequencies it is possible to test them simultaneously, further reducing recording times (Yanashima 1982).

Several areas for future development were identified:

1. Objective signal detection of steady-state VECPs should be applied to electroperimetry.
2. Measurement of steady-state VECPs using adaptive noise cancelling should be investigated. The ANC has a number of potential advantages over conventional phase insensitive techniques such as the FFT and also has the potential to be developed as a phase sensitive detector.

### **3.2.3 Pseudo Random Binary Stimulation VECPs**

Pseudo random binary stimulation (PRBS) produces rapid aperiodic stimuli at a rate similar to that used in steady-state stimulation. The method has been successfully used to measure VECPs (Fricker and Sanders 1974, Collins and Sawhney 1993) and ERGs (Fricker and Sanders 1975, Fricker and Kuperwaser 1982, Sutter and Duong 1992). The evoked signal is recovered from the recording by cross-correlation with the PRBS sequence. The technique offers a number of advantages over transient stimulation:

1. A response with a higher SNR can be obtained in a similar recording period.
2. The stimulus contains a wide range of frequencies and can therefore test a range of cells with different temporal frequency responses.
3. Simultaneous recordings can be made from a number of stimuli by using a different time shifted PRBS sequence for each stimulus. This method has been used to simultaneously record the ERG from many parts of the retina (Sutter and Duong 1992) and could be extended to VECP recordings to reduce recording times.

PRBS is suitable for developing VECP electroperimetry techniques because it is rapid and because it enables multiple areas of the visual field to be tested simultaneously.

The electrophysiology system developed in this laboratory (Chapter 2) has recently been used to develop techniques for PRBS VECP electroperimetry. A major aim of this work is to develop algorithms and software so that the signal recovery can be

performed in real-time during the recording. These developments would not have been possible on commercial electrophysiology systems which further illustrates the versatility of the system developed in this laboratory. Commercial systems do not enable PRBS and are limited to signal averaging for real-time DSP.

### **3.2.4 Conclusion and Summary of Aims**

Steady-state and pseudo random binary stimulation together with their associated signal processing techniques offer significant advantages over transient stimuli for developing techniques in electroperimetry. They use faster stimulation rates, provide an improved SNR and will enable simultaneous testing of multiple areas of the visual field.

To date few people have applied steady-state stimuli to electroperimetry and there are no published papers on the use of PRBS applied to electroperimetry. Presumably this is due to the limited range of stimuli and signal processing facilities on most electrophysiology systems.

The main aims of the novel signal processing developments described in this thesis are:

1. Investigation of the use of a novel ANC for the measurement of steady-state VECs.
2. Application of objective signal detection techniques to electroperimetry.

In addition to these developments, some basic DSP techniques were developed for transient stimuli. Transient stimuli were required for system validation, for routine clinical use and for the development of novel stimuli which could not be presented at steady-state frequencies.

### 3.3 TRANSIENT SIGNAL PROCESSING DEVELOPMENT

#### 3.3.1 Signal averaging

The signal averaging was time-locked to the stimulus onset so that the signal average  $\bar{x}_i$  was defined as:

$$\bar{x}_i = \sum_{n=1}^{n=N} x_{n,i} / N$$

where  $x_n$  was the  $n$  th recording,  $N$  was the total number of recordings and  $i$  was the  $i$  th sampled point from stimulus onset.

#### 3.3.2 Signal addition

The software enabled the addition of signal averaged recordings. In order to maintain an optimum SNR, the addition was weighted by the number of recordings in each average according to the equation:

$$\bar{x}_{\text{sum } i} = \frac{\bar{x}_{1i} N_1 + \bar{x}_{2i} N_2}{N_1 + N_2}$$

where  $\bar{x}_{\text{sum}}$  was the composite sum,  $\bar{x}_1$  and  $\bar{x}_2$  were the averages being added,  $N_1$  was the number of recordings averaged in  $\bar{x}_1$ ,  $N_2$  was the number of recordings averaged in  $\bar{x}_2$  and  $i$  was the  $i$  th sampled point from stimulus onset.

#### 3.3.3 Filtering

A digital low-pass filter was designed to attenuate high frequency noise. The specification of the filter was:

1. The ripple in the pass-band should be less than 1 % up to a frequency of 20 Hz.
2. The filter attenuation should be 90 % at a frequency of 70 Hz.

A Butterworth filter response was chosen because it has the flattest pass-band response (Kuo 1966). Unfortunately, this pass-band response is at the expense of a relatively slow roll-off in the stop-band. The amplitude response of the filter is:

$$\frac{V_{out}}{V_{in}} = \frac{1}{\sqrt{\left[1 + \left(\frac{\omega}{\omega_c}\right)^{2n}\right]}}$$

where  $\omega$  is the input frequency in radians,  $\omega_c$  is the filter cut-off frequency in radians and  $n$  is the order of the filter. Unlike the analogue Butterworth filter, which causes a frequency dependent phase lag (Kuo 1966), the digital filter was designed to produce no phase lag.

The desired filter transfer function was obtained with a fourth order Butterworth filter with a cut-off frequency of 40 Hz. The filter was implemented in the time domain by convolution with the input signal. The processing time was minimised by truncating the number of filter coefficients. The actual number of coefficients was chosen by finding the minimum number required for the filter transfer function to remain within the design specification. The number of filter coefficients required was dependent on the data sampling frequency. At a sampling frequency of 512 Hz, 31 coefficients were required (Figure 3.4), whilst at a sampling frequency of 1 kHz, 61 coefficients were required.

### 3.3.4 Cross-correlation

The cross-correlation function was used to measure the repeatability of signal averaged VECP recordings.

The generalised cross-correlation function  $r_{12}(\tau)$  relating two continuous time-varying signals  $f_1(t)$  and  $f_2(t)$  is defined as:

$$r_{12}(\tau) = \lim_{T_o \rightarrow 0} \frac{1}{T_o} \int_{-T_o/2}^{T_o/2} f_1(t) \cdot f_2(t + \tau) dt$$

where  $\tau$  is a time-shift imposed on one of the signals (Lynn 1989).

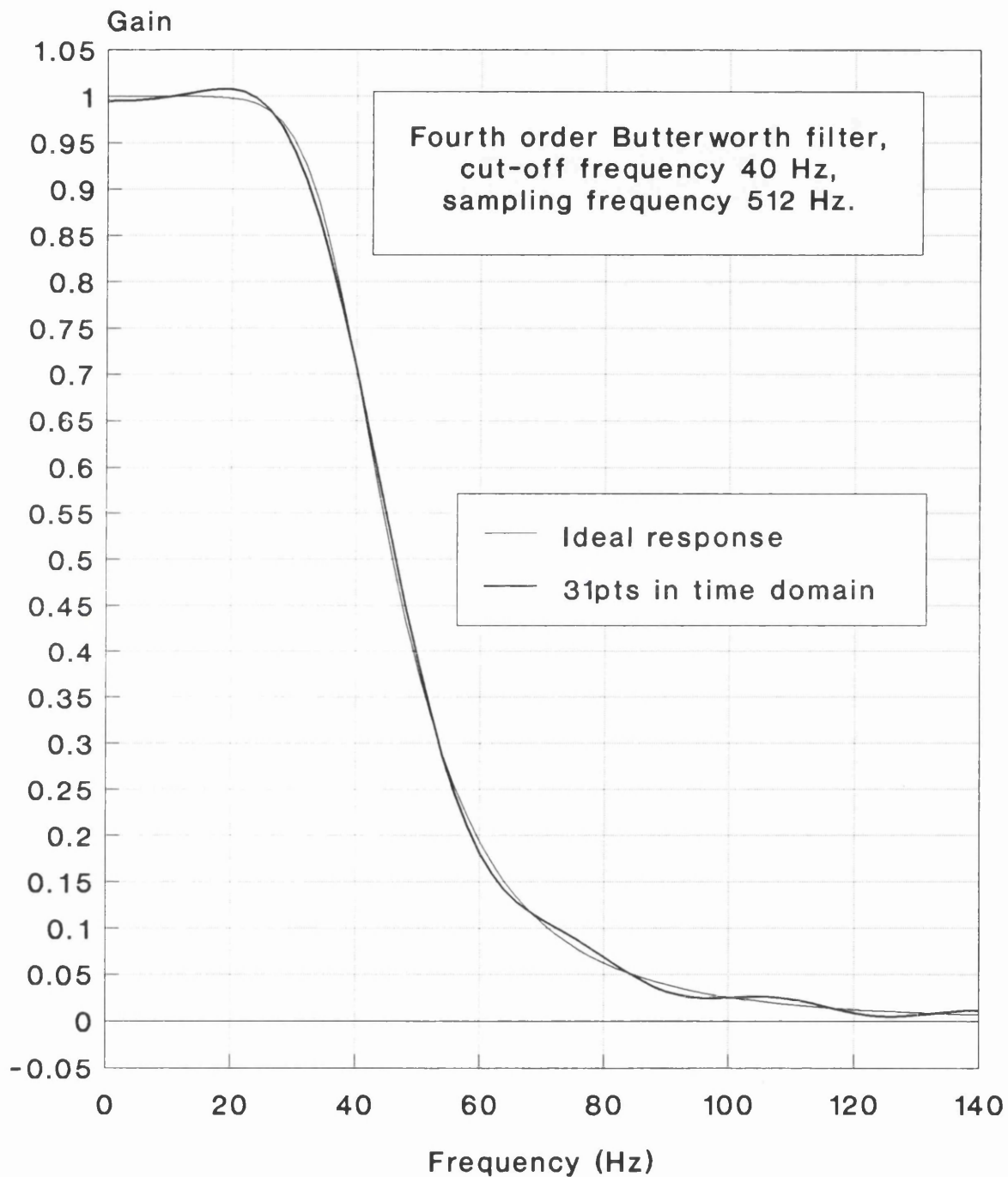


Figure 3.4 Effect of truncation in the time domain on the frequency response of the Butterworth filter

For a signal sampled over a finite period the function is expressed by the equation:

$$r_{12}(\tau) = \frac{1}{M} \sum_{i=1}^{i=M} f_{1i} f_{2i}$$

where  $i$  is the  $i$ th sampled point and  $M$  is the total number of sampled points.

When VECP recordings are averaged, it is assumed that the cortical responses are the same for identical stimuli (Section 3.2.1). Consequently, in order to test the repeatability of two averaged VECP recordings,  $\bar{x}_1$  and  $\bar{x}_2$ , the cross-correlation should be calculated for  $\tau$  equal to zero. In order that the cross-correlation values from different studies could be compared the equation was normalised as below so that it was independent of signal power.

$$\frac{\sum_{i=1}^{i=M} \bar{x}_{1i} \bar{x}_{2i}}{\frac{1}{2} \sum_{i=1}^{i=M} ((\bar{x}_{1i} \bar{x}_{1i}) + (\bar{x}_{2i} \bar{x}_{2i}))}$$

In practice it was found that the cross-correlation function was affected by DC voltage offsets in the signal base-line. This effect was minimised by subtracting the mean of each signal average from the value of each point in the average.

The final expression for cross-correlation was thus:

$$\frac{\sum_{i=1}^{i=M} \left( \bar{x}_{1i} - \frac{\sum_{j=1}^{j=M} \bar{x}_{1j}}{M} \right) \left( \bar{x}_{2i} - \frac{\sum_{j=1}^{j=M} \bar{x}_{2j}}{M} \right)}{\frac{1}{2} \sum_{i=1}^{i=M} \left( \left( \bar{x}_{1i} - \frac{\sum_{j=1}^{j=M} \bar{x}_{1j}}{M} \right)^2 + \left( \bar{x}_{2i} - \frac{\sum_{j=1}^{j=M} \bar{x}_{2j}}{M} \right)^2 \right)}$$

where  $j$  is the  $j$ th sampled point.

Ideally, if the two averaged recordings are identical the expression is equal to unity whilst if there is no correlation the expression is equal to zero. In practice, average VECP recordings contain residual EEG noise, so if the VECP response is repeatable the expression tends to unity as more signals are averaged and the SNR is increased. In order to use cross-correlation as an objective means of signal detection it needs to be determined what value of correlation to consider significant (Section 3.2.1). By modelling VECP signals in EEG noise it would be possible to empirically determine what value of cross-correlation corresponds to what probability of signal detection.

In a transient VECP recording, the signal power varies with time, therefore, the cross-correlation value is dependent on the time window tested. To date, cross-correlation values have been calculated for the whole recording period, typically 0 to 500 ms from stimulus onset (Sections 2.11.2, 2.11.3 and 2.11.4). The values could, however, be increased by using an analysis time window which only includes the main signal components, typically 50 to 200 ms from stimulus onset.

### **3.3.5 Automatic peak picking**

The amplitude and latency of the main features of interest in the VECP were measured by positioning cursors on the waveform. In order to quickly position the cursors, an algorithm was developed for automatic peak picking. The algorithm first searched for the highest positive peak in the range 70 to 140 ms. This point corresponded to  $\overline{P100}$  in the analysis of pattern-reversal VECPs. The algorithm then searched for the negative peak either side of the main positive peak. These points corresponded to  $\overline{N75}$  and  $\overline{N145}$  in the pattern-reversal VECP. The algorithm was tested on 36 waveforms. Each waveform was filtered to remove high frequency noise and the algorithm correctly picked 102 out of 108 peaks.

## **3.4 STEADY-STATE SIGNAL PROCESSING DEVELOPMENT**

### **3.4.1 Introduction**

This section describes the implementation and evaluation of a new measurement technique for steady-state VECPs based on the concept of adaptive noise cancelling (Widrow et al 1975, Widrow and Stearns 1985). The ANC offers a number of potential advantages over conventional analysis methods including the ability to

operate as either a phase insensitive or phase sensitive detector. In its phase insensitive state the ANC automatically tracks the signal phase and amplitude. If the ANC is phase-locked it acts as a phase sensitive detector and will only track changes in the signal amplitude. The ANC has been investigated using simulated and physiological signals; the accuracy and precision of measurement and the reliability of signal detection were compared with the FFT.

### **3.4.2. Theory of the ANC**

#### **Basic concept of adaptive noise cancelling**

The principles of adaptive noise cancelling were formulated by Widrow et al (1975) and the basic structure is illustrated in Figure 3.5. The primary input to the ANC is a signal corrupted by uncorrelated noise. The aim of the ANC is to produce an output which is as close an estimate as possible of the signal. To achieve this, the ANC requires a second, reference, input. The reference is traditionally composed of noise; this noise is uncorrelated with the signal but correlated in an unknown way with the noise in the primary input. The reference input is filtered using an adaptive filter to produce an output which is subtracted from the primary input. The impulse response of the adaptive filter is automatically adjusted using an algorithm to minimise the output power of the ANC. In so doing, the output of the adaptive filter is an estimate of the noise in the primary input and the ANC output is an estimate of the signal in the primary input.

#### **Adaptive noise cancelling of a steady-state VECP**

When recording a VECP signal corrupted by EEG noise the structure of the ANC must be modified because it is difficult to obtain a suitable noise reference. This is because the EEG is not well correlated across the scalp, so it is difficult to find a suitable recording site which simultaneously has a high EEG noise correlation and a negligible VECP signal contribution. Fortunately, the exact stimulus frequency is known and an alternative structure has been developed (Figure 3.6) which uses a synthesised signal, rather than noise, as a reference input.

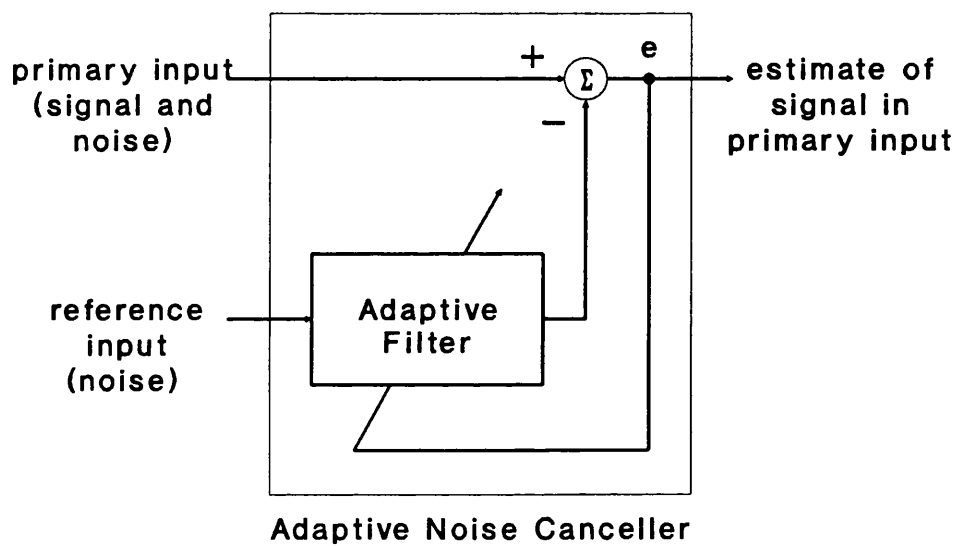


Figure 3.5 Basic structure of an adaptive noise canceller

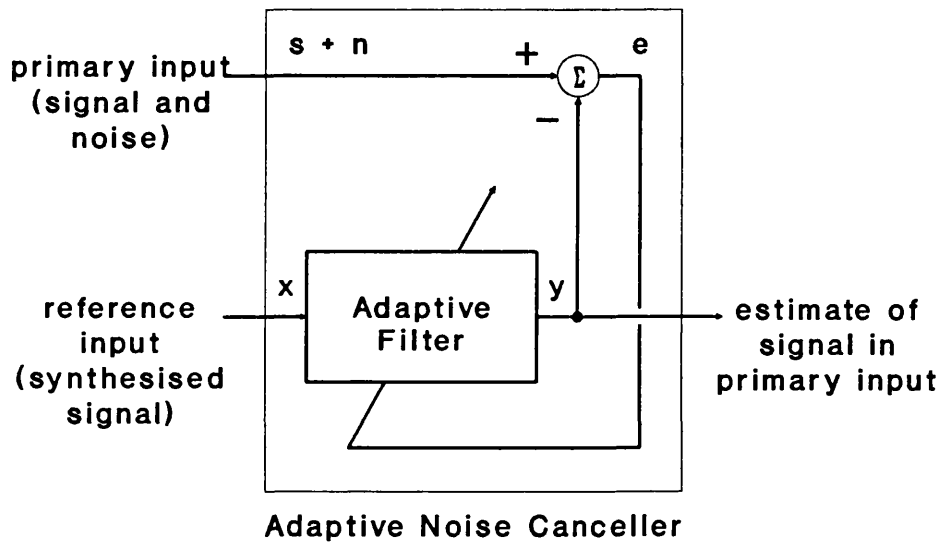


Figure 3.6 Structure of modified adaptive noise canceller.

The primary input to the ANC (Figure 3.6) is a recorded signal  $s$ , corrupted by uncorrelated noise  $n$ . The reference input  $x$  is a synthesised signal, uncorrelated with noise  $n$  but correlated in an unknown way with signal  $s$ . The desired estimate of the signal  $s$  is obtained at the output of the adaptive filter  $y$  as shown below.

$s$ ,  $x$ ,  $n$  and  $y$  are each assumed to be statistically stationary and have zero mean. The output  $e$  is then:

$$e = n + s - y \quad (1)$$

Squaring equation (1) and taking expectations of each side:

$$E[e]^2 = E[n]^2 + E[(s - y)]^2 + 2E[n(s - y)] \quad (2)$$

But  $n$  is uncorrelated with  $s$  and  $y$ , so equation (2) simplifies to:

$$E[e]^2 = E[n]^2 + E[(s - y)]^2 \quad (3)$$

The filter is adjusted to minimise the ANC output power  $E[e]^2$ . The noise power  $E[n]^2$  is unaffected by this process so as  $E[e]^2$  is minimised,  $E[(s - y)]^2$  is also minimised. The adaptive filter output  $y$  is then a least mean square estimate of the primary signal  $s$ .

### Adaptive filter

The adaptive filter module of the ANC is an adaptive linear combiner which is a time-varying, non recursive digital filter. It has an input signal vector  $X_k^T$ , a set of adjustable weights  $W$ , a summing unit and a single output  $y$ .  $y$  is defined by the expression:

$$y_k = X_k^T W_k \quad (4)$$

The output is a linear combination of the input components. The weights are modified using an algorithm which adapts to minimise  $E[e]^2$ .

## Adaptive algorithm

The simplest and most widely used adaptive algorithm, for the adaptive linear combiner, is the Least Mean Square (LMS) algorithm of Widrow and Hoff (Widrow et al 1976). The weights are updated iteratively according to the algorithm:

$$W_{k+1} = W_k + 2\mu e_k X_k \quad (5)$$

where  $\mu$  is a constant that controls the rate of convergence of the weights on the optimal solution and consequently controls the stability of the adaptation process.  $\mu$  has dimensions of reciprocal signal power. The simplicity of the algorithm enables it to be implemented in real-time.

## Synthesis of the reference signal

Most of the steady-state VECF energy is contained in a single frequency component at the stimulus frequency ( or the reversal frequency for pattern-reversal stimuli ). The reference input to the ANC is  $X_k$  which is a sampled signal at the stimulus frequency and comprises two orthogonal components  $x_{1k}$  and  $x_{2k}$ :

$$x_{1k} = C \cos (k\omega_o + \phi) \quad (6a)$$

$$x_{2k} = C \sin (k\omega_o + \phi) \quad (6b)$$

where  $C$  is the reference signal amplitude,  $\omega_o$  is the stimulus frequency in radians multiplied by the sampling period and  $\phi$  is a phase delay.

The input is processed using a two weight filter which is updated according to equation (5) so that:

$$w_{1,k+1} = w_{1k} + 2\mu e_k x_{1k} \quad (7a)$$

$$w_{2,k+1} = w_{2k} + 2\mu e_k x_{2k} \quad (7b)$$

The ANC is an adaptive filter which automatically tracks changes in the amplitude and phase of the recorded VECP signal. Once the filter has adapted, the best estimate of the VECP signal amplitude is:

$$C\sqrt{(w_1^2 + w_2^2)} \quad (8)$$

and the best estimate of the signal phase is:

$$\tan^{-1}\left(\frac{w_2}{w_1}\right) \quad (9)$$

At any instant in time the filter is phase sensitive. However, because of input noise, the filter continues to adapt its phase and its time averaged output is phase insensitive. In clinical practice, for a non swept stimulus, the phase of a VECP is stable. If the signal phase can be reliably estimated to within 45 degrees, the reference signal can be replaced by a single sinusoid input with the same phase. The adaptive filter then operates as a phase sensitive detector and the SNR is increased.

### Filter time constant

The time constant  $t_c$  of the learning curve of the LMS algorithm (Widrow and Stearns 1985) is:

$$t_c = \text{Number of weights} / 4\mu(\text{signal power}) = 1 / \mu C^2 \quad (10)$$

Adaptive transients become insignificant after four time constants.

### Filter transfer function

The time-invariant open loop transfer function  $G(z)$  of the adaptive filter has been described by Widrow and Stearns (1985) as:

$$G(z) = 2\mu C^2 (z \cos \omega_o - 1) / (z^2 - 2z \cos \omega_o + 1) \quad (11)$$

The overall transfer function of the filter  $H(z)$  with respect to the EEG input is calculated by closing the feedback loop:

$$H(z) = G(z)/(1 + G(z)) \quad (12)$$

substituting for  $G(z)$ :

$$H(z) = 2\mu C^2(z \cos \omega_o - 1)/(z^2 - 2(1 - \mu C^2)z \cos \omega_o + (1 - 2\mu C^2)) \quad (13)$$

This function describes a bandpass filter, the bandwidth of which is simply controlled using the convergence parameter  $\mu$ . There is a trade-off in the choice of the value of  $\mu$ . If  $\mu$  is small a narrow bandwidth is obtained but this is at the expense of a slow adaptation rate.

### 3.4.3. Practical evaluation of the ANC

#### Evaluation strategy

The practical performance of the ANC was evaluated using both simulated and real physiological signals. Simulated signals enabled the performance to be evaluated under a range of precisely defined input conditions and this included the use of stationary and non stationary signals.

The ANC was implemented as a phase insensitive detector for all the simulations. In addition, the accuracy and precision of measurement was evaluated with the ANC implemented as a phase sensitive detector.

#### Simulated VECP signals

The steady-state VECP was modelled as a sine wave at the stimulus frequency most often used in clinical practice in this laboratory, 11.57 Hz. The sampling frequency was 493.48 Hz.

### Filter settling time

The settling time of the ANC was checked with time constants in the range 2 to 8 s for representative VECP signals with amplitudes in the range 0.1 to 5  $\mu\text{V}$ .

### Simulated EEG activity

The next stage in the evaluation was to include a realistic simulation of EEG noise activity. A simple solution was to use real EEG recordings. However, the EEG has considerable intra- and interindividual variation, so the simulations used broadly typical EEG data, generated using a coloured noise model. The coloured noise was produced by bandwidth limiting white noise, by convolution with a 512 point filter in the time domain. Most EEG energy is below 20 Hz so the filter included a low-pass cut-off at 20 Hz with a first order roll-off. The amplifier settings used when recording signals were also included; a high-pass cut-off at 0.8 Hz with a first order roll-off and a low-pass cut-off at 100 Hz with a second order roll-off. The power of this simulated EEG was matched to typical values obtained practically in the laboratory.

### Tracking non-stationary signals

The ability of the filter to track non-stationary signals was assessed qualitatively by simulating a time varying VECP buried in EEG activity. One simulation involved linearly changing the signal amplitude from 5 to 3  $\mu\text{V}$  over a period of one minute. A second simulation varied the phase of the signal by 90 degrees over a period of one minute. The effect of using different filter time constants was also investigated.

### Accuracy and precision of measurement

The ANC was used as a phase sensitive detector and as a phase insensitive detector to measure simulated signal amplitudes of 0, 0.1, 0.25, 0.5, 1, 2.5 and 5  $\mu\text{V}$  buried in EEG noise. Four simulations, each of one minute's duration were performed for each amplitude. To obtain temporal information on the filter adaptation the output was vector averaged over consecutive two second periods of data (i.e. phase information was preserved). The settling time of the filter was two seconds. After the filter had settled the output from each two second data segment was averaged to obtain an estimate of the signal amplitude.

For comparison, the same data was processed using an FFT. The accuracy and precision of each measurement technique was determined by calculating the mean and standard deviation of the estimates of the signal amplitude.

### Reliability of signal detection

The temporal information from the above simulations was used to test the reliability of the signal detection. Each vector average comprised a two dimensional estimate of the sine and cosine components of the signal. These components can also be expressed in terms of amplitude and phase.

The significance of the results from the phase insensitive ANC, and the FFT, were determined by applying the two dimensional Hotelling  $t^2$  test (Hotelling 1931, Anderson 1958, Morrison 1976) to the estimates of the sine and cosine components of the signal.

When the ANC was used in its phase sensitive mode, the output phase was constant and a t-test was used to determine whether the mean estimate of the signal amplitude was significantly different from zero.

## **Real physiological signals**

### Recording system

Real physiological signals were recorded using the system described in Chapter 2. The stimulus was generated using computer graphics and presented on the computer monitor. The mean screen luminance was  $10 \text{ cd/m}^2$ . Monocular recordings were made from a mid-occipital electrode relative to a mid-frontal electrode. The amplifier low frequency cut-off was 0.8 Hz and the high frequency cut-off was 100 Hz. Raw EEG data was saved onto floppy disc and processed off-line using the ANC. The adaptive filter time constant was two seconds and the output was vector averaged over two second periods.

### Tracking amplitude changing signals

The ability of the ANC to track amplitude changing VECPs was assessed by varying the contrast of a checkerboard pattern-reversal stimulus over a period of 110 s. The

contrast was reduced in approximately linear steps from a maximum contrast, greater than 98 %, to zero and then increased again. The mean screen luminance remained constant and the pattern reversed at a rate of 11.57 reversals per s. Each check subtended 60' and the total stimulus size was 24° x 24°.

The steady-state VECP is processed by the magnocellular pathway of the visual system which has a non-linear amplitude versus contrast function (Shapley and Perry 1986). For zero contrast there should be no VECP. The VECP amplitude increases with increasing contrast, saturating at about 30 % contrast and reaching a maximum at about 60 % contrast (Shapley and Perry 1986).

#### Tracking phase changing signals

The ability of the ANC to track changes in the phase of a VECP signal was assessed with a checkerboard pattern-reversal stimulus, reversing at a rate of 11.57 reversals per second. The screen subtended 24° x 24°. By using small checks each subtending 30', the stimulus was optimised for stimulation of the central retina (Harter 1970) and only a small part of the screen adjacent to the fixation caused the VECP. The pattern-reversal was time-locked to the refresh of the monitor screen, so the phase of the signal could be increased by moving the fixation marker down the screen. Taking the refresh rate into account, a theoretical phase change of 50 degrees was predicted between signals recorded whilst viewing a fixation marker at the top of the screen as against viewing a marker at the bottom. The fixation marker was moved down the screen by 2° every 10 s, the total recording time was 110 s.

### **3.4.4. Results**

#### **Evaluation with simulated signals**

##### Filter settling time

Figure 3.7 demonstrates the response of the ANC to a constant 5  $\mu\text{V}$  input signal with no added noise for time constants of 2, 4 and 8 s. The practical settling time matched the theoretical prediction, the output settling to 95 % of the input value after four time constants.

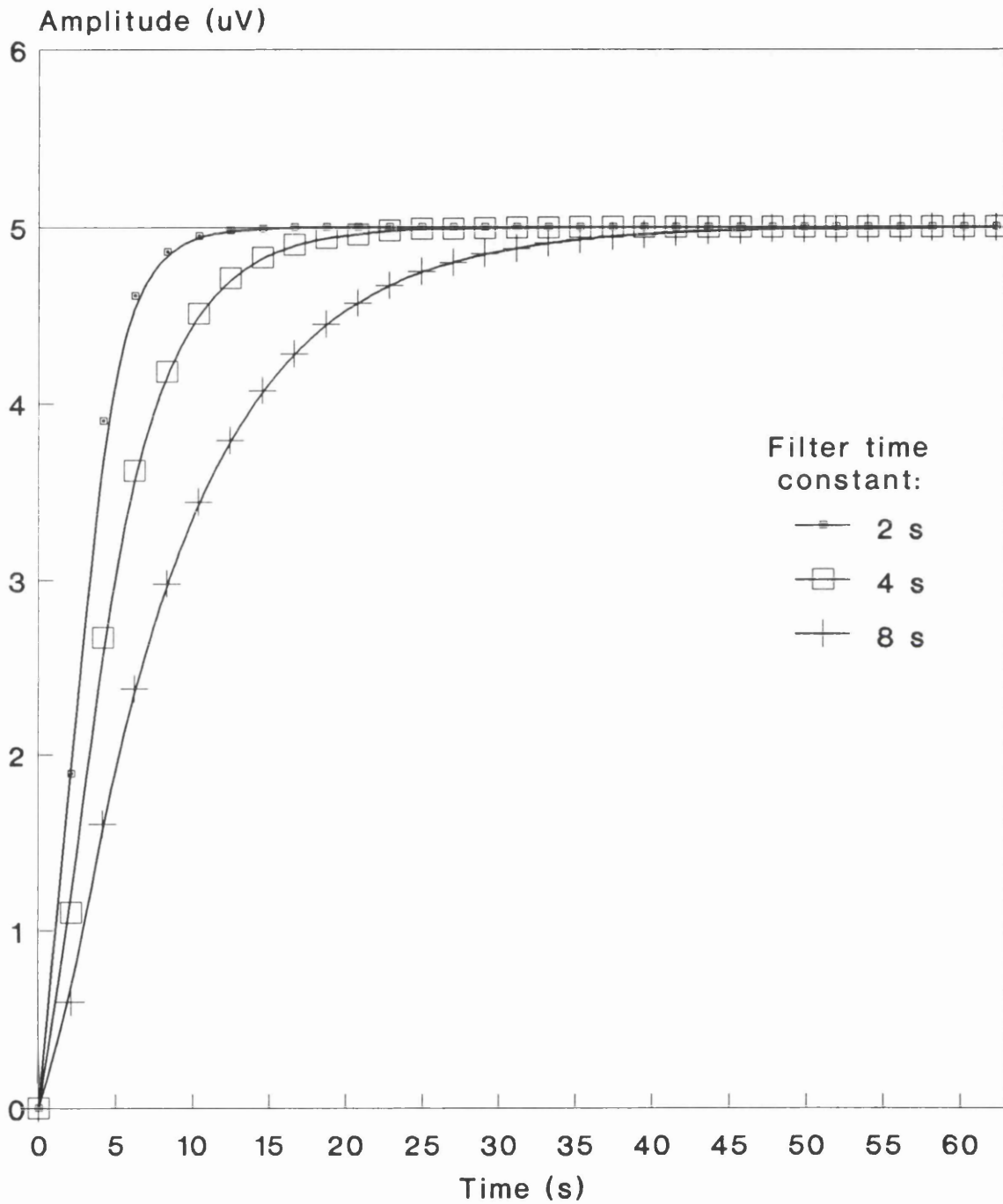


Figure 3.7 Response of the adaptive noise canceller to a 5  $\mu\text{V}$  signal, using various time constants.

### Simulated EEG activity

With the addition of simulated EEG activity the LMS algorithm made noisy adjustments resulting in a noisy estimate of the VECF signal. Figure 3.8 illustrates the result using filter time constants of 2 and 8 s for a signal input of 5  $\mu\text{V}$ . The filter output settled at a rate dependent on the filter time constant which is a function of the convergence parameter  $\mu$  (equation 10). The final estimate of the signal was also dependent on  $\mu$ ; the slower the rate of convergence, the smaller the final measurement error. For a slower rate of convergence the filter effectively had a narrower bandwidth causing it to filter out more noise.

### Tracking non-stationary signals in noise

The simulation in which the amplitude of a signal was linearly reduced is illustrated in Figure 3.9 and the simulation in which the phase was changed is illustrated in Figure 3.10. Due to the finite response of the filter the output tracked the input with a time lag. For slower rates of convergence the lag was longer because the filter required longer to respond to changes in the signal form.

### Accuracy and precision of measurement

The results of the comparison between the ANC and the Fourier transform are illustrated in Figure 3.11. In all cases the signal amplitude was overestimated due to noise. The results from the phase insensitive ANC and the FFT were very similar. The phase sensitive ANC was more precise due to an improved SNR.

### Reliability of signal detection

The phase sensitive ANC was the most sensitive signal detector. Signals of 0.5  $\mu\text{V}$  amplitude were detected with greater than 99 % confidence. Signals of 0.25  $\mu\text{V}$  amplitude were detected with greater than 97.5 % confidence in three cases and with greater than 95 % confidence in one case.

The phase insensitive ANC was able to detect signals of 0.5  $\mu\text{V}$  amplitude with a probability of greater than 99 %. A signal of 0.25  $\mu\text{V}$  amplitude was detected in one case ( $p > 0.975$ ) but in other three cases the probability of signal detection was not significant ( $p < 0.95$ ).

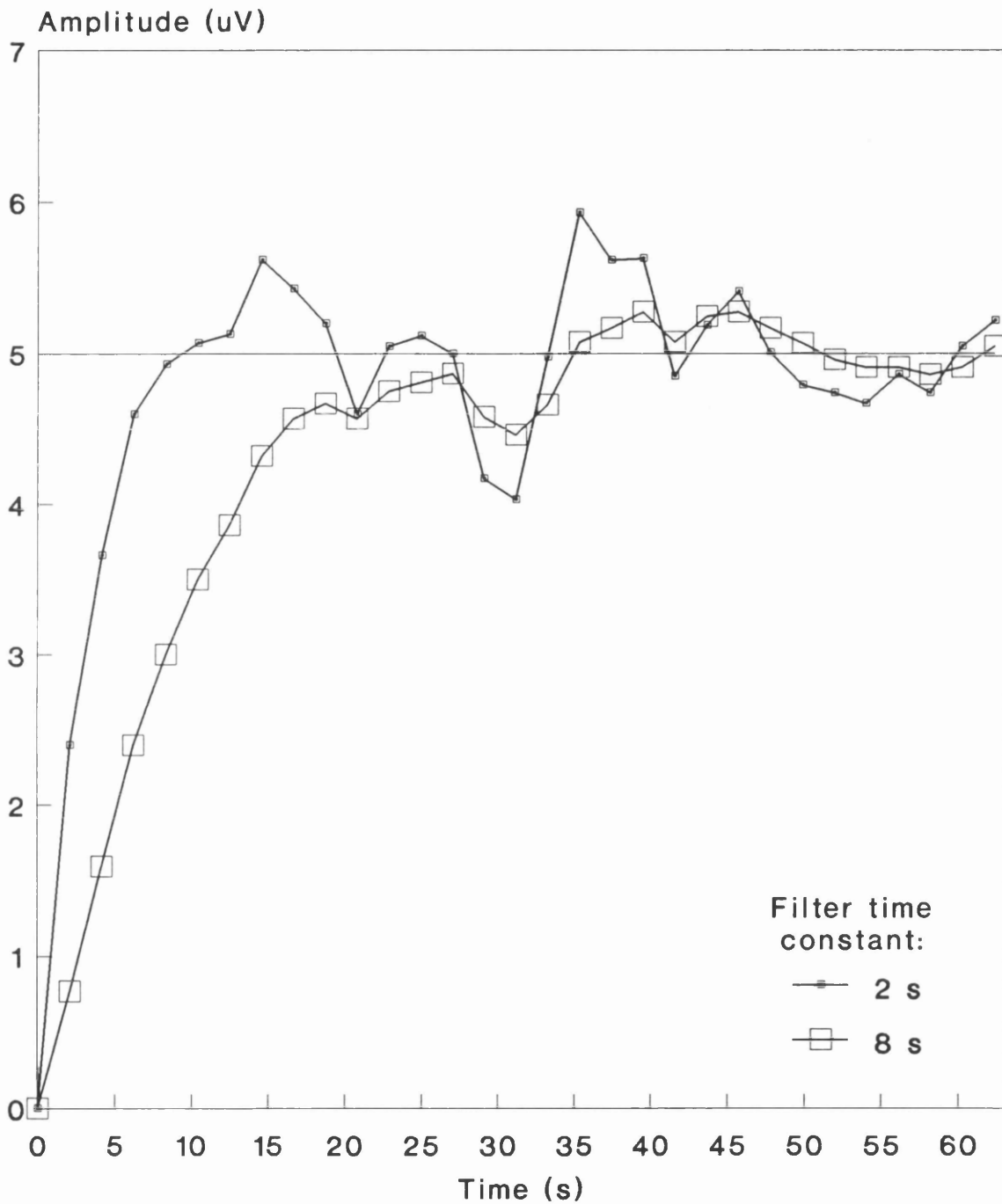


Figure 3.8 Response of the adaptive noise canceller to a 5  $\mu\text{V}$  signal in simulated EEG activity.

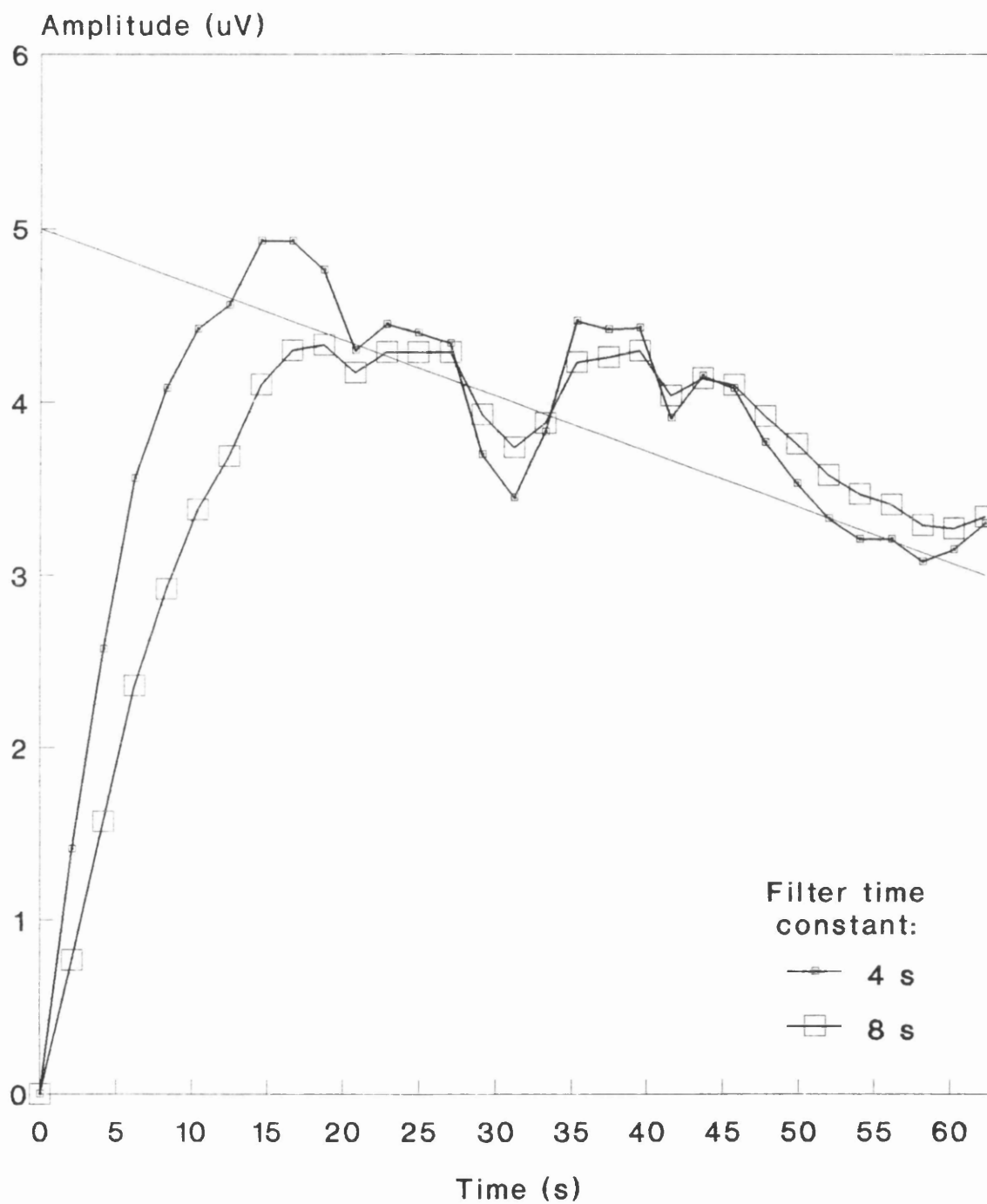


Figure 3.9 Response of ANC to a time varying signal in simulated EEG activity  
Signal amplitude varied from 5 to 3  $\mu\text{V}$ .

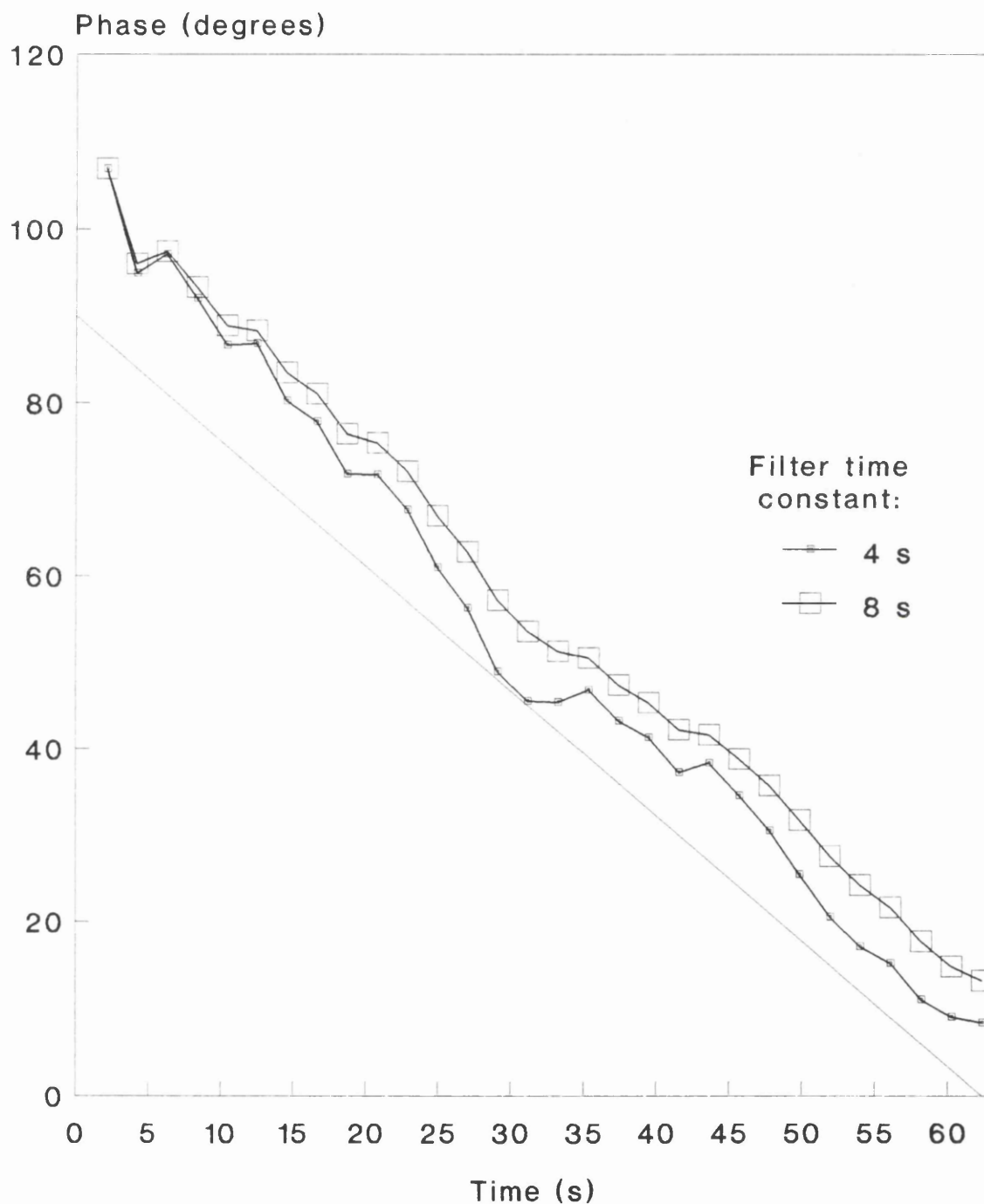
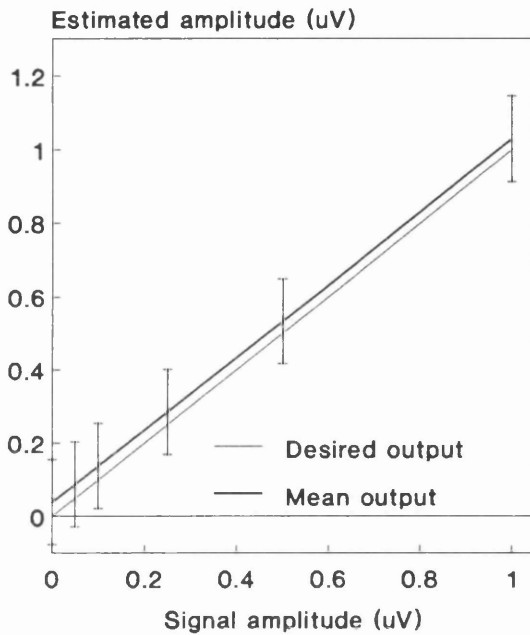
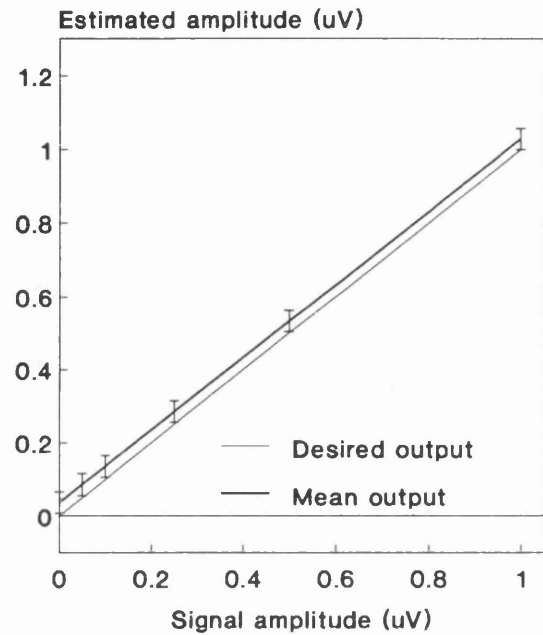


Figure 3.10 Response of ANC to a time varying signal in simulated EEG activity  
Signal phase varied from 90 to 0 degrees

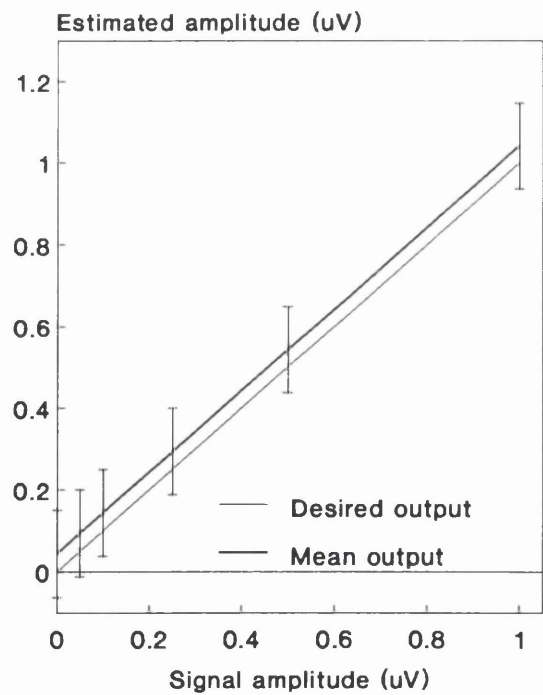


a) Using the phase insensitive adaptive noise canceller (ie. equally sensitive to all phases).



b) Using the phase sensitive adaptive noise canceller (ie. optimally sensitive to the signal phase).

Figure 3.11 Accuracy and precision of signal measurement using various methods of signal analysis.



c) Using the fast Fourier transform.

The FFT was the least sensitive detector. Signals of  $0.5 \mu\text{V}$  amplitude were detected with greater than 99 % confidence in three cases and with a probability greater than 97.5 % confidence in one case. For signal amplitudes of  $0.25 \mu\text{V}$  the probability of signal detection was not significant ( $p < 0.95$ ).

## **Evaluation with real physiological signals**

### Effect of filter time constant

Figure 3.12 shows the response recorded from a normal subject using a pattern-reversal stimulus. The filter output rose at a rate dependent on the filter time constant. There is evidence of a large initial signal amplitude which was missed by the longer time constants.

### Tracking amplitude changing signals

When the stimulus contrast was reduced to zero the filter output correctly reduced towards zero (Figure 3.13) and then increased when the contrast was increased. A three point smoothing filter was applied to the displayed data. The finite response time of the adaptive filter and the presence of EEG noise prevented the output from falling exactly to zero.

### Tracking phase changing signals

As predicted the phase of the filter output increased as the fixation position moved down the monitor screen (Figure 3.14). Using linear regression the measured phase change was 46 degrees, this agrees closely with the theoretical prediction of 50 degrees.

## **3.4.5. Discussion**

The ANC is a self-optimising detector or filter and it can be applied to the measurement of steady-state VECPs. Its performance has been evaluated using both real and simulated data and the results have closely matched the theoretical predictions.

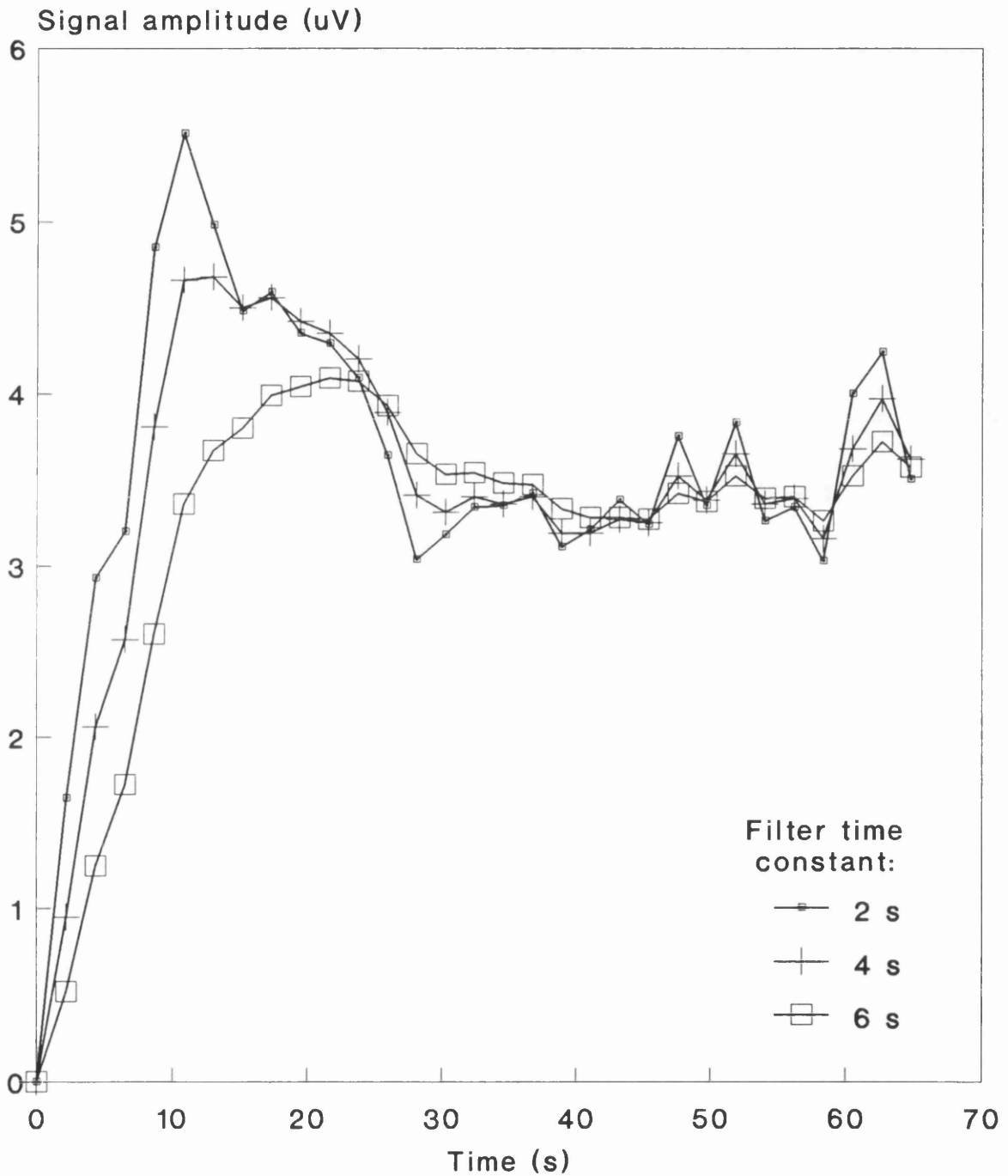


Figure 3.12 Response of the adaptive noise canceller to a steady-state VECF recording.

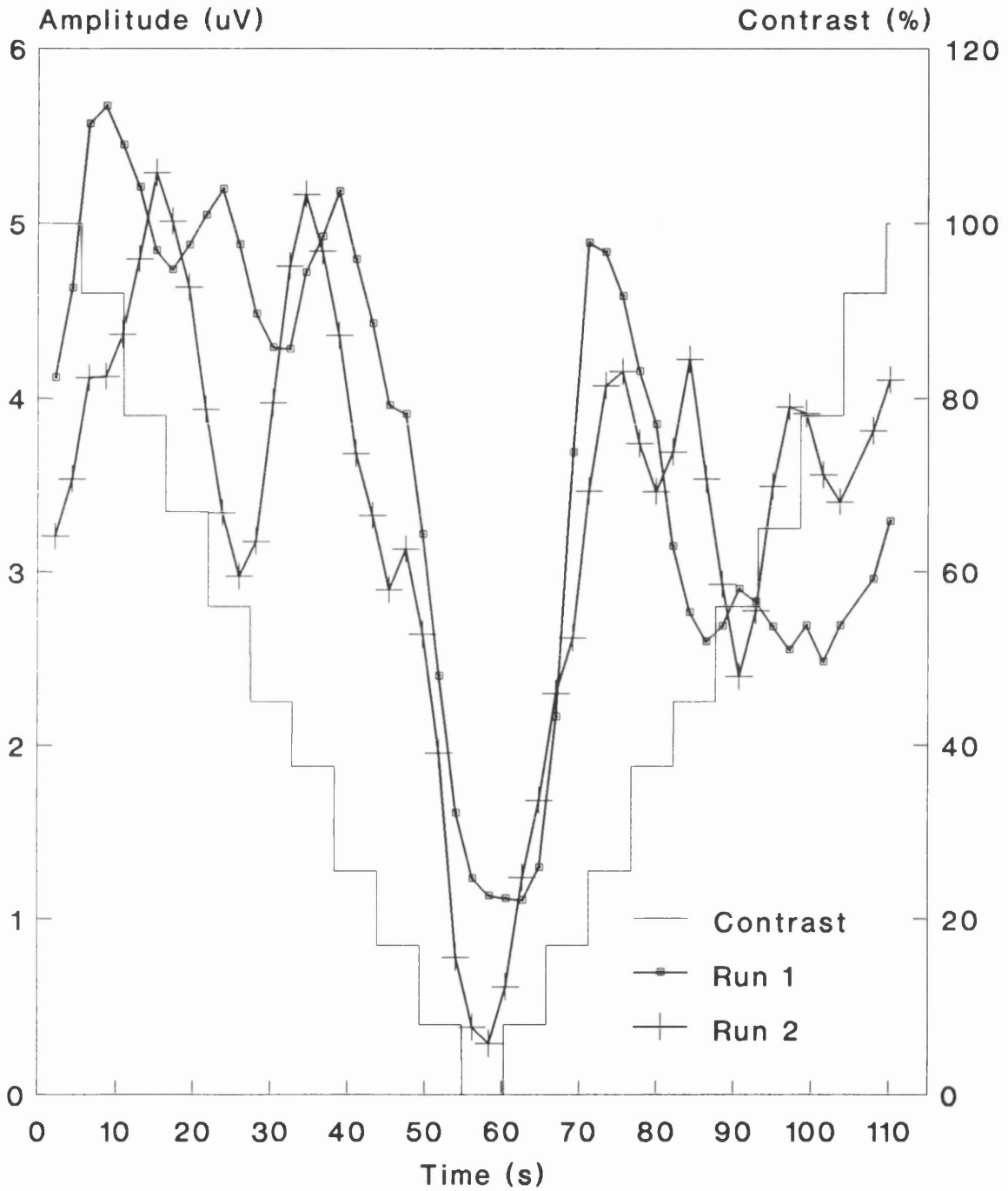


Figure 3.13 Response of the ANC to a time varying steady-state VECP. The amplitude varied with stimulus contrast.

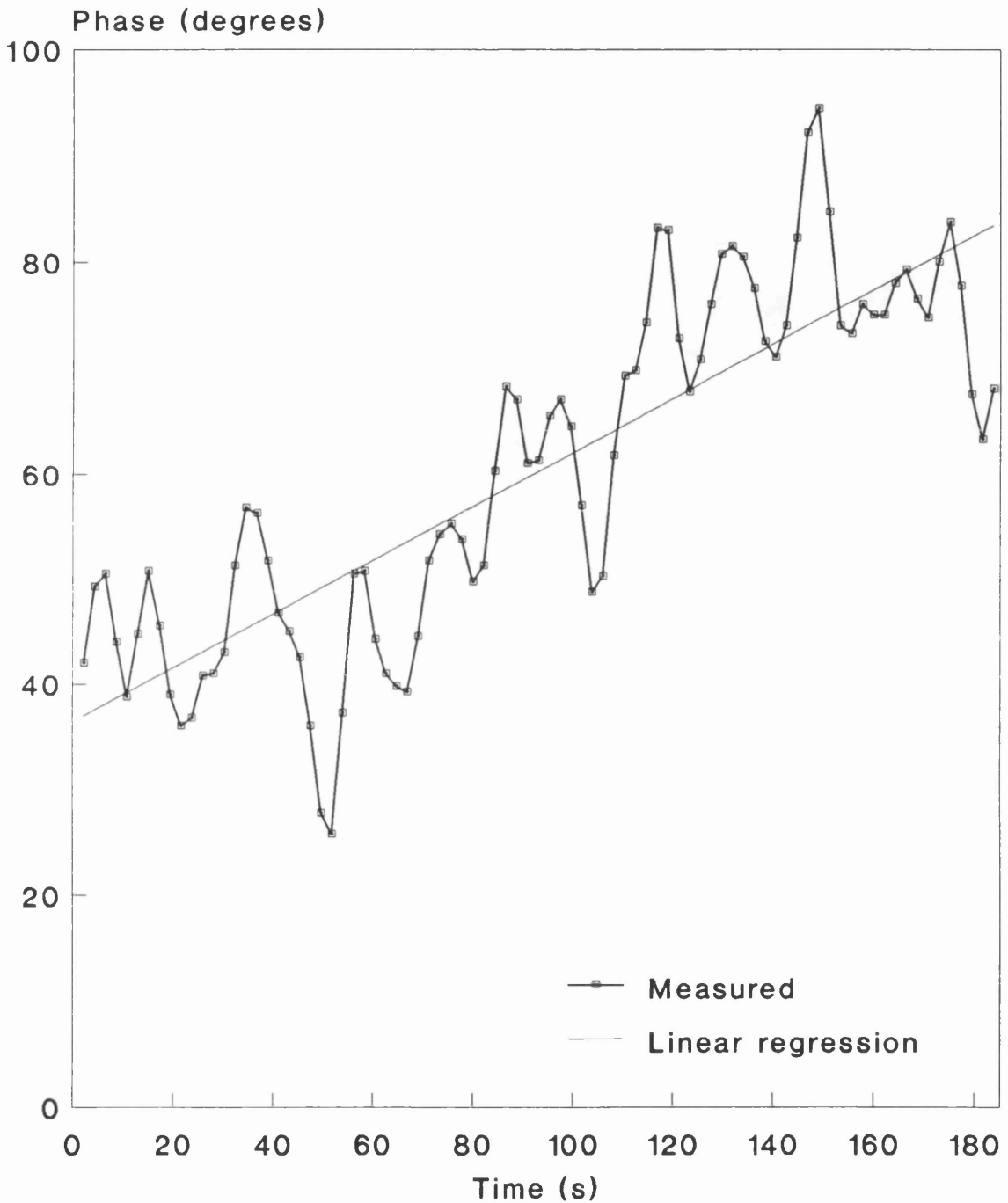


Figure 3.14 Response of the ANC to a time varying steady-state VECP, due to a variation in the stimulus phase.

The filter bandwidth is simply controlled using one parameter, the convergence parameter. The slower the rate of convergence, the narrower the filter bandwidth and the smaller the measurement error. In practice, a compromise is made between the response time and the accuracy of the measurement. The ANC uses a very simple algorithm and so is very flexible; the convergence rate could even be modified during a recording according to the SNR or presence of artefact.

When the ANC is implemented as a phase insensitive detector, temporal information on the signal amplitude and phase is available from the filter output. This information is obtained by vector averaging the output over a period of time, dependent on the convergence rate. For a constant stimulus the temporal information can be used to assess the stability of the recording. If the phase of the adaptive filter output is relatively stable, the phase of the reference signal can be fixed and the ANC can then be used as a phase sensitive detector with an enhanced SNR. If the filter output is not stable this may indicate adaptation to the stimulus, habituation, fatigue, poor fixation or a low SNR. In such instances it would be inappropriate to use the adaptive filter as a phase sensitive detector unless prior information on the signal phase was known.

The ability of the ANC to track temporal changes in the signal amplitude and phase means that it can also be applied to the measurement of sweep VECPs where the stimulus parameters are swept with time. During sweep measurements the VECP can shift phase by nearly 360 degrees (Norcia et al 1985). In this situation it would be inappropriate to use the ANC as a phase sensitive detector because it would severely distort the measurement.

The ANC is very simple to implement in the laboratory. The LMS algorithm is computationally efficient and each iteration of a two weight adaptive linear combiner requires only six multiplications and three additions. With low-cost, high-speed digital signal processors available on commercial cards the ANC can be implemented in real-time in a personal computer.

The assumption that most of the steady-state VECP energy is contained in a single frequency component at the stimulus frequency is a good approximation for stimulus frequencies in excess of 10 reversals per s. For stimulus frequencies of less than 10 reversals per s a greater proportion of the signal energy is contained in the signal harmonics. Each harmonic adds an additional sine and cosine component to the reference signal and two weights to the adaptive linear combiner.

The ANC has a number of advantages over the popular FFT:

1. The ANC can be used as a phase sensitive or phase insensitive detector whilst the FFT can only be used as a phase insensitive detector.
2. When used as a phase sensitive detector the ANC provides a larger SNR, improving signal detection.
3. A standard two weight adaptive linear combiner requires approximately one third the number of multiplications as an FFT. Taking a 1024 point data sample as an example the ANC requires  $6 \times 1024$  multiplications whilst the FFT requires 5120 complex multiplications ( $\frac{N}{2} \log_2 N$  complex multiplications where N is the number of data points (Bergland 1969)). If more than three harmonics are to be measured the ANC loses its computational advantage.
4. The ANC requires virtually no memory whilst the FFT requires a large amount of memory to store both the data being processed and the result.
5. The ANC is less computationally intensive. The FFT is calculated at the end of the data collection period whilst the ANC is updated after each data point is recorded.
6. The ANC is very versatile and unlike the FFT it would be possible to improve it to include artefact rejection. Artefact rejection is widely used in signal averaging. For example, if the amplitude of the input data exceeds a predetermined threshold amplitude the data is assumed to include artefact, such as a blink, and is ignored. Similarly the ANC could ignore artefact by temporally 'holding' or 'freezing' the values of the weights in the adaptive linear combiner.

### 3.5 CONCLUSION

The steady-state VECP has a number of significant advantages over the transient VECP for developing techniques in electroperimetry. In the frequency domain, the steady-state VECP is represented by discrete components at the stimulus frequency and its harmonics (Spehlmann 1985, Regan 1989). Frequency domain analysis enhances the SNR and the recording can be made faster (Regan 1989). Objective signal detection methods can be used to determine whether a signal has been detected

(Norcia et al 1985, Strasburger 1987, Norcia et al 1989, Eizenman et al 1993). Furthermore, different parts of the visual field can be tested simultaneously if each area is stimulated with a different frequency (Yanashima 1982).

If the phase of the steady-state VECF varies or is unknown then a phase insensitive detector should be used, such as the FFT, which is equally sensitive to all phases (Norcia et al 1985, Strasburger 1987). If the phase is known, a phase sensitive detector can be used to further enhance the SNR (Norcia et al 1985, Strasburger 1987).

The most significant signal processing development described in this chapter is the novel application of adaptive noise cancelling principles to the detection and measurement of steady-state VECFs. The ANC can be implemented as a phase insensitive or a phase sensitive detector. The ANC has a number of operating advantages over the FFT; it is less computationally intensive, it requires less memory, it can be implemented in real-time and it provides continuous temporal information on variation of the VECF signal. The theoretical performance of the ANC has been verified using simulated and real physiological signals.

Objective signal detection of the steady-state VECF has been implemented using Hotelling's  $t^2$  test for the first time.

## 4. STIMULUS DEVELOPMENT

### 4.1 INTRODUCTION

This chapter describes the evaluation and development of visual stimuli for electroperimetry.

Previous studies have used steady-state pattern-reversal quadrant checkerboard stimuli (Cappin and Nissim 1975, Howe and Mitchell 1980, Yanashima 1982). A significant problem with the use of the checkerboard stimulus is that the optimum check-size varies across the visual field, increasing with retinal eccentricity (Harter 1970). So, it was decided to verify these results and to proceed to determine experimentally the optimum check-size for stimulating visual field quadrants of varying angular subtense.

A further limitation of the pattern-reversal checkerboard stimulus is that the VECF amplitude is smaller for stimulation of the peripheral visual field (eccentricity greater than  $12.5^\circ$ ) than for stimulation of the central field (Harter 1970). It has been suggested that motion-onset stimuli produce larger amplitude VECFs than pattern-reversal stimuli when testing the extramacular area of the visual field (Kubova et al 1990, Kubova and Kuba 1992, Kuba and Kubova 1992). It was therefore decided to develop motion-onset stimuli and compare them with pattern-reversal stimuli.

An aim of the current research was to develop an instrument for patients who are unable to fixate on the monitor screen. The instrument would enable VECFs to be recorded whilst patterned stimuli were positioned on the retina under the view of an observer. Due to operational and technical constraints, the optimum stimulus for this instrument was a transient dark pattern-onset stimulus (Section 5.4.1).

## 4.2 STUDY OF STEADY-STATE VECPS FROM PATTERN-REVERSAL STIMULATION OF VISUAL FIELD QUADRANTS

### 4.2.1 Introduction

Steady-state pattern-reversal VECPs from quadrant field stimuli have been used to assess visual field defects in glaucoma (Cappin and Nissim 1975) as well as homonymous hemianopia and quadrantanopia due to cortical lesions (Halliday 1972, Howe and Mitchell 1980, Halliday 1982, Yanashima 1982). The checkerboard pattern-reversal stimulus has a number of advantages over the flash stimulus. It is less variable and has a smaller interindividual range (Spehlmann 1985). In addition, the pattern has a constant mean luminance which minimises the effect of scattered light on the surrounding retina.

The amplitude of the VECP is dependent on the size of the checks in the pattern (Spehlmann 1965, Harter 1970). The optimum check-size increases with retinal eccentricity (Harter 1970). From studies on three subjects, Harter (1970) found that when retinal stimulation was limited to the foveal area, at an eccentricity of  $0^\circ$  to  $1.5^\circ$ , the optimum check-size was between  $15'$  and  $30'$  of arc. When more peripheral areas of the retina were tested (at eccentricities of  $1.5^\circ$  to  $4.5^\circ$ ,  $3^\circ$  to  $6^\circ$  and  $4.5^\circ$  to  $7.5^\circ$ ) the check-size producing the largest amplitude VECP increased (to  $30'$ ,  $30'$  to  $60'$  and  $60'$  of arc respectively). Therefore, for VECP studies of visual field quadrants, the optimum check-size should vary according to the stimulus field-size.

As a result of his findings, Harter (1970) proposed that the most effective check-size for stimulating a particular retinal location corresponds to the modal size of the ganglion receptive fields at that location. However, studies on visual resolution and contrast sensitivity in man (Virsu and Rovamo 1979, Hess and Pointer 1988), together with studies on visual resolution and ganglion cell dendritic field sizes in the macaque monkey (Crook et al 1988, Perry and Cowey 1981), have shown that the ganglion receptive fields are about an order of magnitude smaller than the optimum check-sizes determined by Harter. In man, the visual resolution can reach 60 cycles per degree ( $0.5'$ ) in the fovea and a few cycles per degree ( $15'$ ) in the peripheral retina (Virsu and Rovamo 1979). Consequently, the most effective check-size for VECP recording is not directly related to the receptive fields of the retinal ganglion cells and must be determined by a higher level of image processing, presumably in the visual cortex.

It is possible that the most effective check-size for stimulation at a particular retinal eccentricity is related to the cortical magnification factor. The cortical magnification factor is a linear scale for mapping from the visual field to the striate cortex and was defined by Daniel and Whitteridge (1961) as the distance in mm in the striate cortex corresponding to a  $1^\circ$  angle for a particular location in the visual field. The cortical magnification factor is proportional to the linear density of the retinal ganglion cell receptive fields (Rovamo and Virsu 1979, Curcio and Allen 1990) and is inversely proportional to retinal eccentricity (Rovamo and Virsu 1979, Horton and Hoyt). Visual resolution and contrast sensitivity are inversely proportional to the cortical magnification factor (Virsu and Rovamo 1979, Rovamo and Virsu 1979) and it is possible that the most effective check-size for recording VECF signals is similarly related.

A number of formulae have been derived to estimate the cortical magnification factor at different retinal eccentricities (Rovamo and Virsu 1979, Horton and Hoyt 1991). Rovamo and Virsu (1979) based their formulae on published data on the density distribution of retinal ganglion cells. The density of the ganglion cells varies slightly along different retinal meridians (Rovamo and Virsu 1979, Curcio and Allen 1990) so they derived a different formula for each of the principal half-meridians (nasal, superior, temporal and inferior). The retinal ganglion cells are displaced in the fovea (Section 1.1.1), so for this region Rovamo and Virsu had to estimate the cortical magnification from the density of the cones, assuming that there are 0.9 ganglion cells per cone (Missotten 1974). Horton and Hoyt (1991) based their formula on published formulae for the macaque monkey (Hubel and Freeman 1977, Van Essen and Newsome 1984, Dow et al 1985, Le Vay et al 1985, Schein and de Monasterio 1987 and Tootell et al 1988) which they then scaled to the size of the human striate cortex.

The main aims of this study were:

1. To determine the most effective check-size for VECF recording from visual field quadrants of varying angular subtense.
2. To confirm the most effective check-sizes for VECF recording from different retinal eccentricities (Harter 1970).
3. To investigate whether the optimal check-sizes are inversely proportional to the cortical magnification factor.

A recent study of central field stimuli, up to  $12^\circ \times 12^\circ$  in size, showed that there is a maximum number of pattern elements, 300 to 400, above which the VECF amplitude shows little or no increase (Katsumi et al 1988). It was decided to investigate whether a similar effect occurs when visual field quadrants are stimulated.

#### **4.2.2 Subjects and methods**

Seven normal subjects, six males and one female, ranging in age from 23 to 48 years (mean age 31 years) were investigated. All subjects had normal visual fields, had a visual acuity better than or equal to 6/6, were optically corrected for the viewing distance of 40 cm and had normal pupils (3 to 6 mm).

The stimulus was presented on the computer monitor. Monocular recordings from the left eye were made for separate stimulation of the inferior nasal and superior nasal field quadrants. Six check-sizes were investigated (15', 30', 60', 90', 120' and 180') for a combination of stimulus field-sizes (including  $2^\circ \times 2^\circ$ ,  $3^\circ \times 3^\circ$ ,  $4^\circ \times 4^\circ$ ,  $6^\circ \times 6^\circ$ ,  $9^\circ \times 9^\circ$ ,  $12^\circ \times 12^\circ$ ,  $18^\circ \times 18^\circ$  and  $24^\circ \times 24^\circ$ ). The pattern contrast was greater than 99 %, and the mean luminance was  $3 \text{ cd} / \text{m}^2$ . The stimulus frequency was chosen to be close to the 12 pattern-reversals per second used in previous studies (Cappin and Nissim 1975, Katsumi et al 1988). The exact frequency was 11.6 reversals per second, since the pattern-reversal was synchronised to the screen refresh rate to prevent latency jitter of the stimulus.

A grey background was generated on the screen with a luminance equal to the mean pattern luminance. This background ensured that the overall screen luminance remained constant during the experiments and also minimised retinal stimulation due to scattered light. The test subjects viewed a fixation letter, which helped them to focus in the plane of the screen. The fixation letter was 20' wide and 40' high, so it only obscured a small corner of the stimulus field. The experiments were performed in a darkened room, with an ambient illumination of 10 lux, to prevent light adaptation due to scattered room lighting and reflections.

Recordings were made from the occipital sites MO, RO and LO relative to the mid-frontal position MF (Section 2.9.2). A guard electrode was positioned on the scalp within the hairline. The amplifier low frequency cut-off was 0.8 Hz and the high frequency cut-off was 100 Hz.

The VECPs were digitised and processed in the DSP card. The signals were initially analysed by Fourier analysis of time-averaged data. Fifty sweeps of six integer cycles were averaged. This technique generally worked well; however, if averaging precedes spectral analysis, information can be lost irretrievably (Regan 1989). To overcome this problem, the system software was further developed to average spectra from 8-second segments of raw data.

### 4.2.3 Results

When the inferior nasal quadrant of the left eye was stimulated, the VECP distribution on the scalp followed clear individual patterns for each subject. In three subjects, the largest VECP amplitude was recorded at MO for all stimuli. In one subject, the largest VECP amplitude was recorded at LO for all stimuli. In the other three subjects, the largest amplitude was either at MO or LO; in two subjects it was at MO for stimulus field-sizes greater than  $2^\circ \times 2^\circ$ , and in the third subject it was at the MO location for check-sizes less than  $90'$ . The VECP distribution from stimulation of the superior nasal quadrant showed no clear individual patterns, the maximum VECP occurred at any one of the three recording sites, but most often at LO.

Figure 4.1 shows the relationship between maximum VECP amplitude and check-size for different stimulus field-sizes in the inferior nasal quadrant. The electrode site used for recording the maximum VECP amplitude varied according to the topographic distribution of the VECP. The graphs show that the check-size giving the largest VECP amplitude increased with increasing field-size. Measurements for the superior nasal quadrant are plotted in Figure 4.2; again the electrode site varied according to the topographic distribution of the VECP. In the superior quadrant the amplitudes were smaller, but, as in the inferior quadrant, the check-size giving the largest amplitude tended to increase with increasing field-size.

In Figure 4.3, the mean values from Figure 4.1 are plotted against stimulus field-size. The error bars in Figure 4.1 have not been included in Figure 4.3 for the sake of clarity. Whilst there were inter-individual variations in the VECP amplitude at given field-size and stimulus check-size, all subjects showed a similar pattern of amplitude variation with varying stimulus check-size and field-size. The mean data presented in this graph therefore enable the most appropriate check-size to be chosen for assessing a particular size of visual field. The plots show that there are maximum stimulus sizes above which particular check-sizes yield limited additional information. For example,

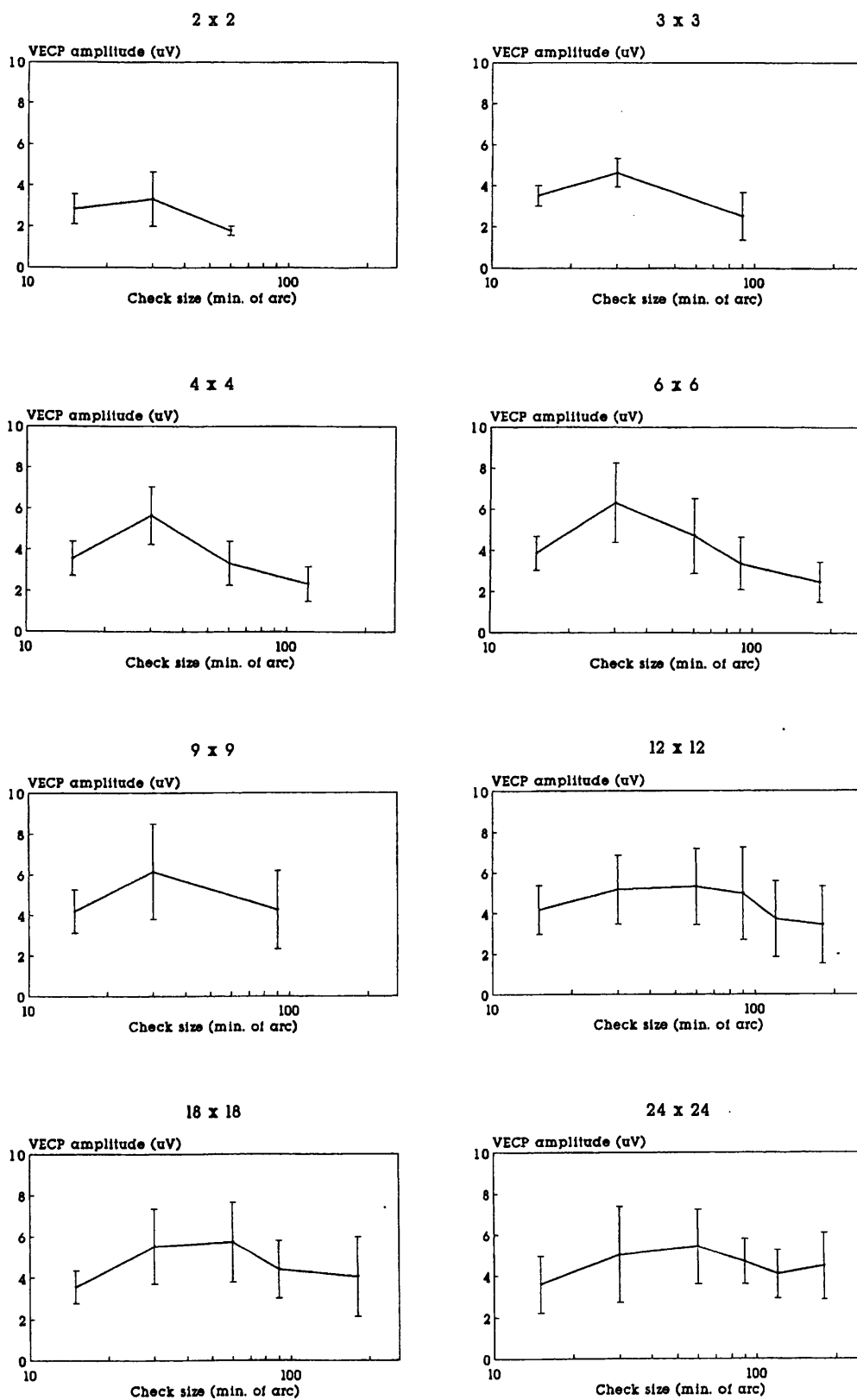


Figure 4.1 The relationship between maximum VECP amplitude and check-size for different stimulus field-sizes in the inferior nasal field quadrant.

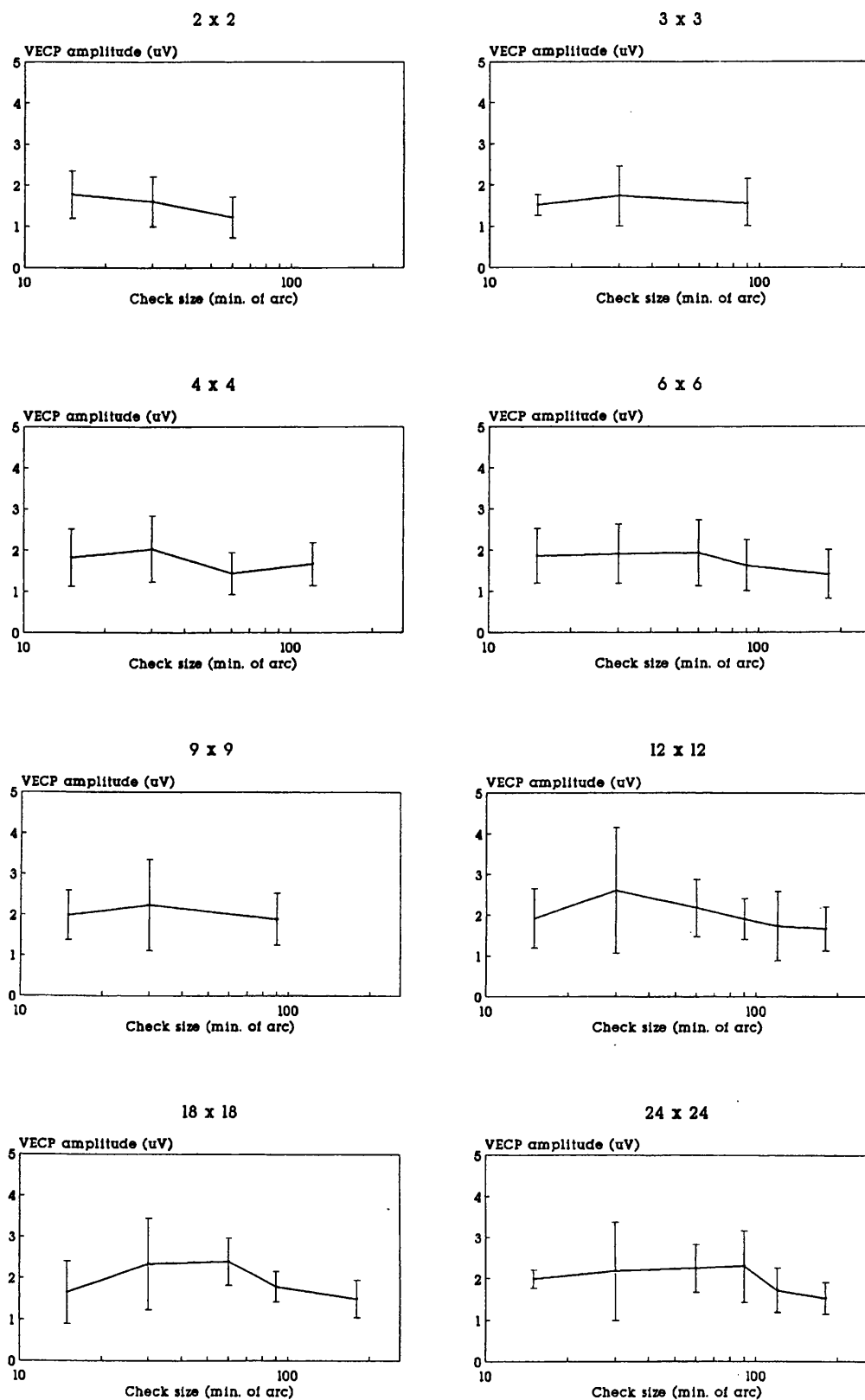


Figure 4.2 The relationship between maximum VECP amplitude and check-size for different stimulus field-sizes in the superior nasal field quadrant.

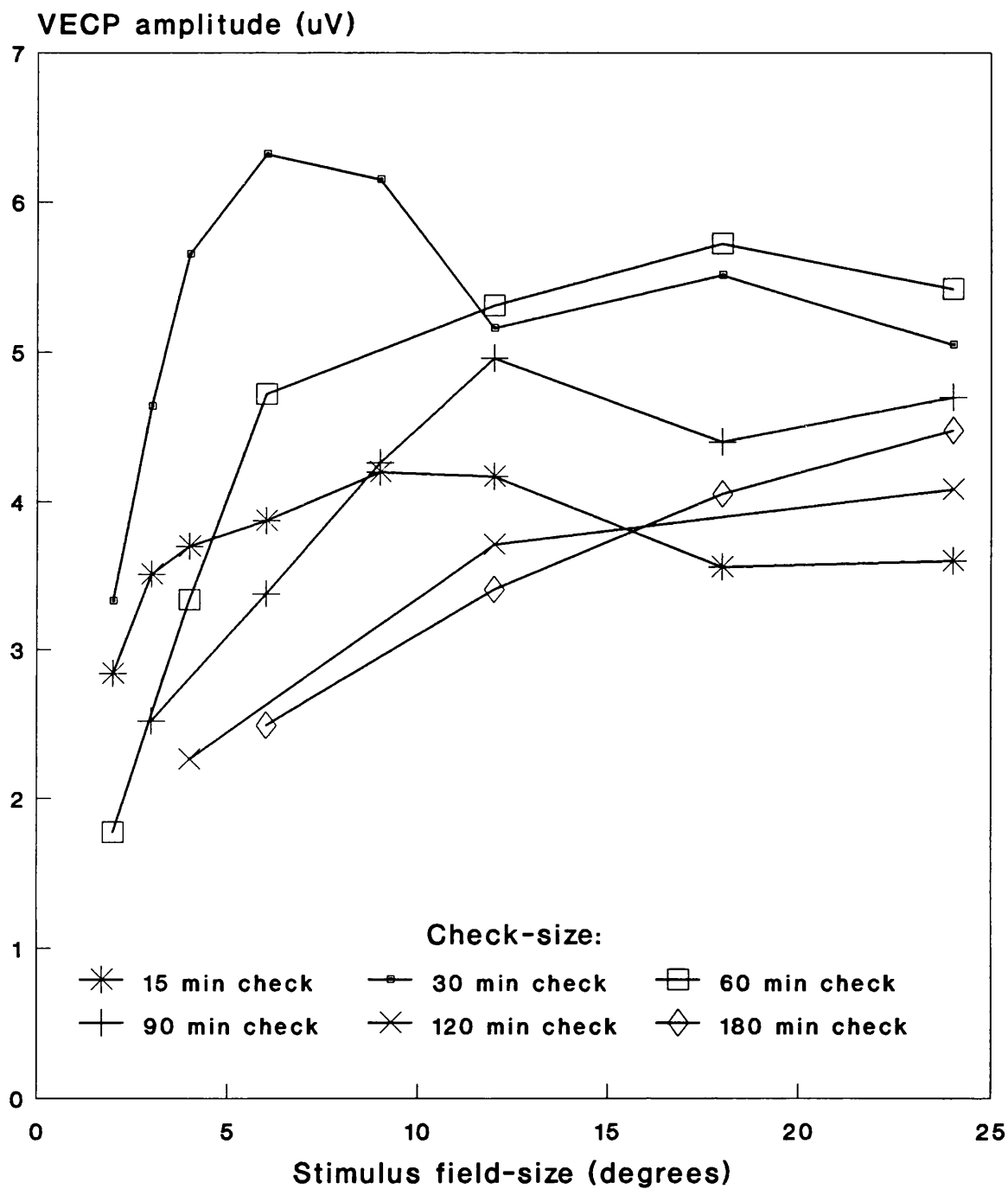


Figure 4.3 VECP amplitude for different stimulus field-sizes and check-sizes in the inferior nasal quadrant

the gradient of the plot for 60' checks is reduced above a stimulus size of 6° x 6°. The 60' check-size is therefore not clinically useful for assessing quadrant fields greater than 6° x 6°, even though it gives slightly larger VECP amplitudes for field-sizes up to 18° x 18°. This is because field areas between 6° x 6° and 18° x 18° are only represented by small proportions of the total VECP signal. The best check-size for assessing a particular field-size is that which gives the largest VECP amplitude, as long as the gradient of the plot has not decreased or become negative. The most effective check-size for assessing each field-size is summarised in Table 4.1.

The most effective check-size for recording VECP signals from different retinal eccentricities can also be derived from Figure 4.3. The most effective check-size is the one that produces the largest VECP signal at a particular retinal eccentricity and this corresponds to the check-size whose VECP amplitude response has the steepest positive gradient. So, for example, the 30' check-size is optimum for stimulation between retinal eccentricities of 2° and 3°. The optimal check-sizes for the complete range of retinal eccentricities are summarised in Table 4.2 and are plotted in Figure 4.4. The optimal check-sizes determined by Harter (1970) are also plotted in Figure 4.4.

In order to investigate whether the optimum check-size is related to the reciprocal of the cortical magnification factor, the formulae for cortical magnification derived by Rovamo and Virsu (1979) and Horton and Hoyt (1991) were used to produce curves estimating the optimal check-size with retinal eccentricity (Figure 4.4). These curves were scaled to give an optimum check-size of 30' at a retinal eccentricity of 2.5°. According to Rovamo and Virsu (1979) the cortical magnification factor for the nasal half-meridian is:

$$7.99 / (1 + 0.33 E + 0.00007 E^3) \text{ mm}/^\circ$$

and the cortical magnification for the inferior half-meridian is:

$$7.99 / (1 + 0.42 E + 0.000055 E^3) \text{ mm}/^\circ$$

where E is retinal eccentricity in degrees. The cortical magnification in the inferior nasal quadrant was estimated by using the mean value of the two equations.

According to Horton and Hoyt (1991) the formula for the cortical magnification factor is:

$$17.3 / (E + 0.75) \text{ mm}/^\circ$$

**Table 4.1 Optimum check-size for assessing visual field quadrants of varying angular subtense, based on mean VECF recordings from seven subjects.**

Field-size (degrees)	Optimum check-size (minutes)
2 x 2	30
3 x 3	30
4 x 4	30
6 x 6	30
9 x 9	90
12 x 12	90
18 x 18	180
24 x 24	180

**Table 4.2 Optimum check-size for VECF recording from varying retinal eccentricities, based on mean recordings from seven subjects.**

Retinal eccentricity (degrees)	Optimum check-size (minutes)
2 to 3	30
3 to 4	30
4 to 6	60
6 to 9	90
9 to 12	90
12 to 18	180
18 to 24	180

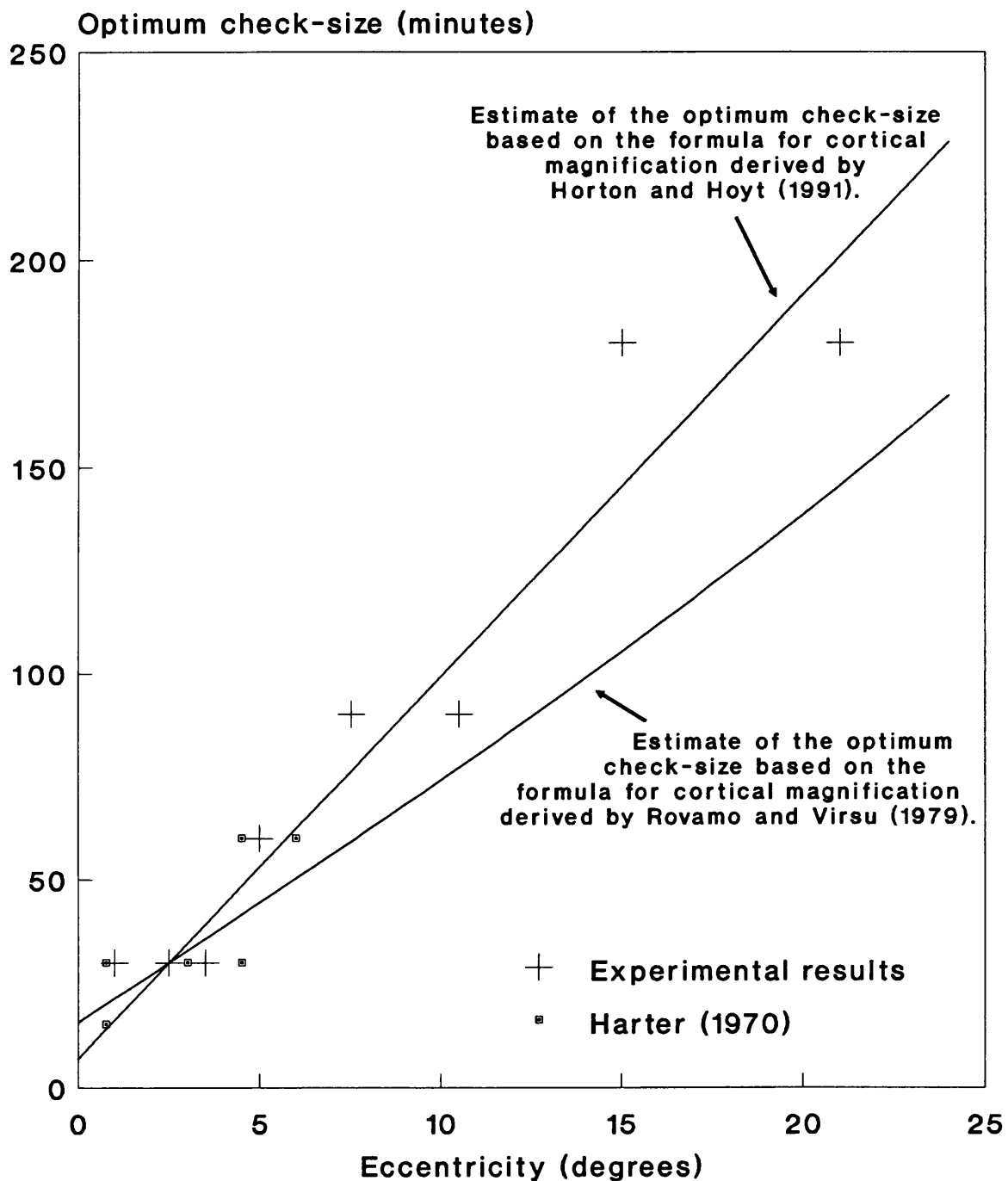


Figure 4.4 Optimum check-size versus retinal eccentricity for the inferior nasal field quadrant.

Referring to Figure 4.4, the curve based on the formula derived by Horton and Hoyt (1991) provides the best fit estimate to the experimentally derived optimal check-sizes.

In Figure 4.5, the mean VECF amplitudes from the superior nasal field quadrant are plotted against stimulus size. For clarity, only data for check-sizes of 30', 60' and 90' are shown. These plots show similar trends to those seen in the data from the inferior nasal quadrant (Figure 4.3).

Figure 4.6 shows the values of Figure 4.3 with the x-axis replotted as the number of pattern elements. The gradients diminish, and in some cases become negative, when the stimulus is composed of approximately 40 to 100 pattern elements. The superior nasal quadrant has not been analysed to this level of detail because of the small signal amplitudes and consequently small SNR.

#### 4.2.4 Discussion

The results of this study have confirmed the findings of Harter (1970) that the optimum check-size for recording VECF signals increases with retinal eccentricity in the central area of the visual field. Furthermore, the optimum check-size for each eccentricity also closely agree with the results of Harter (Figure 4.4).

When Harter tested more peripheral areas of the visual field, between retinal eccentricities of  $12.5^\circ$  and  $27.5^\circ$ , he found that the check-size had little influence on the amplitude of the VECF signal. These findings are contradicted by the current study which suggests that the optimum check-size continues to increase with retinal eccentricity. Both studies agree, however, that the amplitude of the VECF signal is small when this part of the visual field is stimulated. The difference in the results may be due to the fact that Harter (1970) did not use an isoluminant stimulus. As a result, the VECF signals recorded by Harter would have included a luminance response in addition to a pattern specific response and this may have masked the effect of the pattern. Indeed, there is electrophysiological evidence which suggests that for large stimulus checks, the visual system responds more to local luminance stimulation than it does to the contrast difference between pattern elements (Regan 1977, van den Berg et al 1988).

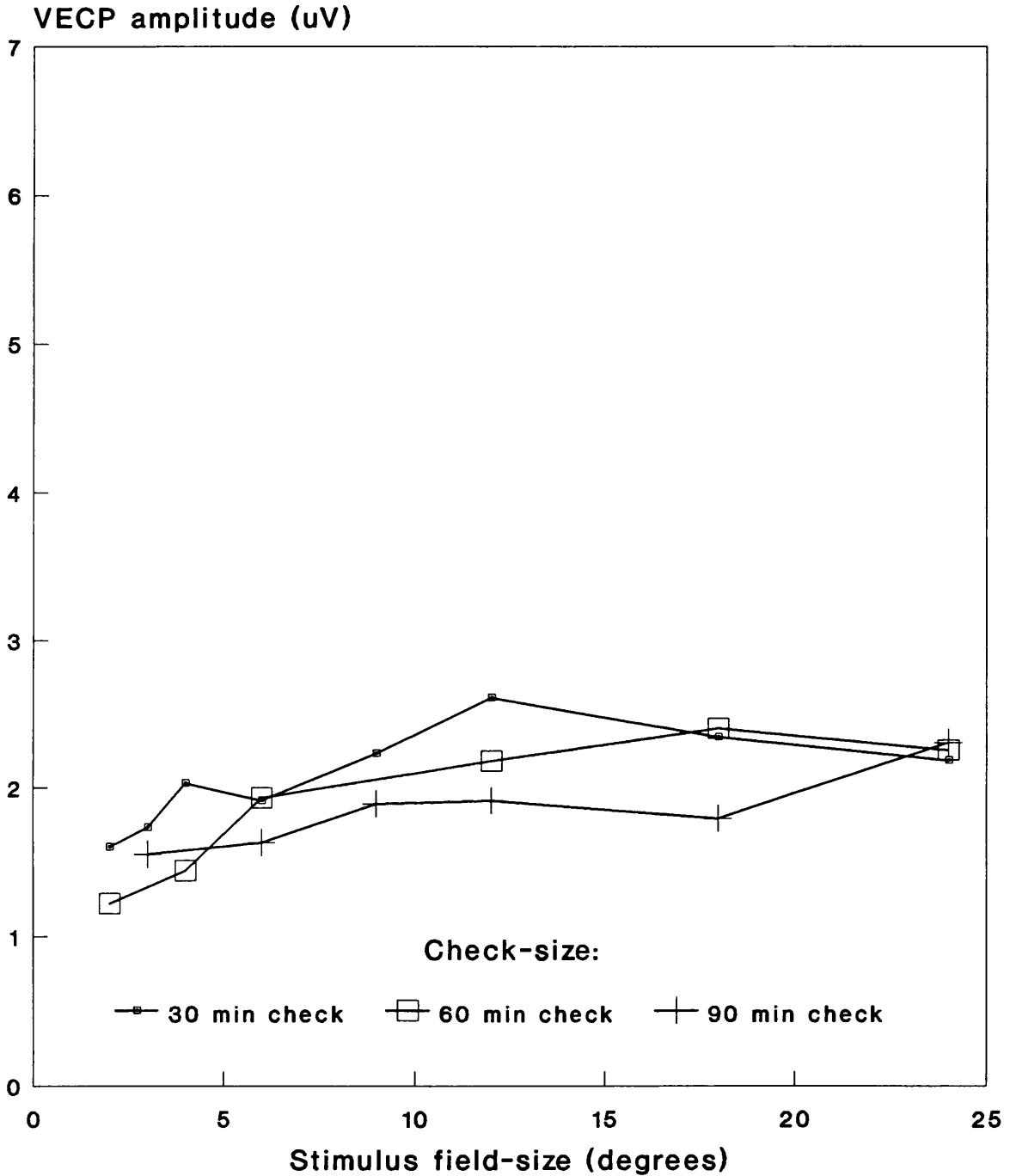


Figure 4.5 VECP amplitude for different stimulus field-sizes and check-sizes in the superior nasal quadrant

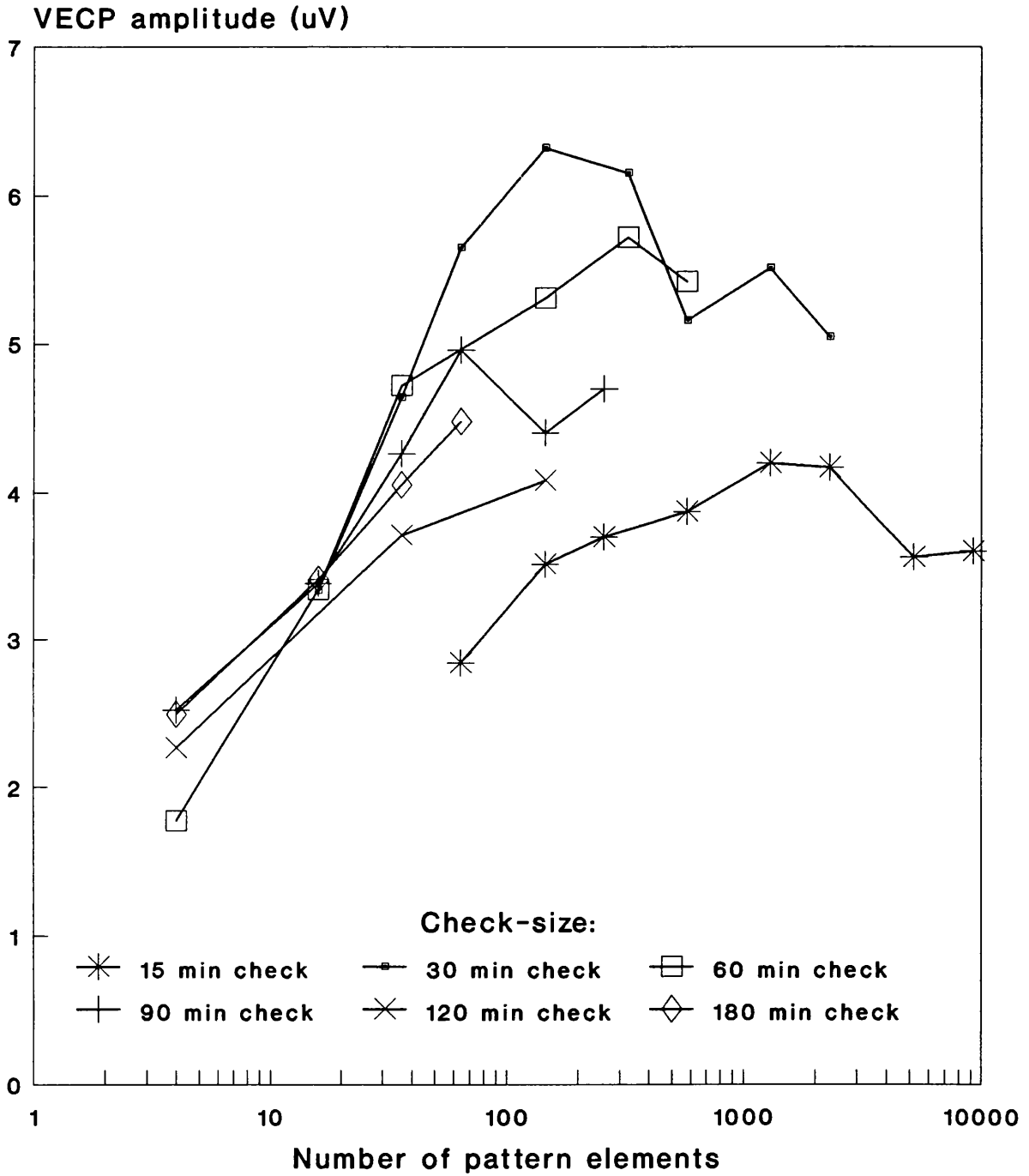


Figure 4.6 VECP amplitude for different numbers of pattern elements in the inferior nasal quadrant

The results of this study are compatible with the hypothesis that the optimum check-size is inversely proportional to the cortical magnification factor. There was good agreement between the experimentally derived optimal check-sizes and an estimated curve based on the formula for cortical magnification derived by Horton and Hoyt (1991). There was, however, less agreement with a curve based on the formulae for cortical magnification derived by Rovamo and Virsu (1979). At this juncture, it is not known which of the formulae for cortical magnification is most reliable. However, Horton and Hoyt were able to verify their formula by means of MRI scans. It is assumed that the optimal check-sizes are the same in each visual field quadrant, although it is possible that there would be a small variation due to differences in the density of ganglion cells in different parts of the retina (Rovamo and Virsu 1979, Curcio and Allen 1990).

When the inferior nasal quadrant was stimulated with a checkerboard composed of checks of size 15' to 120' there was a maximum field-size beyond which the VECF amplitude yielded limited additional information. The maximum field-size corresponded to approximately 40 to 100 pattern elements. A maximum VECF amplitude was not observed for a check-size of 180' because the pattern was limited to a maximum of 64 pattern elements due to the monitor screen size. This feature of an optimal number of pattern elements agrees with the findings of the recent central field study by Katsumi et al (1988), who described it as saturation. The optimal number of pattern elements obtained by Katsumi, 300 to 400 is approximately four times the number found for quadrant field stimulation in our study. Katsumi et al speculated that there exists in the visual system a preferred ratio of check-size to stimulus size related to a certain number of pattern elements and claimed that this was consistent with psychophysical evidence. Whether this speculation is correct or not, the observation of an optimal number of pattern elements is a useful empirical relationship for choosing an appropriate check-size for the investigation of a particular size of visual field quadrant.

The observation of an optimal number of pattern elements can be explained by the fact that the most effective check-size increases with retinal eccentricity. An additional contribution to this effect may be that as the stimulus field-size increases, cortical dipoles of different orientation are stimulated. The summation of the dipoles can cause a change in the VECF distribution on the scalp and a possible reduction in VECF amplitude. There is experimental evidence to support this view, because with some check-sizes the VECF amplitude decreased above a certain field-size. Additional recording sites may be able to overcome the difficulty of the changing

dipole orientations. The sites used in this study are in routine clinical use for left and right hemi-field recordings (Spehlmann 1985) and have also been used in previous quadrant-field studies (Halliday 1972, Halliday 1982). The preparation of more electrode sites would, however, be very time consuming. Furthermore, such studies would be impossible in the many clinics with four-channel recording systems, unless a subset of recording positions could be chosen for each quadrant under investigation.

The VECF amplitudes recorded from stimulation of the superior nasal quadrant were more variable than from stimulation of the inferior nasal quadrant due to a lower SNR. The SNR could be improved by using longer data samples. Alternatively, the stimulus frequency could be increased to well above the alpha frequency range, but the VECF amplitude rapidly decreases with increasing stimulus frequency for pattern-reversal stimulation (Regan 1977).

The observations of this study, in particular the data on optimum check-sizes, provide important information for choosing stimulus variables for making objective measurements of the visual field.

### **4.3 STEADY-STATE VECFs FROM DARTBOARD PATTERN-REVERSAL STIMULATION OF THE VISUAL FIELD**

#### **4.3.1 Introduction**

In section 4.2 the checkerboard stimulus was optimised for stimulation of different stimulus field-sizes. An even better stimulus would be one in which the check-sizes were optimal in all areas of the visual field. The pattern elements would therefore need to increase in size with increasing retinal eccentricity (Section 4.2.4). Barber and Galloway (1976) proposed a stimulus geometry that fits this specification. The checks were arranged radially and the pattern was given the name 'dartboard'; an example is illustrated in Figure 4.7. In 1976 sophisticated computer graphics were not available for stimulus generation. Instead, the pattern was presented using a slide projector and the stimulus produced by chopping the beam. The stimulus gave a larger amplitude VECF than could be obtained using a range of checkerboard stimuli because the check-size was optimal for all retinal locations.

In this study, the possibility of using a dartboard stimulus for electroperimetry was explored. It was hoped that by matching the check-sizes at each eccentricity to the

optimal values determined in Section 4.2, that it would be possible to test smaller areas of the retina than had been possible hitherto.

The aim of the study was to objectively test twelve areas of the visual field outside the fovea. The layout of these areas was designed to objectively detect a range of visual field defects, including:

1. Absolute hemianopia, with or without central sparing.
2. Absolute quadrantanopia, with or without central sparing.
3. Absolute altitudinal field defects, with or without central sparing.
4. Constriction of the visual field.

The SNR of the recording was maximised by using a steady-state stimulus and by analysing the signal in the frequency domain.

#### 4.3.2 Subjects and methods

Four normal male subjects, ranging in age from 31 to 50 years (mean age 38 years) were investigated. All subjects had normal visual fields, had a visual acuity better than or equal to 6/6, were optically corrected for the viewing distance of 40 cm and had normal pupils (3 to 6 mm).

The stimulus was generated using computer graphics and presented on the computer monitor. The ratio of the radii of successive circular divisions was  $r_n/r_{n+1} = 1.15$ , in order that the check-sizes matched the experimentally derived optimal values in Section 4.2 (Figure 4.4). Radial divisions, spaced by  $8.18^\circ$ , were used to divide the pattern into elements that were approximately square. The resultant pattern is illustrated in Figure 4.7. The check-sizes also closely correspond to the optimum values predicted in Section 4.2.3 by means of Horton and Hoyt's (1991) formula for the cortical magnification factor (Figure 4.8). Figure 4.9 shows how the visual field outside the fovea was divided into twelve test areas. The area between  $5^\circ$  and  $15^\circ$  eccentricity was designed to test whether there was central sparing in the visual field; the area could also be used to detect central scotoma. The margins along the vertical and horizontal meridians were designed to prevent inadvertent stimulation of areas

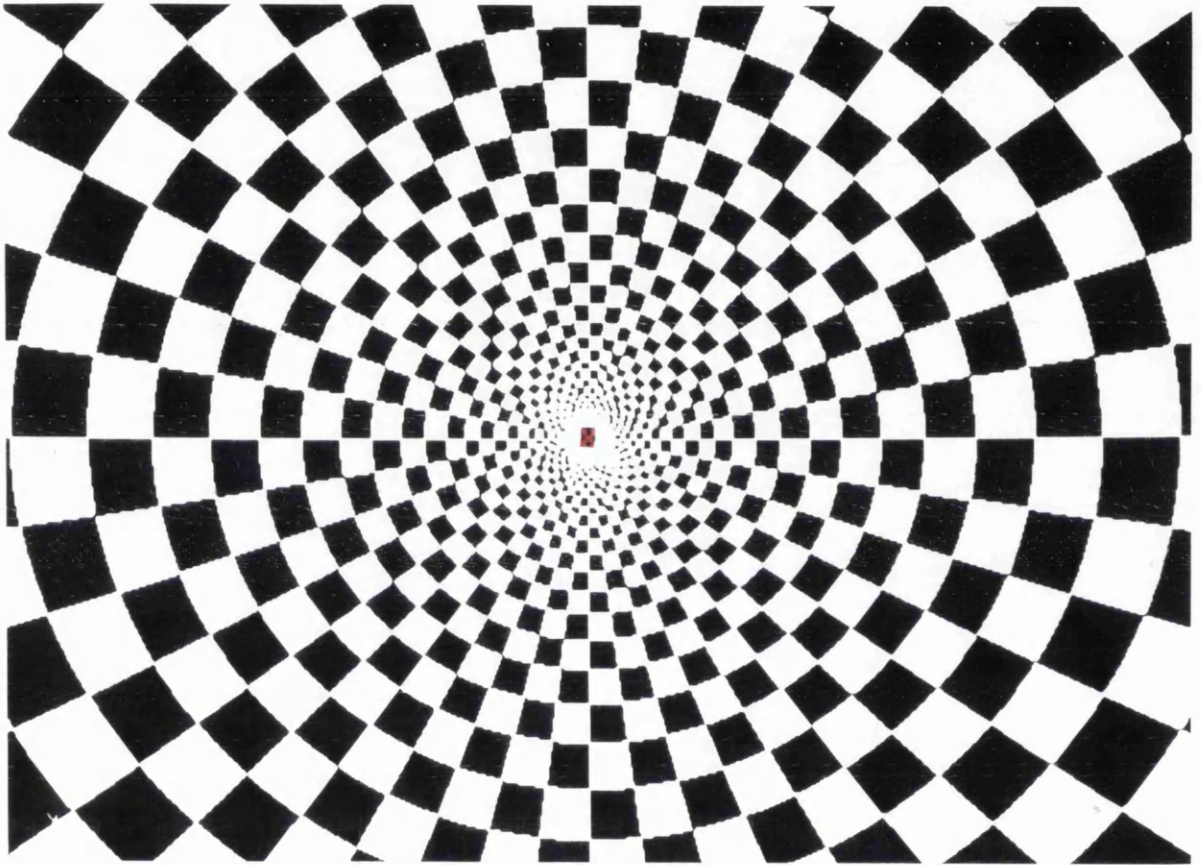


Figure 4.7 Example of a dartboard pattern stimulus.

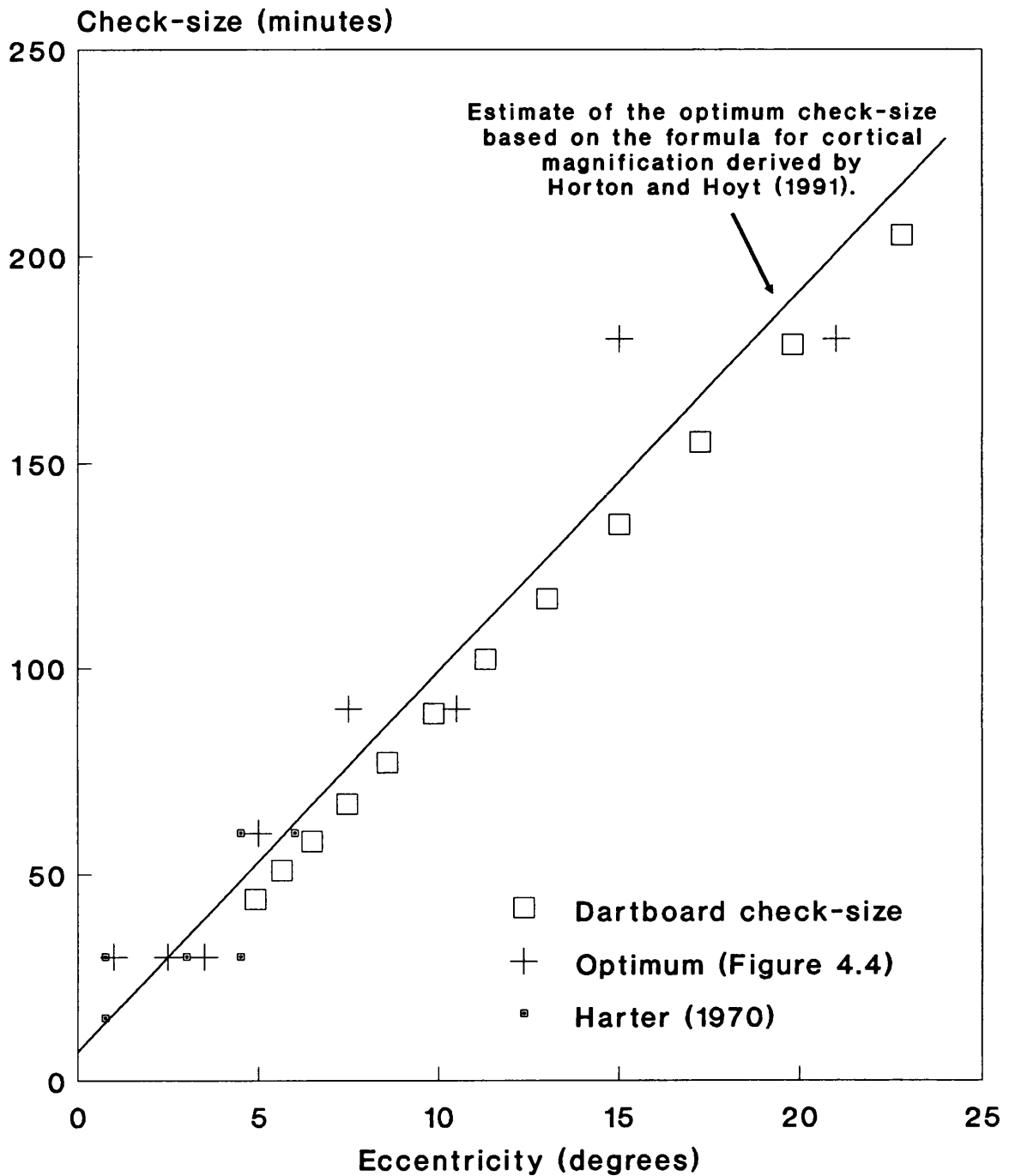


Figure 4.8 Check-size versus retinal eccentricity for the dartboard stimulus, compared with optimal check-sizes.

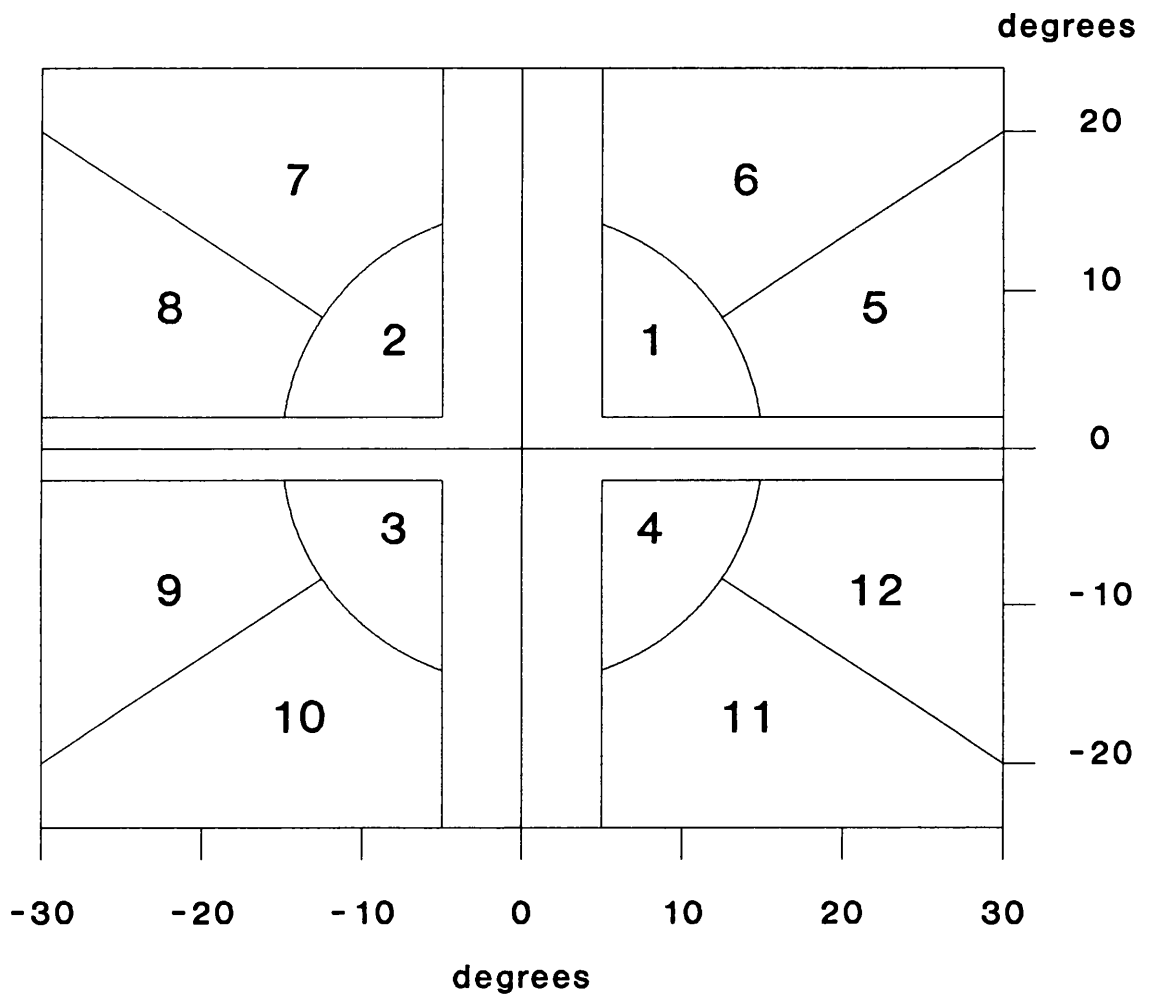


Figure 4.9 The twelve areas of the visual field tested with the dartboard stimulus

not under test, which could be caused by the overlap of ganglion receptive fields and slight losses of fixation. The margin adjacent to the vertical meridian was 5° wide and the margin adjacent to the horizontal margin was 2° wide.

Monocular recordings were made from one eye of each subject. One recording was made from each stimulus area for each subject. The luminance of the white areas was 60 cd/m<sup>2</sup> and the pattern contrast was greater than 99 %. The stimulus rate was 7.71 reversals per second, which is just below the EEG alpha frequency band.

A grey background was generated on the screen, with a luminance equal to the mean pattern luminance, 30 cd/m<sup>2</sup>. This background ensured that the overall screen luminance remained constant during the experiments and also minimised retinal stimulation due to scattered light. The test subjects viewed a fixation letter which helped them to focus in the plane of the screen. In order to ensure that the subject's fixation did not wander, the colour of the letter was intermittently changed for less than one second, the subject had to report the change and the colour. The experiments were performed in a darkened room, with an ambient illumination of 10 lux.

Recordings were made for two minutes from the occipital sites MO, RO, LO and MP relative to the mid-frontal position MF (Section 2.9.2). A guard electrode was positioned on the scalp within the hairline. The amplifier low frequency cut-off was 0.8 Hz and the high frequency cut-off was 100 Hz.

The VECPs were sampled at a rate of 247 Hz, so that one stimulus period corresponded to 32 data points. Successive 1024 points of data were averaged and transformed into the frequency domain using an FFT. The stimulus corresponded to an exact integer frequency in the frequency domain, thus eliminating the effects of spillover in the spectrum (Bergland 1969). The signal was objectively detected by measuring the SNR. The noise power was estimated by performing linear regression on ten frequencies adjacent to the stimulus frequency (Section 3.2.2). The SNR was calculated for the four primary recording channels (MO-MF, RO-MF, LO-MF and MP-MF) and for a further six channels derived from the primary channels (MO-RO, MO-LO, MO-MP, RO-LO, RO-MP and LO-MP).

### 4.3.3 Results

The frequency spectrum of a typical VECP recording is illustrated in Figure 4.10. The recording was made during stimulation of Area 6 (Figure 4.9). The SNR at the stimulus reversal frequency was 4.6. In this example, a signal was also detected at the third, fourth and fifth harmonics of the reversal frequency. EEG alpha activity is observed in the spectrum between 8 and 12 Hz.

The recording channel with the largest signal amplitude varied according to the region of the visual field being stimulated and the individual being tested. Table 4.3 lists how often the largest signal amplitude was recorded from each channel. It should be noted that each channel produced the largest signal amplitude on at least one occasion. When the areas in the superior hemi-field were tested the largest signal amplitude was most often recorded ipsilateral to the excited hemisphere and on the midline (22/24 occasions). Conversely, when the areas in the inferior hemi-field were tested the largest signal was most often recorded contralateral to the excited hemisphere and on the midline (17/24 occasions). A summary of the largest signal amplitudes is given in Table 4.4.

The maximum SNR was usually obtained on the same channel as the maximum signal amplitude. However, if the maximum signal amplitude was obtained from a channel recorded relative to the mid-frontal electrode, then a larger SNR could sometimes be obtained between a pair of adjacent occipital electrodes. In these cases, a larger SNR could be obtained because the background EEG at the two electrodes was very similar and tended to cancel out. Table 4.5 provides a summary of the SNR values obtained in the study. In 44/48 cases the SNR was greater than 2.9, which means the chance of false signal detection was less than 1 % (Section 3.2.2.). In two cases the SNR were between 2.44 and 2.9; the chance of false signal detection was less than 5%. In one case the SNR was 2.2 and the chance of false signal detection was less than 10 %. In the last case the SNR was 1.9 and the chance of false signal detection was greater than 10 %. In several instances the signal was only detectable from one channel.

The fixation monitor worked very well. Fixation was tested 288 times in each subject and was never missed. The simple task required by the test helped the subject to concentrate and reduced the chance of fatigue.

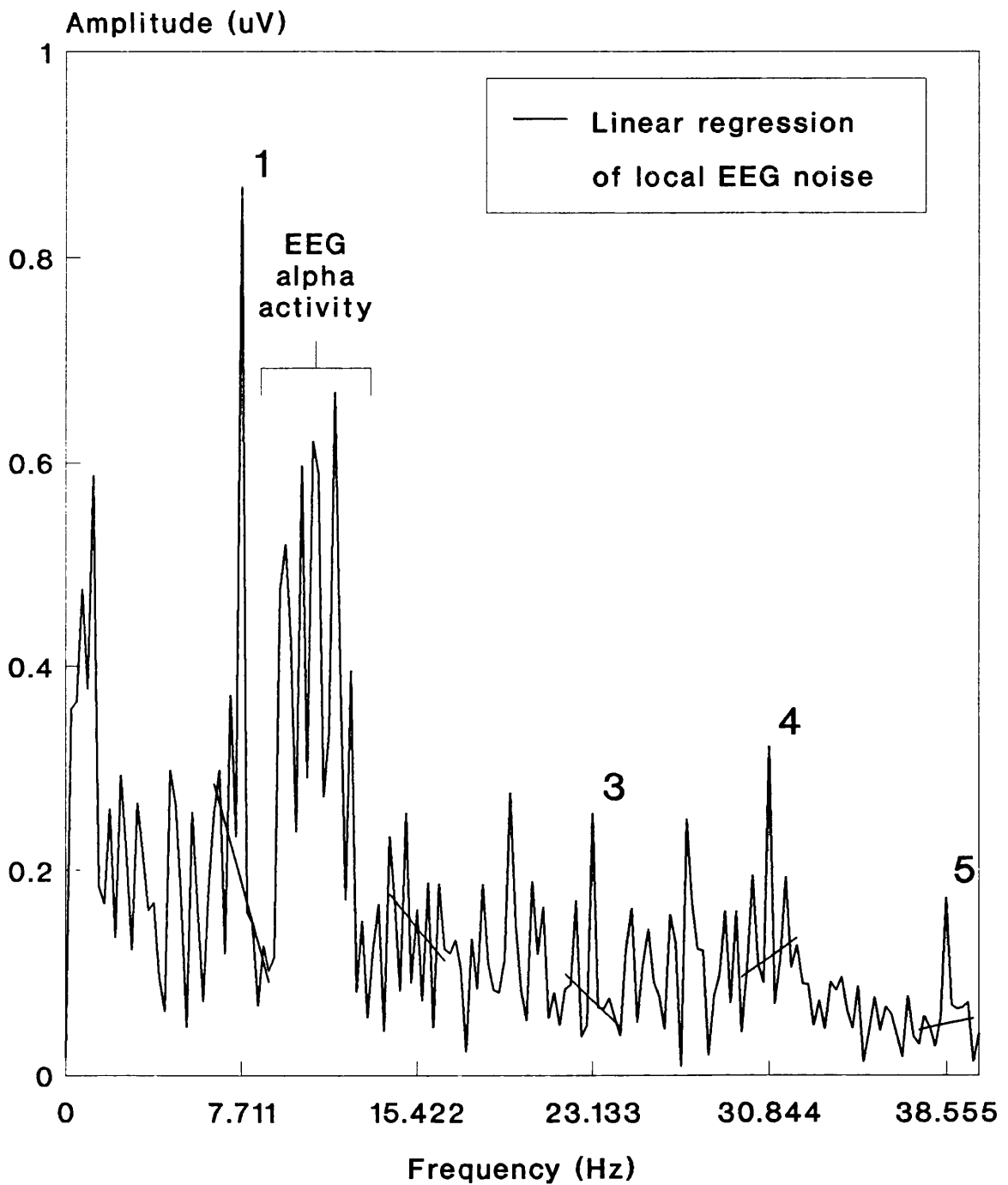


Figure 4.10 Spectrum of VECP recording.  
Stimulus frequency 7.711 revs/s. Signal  
at 1st, 3rd, 4th and 5th harmonics.

**Table 4.3 Frequency of largest VECF amplitude occurring on each recording channel.**

Primary recording channels	Frequency
MO-MF	6/48
RO-MF	9/48
LO-MF	3/48
MP-MF	9/48
Derived recording channels	
MO-RO	3/48
MO-LO	1/48
MO-MP	2/48
RO-LO	6/48
RO-MP	4/48
LO-MP	5/48

**Table 4.4 VECP amplitude from dartboard stimulation, for four subjects.**

Stimulus area	Largest signal amplitude at stimulus reversal frequency ( $\mu\text{V}$ )			
	Mean	Median	Minimum	Maximum
1	1.67	1.99	0.38	2.34
2	1.61	1.34	1.02	2.74
3	1.53	1.41	0.90	2.41
4	1.35	1.23	1.11	1.83
5	1.35	1.58	0.60	1.63
6	0.90	0.89	0.56	1.26
7	0.88	0.87	0.49	1.28
8	0.95	1.04	0.49	1.24
9	1.67	1.70	0.60	2.7
10	1.52	1.51	1.12	1.92
11	1.18	1.12	0.77	1.69
12	1.64	1.61	1.33	2.00

**Table 4.5 VECP signal-to-noise-ratio from dartboard stimulation,  
for four subjects.**

Stimulus area	Signal-to-noise-ratio at pattern-reversal frequency			
	Mean	Median	Minimum	Maximum
1	8.55	8.40	2.2	15.2
2	5.18	4.70	3.5	7.8
3	6.87	7.30	1.9	11.0
4	7.45	8.10	3.4	10.2
5	4.83	4.95	3.0	6.4
6	4.00	3.95	2.5	5.6
7	4.90	4.55	3.3	7.2
8	3.65	3.65	2.7	4.6
9	6.53	6.40	5.1	8.2
10	6.08	6.30	3.2	8.5
11	6.55	6.35	3.0	10.5
12	4.70	4.75	3.6	5.7

#### 4.3.4 Discussion

This study has demonstrated that it is possible to objectively detect a VECF signal from stimulation of 12 small areas of the visual field outside the fovea. The key to this success has been to maximise the SNR. This has been achieved in three ways:

1. The signal was maximised by matching the size of the stimulus pattern elements to the optimum check-size for each retinal eccentricity (determined in Section 4.2).
2. A steady-state stimulus was used so that the signal could be separated from the background EEG in the frequency domain.
3. Ten recording channels (four primary channels and six derived channels) were used to increase the probability of recording the maximum potential difference on the scalp.

The dartboard stimulus has proved to be very effective in this study. It has, however, been reported that the VECF amplitude is attenuated for obliquely oriented stimuli (Moskowitz and Sokol 1985) due to a phenomenon known as the 'oblique effect'. The work of Barber and Galloway (1976) would indicate that this effect is outweighed by the optimal matching of the pattern elements to receptive field-sizes.

The pattern-reversal frequency was set outside the EEG alpha frequency band otherwise the SNR would have been significantly reduced (Figure 4.10).

The use of four recording electrodes over the visual cortex was essential to detect the small VECF signals recorded in the study. The use of six derived channels was also a significant development. In 21/48 of the recordings, the largest signal amplitude was recorded from the derived channels and sometimes the signal was only detectable from these channels.

The probability of signal detection could be further increased by increasing recording times or by using a phase sensitive detector (Section 3.2.2). In addition, the SNR could be measured at harmonics of the stimulus reversal frequency.

## 4.4 TRANSIENT VECPS FROM MOTION-ONSET STIMULI

### 4.4.1 Introduction

Image motion processing is a fundamental property of biological visual systems and is necessary for navigation, collision avoidance and detecting moving objects. Indeed, whilst many animals lack colour vision or significant binocular vision, no sighted animals have been shown to lack mechanisms for motion processing (Nakayama 1985). Man is no exception and it has been possible to record VECPs from motion-onset, motion-offset and motion-reversal stimuli (Clarke 1973).

Motion stimuli may have important clinical applications in ophthalmology and neuro-ophthalmology (Kubova and Kuba 1992). The motion-onset VECP could, for example, be useful for testing the visual field as it is claimed that the VECP amplitude is significantly larger than the pattern-reversal VECP for extramacular stimulation (Kubova et al 1990, Kuba and Kubova 1992, Kubova and Kuba 1992). Muller et al (1990) were able to record VECPs from motion-onset stimuli at an eccentricity of  $23^\circ$  by means of a stimulus subtending  $3.2^\circ$ . In order to determine the utility of the motion-onset VECP for electroperimetry an attempt was made to reproduce the work of Kubova et al.

For extramacular stimulation Kubova et al (1990) used an annular stimulus field between retinal eccentricities of  $5^\circ$  and  $9^\circ$  (the term 'extramacular stimulation' is in fact misleading because the stimulus was in effect positioned on the macular area surrounding the fovea). The stimulus moved horizontally and consisted of vertical bars with a spatial frequency of 2.3 cycles per degree. This spatial frequency corresponds to a bar width of  $13'$  which, unfortunately, is not optimal for pattern-reversal stimulation of the retina between eccentricities of  $5^\circ$  and  $9^\circ$  (Section 4.2, Harter 1970). Based on results with a pattern-reversal checkerboard stimulus, the optimum bar width would have been in the range  $45'$  to  $90'$  (Figure 4.3). In this work, it was therefore decided to investigate whether the motion-onset VECP was still significantly larger than the pattern-reversal VECP when the central  $10^\circ$  of the visual field were masked and the spatial frequency of the stimulus was optimised for pattern-reversal stimulation.

The motion-onset VECP is believed to be a motion specific response, evoked by the cortical cells responsible for motion processing. There are two reasons for this. Firstly, the response was found to be reduced by adaptation to moving stimuli (Kuba

and Kubova 1992). Secondly, the full-field motion-onset VECF was found to have a maximum amplitude from electrodes placed lateral to the midline of the visual cortex, unlike the full-field pattern-reversal VECF which has a maximum amplitude over the midline of the visual cortex (Kubova et al 1990, Kuba and Kubova 1992). Kuba and Kubova proposed that the response is lateralised because it originates from area V5 (Section 1.1.6), which is located in the region of the temporo-parieto-occipital junction (Zeki et al 1991), and is dedicated to motion processing.

In this work, it was recognised that if the motion-onset VECF was truly a motion specific response from area V5 then it should be possible to maximise the amplitude of the signal by developing a stimulus that stimulates as many cells in V5 as possible.

Area V5 is also known as MT (Section 1.1.6). Our current knowledge of the function of V5 is derived from microelectrode studies of MT in monkeys such as the owl monkey (Zeki 1980) and the macaque (Maunsell and Van Essen 1983). Behavioural studies in the macaque (Newsome et al 1985) and the rhesus monkey (Newsome and Pare 1988) have also confirmed that MT is dedicated to motion processing. The function of V5 in man was recently confirmed by Zeki et al (1991). Using PET, they showed that there was an increase in blood flow in V5 during motion stimulation.

MT in the macaque has been shown to contain a representation of the visual field that is similar to that of the striate cortex (Gattass and Gross 1981). Like the striate cortex, the receptive fields increase in size with retinal eccentricity. However, because MT is much smaller than the striate cortex, the receptive fields are much larger. Maunsell and Van Essen (1983) found that many cells showed a high degree of selectivity for stimulus direction, speed and orientation. Albright et al (1984) found that sixty percent of the cells tested responded exclusively to one direction of motion, 24 % responded best to one direction with a weaker response in the opposite direction, 8 % responded equally well to two opposite directions of motion and 8 % responded equally well to all directions of motion.

The stimulus used by Kubova et al (1990) was restricted to motion along one axis. In order to stimulate more cells in area V5, in this work it was proposed that the stimulus should include motion along additional axes. It is physically impossible to produce a stimulus which simultaneously moves in all directions in all areas of the visual field. Nevertheless, because the receptive fields of the cells in V5 are large (Gattass and Gross 1981), it should be possible to stimulate many of them using

stimulus elements moving in random directions in different parts of the visual field. Unfortunately, however, such a stimulus is not easy to program in VGA computer graphics. Consequently, for a preliminary investigation a less complex stimulus was developed that consisted of circular rings that moved towards the patient's point of fixation (Figure 4.11). In this way, each receptive field would simultaneously contain pattern elements moving along several axes of motion and was therefore more likely to be stimulated.

#### **4.4.2 Subjects and methods**

##### **Vertical bars**

Motion-onset VECs were compared with pattern-reversal VECs for vertical black and white bars. The stimuli were presented on the computer monitor screen and the stimulus field subtended  $30^\circ \times 24^\circ$ . Recordings were made with full-field stimulation and with the central  $10^\circ$  masked. The luminance of the white bars was  $56 \text{ cd/m}^2$  and the mean screen luminance was constant at  $28 \text{ cd/m}^2$ . Subjects viewed a red fixation letter in the middle of the screen (Figure 4.12) and their eyes were observed to check that there were no eye movements. Furthermore, in some studies an EOG recording was made simultaneously with the VEC to show that there were no eye movements.

For pattern-reversal stimulation the position of the bars was reversed every 0.8 s.

For motion-onset stimulation the bars moved from left to right across the screen. This apparent movement was achieved by means of colour palette animation. The duration of motion was 200 ms as used by Kubova and Kuba (1992). Kubova et al (1990) found that the duration of motion must be at least 100 ms in order to evoke a motion-onset VEC in all subjects. The interstimulus interval was approximately 3.6 s in order to prevent adaptation to the stimulus. The stimulus duty cycle was therefore 5.3 % (the stimulus duty cycle is the duration of motion divided by the period between successive stimulus onsets). The interstimulus interval was varied by 50 ms between successive stimuli so that EEG alpha activity did not become synchronised to the VEC.

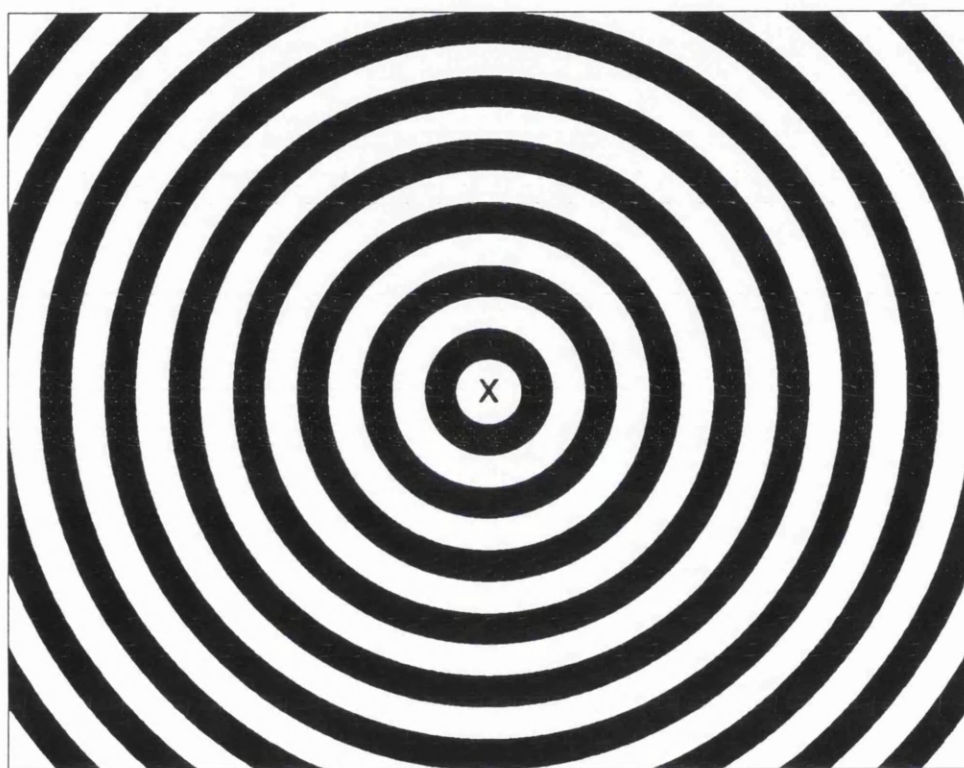
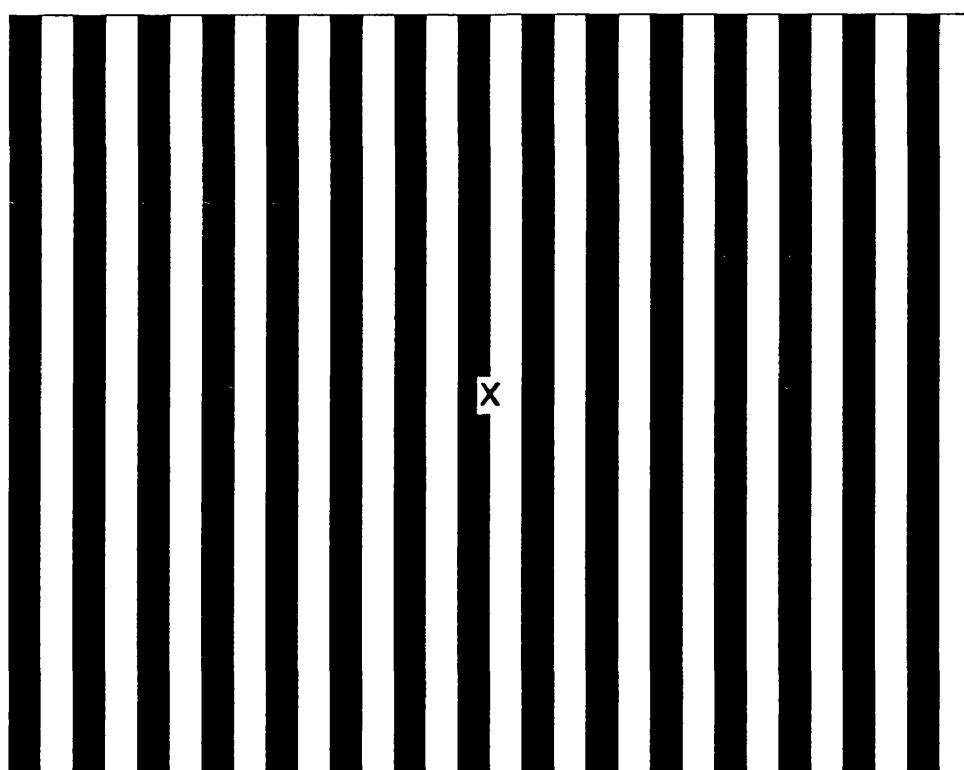


Figure 4.11 Novel motion stimulus.  
The circular rings move towards the  
fixation letter in the centre.



**Figure 4.12 Vertical bar stimulus.**  
Note the fixation letter in the centre  
of the screen.

Patterns with a spatial frequency of 1.1 cycles per degree (bar width 27') were investigated in eight male subjects, aged 22 to 48 years (mean 32 years). Three velocities were used: 3.6, 5.4 and 10.7° /s. Kuba and Kubova (1992) currently use bars with a spatial frequency of 1.3 cycles per degree (bar width 23') that move with a velocity of 5.6° /s.

Patterns with a spatial frequency of 0.33 cycles per degree (bar width 90') were investigated for three velocities: 6, 8.9 and 17.9° /s. The bar width was optimal for stimulating the retina at an eccentricity of 10° (Section 4.2.3). Eight subjects were studied, four of whom were male, with ages ranging from 20 to 51 years (mean 31 years).

### **Circular ring stimulus**

Motion-onset VECs from the novel circular ring stimulus were investigated in 14 subjects, nine of whom were male. Their ages ranged from 20 to 51 years (mean age 31 years). The stimulus rings had a spatial frequency of 0.66 cycles per degree (ring width 45') and moved with a velocity of 8.9° /s. The motion duration was 170 ms and the interstimulus interval was 3.6 s. Recordings were made with full-field stimulation and with the central 10° masked. The luminance of the white bars was 56 cd/m<sup>2</sup> and the mean screen luminance was constant at 28 cd/m<sup>2</sup>. Subjects viewed a red fixation letter in the middle of the screen (Figure 4.11).

### **Recording methods**

All subjects had normal visual fields, had a visual acuity better than or equal to 6/6, were optically corrected for the viewing distance of 40 cm and had normal pupils (3 to 6 mm). Monocular recordings were made from the left eye, except for one subject in whom the right eye was tested because of a reduced acuity in the left eye.

Recordings were made using an electrode montage based on the ten-twenty system (Section 2.9.2). Three recording sites were used O<sub>z</sub> and 5 cm to the right and left of O<sub>z</sub>, O<sub>R</sub> and O<sub>L</sub> respectively (Kubova et al 1990). Linked ear lobes A<sub>1+2</sub> were used as a reference and a guard electrode was positioned on the scalp within the hairline.

The amplifier low frequency cut-off was 0.8 Hz and the high frequency cut-off was 100 Hz. Signals were digitised at a rate of 512 Hz and recorded for 500 ms from stimulus presentation. Two averages of forty responses were recorded for each stimulus.

### 4.4.3 Results

#### Vertical bars

The pattern-reversal VECP was characterised by a triphasic response labelled N1, P1 and N2 as shown in Figure 4.13. For each subject, the recording channel with the largest P1-N2 amplitude was used to measure the latency of P1 and N2. The largest signal was recorded from channel  $O_z - A_{1+2}$  in 94 % of the studies. The amplitude and latency measurements are presented in Table 4.6. When the 10° diameter foveal mask was applied to the stimulus, the VECP signal amplitude was reduced by an average of 57 % for a spatial frequency of 1.1 cycles per degree and by 49 % for a spatial frequency of 0.33 cycles per degree. With the foveal mask in place, the largest amplitude pattern-reversal VECP was recorded by means of the pattern with the spatial frequency of 0.33 cycles per degree. These results were expected because a spatial frequency of 0.33 cycles per degree is optimum for recording VECPs from a retinal eccentricity of 10° (Section 4.2.3), whilst 1.1 cycles per degree is optimum for recording VECPs from an eccentricity of 2° to 3°.

The motion-onset VECP was characterised by a negative peak N2, approximately 150 ms from the stimulus onset, preceded by a peak or turning point labelled P1 as shown in Figure 4.14. In some subjects, two further features N1 and P2 were observed. N1 had a latency of approximately 50 ms and preceded P1 (Figure 4.14). P2 had a latency of 200 to 250 ms and followed N2. For each subject, the recording channel with the largest P1-N2 amplitude was used to measure the latency of N2 and P1. The largest signal was recorded from channel  $O_z - A_{1+2}$  in 54 % of the studies and from  $O_R - A_{1+2}$  in a further 40 % of the studies. The amplitude and latency measurements are presented in Table 4.7. The signal amplitude was reduced following the application of the foveal mask. The average reduction was only 19 % for both spatial frequencies. There was no evidence, either from observing eye

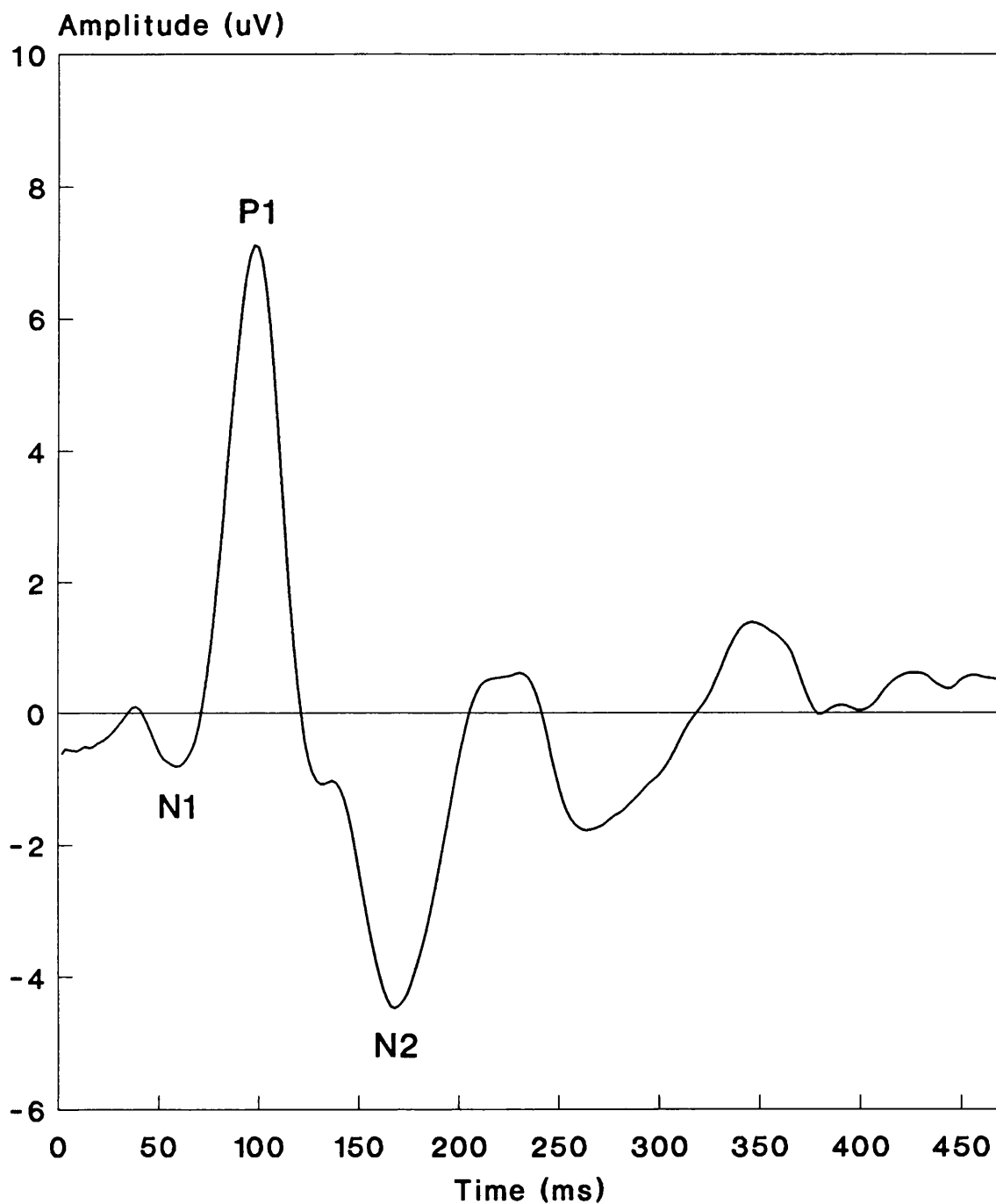


Figure 4.13 Typical pattern-reversal VEP from bar stimulus pattern, showing typical N1, P1 and N2 peaks.

**Table 4.6 Results using pattern-reversal stimulus**

The table shows the mean values and range for the average of two recordings from eight subjects.

Stimulus	Foveal mask	P1 latency (ms)	P1-N2 amplitude ( $\mu$ V)	N2 latency (ms)
Bars 1.1 cycles per degree	No	99 (90 - 106)	9.1 (4.3 - 14.6)	157 (121 - 180)
	Yes	94.3 (68 - 106)	3.9 (1.6 - 7.0)	147.8 (123 - 172)
Bars 0.33 cycles per degree	No	98.5 (90 - 106)	10.9 (5.7 - 18.5)	158.6 (147 - 178)
	Yes	100.5 (72 - 117)	5.6 (2.8 - 9.9)	146.8 (121 - 162)

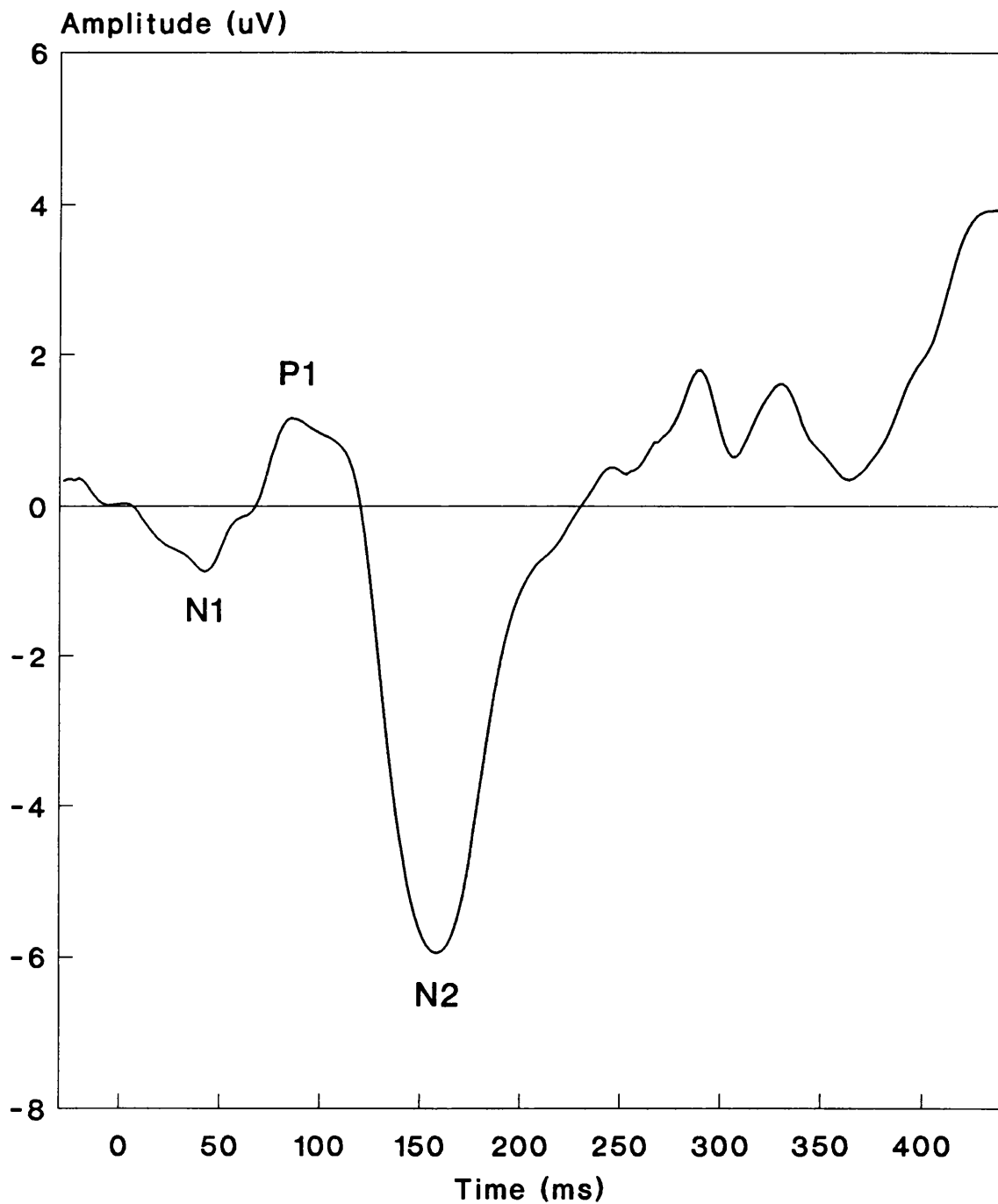


Figure 4.14 Typical motion-onset VECP showing the characteristic negative peak N1 about 150 ms from stimulus onset.

**Table 4.7 Results using motion-onset stimulus****Vertical bars, 1.1 cycles per degree**

The table shows the mean values and range for the average of two recordings from eight subjects.

Stimulus velocity ( $^{\circ}$ / s)	Foveal mask	P1 latency (ms)	P1-N2 amplitude ( $\mu$ V)	N2 latency (ms)
3.6	No	109 (94 - 121)	6.6 (2.8 - 10.6)	153.8 (129 - 186)
3.6	Yes	107 (78 - 133)	4.5 (2.4 - 6.5)	162.9 (137 - 188)
5.4	No	96.1 (67 - 124)	6.9 (4 - 8.7)	145.6 (124 - 198)
5.4	Yes	91.1 (57 - 126)	5.7 (3.8 - 7.4)	153.4 (126 - 192)
10.7	No	104.4 (74 - 128)	6.3 (2.3 - 9.2)	152 (128 - 199)
10.7	Yes	91.1 (74 - 113)	5.8 (4.3 - 7.5)	146.9 (120 - 197)

**Table 4.7 Results using motion-onset stimulus (continued)****Vertical bars, 0.33 cycles per degree**

The table shows the mean values and range for the average of two recordings from eight subjects.

Stimulus velocity (°/s)	Foveal mask	P1 latency (ms)	P1-N2 amplitude ( $\mu$ V)	N2 latency (ms)
6	No	98.9 (70 - 147)	6.7 (4.4 - 12)	165.5 (141 - 195)
6	Yes	88.4 (68 - 133)	5.0 (3.7 - 7.7)	149.8 (127 - 176)
8.9	No	90.6 (69 - 116)	6.7 (4.4 - 10)	156 (134 - 169)
8.9	Yes	94.7 (67 - 118)	5.3 (3.0 - 8.4)	152.6 (134 - 167)
17.9	No	103.1 (76 - 126)	5.6 (2.9 - 10)	154.4 (140 - 165)
17.9	Yes	103.2 (64 - 163)	5.1 (2.1 - 9.7)	157.1 (136 - 201)

**Table 4.7 Results using motion-onset stimulus (continued)****Circular ring stimulus, 0.66 cycles per degree**

The table shows the mean values and range for the average of two recordings from 14 subjects.

Stimulus velocity ( $^{\circ}$ / s)	Foveal mask	P1 latency (ms)	P1-N2 amplitude ( $\mu$ V)	N2 latency (ms)
8.9	No	92 (68 - 125)	11.2 (6 - 18)	150.1 (130 - 197)
8.9	Yes	85 (39 - 125)	8.1 (4.8 - 12)	144.4 (123 - 184)

movements or from recording the EOG, that subjects lost fixation during the measurements. Despite the small stimulus duty cycle used, there was evidence in one subject's motion-onset VECP recording that the visual system adapted to motion during the test.

A Wilcoxon test was used to compare the amplitude of the VECPs from motion-onset and pattern-reversal stimuli. At a spatial frequency of 1.1 cycles per degree there was no statistical difference between the results obtained from the full-field stimulus. However, when the foveal mask was applied the amplitude of the motion-onset VECP was significantly larger ( $p < 0.05$ ) than the pattern-reversal VECP for velocities of 5.4 and 10.7° / s. At a spatial frequency of 0.33 cycles per degree the full-field pattern-reversal VECP was significantly larger ( $p < 0.05$ ) than the motion-onset VECP for all velocities. When a foveal mask was applied there was no significant difference between the amplitude of the motion-onset VECP and the pattern-reversal VECP.

### **Circular ring stimulus**

As with the vertical bars stimulus, the motion-onset VECP was characterised by a negative peak N2, approximately 150 ms from the stimulus onset. For each subject, the recording channel with the largest P1-N2 amplitude was used to measure the latency of N2 and P1. The largest signal was recorded from channel  $O_R - A_{1+2}$  in 52 % of the studies and from  $O_L - A_{1+2}$  in a further 30 % of the studies. The amplitude and latency measurements are presented in Table 4.7. The signal amplitude was reduced by an average of 28 % following the application of the foveal mask.

A Mann-Whitney test was used to compare the results obtained from the circular ring stimulus with those obtained from the vertical bars. For a full-field stimulus, the motion-onset VECPs recorded using the circular ring stimulus were significantly larger ( $p < 0.05$ ) than the motion-onset VECPs recorded using the vertical bars. When the foveal mask was applied, the motion-onset VECPs recorded using the circular ring stimulus were significantly larger ( $p < 0.05$ ) than all the VECPs recorded using the vertical bars.

#### 4.4.4 Discussion

The results of the studies with the motion-onset VECP confirm a number of findings reported in the literature:

1. The motion-onset VECP was characterised by a negative peak with a latency of approximately 150 ms (Kubova et al 1990, Muller et al 1990, Kuba and Kubova 1992, Kubova and Kuba 1992).
2. The motion-onset VECP was often lateralised, with the largest amplitude often recorded on the right side of the scalp (Kubova et al 1990, Kuba and Kubova, Kubova and Kuba 1992). In contrast, the maximum pattern-reversal VECP amplitude was almost without exception recorded on the midline over the primary visual cortex (Kubova et al 1990, Kuba and Kubova 1992).
3. The motion-onset VECP was reduced by adaptation to the moving stimulus and so it was necessary to have long interstimulus intervals (Kuba and Kubova 1992).

As these findings agree with the work of Kubova et al they do not contradict their hypothesis that the motion-onset VECP originates from the extrastriate cortex (Kubova et al 1990, Kuba and Kubova 1992).

There is, however, some controversy regarding the shape of the typical VECP in response to motion-onset stimuli. Some workers (Spekreijse et al 1985, De Vries et al 1989) have described the typical response as having a dominant positive peak with a latency of about 130 ms in contrast to the dominant negative peak reported in this work. The apparent conflict in these results can be explained by differences in the stimuli used (Kuba and Kubova 1992). It is likely that the response obtained by Spekreijse et al and De Vries et al was not a true motion specific response but a pattern-offset VECP caused by the blurring of the stimulus. In particular, Spekreijse et al and De Vries et al used fine bars, 12' wide, and only stimulated the central 6° of the visual field. Furthermore, the duty cycle was 50 % so there was no opportunity for recovery from motion adaptation. In addition, the resultant VECP had a maximum amplitude on the midline of the scalp over the visual cortex.

As explained above, a hypothesis has been proposed to explain the lateralisation of the motion-onset VECP (Kubova et al 1990, Kuba et al 1992). However, it is not

clear why the maximum amplitude signal was most often recorded on the right side of the scalp, in preference to the left side, and this needs further investigation.

The degree of motion adaptation is dependent on the stimulus duty cycle. Even with the small duty cycle used in these studies there was evidence that motion adaptation reduced the amplitude of some VECPs. Therefore, in order to ensure the repeatability of measurements it was essential that the same number of stimulus presentations was used for each recording. Kubova et al (1990) similarly used a small duty cycle of 7.3 %, although they later reported using a duty cycle of 16 % (Kubova and Kuba 1992). These small duty cycles required long interstimulus intervals which unfortunately resulted in long recording times, typically five times longer than that required for a pattern-reversal recording. This will be discussed further below.

In agreement with the findings of Muller et al (1990), the amplitude of the motion-onset VECP was found to be fairly independent of the spatial frequency of the vertical bars, for the motion velocities tested. This finding is consistent with the presumed extrastriate cortical origin of the motion-onset VECP in area V5 because in the MT area of the macaque monkey many cells were found to be selective for stimulus direction, speed and orientation but were not significantly effected by stimulus width (Maunsell and Van Essen 1983).

When the foveal mask was used, the novel circular ring stimulus produced a significantly larger motion-onset VECP than any of the other stimuli. This finding supports the hypothesis, proposed in Section 4.4.1, that the amplitude of the motion-onset VECP could be increased by using a stimulus with motion along more than one axis. It is therefore likely that a stimulus with elements moving in random directions in different parts of the visual field would further increase the amplitude of the signal because even more receptive fields in area V5 would be stimulated.

The effect of eye movements on the motion-onset VECP was not investigated. Instead, it was ensured that subjects maintained fixation which was important if motion stimuli were to be used ultimately to test small specific areas of the visual field. No eye movements were observed during the tests. However, there is a natural tendency for the eyes to pursue a moving stimulus, especially when the stimulus covers a large field of view. This involuntary response is called optokinetic nystagmus. The recordings with the moving vertical bars were therefore particularly tiring for the test subjects as they had to concentrate hard, in order not to track the pattern. This highlights another advantage of the circular ring stimulus. In this

stimulus, all the pattern elements moved towards the point of the subject's fixation, there was therefore no tendency to loose fixation and the test was less tiring. Even if subjects had followed the horizontally moving bars it is unlikely that this would have effected the recorded VECF because the interstimulus interval was aperiodic, which meant the stimulus onset was unexpected. The latency of eye movements to unexpected stimuli is typically 200 ms for saccades and 150 ms for pursuit movements (Fender 1964). If the stimulus period had been periodic the average latency of eye movements could have been almost zero (Fender 1964) which may have affected the recorded response.

In this study, the motion-onset stimulus composed of circular rings produced the largest amplitude VECF signal for stimulation of the retina outside the fovea. The stimulus could therefore be used for electroperimetry to study small parts of the visual field. The main drawback with the motion-onset stimulus, however, is that the test is very time consuming because long interstimulus intervals are required. In practice, the pattern-reversal stimulus is better for testing the visual field because long interstimulus intervals are not required, so the VECF can be recorded rapidly by means of steady-state stimuli. The motion-onset VECF may, however, still have an important clinical role for testing the motion specific pathway of the visual system, which cannot be tested by other stimuli. For example, when the motion-onset VECF was used in addition to the conventional pattern-reversal VECF for detecting the presence of multiple sclerosis, the sensitivity of the test was increased (Kubova and Kuba 1992). This is presumably because the motion sensitive pathway of the visual system was predominantly affected in some subjects, rather than the pathway responsible for producing the pattern-reversal VECF.

## **4.5 TRANSIENT VECFs FROM DARK AND BRIGHT PATTERN-ONSET STIMULI**

### **4.5.1 Introduction**

The aims of the study were to determine whether reproducible VECFs could be recorded from dark pattern-onset stimuli and if so, how they varied compared to the VECFs produced by light pattern-onset stimuli. There were two reasons for the study. Firstly, it was proposed that the dark stimulus should be used for a new stimulus delivery system under development in the laboratory. Secondly, other

workers in the laboratory wished to study differences between the on- and off-pathways of the visual system.

The new stimulus delivery system under development (Chapter 5) enabled VECPs to be recorded whilst the stimulus was simultaneously positioned on the retina by an observer. The stimulus was presented on an LCD screen which had a relatively slow response time compared to a monitor screen. In a preliminary investigation (Section 5.4.1), it was found that with this slow response time, pattern-onset stimuli produced larger VECPs than pattern-reversal stimuli. In order that the observer had a clear view of the retina it was essential that the stimulus background was clear and consequently the stimulus had to be dark.

The on- and off- pathways of the visual system selectively carry information on light increments and decrements respectively (Schiller et al 1986). Consequently, a light pattern stimulus would preferentially stimulate the on-pathway whilst a dark pattern stimulus would preferentially stimulate the off-pathway. The on-pathway is formed by on-centre retinal ganglion cells and the off-pathway is formed by off-centre retinal ganglion cells (Schiller 1986, Schiller et al 1986, Wassle and Boycott 1991) and their connections largely remain separate until they reach the visual cortex (Schiller et al 1986). The two pathways originate at the bipolar cell layer (Schiller 1986); on-bipolar cells are depolarised by a light spot whilst off-bipolar cells are depolarised by a dark spot (Wassle and Boycott 1991). As the on- and off-pathways are independent, it was proposed that there would be differences in the VECP produced by equal and opposite luminance changes.

#### **4.5.2 Subjects and methods**

Five normal subjects were examined, three male and two female, ranging in age from 26 to 35 years (mean age 30 years). All subjects had normal visual fields, had a visual acuity better than or equal to 6/6, were optically corrected for the viewing distance of 40 cm and had normal pupils (3 to 6 mm). The superior hemi-field of the left eye was tested. The stimulus field subtended  $24^{\circ} \times 24^{\circ}$  and consisted of 144 discs, each subtending a visual angle of  $60'$  and separated by a distance equal to their diameter (similar to Figure 2.6). The subjects maintained fixation by viewing a letter at the inferior edge of the stimulus field.

Measurements were made in a darkened room. Prior to making the recordings, there was a three minute period for retinal light adaptation during which the subjects viewed the stimulus background,  $20 \text{ cd/m}^2$ . Three values of stimulus luminance were investigated,  $0.1 \text{ cd/m}^2$  (black),  $10 \text{ cd/m}^2$  (grey) and  $40 \text{ cd/m}^2$  (white), giving Michaelson contrasts of -100 %, -30 % and +30 % respectively. Thus equal and opposite stimulus luminance and equal and opposite stimulus contrast were investigated. In order to separate the stimulus onset response from the stimulus offset response, it was necessary to present the pattern on the screen for 400 ms. The period between stimulus presentations was 2 s, giving a pattern on-time/pattern off-time ratio of 1:5. In order to minimise retinal light adaptation to the stimulus, the pattern was presented alternately in one of two positions (similar to Figure 2.6) providing an effective pattern on-time/off-time ratio of 1:11.

The VECPs were recorded from the mid-occipital location 5 cm above theinion, relative to a mid-frontal electrode placed 12 cm above from the nasion (Section 2.9.2). A guard electrode was positioned on the scalp within the hairline. A physiological amplifier (PA 400, Biodata Ltd, Manchester, UK) was used to amplify and filter the signals. The filter 3 dB cut-off points were set at 0.8 Hz and 100 Hz. The recordings were digitised at a rate of 320 Hz and 800 ms epochs were averaged. The averaging was triggered from stimulus onset, the onset response was contained in the first 400 ms of the recording and the offset response was contained in the second 400 ms of the recordings. One hundred pattern-onset and pattern-offset responses were recorded for each stimulus type. Recordings were made as two sets of 50 responses and signal reproducibility was checked by means of cross-correlation. The two recordings were summed and filtered with a digital low-pass filter to attenuate residual high frequency noise.

The recordings were evaluated by identifying their common reproducible features which were then quantified by measuring their latency and relative amplitude. A statistical evaluation of the results was made by means of the paired t-test.

### 4.5.3 Results

Figure 4.15 shows a typical VECP waveform recorded in response to the stimulus onset and offset. The waveforms were reproducible and the values for cross-correlation are presented in Table 4.8. The values for cross-correlation were lower than those obtained using a pattern-reversal stimulus (Section 2.11.2) but this was to

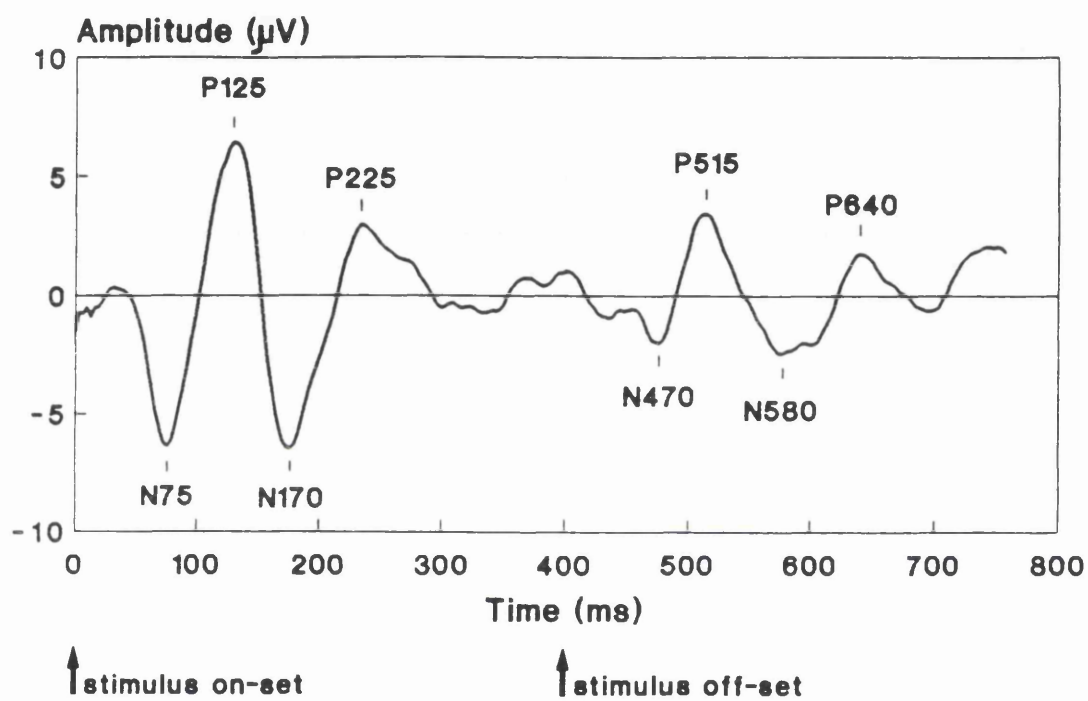


Figure 4.15 Typical VECP waveform following stimulus onset and offset.

This response was recorded using the black stimulus pattern.

**Table 4.8 Cross-correlation values for pairs of recordings from five subjects.**

	Stimulus		
	black	grey	white
Mean	0.63	0.62	0.75
Median	0.61	0.62	0.83
Minimum	0.45	0.47	0.45
Maximum	0.84	0.78	0.89
First quartile	0.45	0.51	0.54
Third quartile	0.82	0.74	0.88

be expected because the SNR was lower due to the fact that the signal amplitude was smaller and fewer responses were averaged.

The onset response had characteristic negative peaks at latencies of 75 and 170 ms and positive peaks at latencies of 125 and 225 ms. These peaks were labelled  $\overline{N75}$ ,  $\overline{P125}$ ,  $\overline{N170}$  and  $\overline{P225}$  respectively. A statistical analysis of the latencies and peak-to-peak amplitudes is presented in Tables 4.9 and Table 4.10.

The offset response had characteristic negative peaks at latencies of 470 and 580 ms and positive peaks at latencies of 515 and 640 ms. These peaks were labelled  $\overline{N470}$ ,  $\overline{P515}$ ,  $\overline{N580}$  and  $\overline{P640}$  respectively.

The onset of the bright (white) stimulus produced larger amplitude VECPs than the onset of the dark (black and grey) stimuli. The  $\overline{P125-N170}$  and  $\overline{N170-P225}$  amplitudes were significantly larger for the white stimulus than for the dark stimuli ( $p < 0.01$ ). There were, however, no significant differences in the  $\overline{P125-N75}$  amplitudes for the three stimuli ( $p > 0.05$ ), nor were there any significant differences in the latencies of the characteristic peaks ( $p > 0.05$ ).

The offset of the dark (black and grey) stimuli produced larger amplitude VECPs than the offset of the bright (white) stimulus. This finding is consistent with the results from the onset stimuli because offset of a dark stimulus creates a light increment. The  $\overline{P515-N470}$  amplitudes were significantly larger for the black and grey stimuli than for the white stimulus ( $p < 0.01$  and  $p < 0.05$  respectively). The  $\overline{P515-N580}$  amplitudes for the black and grey stimuli were larger by 80 % and 37 % respectively. There were no significant differences in the  $\overline{P640-N580}$  amplitudes for the three stimuli ( $p > 0.05$ ) and, as with the onset stimuli, there were no significant differences in the latencies of the characteristic peaks ( $p > 0.05$ ).

**Table 4.9 Peak Latencies**

Mean latency and standard deviation in milliseconds for the average of two recordings from five subjects..

Peak	Stimulus		
	black	grey	white
Onset response			
$\overline{N75}$	80.1 $\pm$ 10.8	81.4 $\pm$ 8.7	70.2 $\pm$ 9.6
$\overline{P125}$	122.4 $\pm$ 9.8	129.3 $\pm$ 11.8	124.9 $\pm$ 6.9
$\overline{N170}$	169.1 $\pm$ 9.1	174.8 $\pm$ 10.6	165.9 $\pm$ 9.1
$\overline{P225}$	213.4 $\pm$ 30.4	234.2 $\pm$ 25.6	231.7 $\pm$ 17.6
Offset response			
$\overline{N470}$	473.8 $\pm$ 4.1	478.2 $\pm$ 22.9	467.5 $\pm$ 13.8
$\overline{P515}$	514.2 $\pm$ 6.3	516.7 $\pm$ 15.4	515.5 $\pm$ 8.5
$\overline{N580}$	580.4 $\pm$ 12.6	584.2 $\pm$ 16.6	577.3 $\pm$ 8.5
$\overline{P640}$	641.2 $\pm$ 15	634.9 $\pm$ 2.9	641.6 $\pm$ 22.7

**Table 4.10 Peak-to-peak amplitudes**

The mean amplitude and range in microvolts for the average of two recordings from five subjects.

Peaks	Stimulus		
	black	grey	white
Onset response			
$\overline{P125-N75}$	7.3 (1.8 - 12.8)	6.8 (5 - 8.8)	7.2 (3.7 - 12.8)
$\overline{P125-N170}$	9.2 (5.5 - 12.9)	8.3 (2.7 - 11.5)	12.5 (9.9 - 16.2)
$\overline{P225-N170}$	7.3 (4.0 - 11.9)	7.3 (3.9 - 12.4)	11.2 (7.1 - 15.0)
Offset response			
$\overline{P515-N470}$	5.7 (3.3 - 7.9)	4.2 (2.6 - 5.6)	3.7 (2.4 - 4.8)
$\overline{P515-N580}$	8.3 (5.8 - 12.1)	6.3 (3.2 - 10.8)	4.6 (3.3 - 6.2)
$\overline{P640-N580}$	5.4 (2.4 - 7.7)	4.3 (1.9 - 6.7)	4.9 (1.5 - 7.3)

#### 4.5.4 Discussion

This study has shown that reproducible VECPs could be recorded from dark pattern-onset stimuli. The stimuli were therefore suitable for further study in the new stimulus delivery system (Chapter 5).

The visual system is non-linear so it is not surprising that light increment stimuli should produce larger VECF signals than equal and opposite light decrement stimuli. There are, for instance, fundamental differences between the on- and off-pathways: in morphology, physiology, pharmacology and psychophysiology (Schiller 1986, Liu and Wong-Riley 1990, Wassle and Boycott 1991, Mutlukan and Damato 1992). Furthermore, in the macaque monkey the metabolic activity of the on-pathway neurones was found to be higher than that of the off-pathway (Liu and Wong-Riley 1990) and in work with rhesus monkeys the number of on-centre ganglion cells was found to be greater than the number of off-centre cells (Schiller 1986). If these differences exist in man they would be consistent with the larger VECF signals recorded from the light increment stimuli.

A further issue which needs investigation is the affect of the background luminance on the VECF. The level of the luminance would, for example, affect the resting discharge rate of the on- and off-centre ganglion cells.

Due to the fundamental differences in the morphology, physiology and pharmacology of the on- and off-pathways (Schiller 1986, Liu and Wong-Riley 1990, Wassle and Boycott 1991) it is possible that they differ in their susceptibility to various neuro-ophthalmic disorders. It might therefore be useful to test the on- and off-pathways separately when performing electrophysiological and perimetric examinations (Mutlukan and Damato 1992, Mutlukan et al 1992). There is evidence, for example, that some children with cerebral palsy perform poorly to tasks involving black on white visual material (Uhlen and Dickson 1970, May 1978, Marozas and May 1985) and this could be due to a deficit in the off-pathway.

#### 4.6 CONCLUSION

Motion-onset stimuli produced larger amplitude VECFs than pattern-reversal VECFs when the fovea was masked (Section 4.4). However, relatively long interstimulus intervals were required to minimise adaptation to the motion stimuli. From the

studies in this chapter the most suitable stimulus for studying the visual field appears to be the steady-state pattern-reversal dartboard presented in Section 4.3. With this stimulus it was possible to objectively detect a VECP signal from stimulation of 12 small areas of the visual field outside the fovea. The key to this success was to maximise the SNR of the VECP; this was achieved by matching the size of the stimulus pattern elements to the optimum check-size at each retinal eccentricity and by analysing the VECP signal in the frequency domain.

## **5. NEW STIMULUS DELIVERY SYSTEM**

### **5.1 INTRODUCTION**

This chapter describes the development of a prototype stimulus delivery system which enables VECPs to be recorded whilst patterned stimuli are simultaneously positioned on the retina by the system operator. The ultimate aim of this development is to produce a stimulus delivery system that can be used with patients who are unable to fixate reliably on a computer monitor screen.

Possible stimulus delivery methods were reviewed. As a result of this review, a new stimulus delivery system was developed which was based upon an indirect ophthalmoscope. The stimulus was presented in the plane of the retinal image using a miniature transmissive liquid crystal display (LCD). Radiometric measurements were made to ensure that the patient's exposure to blue light was within the safety guidelines published by the American Conference of Governmental Industrial Hygienists (1983).

Preliminary studies with the prototype system are described and they confirm that reproducible VECP recordings can be made. VECPs were successfully recorded during indirect ophthalmoscopy in one normal subject using full-field and quadrant field stimuli.

As a result of these experiments a robust instrument housing was constructed and plans for further experiments are presented.

The system has a wide range of potential clinical applications and these are briefly described.

## 5.2 REVIEW OF STIMULUS METHODS

Copenhaver and Eisenberg (1967) were the first to demonstrate that VECPs can be recorded during ophthalmoscopy whilst a stimulus is positioned on the retina. They connected a fibre optic system to a direct ophthalmoscope and this enabled a focal flickering stimulus to be focused on the fundus. Other similar systems were subsequently described (Shiple 1969, Inoue et al 1973, Sandberg and Ariel 1977). One such system is now commercially available for recording focal flicker ERGs to test cone function (Maculoscope, Doran Instruments, Mass, USA).

An alternative system using a helium-neon laser mounted on a slit-lamp table was developed by Hirose et al (1977). By chopping the laser beam with a mechanical shutter a flickering stimulus was produced. A joy stick was then used to position the stimulus on the retina. In this way the system was used to record ERGs and VECPs simultaneously.

The main disadvantage of these systems was that the stimulus was limited to a flickering disc superimposed upon a constantly illuminated background. The development of the scanning laser ophthalmoscope (SLO), however, has provided the opportunity to use more effective patterned stimuli.

The SLO employs a laser raster scan to image the retina. This enables relatively low levels of illumination to be used. By modulating the laser beam with an acoustic-optical modulator it is possible to superimpose patterns on the retina. Several groups have now recorded VECPs using these systems (Le Gargasson et al 1989, Katsumi et al 1989, Teping et al 1989). Simultaneous recordings of the VECP and PERG are also possible and they may prove to be an important tool in the investigation of focal retinal disease (Katsumi et al 1991). The SLO is, however, currently too expensive for widespread clinical use. As a result, the possibility of developing a new lower cost stimulus delivery system, based on an indirect ophthalmoscope, was investigated.

## 5.3 STIMULUS DELIVERY USING AN INDIRECT OPHTHALMOSCOPE

Figure 5.1 illustrates the optics of the indirect ophthalmoscope. A real, inverted, magnified image of the retina is formed in space at the second principal focus of the convex lens, known as a condensing lens. The observer holds this condensing lens at arms length and typically views the retinal image from a distance of 40 to 50 cm.

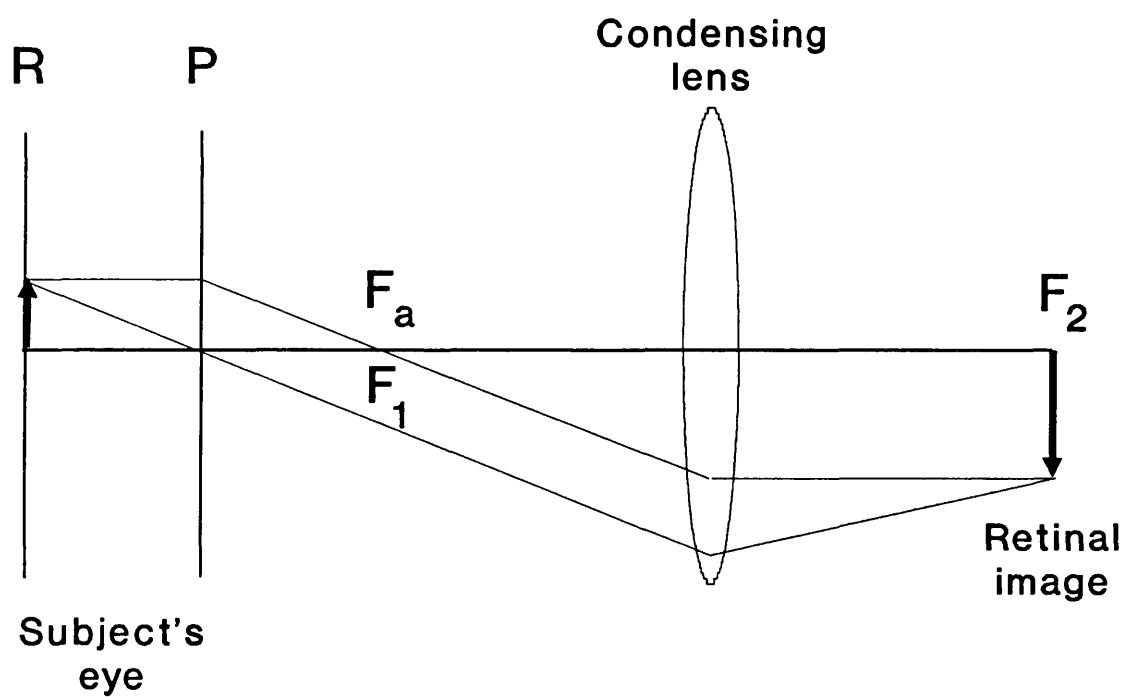


**Figure 5.1 Optics of the indirect ophthalmoscope.**  
 A real inverted image of the subject's retina is formed at the second principal focus of the condensing lens.  
 R, retina of subject; P, principal plane of subject's eye;  
 $F_a$ , anterior focus of subject's eye;  $F_1$ , first principal focus of condensing lens;  $F_2$ , second principal focus of condensing lens.

Illumination is provided by a bright electric lamp mounted on the observer's head. The subject's pupil size determines the field of retinal illumination and it is therefore usual to dilate the pupil widely prior to indirect ophthalmoscopic examination. Due to the linear nature of the optics, a point at the second principal focus of the condensing lens forms its own image on the retina. This simple principle is the key to the new stimulus delivery system.

A transparent screen was positioned at the second principal focus of the condensing lens so that the retina formed an image on the screen. By superimposing a stimulus on the screen, the stimulus was automatically focused onto the subject's retina. The stimulus and retina were also simultaneously visible to the observer, so it was possible for the observer to position and focus the stimulus anywhere on the retina.

Recent advances in transmissive LCD technology have allowed computer generated pattern stimuli to be used. The optical arrangement of the system is illustrated in Figure 5.2. A miniature transmissive black/white chip-on-glass LCD (Kyocera KL6448E-STP-FFW, supplied by Anders Electronics, London, UK) shown in Figure 5.3 was positioned in the plane of the retinal image. The display had an active area of 66 x 51 mm, with a resolution of 640 x 480 pixels. The pixels contained a fast response super twisted nematic fluid with a maximum contrast of 67 % (at 20° C). When the fluid was switched between states, the contrast changed exponentially providing 90 % of the contrast change in 250 ms (at 20° C). The LCD was interfaced to a personal computer using a Vidi III VGA card and a custom-built adapter card (Anders Electronics, London, UK). Referring to the system block diagram in Figure 2.1, the dual VGA card was replaced by the Vidi III card and the LCD was used for the stimulus display. The adapter card was connected between the output of the Vidi III card and the input to the LCD. This card was required to set the voltage levels used by the LCD.

A 15 dioptre double aspheric lens was used for the indirect ophthalmoscope and Figure 5.4 shows a reduced eye used to calculate the magnification of the instrument. CF is the focal length of the lens and corresponds to 66.7 mm for a 15 dioptre lens. N is known as the nodal point of the eye. BN is the distance between the subject's retina and the nodal point. The linear magnification is  $ab/AB$ . The angle made by aCF is equal to the angle ANB because the rays Ca and AN are parallel. Consequently,  $ab/CF = AB/BN$  and  $ab/AB = CF/BN$ . The distance BN is assumed to be 15 mm (Elkington and Frank 1984), so the magnification is simply the

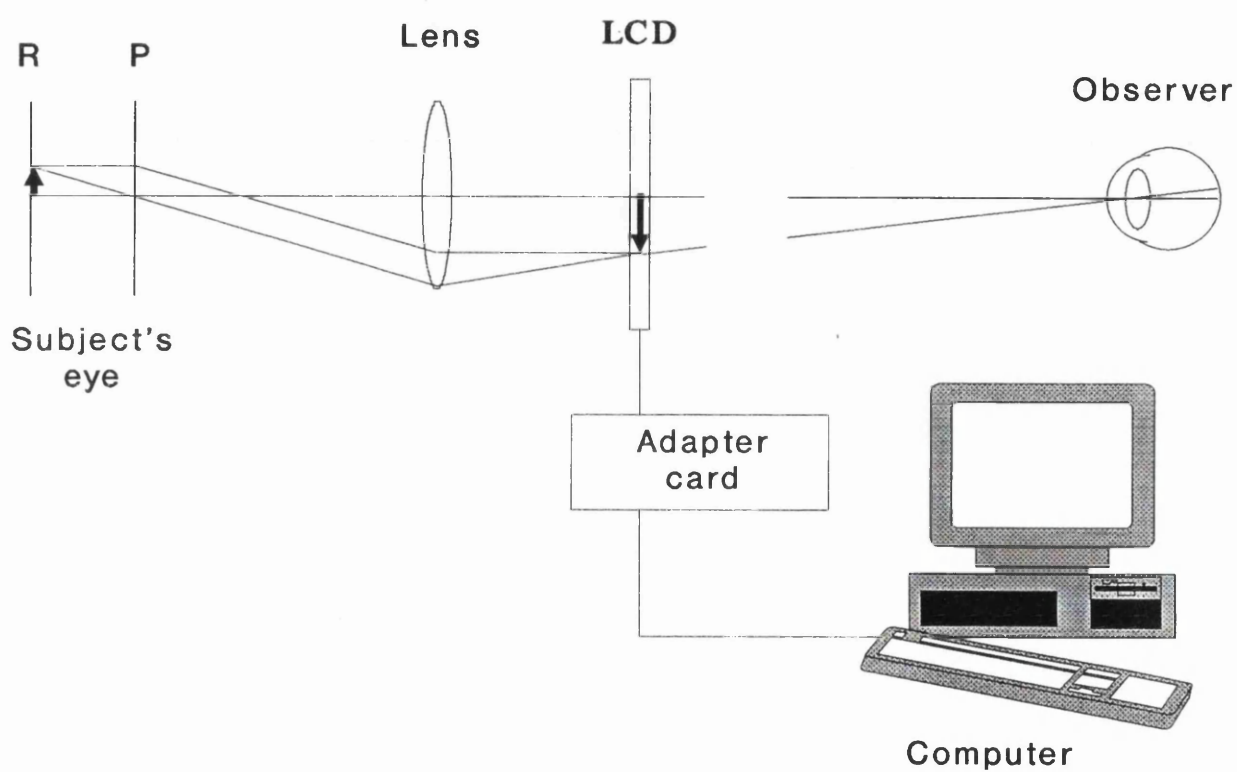


Figure 5.2. LCD stimulation of the retina during indirect ophthalmoscopy. The LCD screen is positioned in the plane of the retinal image formed by the condensing lens. R, subject's retina; P, principal plane of subject's eye.

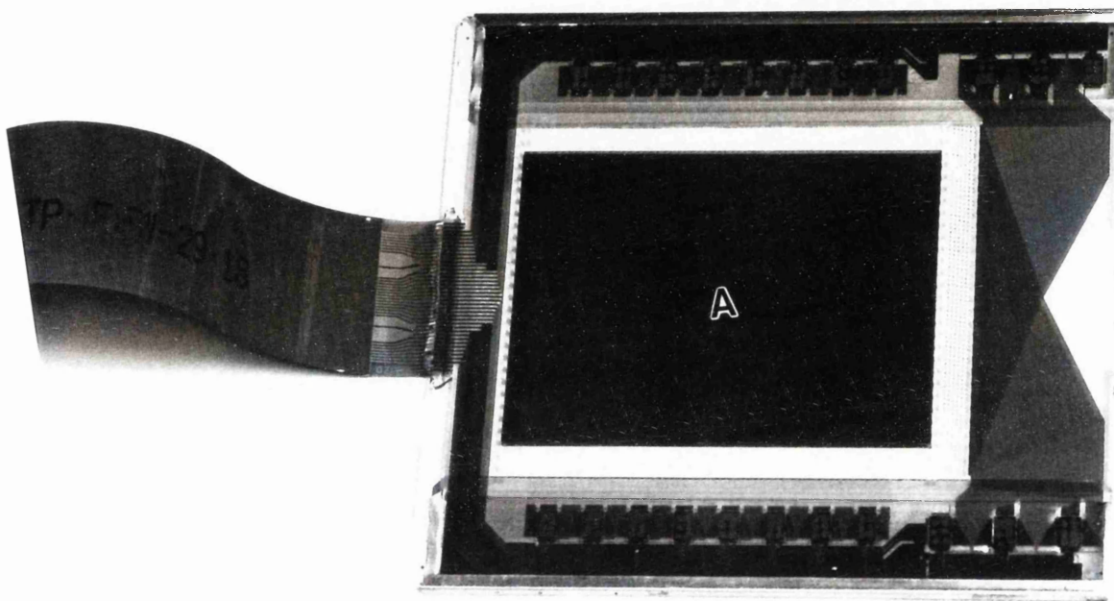


Figure 5.3 Kyocera KL6448E-STP-FFW LCD, showing active area (A).

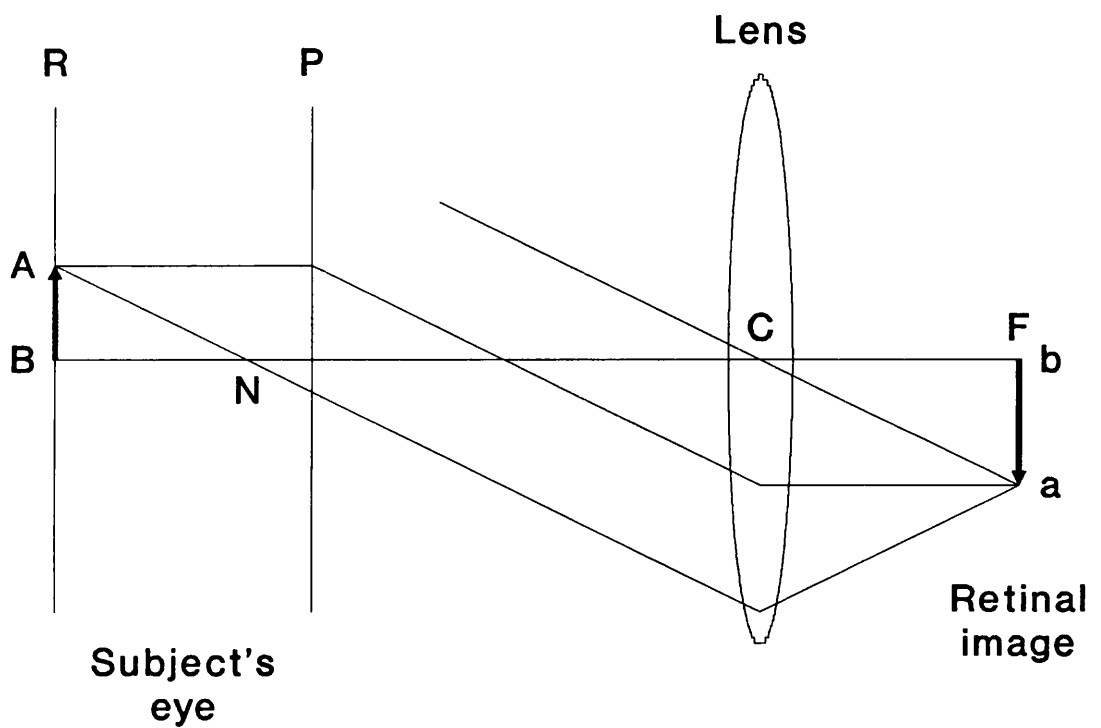


Figure 5.4 Magnification of the indirect ophthalmoscope. R, retina of subject; P, principal plane of subject's eye. Linear magnification =  $ab/AB$ . (Adapted with permission of the publisher from Elkington AR and Frank HJ (1984). Clinical optics. Blackwell Scientific, Oxford.)

focal length of the lens in millimetres divided by 15. The magnification of the 15 dioptre lens is therefore 4.44.

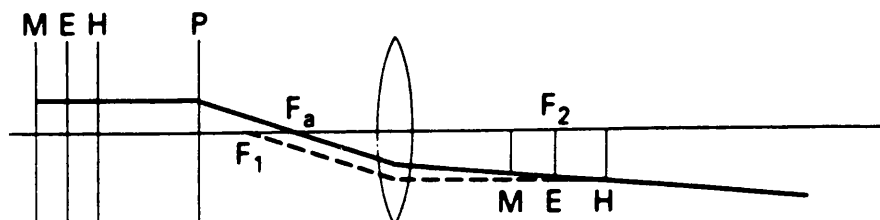
The diameter of the retinal field of view is equal to the diameter of the lens divided by the magnification of the indirect ophthalmoscope,  $50/4.44 = 11.25$  mm. Assuming a retinal magnification of  $276\mu\text{m}/\text{degree}$  (Holden and Fitzke 1988) this distance corresponded to a field of view of 40 degrees.

The above description of the stimulus system assumes that the subject is emmetropic. If the subject is ametropic the stimulus screen has to be repositioned relative to the lens of the indirect ophthalmoscope. In myopia, the retina is brought into focus in front of the second principal focus of the lens whilst in hypermetropia the retina is brought into focus behind the second principal focus of the lens.

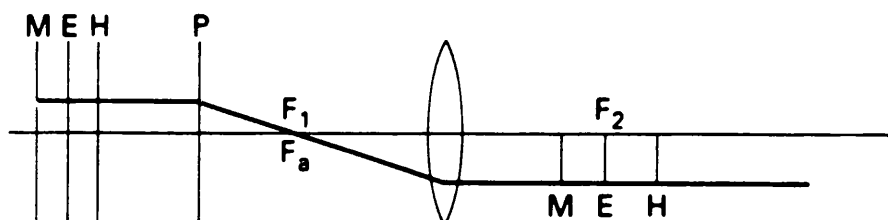
In order to avoid magnification errors due to ametropia it is also important to correctly position the condensing lens relative to the subject's eye. Figure 5.5 illustrates how the image size can vary according to the position of the condensing lens. In ametropia because rays emerging from the eye are not parallel, it is essential that the first principal focus of the condensing lens is coincident with the anterior focus of the eye, otherwise the size of the retinal image is either increased or decreased. Montgomery (1991) has calculated the retinal magnification error for different lens positions and for varying degrees of ametropia. If, for example, the lens is incorrectly positioned by 10 mm then a 5 % error in retinal magnification is obtained for 6 dioptres of ametropia. By contrast, in emmetropia the size of the retinal image is independent of the lens position because the rays emerging from the eye are parallel.

Prior to recording VECPs during indirect ophthalmoscopy, some preliminary measurements were made using the stimulus to ensure that reproducible recordings could be made. In addition, as recordings would take an extended period of time, it was necessary to assess the retinal blue light hazard during indirect ophthalmoscopy.

- a The first principal focus of the condensing lens  $F_1$  is closer to the eye than the anterior focus of the eye  $F_a$



- b The first principal focus of the condensing lens  $F_1$  is at the anterior focus of the eye  $F_a$



- c The first principal focus of the condensing lens  $F_1$  is beyond the anterior focus of the eye  $F_a$

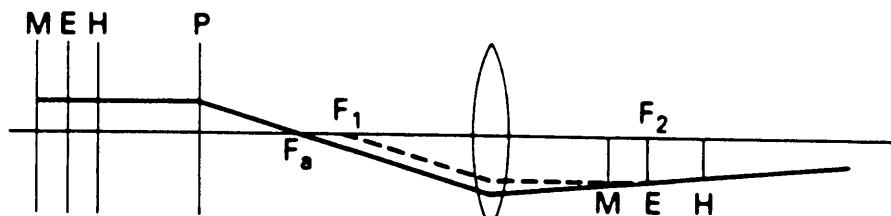


Figure 5.5 Optics of the indirect ophthalmoscope to show the effect of the position of the condensing lens on the retinal magnification. Relative positions of the retina and retinal image in myopia, M, emmetropia, E and hypermetropia, H. P is the principal plane of the subject's eye,  $F_a$  is the anterior focus of the subject's eye,  $F_1$  is the first principal focus of the condensing lens and  $F_2$  is the second principal focus of the condensing lens. (from Elkington and Frank, 1984).

## 5.4 PRELIMINARY STUDIES

### 5.4.1 Introduction

The feasibility of recording VECPs from an LCD stimulus was first evaluated using an LCD overhead projection screen (PCV6448C+2, LSK Kommunikations-System, Dieburg, Germany) which had the same rate of fluid contrast change as the miniature Kyocera screen. Five subjects were studied using pattern-reversal, pattern-onset and motion-onset stimuli. The results from these experiments indicated that the largest VECP signal was produced by a pattern-onset stimulus. Pattern-reversal stimuli and motion-onset stimuli produced significantly smaller signals and this was probably due to the slow contrast change of the LCD fluid. In the indirect ophthalmoscope stimulus delivery system, the observer was required to see the retina at all times. Therefore, it was decided to use a clear background and a dark pattern-onset stimulus so that the observer would have a clear view of the retina between stimulus presentations. This stimulus would therefore theoretically produce a VECP in response to the presentation of the pattern and a net luminance change. Dark and light pattern-onset stimuli were investigated in detail in a separate study using a computer monitor screen stimulus (Section 4.5).

Prior to evaluating the miniature Kyocera LCD screen during indirect ophthalmoscopy, it was necessary to check that the rate of contrast change was sufficiently fast to elicit a measurable VECP. During ophthalmoscopy the display and its associated drive circuitry needed to be positioned about 15 cm from the subject. It was therefore necessary to assess the potential vulnerability of recordings to electromagnetic interference. By back-lighting the LCD and lens assembly with an x-ray viewing box, time was spent evaluating these aspects at relatively low levels of illumination.

### 5.4.2 Method

Five normal male subjects, ranging in age from 26 to 50 years (mean age 34 years) were investigated with full-field and quadrant field stimuli. All subjects had normal visual fields, had a visual acuity better than or equal to 6/6, and were optically corrected. One eye was tested in each subject.

Dark checkerboard pattern-onset stimuli were presented from a clear background. For full-field stimulation, check-sizes of 30', 60' and 120' with a contrast of 67 % were used. In order to investigate the contribution of the net luminance change to these VECPs, a uniform full-field dark stimulus was also investigated. The quadrant field stimulus was used to test the right inferior visual field quadrant and the check-size was 120', which is the most effective check-size for stimulation at a retinal eccentricity of 12° (Section 4.2). During quadrant field stimulation, the fovea was masked by means of a disc with a five degree radius. It was recognised that the signal amplitude from superior field quadrants was likely to be smaller than from inferior quadrants (Section 4.2), but it was considered adequate to limit measurements to one inferior quadrant for this preliminary study. Subjects viewed a fixation letter to correctly position the stimulus on the retina. The stimulus presentation time was 800 ms and the interstimulus interval was 1.8 s. The position of the dark and light checks was alternated on successive presentations in order to minimise adaptation to the stimulus.

The LCD was placed on an x-ray viewing box and a yellow coated 15 dioptre condensing lens (Volk, Mentor, Ohio, USA) was positioned 67 mm (i.e. focal length of the lens) anterior to the LCD using a cardboard tube. The subject's cornea was positioned 82 mm anterior to the condensing lens so that the anterior focus of the subject's eye coincided with the first principal focus of the lens. In order to assess any problem with electromagnetic interference, two control recordings were made with the 60' check full-field stimulus presented on the LCD and with the light source obscured so that there was no visual stimulation.

VECPs were recorded from a mid-occipital electrode, placed 5 cm superior to theinion, and were measured relative to an electrode placed on the right earlobe. When quadrant field stimuli are used, the maximum VECp may be over the right or the left occipital cortex (Section 4.2) and additional recording sites should be used to detect the maximum signal. Unfortunately, only a single channel amplifier was available for the study. Nevertheless, this was considered adequate to determine whether VECps could be recorded from stimuli presented on the LCD. The amplifier gain was 10,000 and the filter bandwidth was 1 to 300 Hz. The responses to 50 stimulus presentations were averaged. Two signal averages were recorded for each stimulus and signal reproducibility was measured using cross-correlation. The recording time was about 1.5 minutes for each stimulus.

### 5.4.3 Results

Reproducible VECP signals were recorded from each of the five subjects and the results are summarised in Table 5.1.

The signals evoked by the pattern stimuli were larger than that evoked by the uniform dark stimulus. The VECPs were characterised by a large negative peak, N1, which was preceded and followed by a positive peak, P1 and P2. Figure 5.6 shows representative recordings made from one subject, aged 50 years.

Like the pattern stimuli, the signals obtained from the uniform luminance stimulus were characterised by a negative peak, N1. This peak was however, smaller and later than that obtained with the pattern stimuli. Furthermore, there was no clear P1 component. The values for cross-correlation were also smaller than those obtained from the pattern stimuli.

The control recordings contained residual EEG noise activity as a result of signal averaging. No reproducible features were obtained in these recordings.

### 5.4.4 Discussion

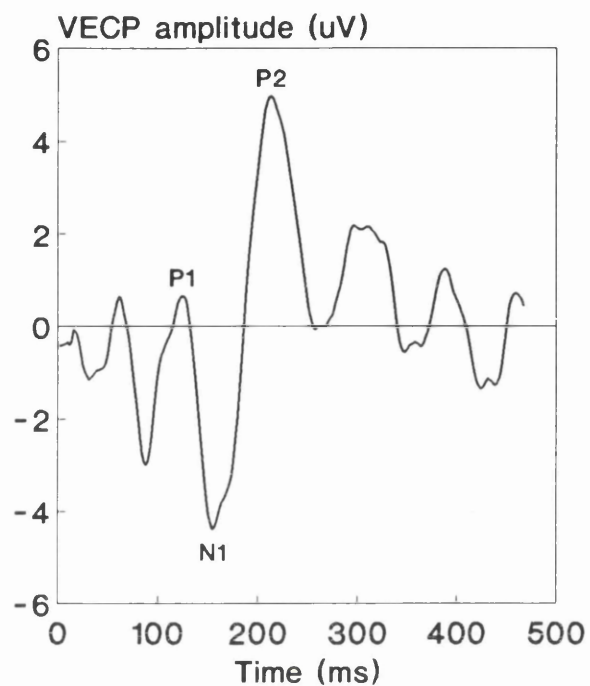
Electromagnetic interference from the LCD and its drive circuitry was not found to be a significant problem as no signal was measured in the control recordings. The results also confirmed that the contrast of the LCD fluid changed sufficiently rapidly to elicit a measurable VECP. The values for cross-correlation were low compared to those obtained for full-field stimuli in Section 2.11; however, this was to be expected because in this study the SNR was reduced due to the fact that the signal amplitude was smaller and fewer signals were averaged.

During the pattern-onset stimulation there was also a net luminance decrease. The signals evoked by these patterns could therefore have been produced by the pattern presentation and/or the luminance change. The VECPs recorded from the pattern stimuli were larger than those recorded from the uniform stimulus and also differed in shape. The results therefore indicated that the VECP produced by the pattern stimuli included a pattern specific component. The finding that a larger amplitude signal can be recorded by means of a patterned stimulus is consistent with results obtained using conventional stimulus delivery systems (Spehlmann 1965, Harter 1970).

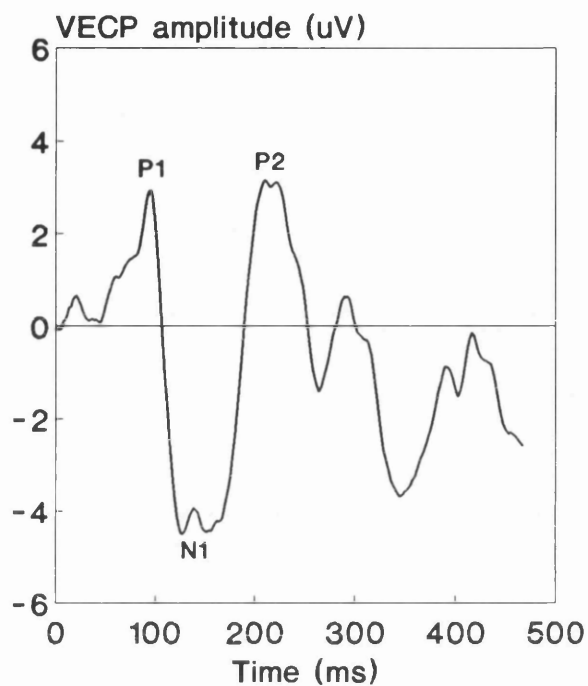
**Table 5.1 Summary of VECP results obtained using pattern-onset stimulation on the Kyocera KL6448E-STP-FFW LCD screen.**

The table shows the mean values and range for the average of 100 responses from five subjects.

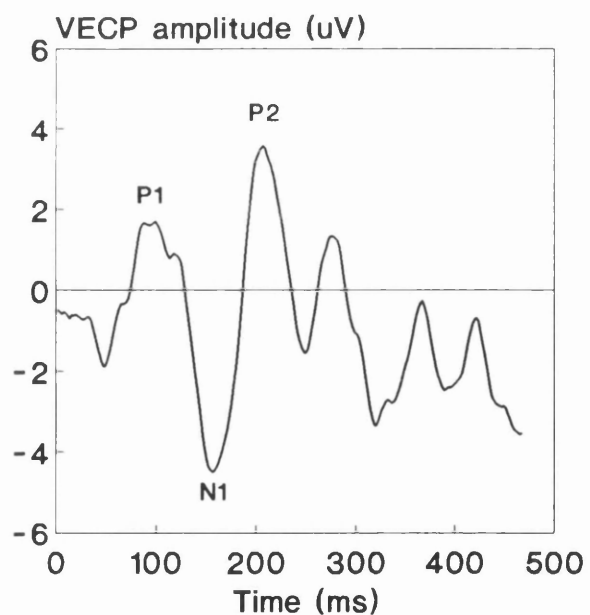
Stimulus	Cross-corrn.	Latencies			Amplitudes	
		P1 (ms)	N1 (ms)	P2 (ms)	P1-N1 ( $\mu$ V)	P1-N2 ( $\mu$ V)
Full-field stimuli						
30' check-size	0.53 0.39-0.75	92 74-125	148 125-168	232 211-262	6.8 4.4-9.9	7.6 5.3-10
60' check-size	0.69 0.56-0.81	87 80-96	130 104-156	220 197-244	8 6.7-9.4	8.9 5.8-11.5
120' check-size	0.64 0.36-0.87	89 76-102	140 98-180	215 207-236	6.8 5.5-8.4	9.3 6.1-13.2
Uniform stimulus	0.44 0.19-0.73	106 96-125	163 137-234	225 193-275	2.3 1.5-3.7	4 2.7-5.4
Quadrant field stimulus						
120' check-size	0.48 0.15-0.77	89 76-109	154 106-172	213 168-260	5.7 3.9-7.6	4.9 4.2-6.4



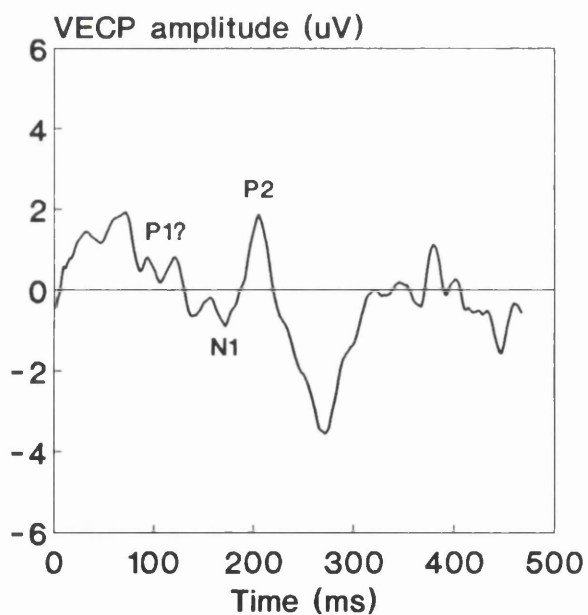
a) 30 minute checksize



b) 60 minute checksize



c) 120 minute checksize



d) Dark uniform stimulus

Figure 5.6 Pattern-onset VECPs recorded from LCD stimulus

The finding that VECPs could be recorded from quadrant field stimulation showed that the system was capable of testing areas of the retina outside the fovea. The amplitude of the signal from the quadrant stimulus was smaller than that obtained when the central visual field was stimulated (Table 5.1). This finding is consistent with the results obtained using conventional stimulus delivery systems (Harter 1970). Larger amplitude VECP signals may have been recorded from the quadrant field stimuli if additional recording electrodes had been placed over the right and left occipital cortex (Section 4.2).

## **5.5 BLUE LIGHT HAZARD ASSESSMENT**

### **5.5.1 Introduction**

The potential hazard to patients from excessive light exposure during ophthalmic procedures is well recognised (Calkins and Hochheimer 1980, Calkins et al 1980, Mainster et al 1983). The indirect ophthalmoscope is a blue light hazard, potentially causing photochemical injury to the retina (Sloney 1983). Damage from blue light is linearly additive for periods as great as four hours, with some slight cumulative effect for periods of up to almost four days.

Patient safety in the introduction of any new clinical technique must be paramount. A blue light hazard assessment of the new stimulus delivery system was therefore undertaken.

### **5.5.2 Blue light hazard**

The American Conference of Governmental Industrial Hygienists (ACGIH) have published criteria (1983) for determining the maximum permissible daily exposure to blue light based on current knowledge of acute and chronic injury. The exposure limits are expressed in terms of radiance and are calculated by spectrally weighting the source spectrum,  $L_\lambda$ , with a blue light hazard function,  $B_\lambda$ .  $B_\lambda$  weights each wavelength relative to a peak hazard at 440 nm (Figure 5.7).

Relative blue light hazard

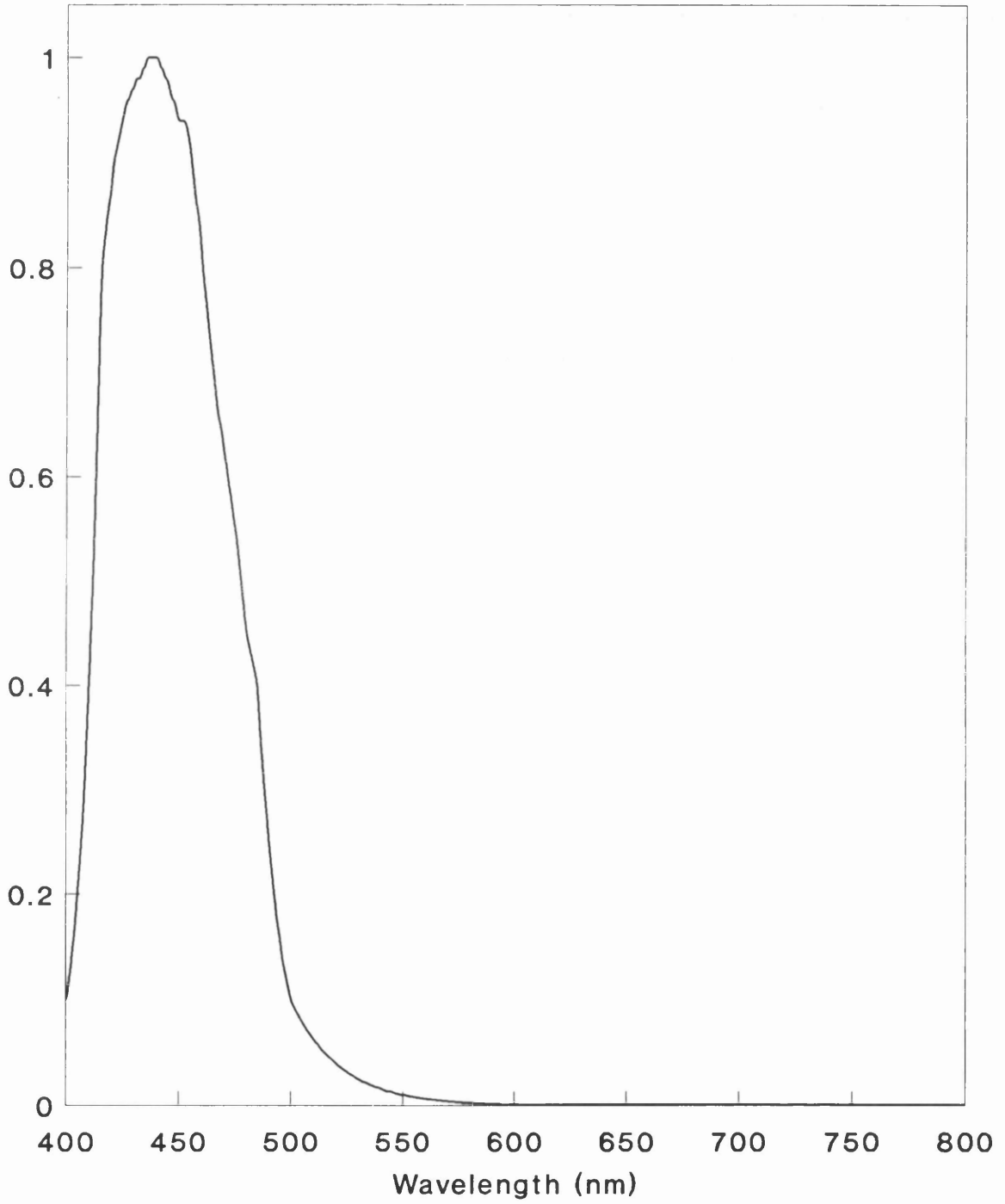


Figure 5.7 Blue light hazard function

The integrated spectrally weighted radiance should not exceed  $100 \text{ J cm}^{-2}\text{sr}^{-1}$  for durations less than  $10^4 \text{ s}$  or exceed  $0.01 \text{ W cm}^{-2}\text{sr}^{-1}$  for durations longer than  $10^4 \text{ s}$ ,

$$L_{\text{haz}} = \sum_{400}^{1400} L_{\lambda} B_{\lambda} \Delta\lambda = 100/t \text{ W cm}^{-2}\text{sr}^{-1}, t \leq 10^4 \text{ s} \quad (1a)$$

$$L_{\text{haz}} = \sum_{400}^{1400} L_{\lambda} B_{\lambda} \Delta\lambda = 0.01 \text{ W cm}^{-2}\text{sr}^{-1}, t \geq 10^4 \text{ s} \quad (1b)$$

where  $L_{\text{haz}}$  is the maximum permissible source radiance,  $\Delta\lambda$  is the wavelength associated with  $L_{\lambda}$  and  $t$  is time in seconds. These limits apply to an extended source with a pupil of 3 mm diameter.

The blue light hazard of the VECP indirect ophthalmoscope recording set up was assessed using spectral radiometric measurements made according to the radiometric method described by Calkins and Hochheimer (1980) and Calkins et al (1980). This method derives retinal irradiance, so in order to calculate the duration for maximum permissible exposure the blue light exposure limit was re-expressed in terms of retinal irradiance.

### 5.5.3 Retinal irradiance exposure limit

For an extended source, retinal irradiance is related to source radiance by the equation:

$$E_{\text{ret}} = L \frac{A}{f^2} n^2 T \quad (2)$$

where  $E_{\text{ret}}$  is the retinal irradiance,  $L$  is the source radiance,  $A$  is the pupil area,  $f$  is the distance from the pupil plane to the retina,  $n$  is the refractive index of the vitreous humor and  $T$  is the transmission of the optic media (Calkins et al 1980).

The retinal irradiance exposure limit,  $E_{\text{haz}}$  is then:

$$E_{\text{haz}} = L_{\text{haz}} \frac{A}{f^2} n^2 T \quad (3)$$

Substituting 2.15 cm for  $f$ , 1.33 for  $n$  (Calkins and Hochheimer 1980, Calkins et al 1980) and 0.5 for  $T$  at a wavelength of 440 nm (WHO 1982), the retinal exposure limit is:

$$E_{\text{haz}} = 1.35/t \text{ W cm}^{-2}, t \leq 10^4 \text{ s} \quad (4a)$$

$$E_{\text{haz}} = 0.135 \text{ mW cm}^{-2}, t \geq 10^4 \text{ s} \quad (4b)$$

#### 5.5.4 Spectral radiometric measurements

Measurements were made between 400 and 610 nm at wavelength intervals of 1 nm using a Bentham DM150 dual monochromator spectroradiometer (Bentham Instruments Ltd, Reading, UK). Between 610 and 800 nm measurements were made at wavelength intervals of 10 nm using an International Light IL700A spectroradiometer (International Light, Newburyport, Mass., USA). The blue light hazard is negligible for wavelengths from 800 to 1400 nm so measurements were not made in this region. Both radiometers were calibrated against sources traceable to standards at the National Physical Laboratory.

The assessment was made using a Keeler Fison binocular indirect ophthalmoscope headset fitted with a tungsten filament bulb. Measurements were made for the maximum recommended output voltage setting, nominally 6 V, and for the maximum obtainable output voltage setting, nominally 7.5 V. The voltage setting was controlled using a rheostat and as with previous measurement practice the bulb was aged (Calkins and Hochheimer 1980, Calkins et al 1980, Kossol et al 1983). A few trial measurements with a new bulb indicated that the radiance of a new bulb was approximately 20 % greater. Two 15 dioptre lenses were assessed. One was clear and the other was yellow coated to attenuate harmful blue wavelengths (Volk, Mentor, Ohio, USA). The LCD transmission was measured with the whole screen clear. The LCD has a contrast control which is normally adjusted to give maximum contrast (67 % at 20°C) between the clear and black states. The transmission was measured with the control set for maximum contrast (normal use) and repeated with the control set for maximum transmission (worst case hazard). The LCD was not normally operated in its maximum transmissive state because the pattern contrast was sub-optimal.

Figure 5.8 shows how the radiometers were used to determine the radiant flux LA of the indirect ophthalmoscope, where L is the radiance of the filament image and A is its projected area:

$$LA = E_{\text{air}} d^2 \quad (5)$$

where  $E_{\text{air}}$  is the irradiance measured in air by the radiometer at a distance  $d$  from the filament image. The distance  $d$  was 16.2 cm and the position of the radiometer was adjusted to obtain the maximum value of  $E_{\text{air}}$ . The lens was positioned 29 cm from the mirror to simulate clinical conditions. At this distance all the light passed through the lens.

In clinical use, a filament image of radiance  $L$  and area  $A$  is formed in the pupillary plane of the patient's eye, from (3) and (5), the retinal irradiance  $E_{\text{ret}}$  is therefore:

$$E_{\text{ret}} = (E_{\text{air}} d^2) \frac{n^2 T}{f^2} \quad (6)$$

In terms of spectral irradiance:

$$E_{\lambda_{\text{ret}}} = (E_{\lambda_{\text{air}}} d^2) \frac{n^2 T}{f^2} \quad (7)$$

The effective blue light retinal irradiance,  $E_b$ , was calculated by weighting  $E_{\lambda_{\text{ret}}}$  with the blue light hazard function as below:

$$E_b = \sum_{400}^{800} E_{\lambda_{\text{ret}}} B_{\lambda} \Delta\lambda = \sum_{400}^{800} E_{\lambda_{\text{air}}} B_{\lambda} \Delta\lambda d^2 \frac{n^2 T}{f^2} \quad (8)$$

Substituting for  $d$ ,  $n$ ,  $f$  and  $T$ :

$$E_b = 50.2 \times \sum_{400}^{800} E_{\lambda_{\text{air}}} B_{\lambda} \Delta\lambda \quad (9)$$

In order that the blue light retinal irradiance exposure limit is not exceeded the value for  $E_b$  calculated in equation (9) should be less than the value for  $E_{\text{haz}}$  in equation (4).

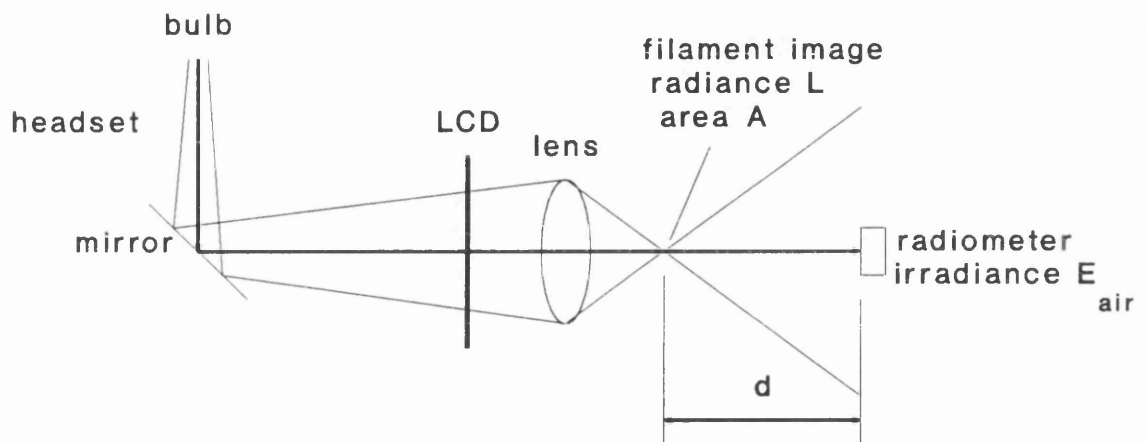


Figure 5.8 Indirect ophthalmoscope radiometry

### 5.5.5 Results

Figure 5.9 shows the spectral irradiance of the indirect ophthalmoscope, measured in air using the clear 15 dioptre lens. Figure 5.10 illustrates the spectral transmission of the yellow lens coating and Figure 5.11 illustrates the spectral transmission of the LCD.

In order to calculate the blue hazard, the measurements illustrated in Figures 5.9, 5.10 and 5.11 were combined and weighted with the blue hazard function. Figures 5.12 and 5.13 show the weighted spectrum using the clear lens for bulb voltage settings of 6 volts and 7.5 volts respectively. Figures 5.14 and 5.15 show the weighted spectrum using the yellow coated lens for bulb voltage settings of 6 volts and 7.5 volts respectively.

The weighted spectra were summed according to equation (9) to calculate the effective blue light retinal irradiance and the duration for maximum permissible exposure (Table 5.2).

The duration for maximum permissible exposure using the clear lens was found to be of the order 20 minutes. The blue light hazard was significantly reduced by the yellow coated lens and the duration for maximum permissible exposure was indefinite.

### 5.5.6 Discussion

The duration for maximum permissible exposure to the indirect ophthalmoscope stimulus delivery system has been calculated and is more than ample to allow VECP recording. These calculated values are compatible with psychophysical and ultrastructural studies using indirect ophthalmoscopes.

Dawson and Heron (1970) exposed eyes to maximum illumination with the indirect ophthalmoscope for 8 minutes and found no significant differences in dark adaptation curves when compared with fellow control eyes.

Robertson and Erickson (1979) studied an eye enucleated for malignant melanoma. Prior to enucleation the eye was exposed to maximum illumination with an indirect ophthalmoscope for 45 minutes. This exposure was sufficiently severe to cause loss of corneal epithelium and electron microscopy showed some changes in photoreceptor outer segments including the disruption of lamellar membranes and the

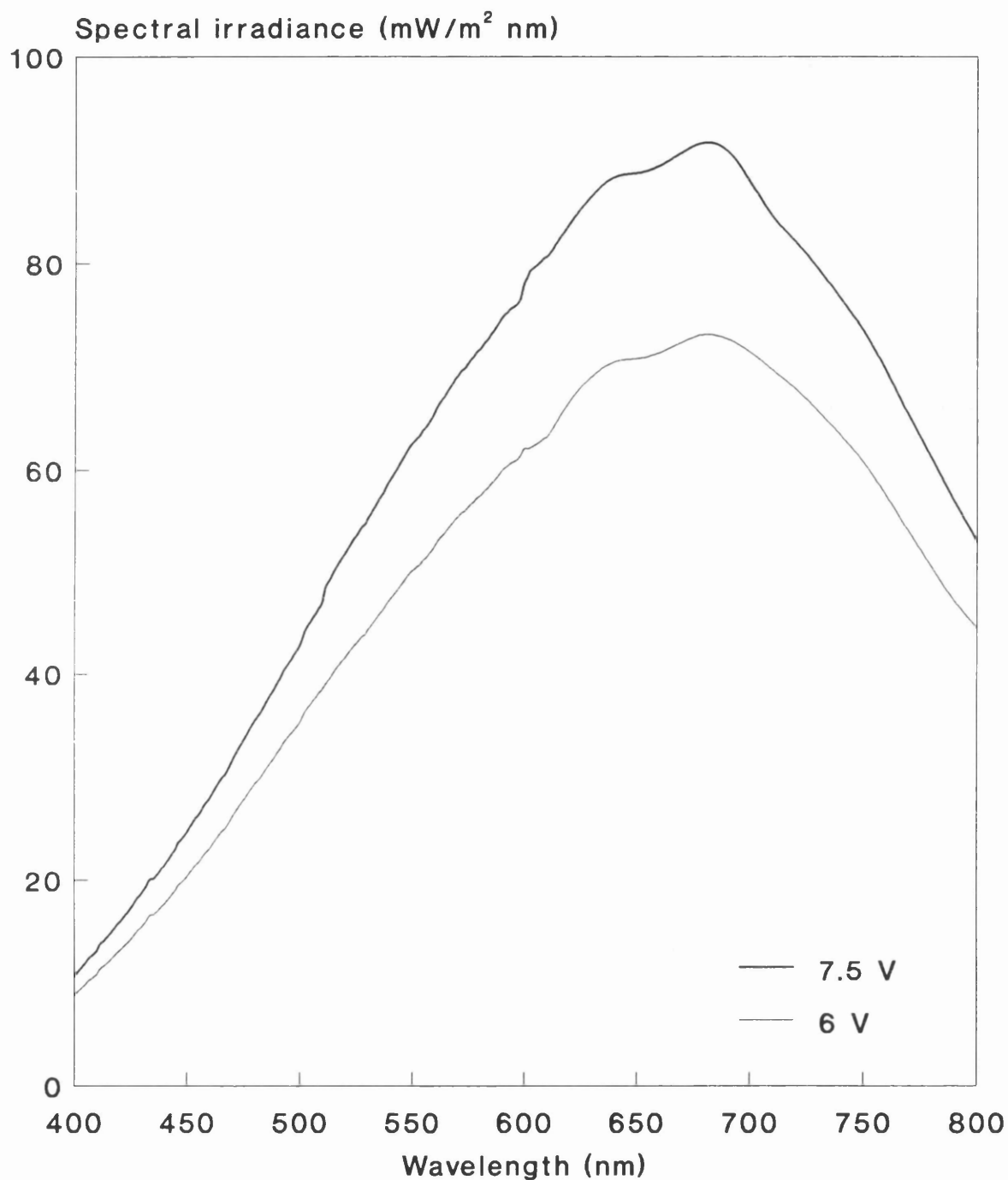


Figure 5.9 Spectral irradiance from indirect ophthalmoscope for two bulb voltage settings (using clear 15D lens).

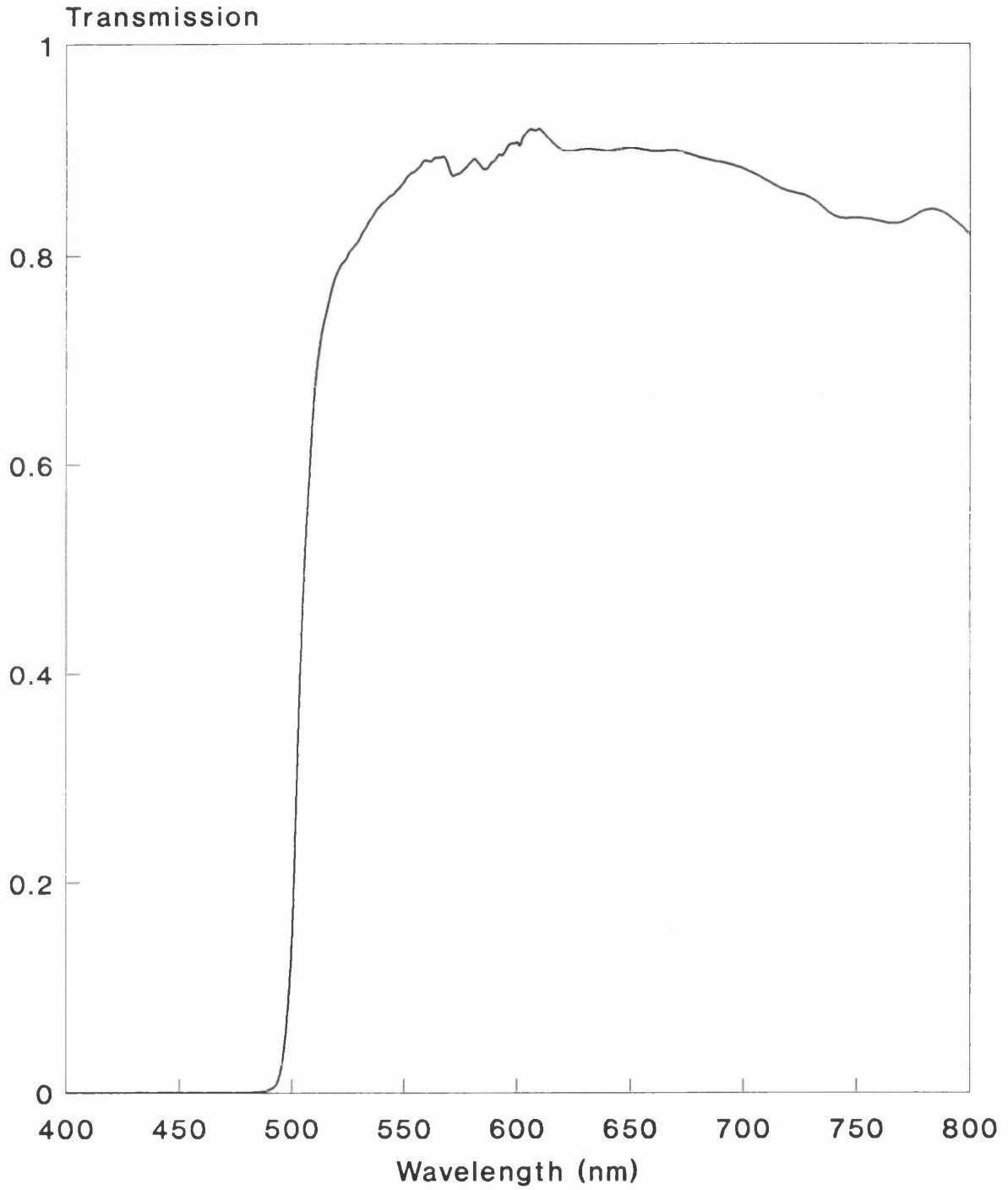


Figure 5.10 Transmission of yellow lens coating

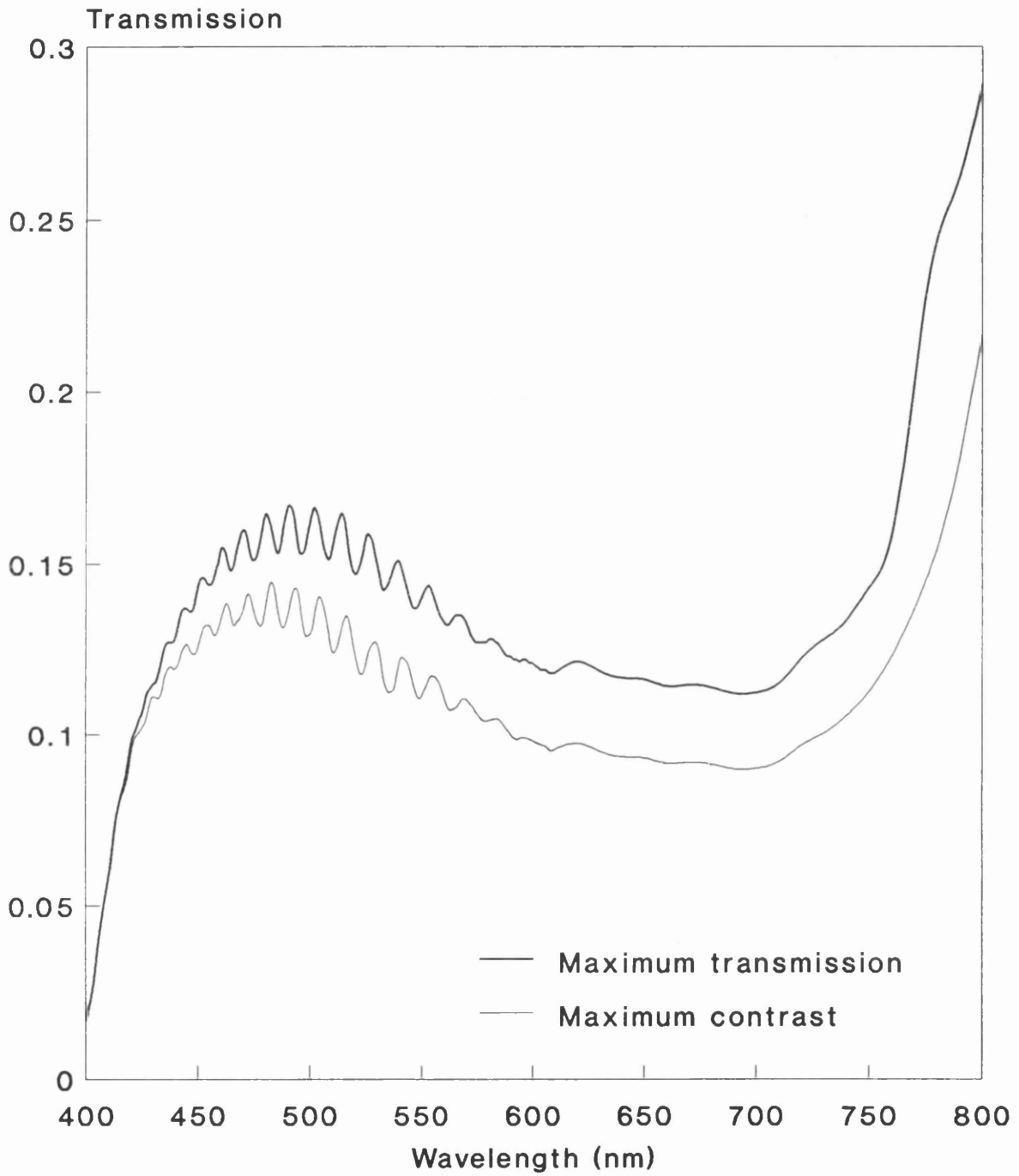


Figure 5.11 Transmission of liquid crystal display in clear transmissive state for two contrast settings.

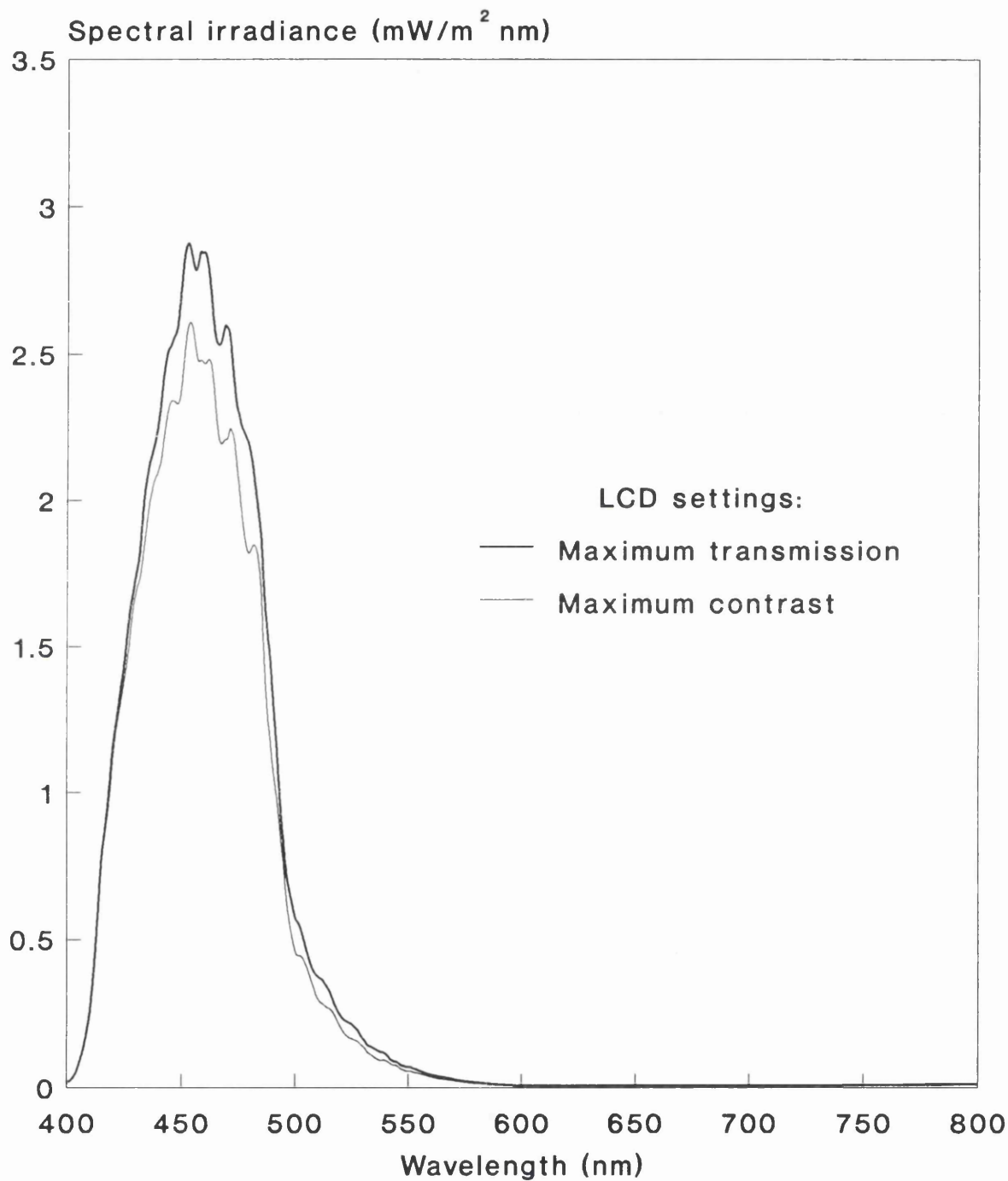


Figure 5.12 Blue light hazard weighted spectral irradiance using 6 Volt bulb setting, clear lens and LCD.

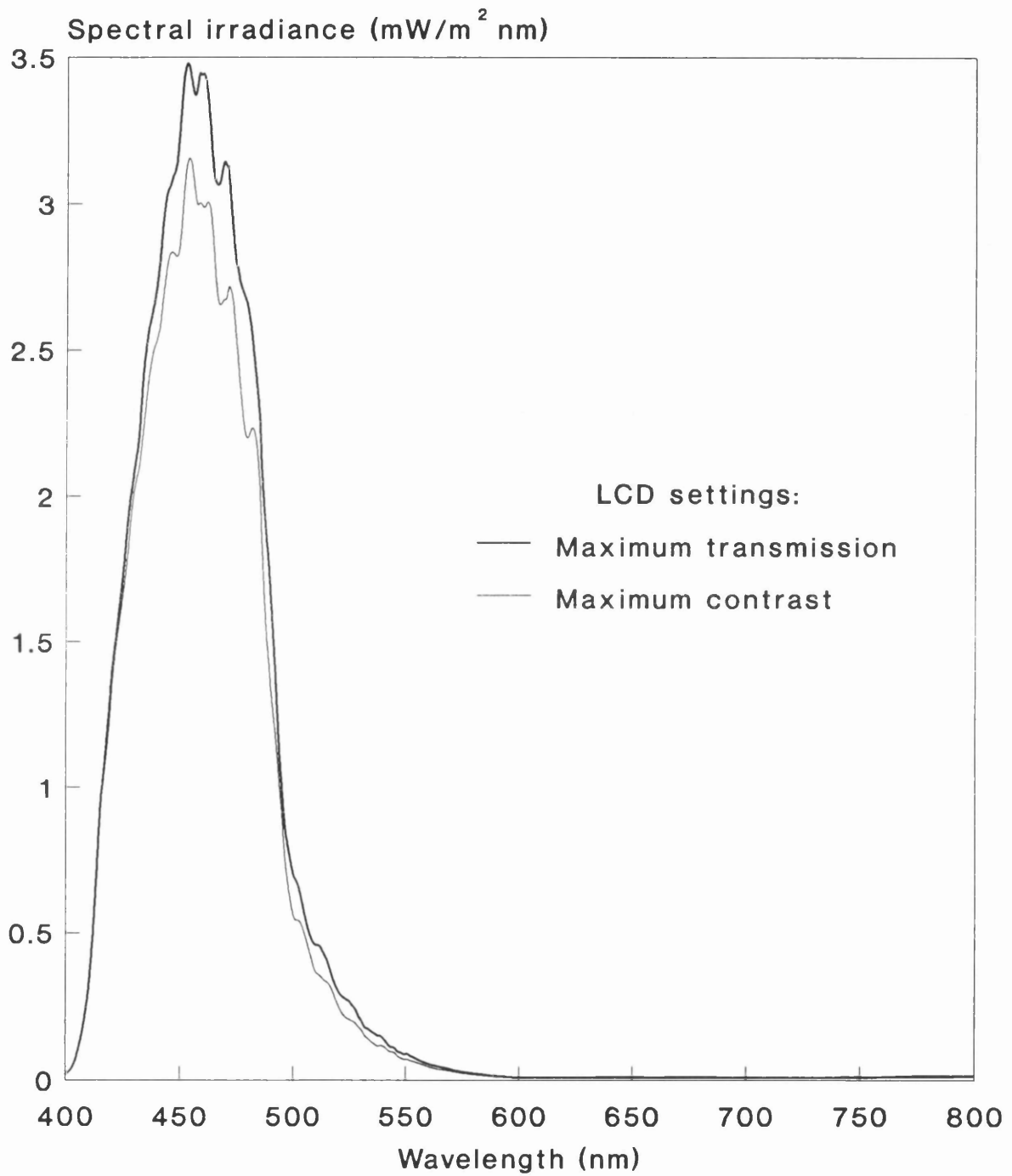


Figure 5.13 Blue light hazard weighted spectral irradiance using 7.5 Volt bulb setting, clear lens and LCD.

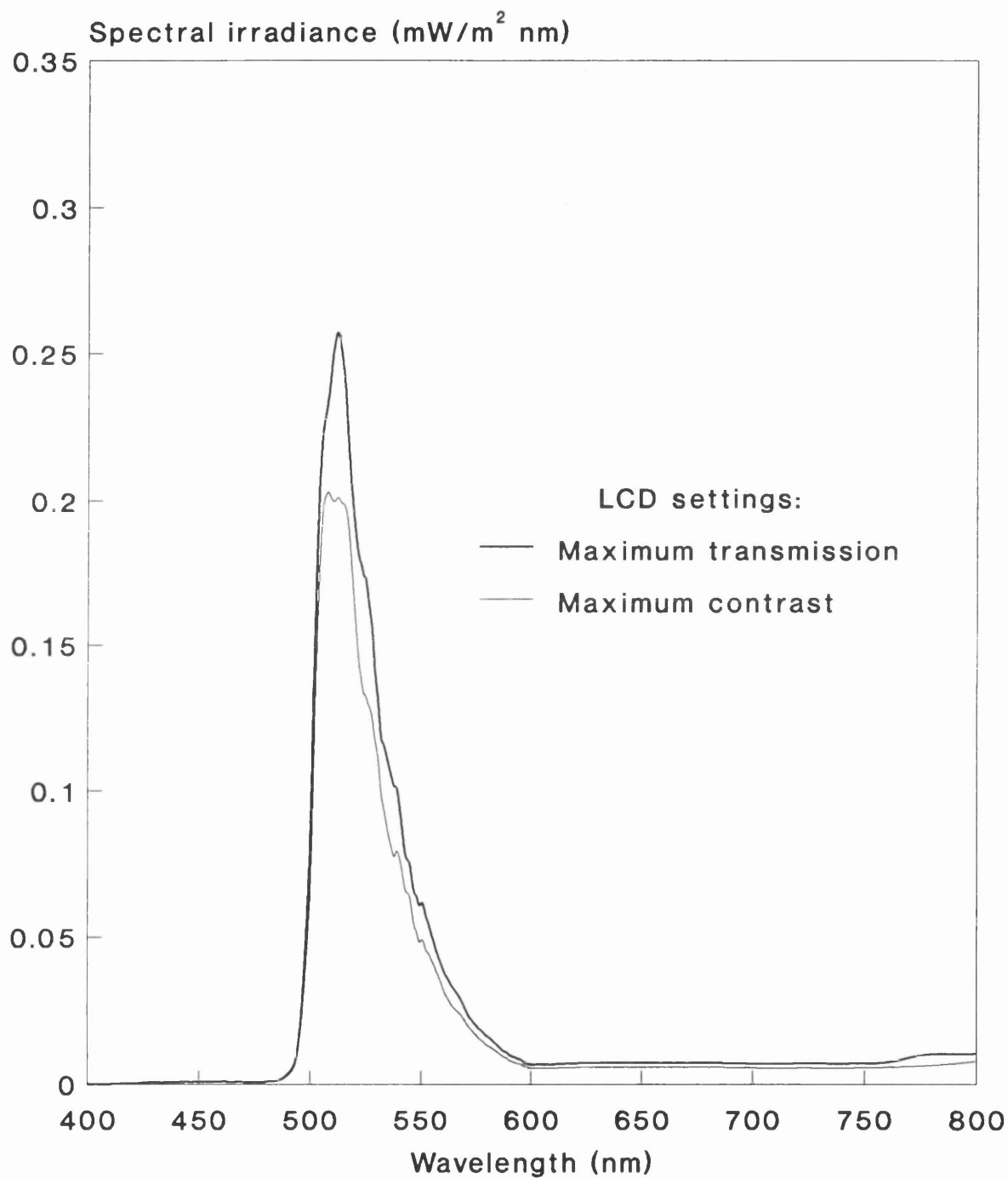


Figure 5.14 Blue light hazard weighted spectral irradiance using 6 Volt bulb setting, yellow coated lens and LCD.

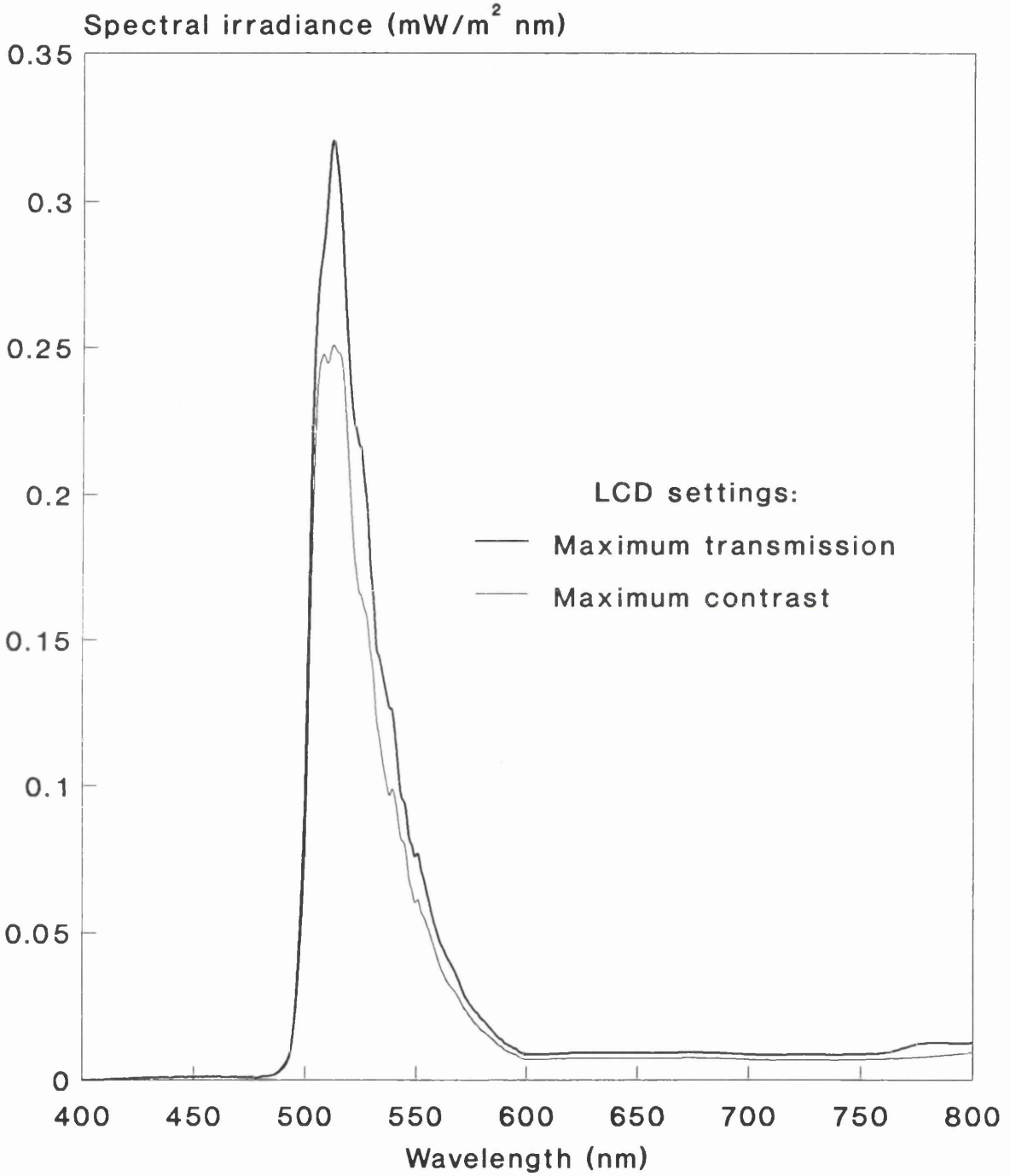


Figure 5.15 Blue light hazard weighted spectral irradiance using 7.5 Volt bulb setting, yellow coated lens and LCD.

**Table 5.2 Effective blue light retinal irradiance and duration for maximum permissible exposure for various measurement conditions**

Lens	Bulb voltage setting (Volts)	LCD contrast setting	Effective blue light retinal irradiance ( $\text{mW cm}^{-2}$ )	Duration for maximum permissible exposure (s)
Clear	6	Maximum contrast	0.85	1600
Clear	6	Maximum transmission	0.95	1400
Clear	7.5	Maximum contrast	1.0	1300
Clear	7.5	Maximum transmission	1.2	1200
Yellow coated	6	Maximum contrast	0.045	$>10^4$
Yellow coated	6	Maximum transmission	0.055	$>10^4$
Yellow coated	7.5	Maximum contrast	0.055	$>10^4$
Yellow coated	7.5	Maximum transmission	0.068	$>10^4$

swelling of mitochondria. These retinal changes were, however, considered to be reversible based on experiments with primates (Ts'o et al 1972).

It should also be noted that the level of retinal illumination in the present experiments was probably less than that used in the above studies because the light source was attenuated by the LCD. Furthermore, in neither of the above studies was there an attempt to filter out the more hazardous blue wavelengths.

Nevertheless, intense light remains a potential hazard, especially as the tolerance of diseased eyes may well be lower than that of healthy eyes. In order to limit the blue light hazard it is necessary to minimise retinal light exposure and this can be achieved in a number of ways:

1. The recording duration should be kept to a minimum.
2. Stimuli should be designed so that the areas of the retina not being investigated are masked.
3. A yellow coated lens should be used.
4. The ophthalmoscope rheostat should be turned to the lowest voltage setting that allows fundus landmarks to be identified.

The retinal exposure could be further reduced if the LCD transmission was increased. Unfortunately, the transmission of light through super twisted nematic fluid LCDs is inefficient (Figure 5.11).

Within the next few years, miniature thin film transistor (TFT) and ferro-electric (smetic) LCD modules should become commercially available. These displays switch rapidly at video refresh rates and this will allow the recording of steady-state VECPs. Using the signal processing techniques developed in Chapter 3, the recording of steady-state VECPs will enable a reduction in the recording time and this will further reduce retinal light exposure.

## 5.6 OPHTHALMOSCOPIC STUDY

### 5.6.1 Introduction

The aim of this study was to confirm that reproducible VECPs could be recorded during indirect ophthalmoscopy from full-field and quadrant field stimuli.

### 5.6.2 Method

One normal male subject, 31 years old, was investigated. The subject had normal visual fields and a visual acuity 6/5. The right eye was tested following full dilatation of the pupil. The LCD and adapter circuit (Section 5.3) are supplied unmounted by the manufacturer and are consequently fragile. Recordings from further subjects during indirect ophthalmoscopy have been postponed until a suitable housing is completed (Section 5.7).

A yellow coated 15 diopetre condensing lens (Volk, Mentor, Ohio, USA) was positioned anterior to the LCD using a cardboard tube. The subject's cornea was positioned 82 mm anterior to the condensing lens so that the anterior focus of the subject's eye coincided with the first principal focus of the lens. The ophthalmologist supported the lens and LCD in his hands. As is usual practice during indirect ophthalmoscopy, the light source was supported on the ophthalmologist's head using a headband. The LCD adapter circuit was supported by the test subject.

Dark checkerboard pattern-onset stimuli were presented from a clear background. For full-field stimulation, the check-size was 60'. The right inferior field quadrant was tested with 120' checks, which is the most effective check-size for stimulation at a retinal eccentricity of 12°. During quadrant field stimulation, the fovea was masked by means of a disc with a five degree radius. It was recognised that the signal amplitude from superior field quadrants was likely to be smaller than from inferior quadrants (Section 4.2), but it was considered adequate to limit measurements to one inferior quadrant for this preliminary study. Steady fixation was maintained with the aid of a fixation letter focused on the fovea. The stimulus presentation time was 800 ms and the interstimulus interval was 1.8 s. The position of the dark and light checks was alternated on successive presentations in order to minimise adaptation to the stimulus. In order to assess any problem with electromagnetic interference, two

control recordings were made with the 60' check full-field stimulus presented on the LCD but with the light source obscured so that there was no visual stimulation.

VECPs were recorded from a mid-occipital electrode, placed 5 cm superior to theinion, and were measured relative to an electrode placed on the right earlobe. When quadrant field stimuli are used, the maximum VECP may be over the right or the left occipital cortex (Section 4.2) and additional recording sites should be used to detect the maximum signal. As in Section 5.4, only a single channel amplifier was available for the study. Nevertheless, this was considered adequate to determine whether VECPs could be recorded during indirect ophthalmoscopy. The amplifier gain was 10,000 and the filter bandwidth was 1 to 300 Hz. The responses to 50 stimulus presentations were averaged. Two signal averages were recorded for each stimulus and signal reproducibility was measured using cross-correlation. The recording time was about 1.5 minutes for each stimulus.

In order to check that retinal function remained normal, the subject's colour vision was assessed using the Farnsworth-Munsell 100-hue test one week after the recordings.

### 5.6.3 Results

The cross-correlation for the full-field recordings was 0.43 and the combined waveform is shown in Figure 5.16. N1 and P1 components were observed at approximately 130 and 240 ms respectively, the P1-N1 amplitude was 9.6  $\mu$ V. The cross-correlation for the quadrant field recording was only 0.19, however, the recordings showed reproducible P1 and N1 components at 98 and 164 ms respectively (Figure 5.17).

The control recordings contained residual EEG noise activity as a result of signal averaging. No reproducible features were obtained in these recordings.

The subject's colour vision error scores were found to be average for his age with no significant difference between the two eyes.

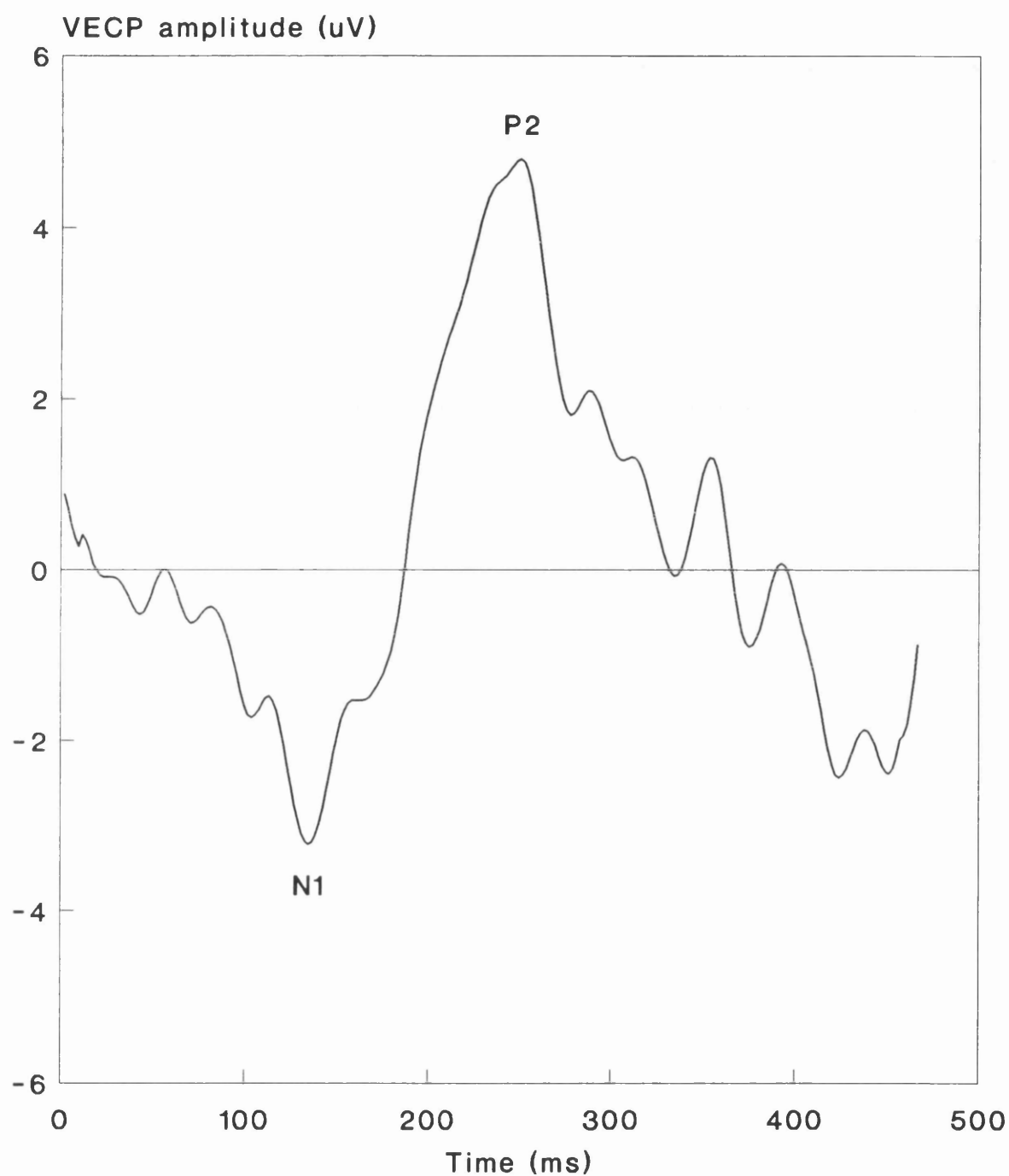


Figure 5.16 Full-field VECP recorded during indirect ophthalmoscopy from a checkerboard pattern-onset (60' checks)

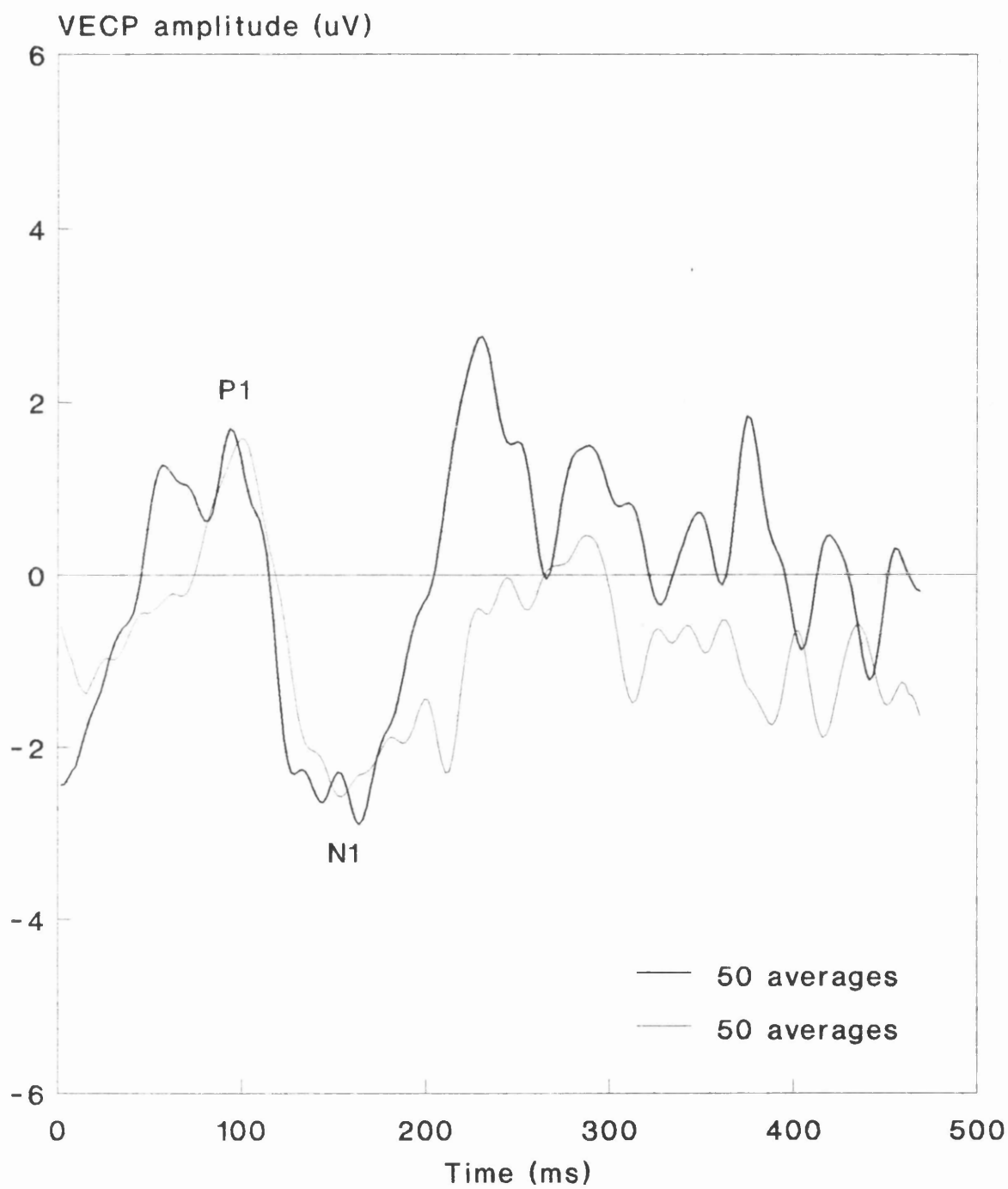


Figure 5.17 Repeat VECP signals recorded during indirect ophthalmoscopy from a quadrant field stimulus.

#### 5.6.4 Discussion

This study has shown that it is feasible to record VECP signals from full-field and quadrant field patterned stimuli during indirect ophthalmoscopy. Stimuli can be accurately positioned by the observer to test specific areas of the retina and their cortical projections.

As in the preliminary study (Section 5.4), the cross-correlation values were lower than those recorded when patterned stimuli were presented on a computer monitor screen (Section 2.11). These lower values were obtained because the SNR was reduced and this was probably due to the fact that the signal amplitudes were smaller and because fewer signals were averaged. In addition, the VECP may have been more variable under the bright stimulus conditions. The reproducibility of the recordings could be improved by averaging the responses to more stimuli. It will probably be necessary to average 100 responses or more for each measurement. If recording times are to be increased it is essential that precautions continue to be taken to minimise the blue light hazard, as recommended in Section 5.5.6.

The LCD adapter circuit may have contributed some noise to the recordings as it was supported by the test subject.

A drawback of the present LCD is the relatively slow switching speed of the fluid, which excludes the use of steady-state stimuli. Due to the slow change in contrast it is possible that the normal components in the VECP blur and overlap. If this is the case, it would be difficult to distinguish normal signals from delayed signals and this will need to be investigated. Nevertheless, the system is effective at recording VECPs from quadrant field stimuli and it should therefore be possible to use it for the purpose for which it was developed, to detect absolute hemi-field and quadrant field defects. High speed TFT LCDs with colour graphics capability are already available in large screen formats for use with overhead projectors. It is likely that miniature versions will follow and these could greatly enhance the performance of the system enabling, for example, the use of steady-state stimuli.

A detailed study of VECPs using the stimulus delivery system has been planned for when the instrument housing (Section 5.7) is complete. Normal recordings from full-field and quadrant field stimuli will be recorded from a group of ten subjects. In order to obtain a high SNR, 200 responses will be averaged for each recording. Group mean average waveforms with standard deviations will be produced and signal

repeatability and intraocular variations will be investigated. For quadrant field stimulation it is essential that multichannel recordings are performed due to the distribution of the VECF over the scalp (Section 4.2). The results will be compared with recordings made using the same stimulus on a monitor screen. Once the data has been collected from normal subjects, patients with absolute visual field defects will be investigated.

Some patients, especially the young, are unlikely to co-operate with indirect ophthalmoscopy. In these cases it will be necessary to sedate or anaesthetise the patients. In many centres visual electrophysiology is routinely performed on young children who are sedated or anaesthetised. In other centres, however, the technique could be restricted to those cases in which examination under anaesthetic is indicated for other reasons. Due to the portability of the system it could be used in theatre and could be used with a supine patient.

The system has wider potential applications in electrophysiology. Some ophthalmologists have expressed interest in using the system to test visual acuity in subjects suspected of malingering or being hysterical. The observer would be able to ensure that the stimulus was correctly focused on the retina and that steady fixation was maintained. The system could also be used to record PERGs which would be especially valuable in the study of maculopathy.

Outside the field of electrophysiology, the system also has a number of potential applications such as making fundus measurements and assessing fixation prior to laser photocoagulation.

This innovative indirect ophthalmoscope system has a number of advantages over other stimulus delivery systems. The system has a wide field of view, 40 degrees in diameter, and can be used to present patterned stimuli. Systems based on direct ophthalmoscopes have a restricted field of view, typically six degrees in diameter, and are not suitable for presenting patterned stimuli.

Like the indirect ophthalmoscope, the SLO can present patterned stimuli and has a wide field of view. The SLO has the advantages that it uses relatively low levels of illumination, does not require dilation of the pupil and it can also be used to present steady-state patterned stimuli (Katsumi et al 1991). The indirect ophthalmoscope system, however, has the advantages that it is compact, portable and relatively inexpensive when compared with the SLO.

## 5.7 INSTRUMENT HOUSING

An instrument housing has been constructed to mount the LCD, the adapter circuit and the lens (Section 5.3) and is shown in Figure 5.18.

The main LCD housing was machined from aluminium to make it light and robust. The LCD is secured by rubber shock mounts within the housing. The adapter circuit is mounted on the side of the LCD housing and is enclosed within a tinned steel box which is itself mounted within a plastic box. The purpose of the tinned steel box is to screen magnetic fields from the subject. Both the LCD housing and the adapter housing are earthed in order to screen electric fields.

The lens assembly was machined from aluminium and is fitted to the front of the LCD housing. The assembly has a telescopic adjustment which enables the distance between the lens and the LCD to be adjusted if the subject is ametropic (Section 5.3). The distance between the lens and the LCD can be varied by 45 mm which enables subjects who require -5.7 to + 4.1 dioptres of optical correction to be tested.

The completed housing weighs 1.3 kg and is sufficiently compact and portable to be hand-held by the observer. The housing can alternatively be mounted on a slit-lamp table by means of standard camera attachments (Figure 5.19).

Unfortunately, the instrument housing was not ready until this thesis was nearing completion. The housing will be used in all future work, including the studies described in Section 5.6.4.

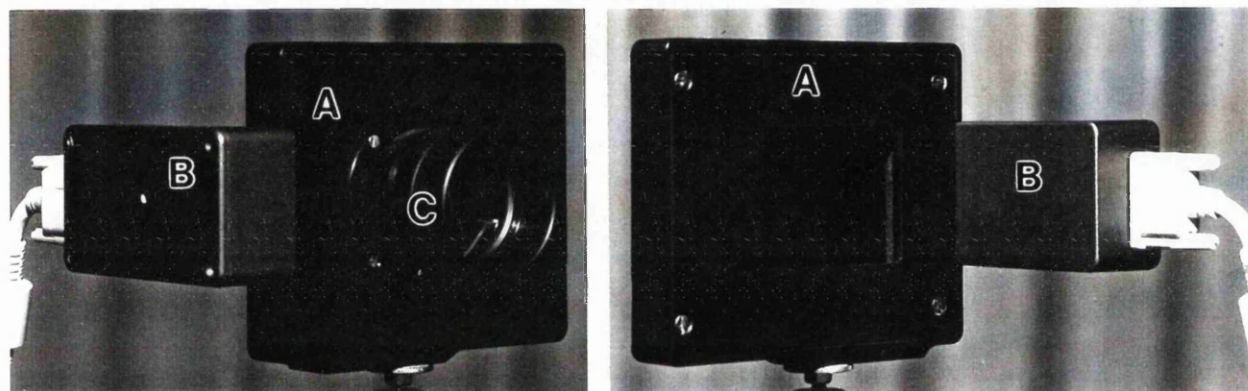


Figure 5.18 Photographs of the indirect ophthalmoscope stimulus delivery system showing the LCD housing (A), adapter circuit housing (B) and lens assembly (C).

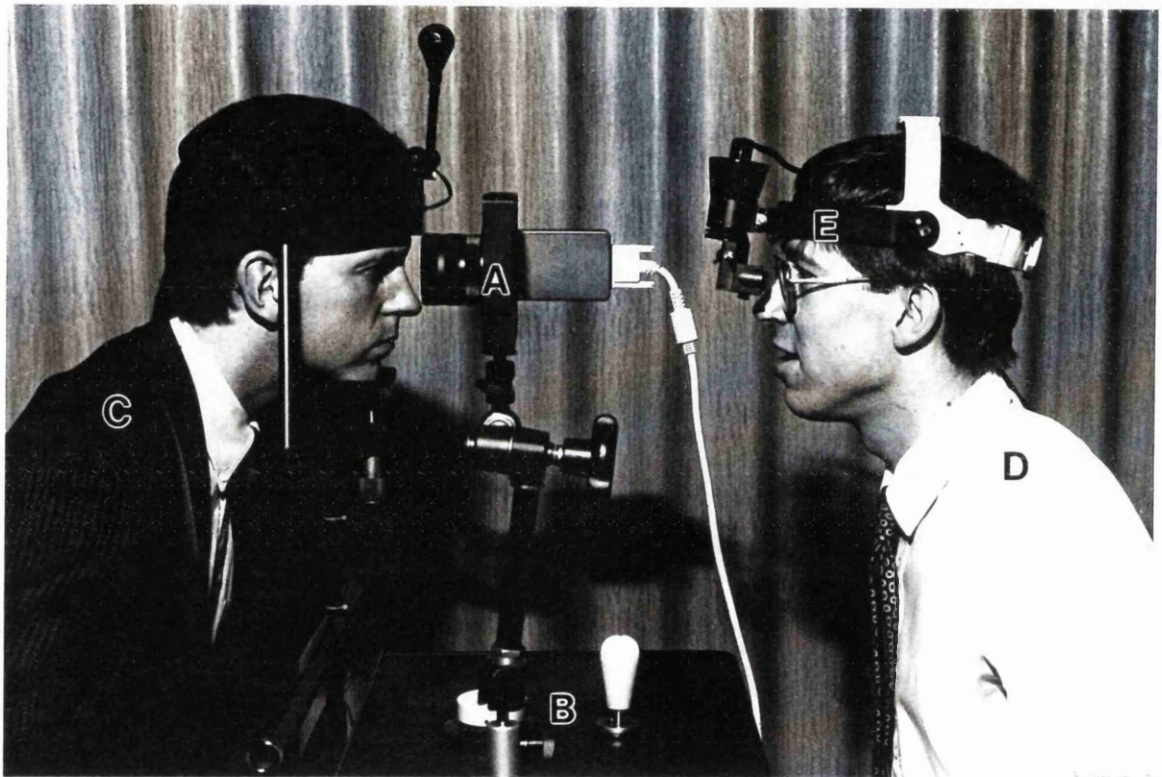


Figure 5.19 Photograph of the indirect ophthalmoscope delivery system (A) mounted on a slit-lamp table (B) in front of a test subject (C). The observer (D) is shown wearing a standard indirect ophthalmoscope headset (E).

## 6. CLINICAL EVALUATION

### 6.1 INTRODUCTION

This chapter describes the clinical evaluation of the stimulus and recording system for objective analysis of the visual field. The aim of this work was to assess the ability of the system to detect complete and absolute hemi-field and quadrant field defects. Quadrant field pattern-reversal checkerboard stimuli were used for the investigation. A steady-state stimulation rate was used so that the SNR could be maximised by using frequency domain analysis. The stimuli were generated by computer graphics software and were presented on a monitor screen. There have been a few previous clinical studies on the use of quadrant field stimuli (Section 1.5.3). A major novel aspect of the work described in this chapter was the use of objective signal detection techniques. A preliminary study of seven subjects is described. As a result of this study two improvements were made: recording times were increased to improve the SNR and a novel method for fixation monitoring was introduced. The main study considers ten further subjects who had a variety of field defects due to pathology affecting the optic nerve, optic chiasm, optic radiation and occipital cortex. The objective results obtained using electrophysiology corresponded well with the patterns of subjective field loss. Two methods for objective signal detection are compared: one method measures the SNR in the frequency domain, the other technique uses Hotelling's  $t^2$  statistic. Finally, recommendations are made for future clinical evaluation.

This study preceded the development of the dartboard stimulus presented in Section 4.3. If the dartboard had been available, it would have been used in preference to the checkerboard because it is a more effective stimulus producing a larger amplitude VECP signal. The increased SNR would have increased the probability of signal detection and it is proposed that this would have improved the optimum sensitivity and specificity of the test. Alternatively, the dartboard could have been used to test smaller areas of the visual field.

## 6.2 PRELIMINARY STUDY

### 6.2.1 Subjects and methods

Seven subjects, five males and two females, ranging in age from 27 to 64 years (mean age 47 years) were investigated. All subjects were optically corrected for the stimulus viewing distance of 40 cm. The subjects had a variety of field defects, most were referred from the Neuro-ophthalmology clinic and they all had subjective perimetry. Six subjects had kinetic perimetry performed with a Goldmann perimeter and one subject had static perimetry performed on a Humphrey field analyser. The referring criteria were that the subjects had an acuity of 6/18 or better and that they had complete and absolute hemi-field or quadrantic field defects.

The stimulus was presented on the computer monitor. Monocular recordings were made from each eye for separate stimulation of each field quadrant. A check-size of 90' was used which is optimal for stimulating the retinal ganglion cells at an eccentricity of about  $10^\circ$  (Section 4.2). The stimulus extended to  $23^\circ \times 23^\circ$  and is illustrated in Figure 6.1. A foveal mask with a radius of  $5^\circ$  was used to prevent cortical stimulation due to foveal sparing of field defects. Masks, two degrees wide, were used along the vertical and horizontal meridians to prevent inadvertent stimulation of areas not under test; due to the overlap of ganglion receptive fields and slight losses of fixation. The stimulus frequency was 7.71 reversals per second, which is just below the alpha frequency band. The pattern contrast was greater than 99 %, and the mean luminance was  $20 \text{ cd/m}^2$ . A grey background was generated on the screen, with a luminance of  $10 \text{ cd/m}^2$ , equal to the mean pattern luminance. This background ensured that the overall screen luminance remained constant during the experiments and also minimised retinal stimulation due to scattered light. A fixation letter was used so that test subjects maintained optical accommodation. For subjects with poor acuity, the letter was replaced with a spot. Fixation was monitored by observing eye movements. The experiments were performed in a darkened room, with an ambient illumination of 10 lux.

The VECPs were sampled at a rate of 247 Hz, so that one stimulus period corresponded to 32 data points. Successive 1024 points of data were averaged and transformed into the frequency domain using an FFT. There was an exact number of pattern reversals per 1024 data points and this eliminated spectral leakage in the frequency domain. Each recording lasted 30 seconds and was repeated. The signal was objectively detected by measuring the SNR. The noise power was estimated by

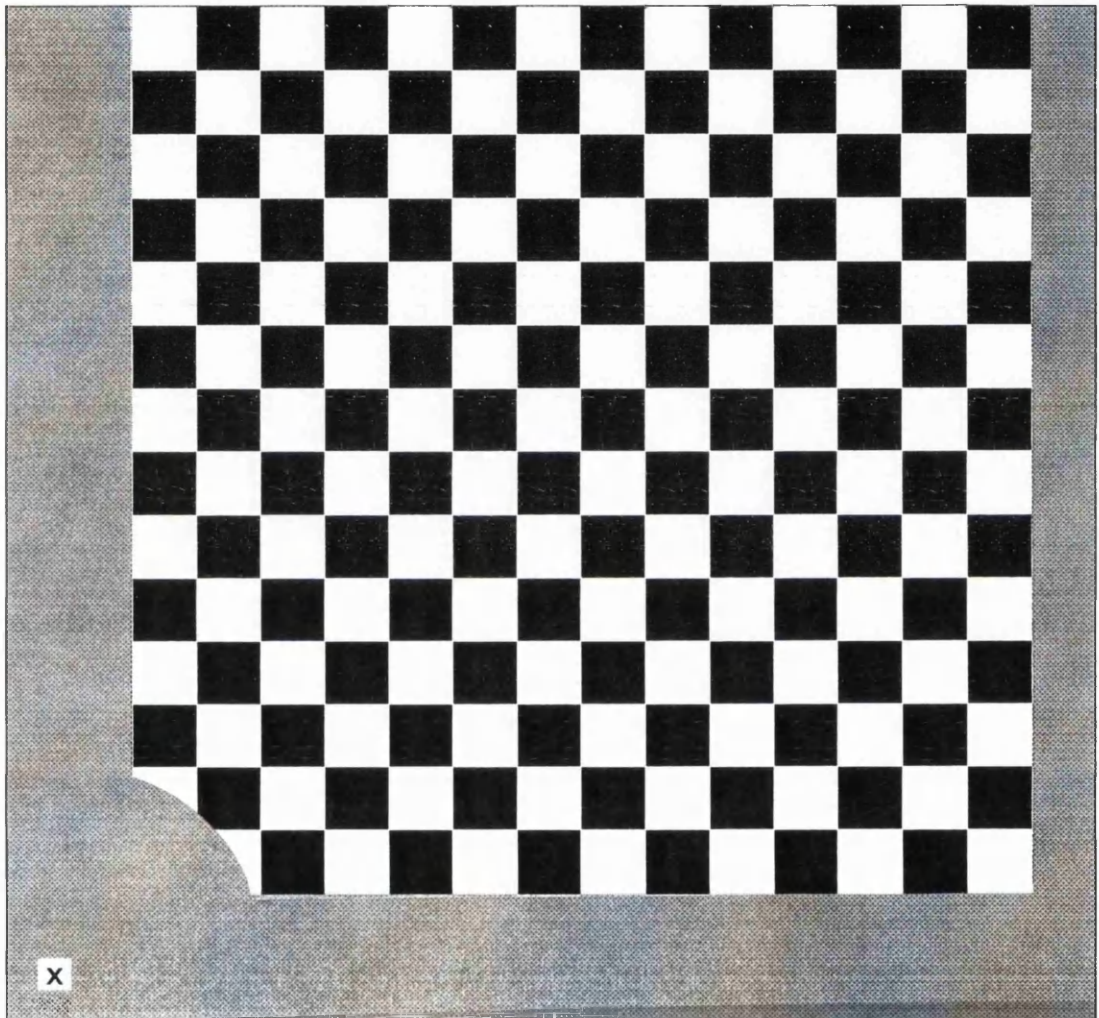


Figure 6.1 Quadrant field stimulus

performing linear regression on ten frequencies adjacent to the stimulus frequency (Section 3.2.2). Three primary recording channels were used, MO-MF, RO-MF, and LO-MF (Section 2.9.2). The topography of the VECP on the scalp varied according to the region of the visual cortex being stimulated. Therefore, in order to increase the chance of detecting the VECP, three derived channels, MO-RO, MO-LO, RO-LO (Figure 6.2) were also used. As the electrodes used for these derived channels were physically very close, the hypothesis was that most of the background EEG noise would be cancelled, potentially producing a large SNR. According to the method of Eizenman (1993) (Section 3.2.2), if the SNR was greater than 2.2, 2.4 or 2.9 on a particular recording channel, the probability of false signal detection on that channel was 10 %, 5 % and 1 % respectively.

### 6.2.2 Results

Figure 6.3 illustrates a typical frequency spectrum from quadrant field stimulation. This particular example was recorded from the MO electrode relative to the MF electrode in response to stimulation of the superior temporal quadrant of a left eye. The figure illustrates how the background noise level was estimated by linear regression of the noise frequencies adjacent to the stimulus frequency. In this example the SNR was estimated to be 5.6 and the probability of false signal detection was less than 1 %.

In some recordings the SNR was not greater than 2.2 yet the signal amplitude and phase were repeatable on successive recordings. Obviously, in some cases the 2.2 threshold was too strict for determining whether a signal had been detected. Criteria for signal detection were arbitrarily set as follows:

1. The maximum signal amplitude had to be on the same recording channel on successive recordings.
2. In addition, the SNR had to be greater than 2.2 or the signal amplitude had to be repeatable to within 50 % and the phase had to be repeatable to within 45°.

Figure 6.4 summarises the visual fields tested. Using the above criteria, a signal was 'detected' in 24 out of 26 'seeing' quadrants. The mean signal amplitude was 4.18  $\mu$ V and the range was 1.3 to 9.3  $\mu$ V. In 21 of the 24 detected signals the SNR was greater than 2.2 on both recordings. In some subjects the signal amplitude and phase

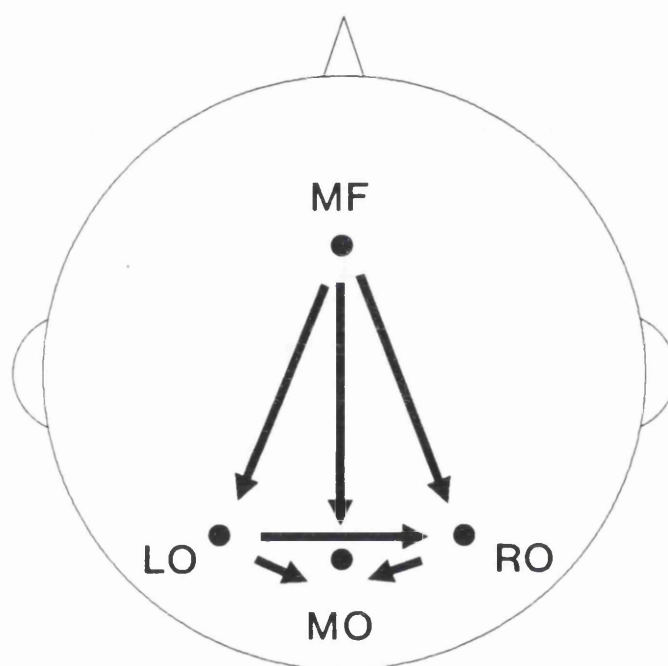


Figure 6.2 Electrode montage: mid occipital (MO) right occipital (RO), left occipital (LO) and mid frontal (MF). Recording channels MO-MF, RO-MF, LO-MF, MO-RO, MO-LO and RO-LO.

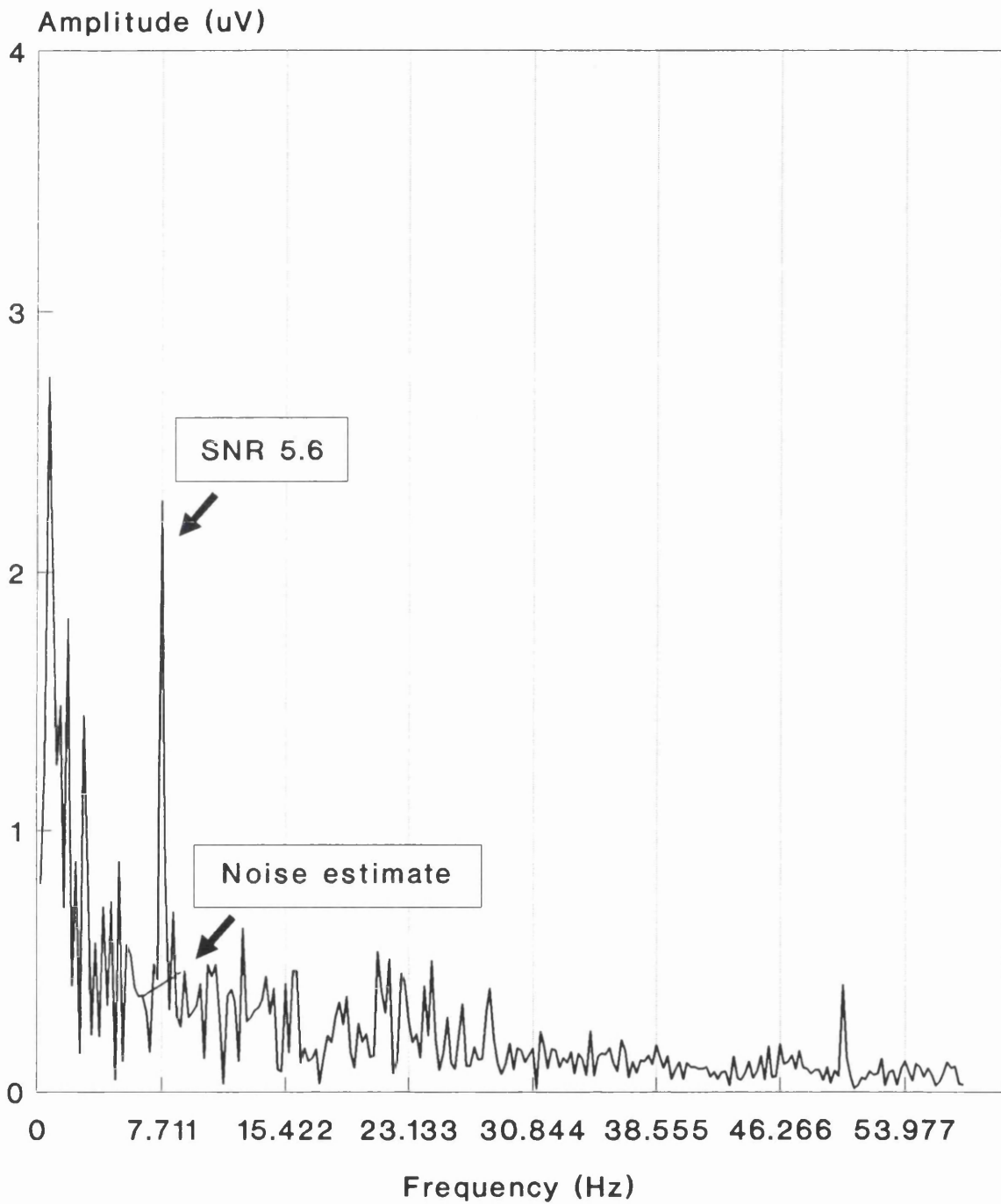
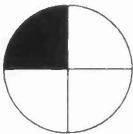
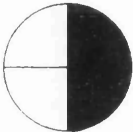
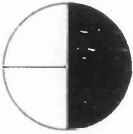
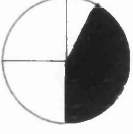
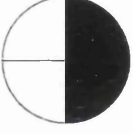
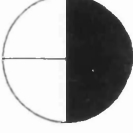
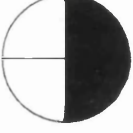
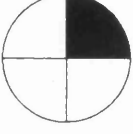
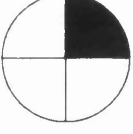


Figure 6.3 Frequency spectrum of recording showing VECP signal at 7.711 Hz and estimate of EEG noise.

	Right eye (OD)	Left eye (OS)	Number of 'seeing' quadrants	Number of 'non-seeing' quadrants
Subject 1			3	1
Subject 2			2	2
Subject 3			2	2
Subject 4			5	3
Subject 5			4	4
Subject 6			4	4
Subject 7			6	2

■ = field defect.

Figure 6.4 A summary of the visual fields tested.

were very repeatable. In one subject, for example, the amplitude was repeatable to within 13 % and the phase was repeatable to within 10° for four quadrants. The three cases for which the SNR did not exceed 2.2 were all in the superior hemi-field; one quadrant in each of three subjects.

A signal was also detected in five out of 18 'non-seeing' quadrants. The mean signal amplitude was 2.7  $\mu\text{V}$  and the range was 0.9 to 6  $\mu\text{V}$ . In three of these cases the signal amplitude was significantly reduced compared to that obtained from the corresponding 'seeing' quadrant on the opposite side of the vertical meridian; the ratios were 0.15, 0.2 and 0.34.

The details of the results for each subject are presented below.

**Subject 1** - A 59 year old man developed a dural fistula of the ophthalmic artery producing a right supero-nasal field defect. A significant signal was recorded from two of the three 'seeing' quadrants. The signal from the third 'seeing' quadrant did not meet the detection criteria defined above. No signal was recorded from the affected quadrant.

**Subject 2** - A 49 year old man developed compression of the optic chiasm due to a craniopharyngioma and this produced a bitemporal hemianopia. Only one eye was tested because the subject was unable to fixate with the other eye. A significant signal was recorded from both 'seeing' quadrants as well as from one affected quadrant.

**Subject 3** - A 46 year old lady developed compression of the optic chiasm due to a pituitary adenoma and this produced bitemporal field defects. One eye with a hemianopia was tested; the other eye had an incomplete quadrantanopia. A signal was recorded from both of the 'seeing' quadrants and a signal with a reduced amplitude was recorded from one of the affected quadrants but not the other.

**Subject 4** - A 43 year old man developed compression of the optic chiasm due to a pituitary adenoma and this produced an incongruous homonymous hemianopia. A significant signal was detected from all five 'seeing' areas and from one affected quadrant with an incomplete quadrantanopia. A signal with a reduced amplitude was recorded from one of the affected quadrants.

**Subject 5** - A 42 year old lady developed a left parietal infarct following a ruptured cerebral aneurysm and this produced an incomplete right homonymous hemianopia. A significant signal was recorded from all four 'seeing' quadrants. A signal with a reduced amplitude was recorded from one affected quadrant, which had an incomplete quadrantanopia.

**Subject 6** - A 27 year old man developed a subdural haematoma following a head injury and this produced a right homonymous hemianopia. A significant signal was recorded from three of the four 'seeing' quadrants. The signal from the fourth 'seeing' quadrant did not meet the detection criteria defined above. No signal was recorded from the affected 'non-seeing' quadrants.

**Subject 7** - A 64 year old man developed an occipital infarct following a cerebrovascular accident and this produced a right superior homonymous quadrantanopia. A significant signal was recorded from three of the four 'seeing' quadrants. No signal was recorded from the 'non-seeing' quadrants.

### **6.2.3 Discussion**

A signal was not detectable in three of the 'seeing' quadrants because the SNR was insufficiently large. It is of interest that these three quadrants were all in the superior hemi-field. The SNR was reduced because in general the signals produced by stimulation of the superior field quadrants are smaller than for stimulation of the inferior field (Section 4.2). The reason for this is due to differences in the position and orientation of the superior and inferior field representation in the visual cortex. One way of improving the SNR would be to increase the recording time.

Signals were sometimes recorded from affected quadrants because the field defects were incomplete. Furthermore, some subjects may not have had absolute field defects. The reason why these subjects may have been referred is that whilst it was routine to use the brightest stimulus target (4e) for kinetic perimetry using the Goldmann perimeter, the largest target size (V) was not necessarily always used.

On other occasions signals would have been recorded from affected quadrants due to statistical chance. It is difficult to calculate the exact probability of false signal detection because the six recording channels were not strictly independent, however,

the probability of false signal detection would have been greater than that quoted for a single recording channel in Section 6.2.1.

A further reason for sometimes detecting a signal from an affected quadrant may have been due to a loss of fixation. This could also have affected the results from 'seeing' quadrants. An improved method for monitoring fixation was therefore required.

## **6.3 MAIN STUDY**

### **6.3.1 Subjects and Methods**

Ten subjects, two males and eight females, ranging in age from 17 to 69 years (mean age 46 years) were investigated. All subjects were optically corrected for the stimulus viewing distance of 40 cm. The subjects had a variety of field defects, most were referred from the Neuro-ophthalmology clinic and they all had subjective perimetry. Six subjects had kinetic perimetry performed with a Goldmann perimeter, three of whom also had kinetic perimetry performed with a Tübingen perimeter. Of the remaining four patients, three had kinetic perimetry performed with a Tübingen perimeter and three had static perimetry performed with a Friedmann field analyser. The referring criteria were that the subjects had an acuity of 6/18 or better and that they had complete and absolute hemi-field or quadrantic field defects.

The stimulus and recording conditions were the same as those described in Section 6.2.1 with two exceptions:

1. The recording time was increased to 2 minutes to improve the SNR.
2. An improved method of fixation monitoring was introduced as described in section 4.3.2. The fixation letter momentarily changed from red to blue or green at varying time intervals. The subject had to correctly report the change. This simple task also helped the subject to concentrate and reduced fatigue.

The data were then analysed in two different ways:

1. The data were transformed into the frequency domain using an FFT and the SNR measured (Section 3.2.2). A signal was detected if the SNR exceeded 2.2.

2. The signal was measured using an ANC (Section 3.4) and the probability of signal detection calculated using Hotelling's  $t^2$  statistic (Section 3.4.3). Artefact rejection was included in the ANC as proposed in Section 3.4.5, point 6. Receiver operating characteristic (ROC) curves were generated to determine the optimum signal detection threshold.

### 6.3.2 Results

#### SNR measurement in the frequency domain

A signal was 'detected' in 37 out of 40 'seeing' quadrants (using an SNR of 2.2 as the signal detection threshold). The mean signal amplitude was  $3.7 \mu\text{V}$  and the range was 1.1 to  $10.1 \mu\text{V}$ . The three quadrants in which the SNR did not exceed 2.2 were all in one subject whose VECP was small. In this subject the mean signal amplitude was  $1.3 \mu\text{V}$  and the range was 1.2 to  $1.4 \mu\text{V}$ .

A signal was also detected in nine out of 34 'non-seeing' quadrants (using an SNR of 2.2 as the signal detection threshold). The mean signal amplitude was  $1.5 \mu\text{V}$  and the range was 0.7 to  $2.7 \mu\text{V}$ . In eight of these nine cases the signal amplitude was reduced compared to that obtained from the corresponding 'seeing' quadrant on the opposite side of the vertical meridian. In four of the nine cases, the field defects were incomplete. In a further two cases, the field defects were not absolute but relative. In one subject the signal recorded from an affected quadrant was 70 % larger than that recorded from the corresponding 'seeing' quadrant and this was probably due to a loss of fixation.

In this study all the recording channels were found to be useful for detecting the VECP signal; the peak SNR could be present on any one of the channels. The maximum signal amplitude however, was most often detected on the RO-LO channel (27/37 cases).

The details for each subject are presented below.

**Subject 1** - A 58 year old lady developed bilateral open angle glaucoma which produced superior altitudinal field defects. The field charts and results of electroperimetry are presented in Figures 6.5 and 6.6. A significant signal was recorded from all four 'seeing' quadrants. In addition, a small but significant signal was also recorded from the right superior quadrant of the right eye. The field defect in this eye was incomplete.

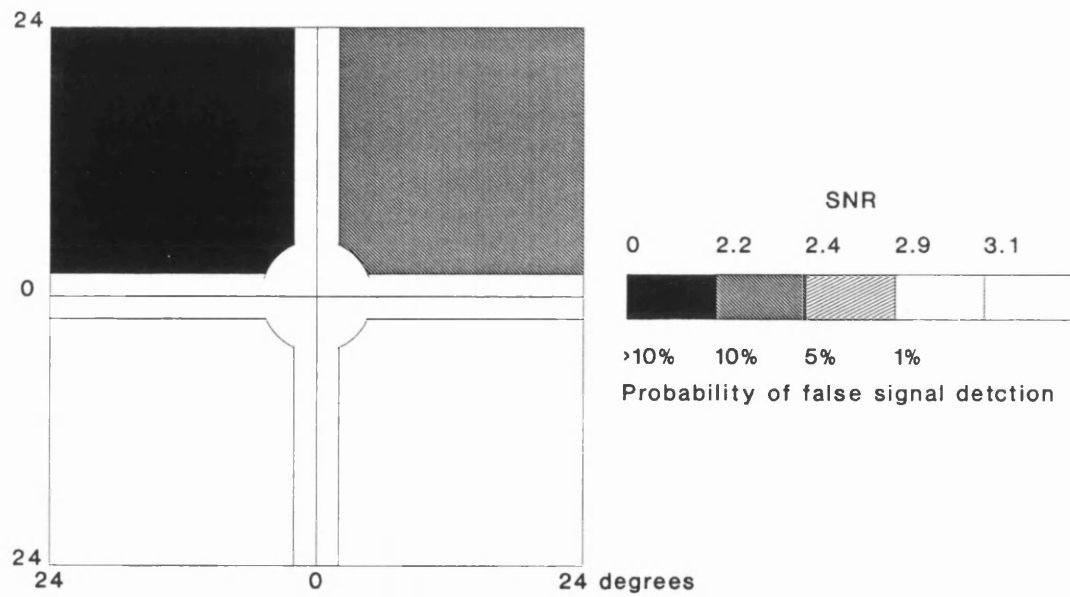
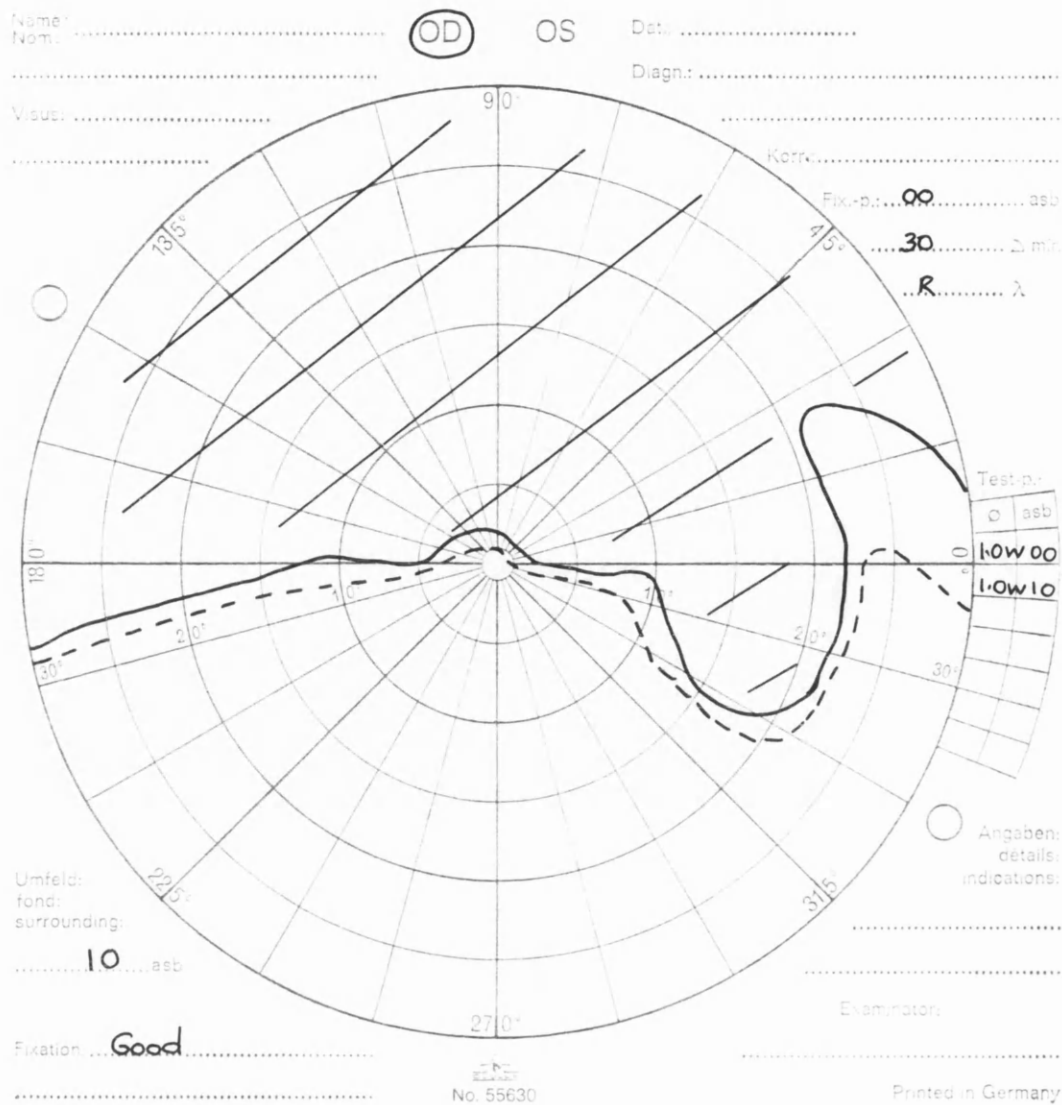


Figure 6.5 Subject 1 - field chart and result of electroperimetry for right eye

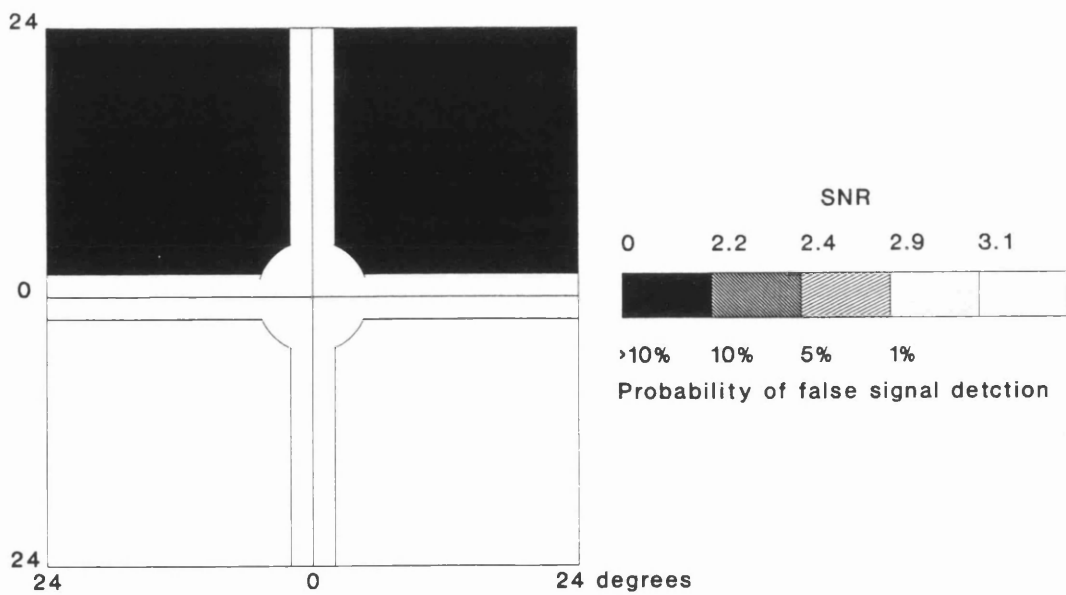
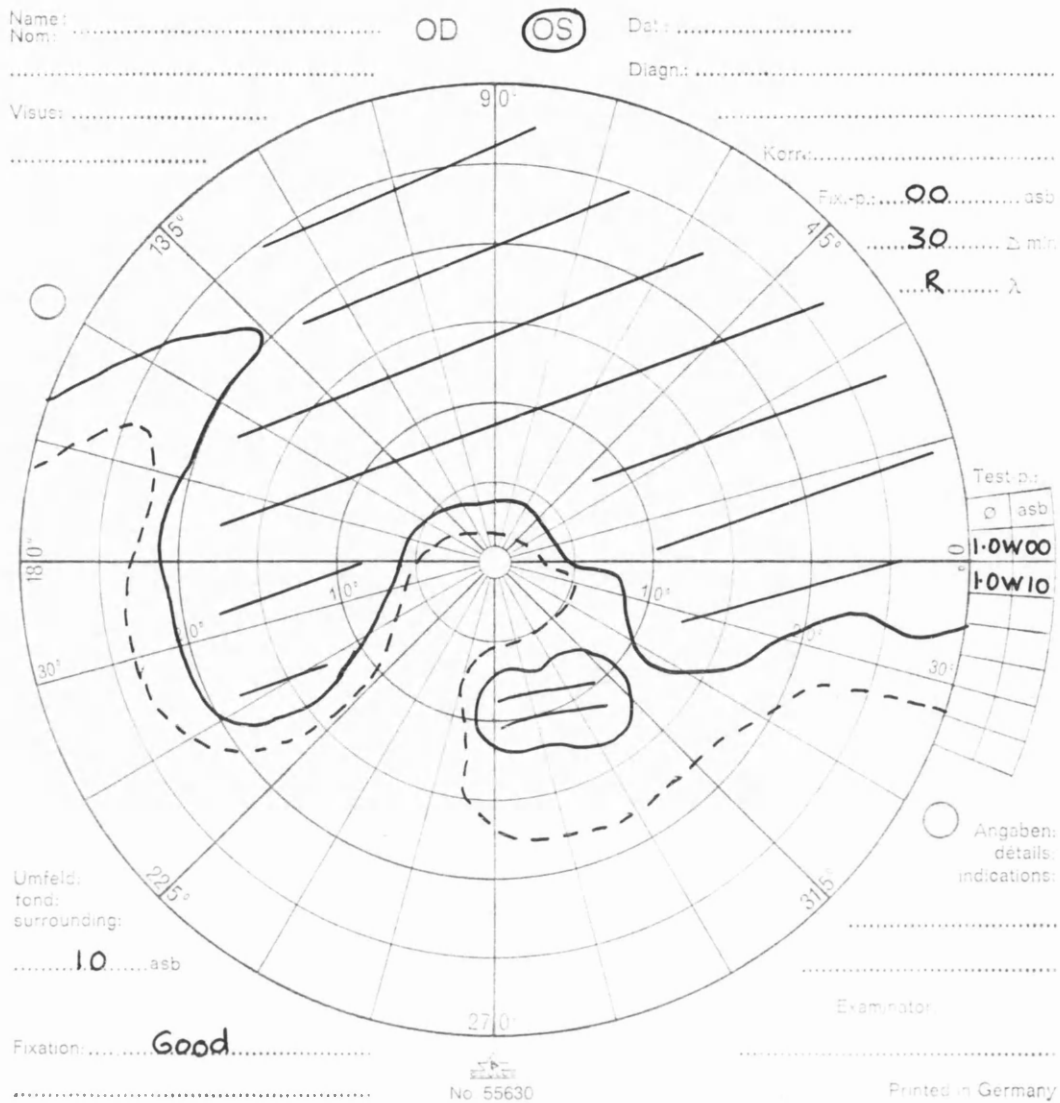


Figure 6.6 Subject 1 - field chart and result of electroperimetry for left eye

**Subject 2** - A 61 year old man developed compression of the chiasm as a result of a pituitary adenoma and this produced bitemporal field defects. The field charts and results of electroperimetry are presented in Figures 6.7 and 6.8. In the right eye a significant signal was recorded from the two 'seeing' quadrants. No signal was recorded from the affected quadrants. In the left eye, no significant signal was recorded from the left inferior quadrant which had a complete field defect. A small, yet significant, signal was recorded from the other quadrants.

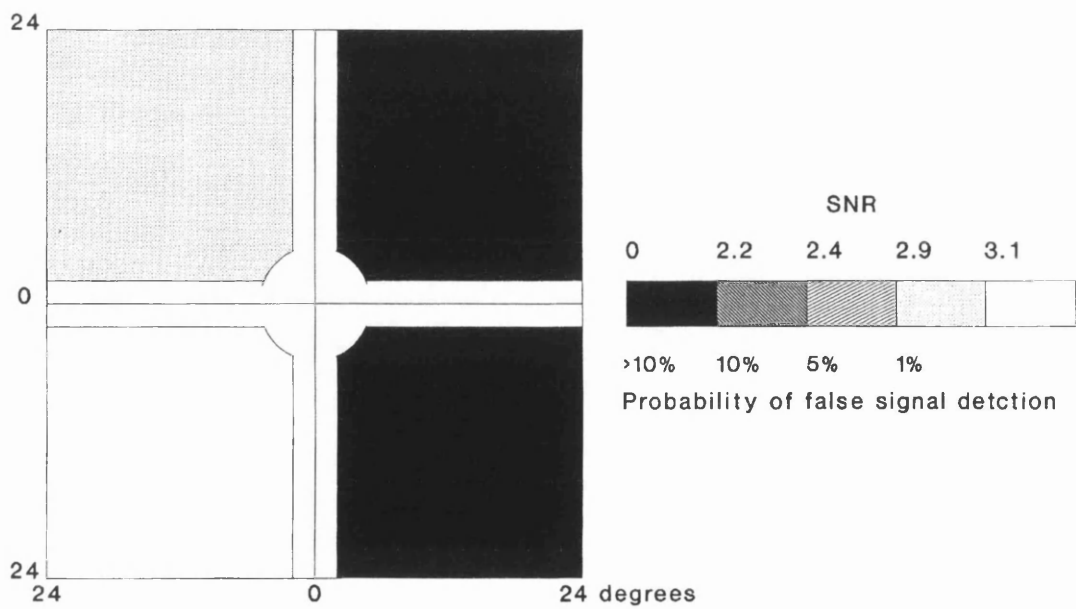
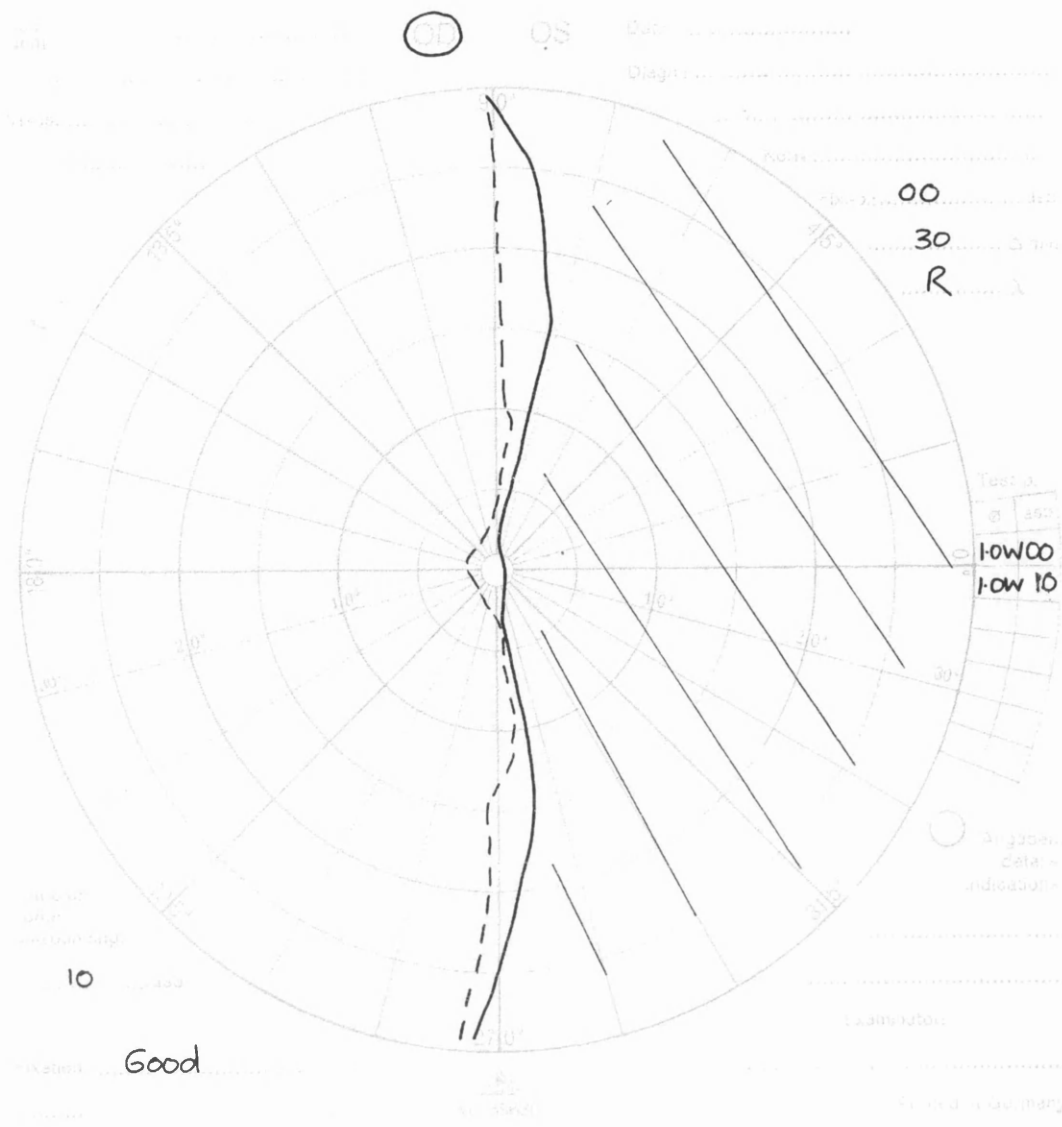


Figure 6.7 Subject 2 - field chart and result of electroperimetry for right eye



**Subject 3** - A 69 year old lady developed compression of the chiasm as a result of a pituitary adenoma and this produced bitemporal field defects. Only two quadrants from the right eye were tested due to time constraints (Figure 6.9). A significant signal was recorded from the 'seeing' quadrant. No significant signal was recorded from the affected quadrant.

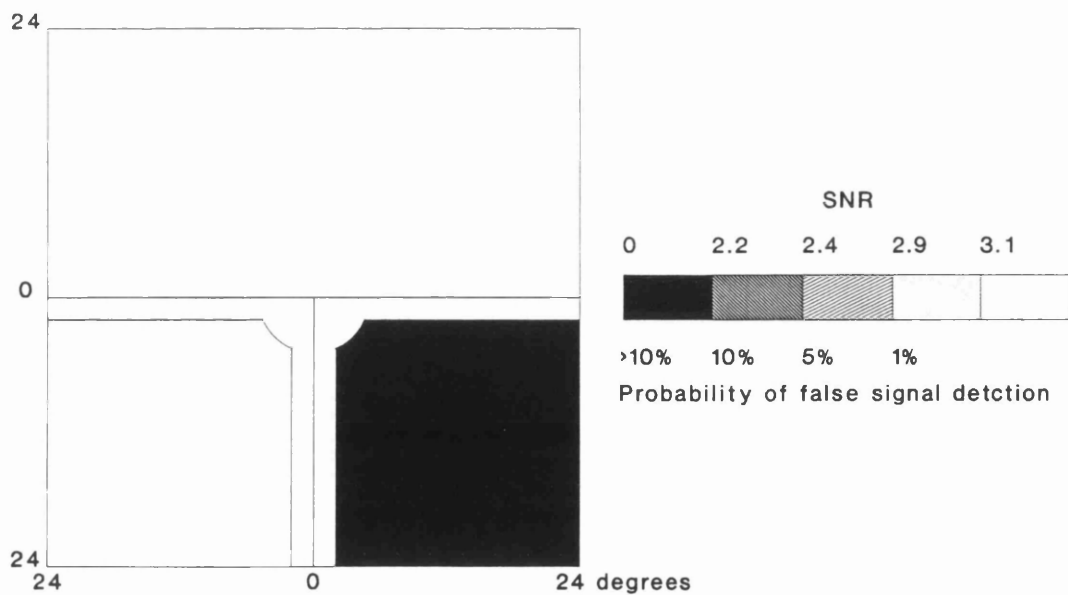
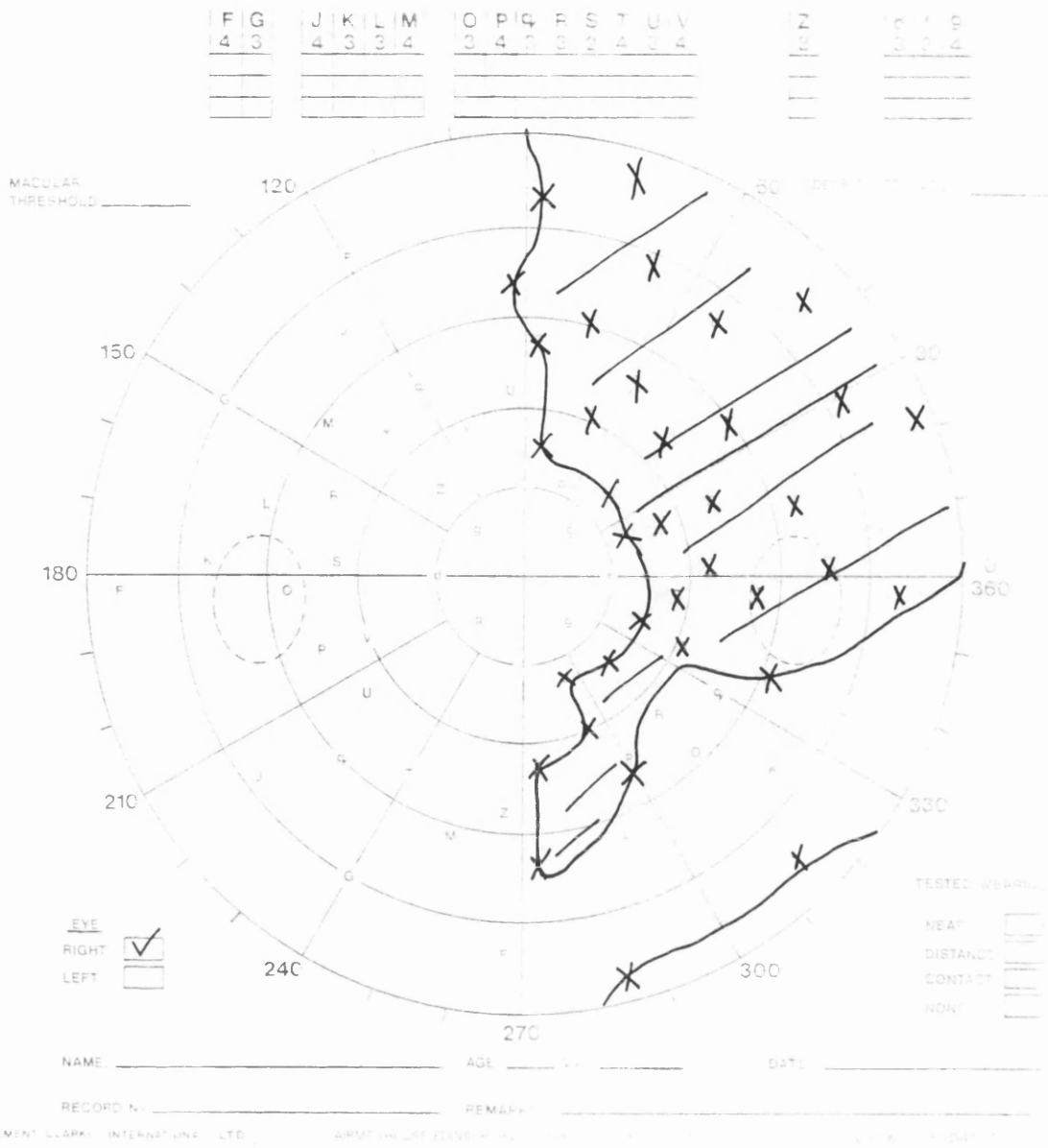
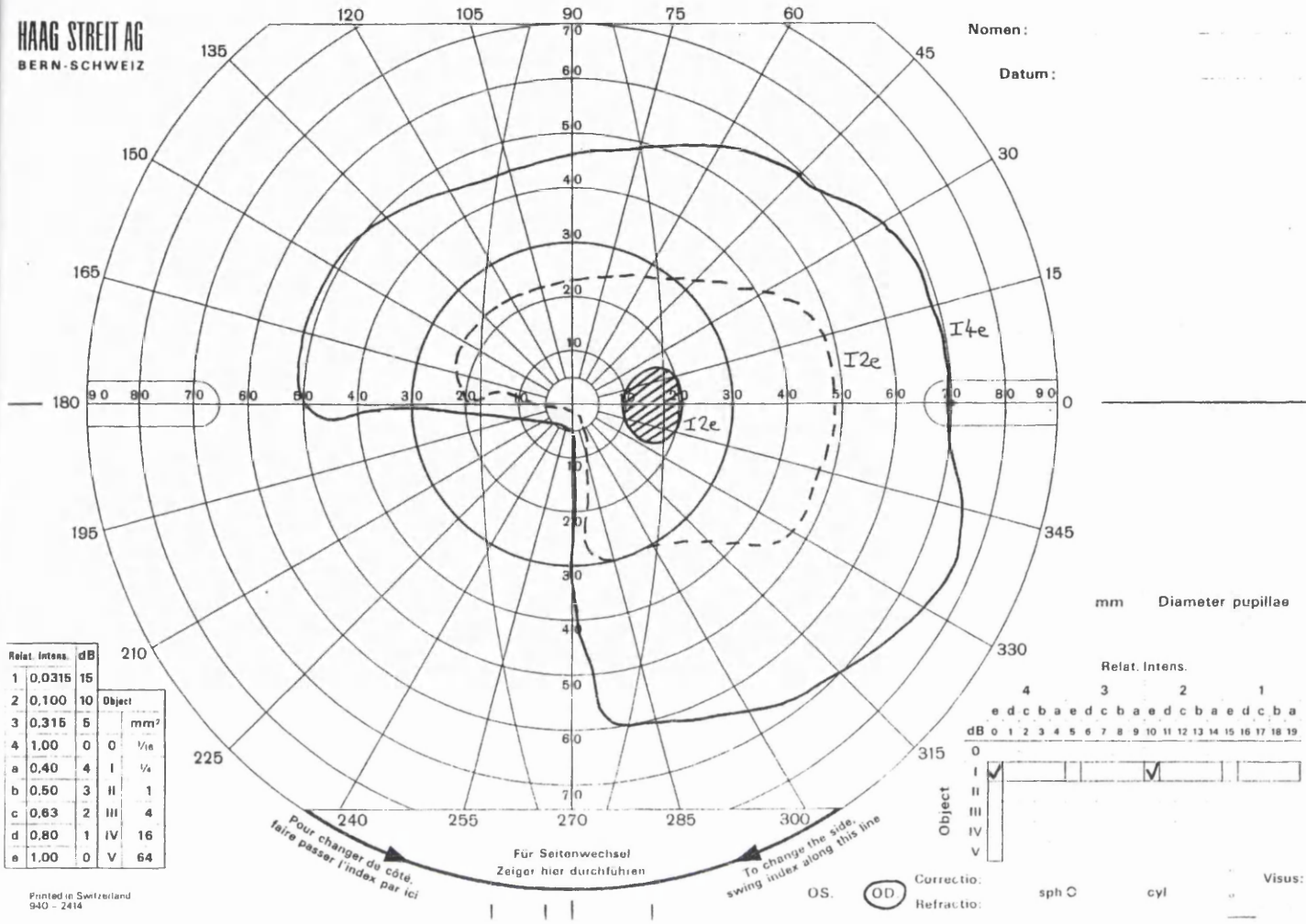


Figure 6.9 Subject 3 - field chart and result of electroperimetry for right eye

**Subject 4** - A 33 year old man developed a right parietal occipital haematoma which produced a left inferior homonymous quadrantanopia. The field charts and results of electroperimetry are presented in Figures 6.10 and 6.11. A significant signal was recorded from the six 'seeing' quadrants and no significant signal was recorded from the two affected quadrants.

HAAG STREIT AG  
BERN-SCHWEIZ



Relat. intens. dB	Object	mm <sup>2</sup>
1 0.0315 15		
2 0.100 10		
3 0.315 5		
4 1.00 0	0	1/16
a 0.40 4	I	1/4
b 0.50 3	II	1
c 0.63 2	III	4
d 0.80 1	IV	16
e 1.00 0	V	64

Printed in Switzerland  
940 - 2414

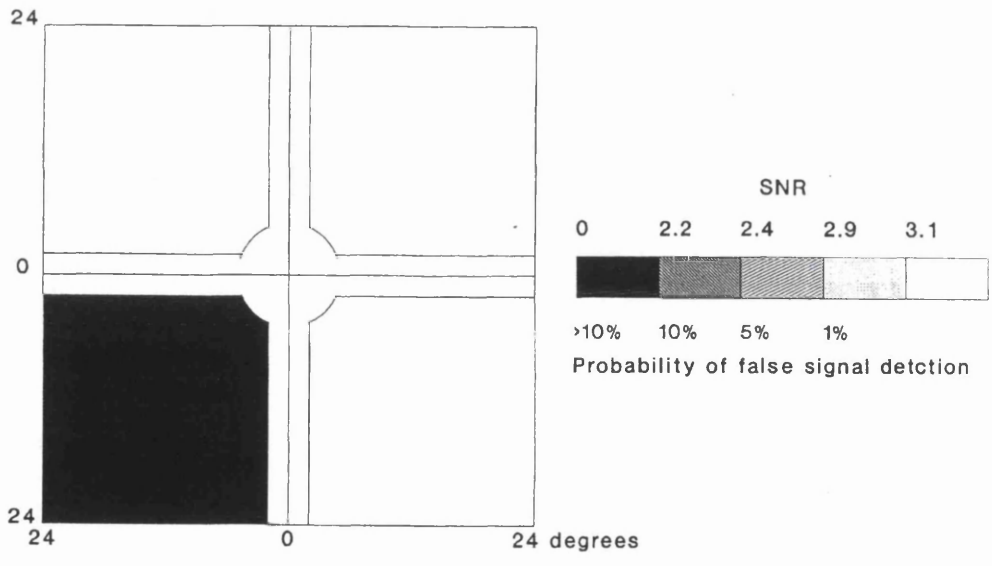
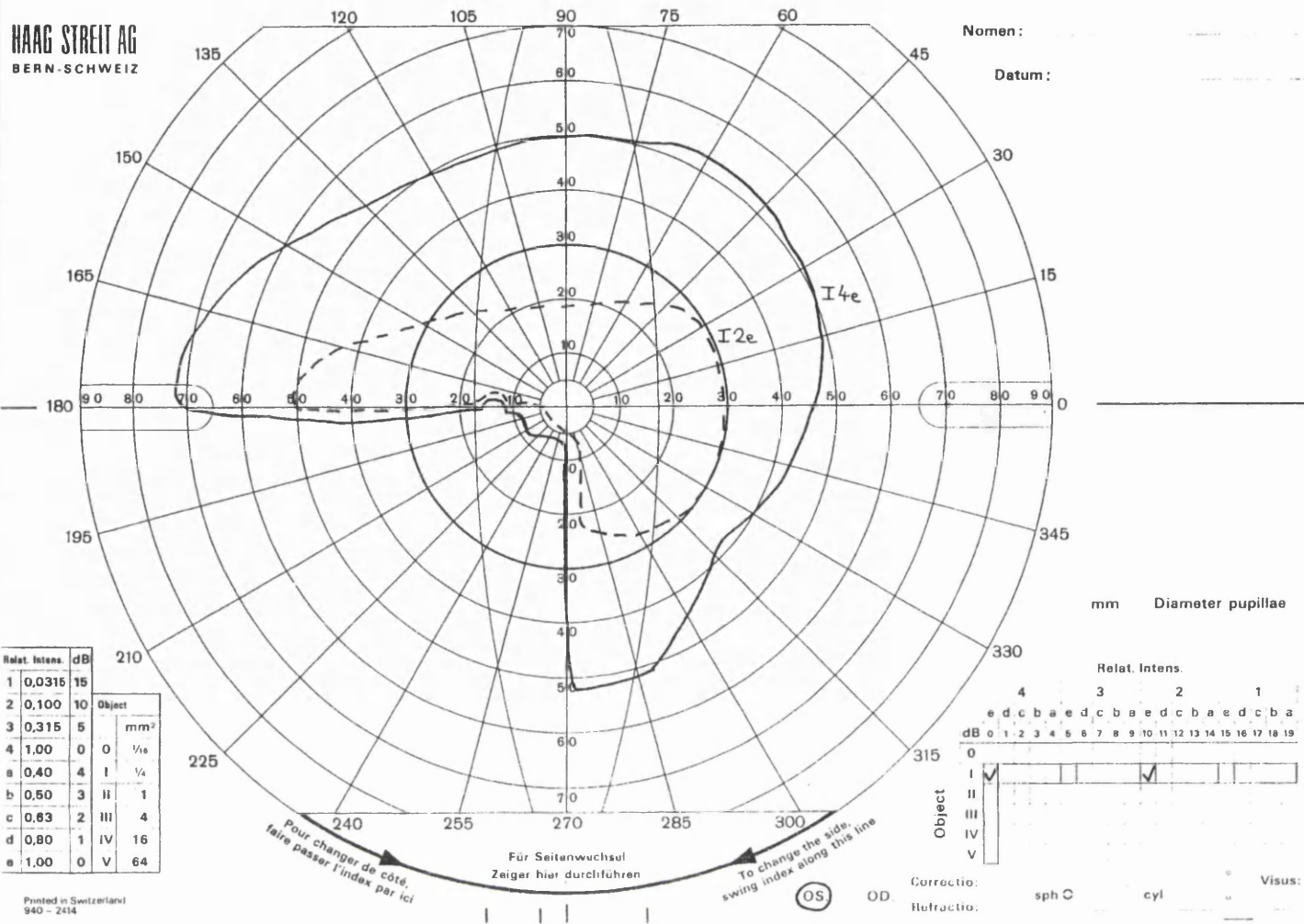


Figure 6.10 Subject 4 - field chart and result of electroperimetry for right eye

HAAG STREIT AG  
BERN-SCHWEIZ

Nomen: \_\_\_\_\_  
Datum: \_\_\_\_\_



Relat. Intens.	dB	Object	mm <sup>2</sup>
1	0,0315	15	
2	0,100	10	
3	0,315	5	
4	1,00	0	1/4
a	0,40	4	I 1/4
b	0,50	3	II 1
c	0,63	2	III 4
d	0,80	1	IV 16
e	1,00	0	V 64

Relat. Intens.		mm Diameter pupillae	
dB	Object	4	3
0	I		
1	II		
2	III		
3	IV		
4	V		

Printed in Switzerland  
940 - 2414

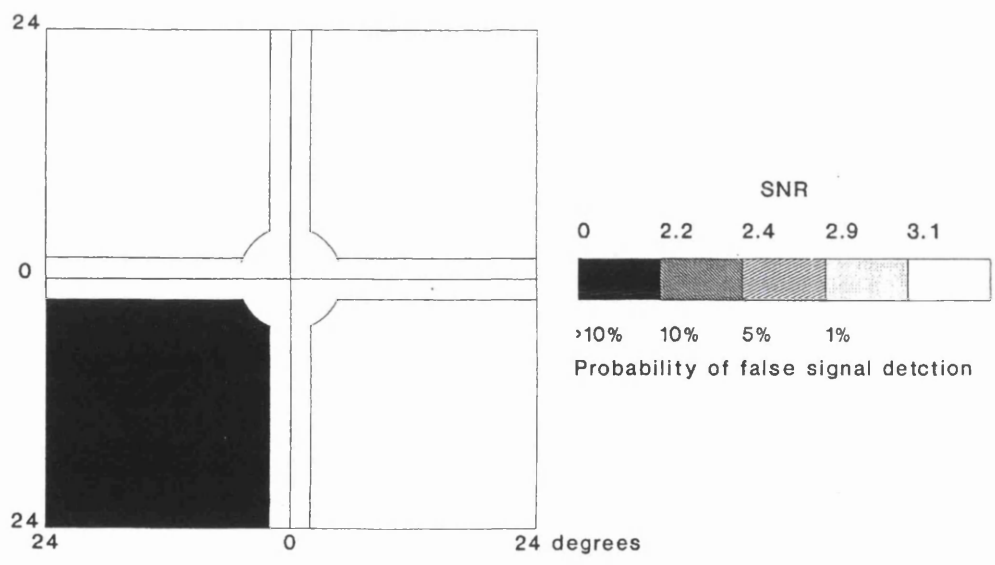


Figure 6.11 Subject 4 - field chart and result of electroperimetry for left eye

**Subject 5** - A 27 year old lady had a right parietal arterio-venous malformation which produced a left homonymous hemianopia. The field charts and results of electroperimetry are presented in Figures 6.12 and 6.13. A significant signal was recorded from the four 'seeing' quadrants. No significant signal was recorded from the four affected quadrants.

HAAG STREIT AG  
BERN - SCHWEIZ

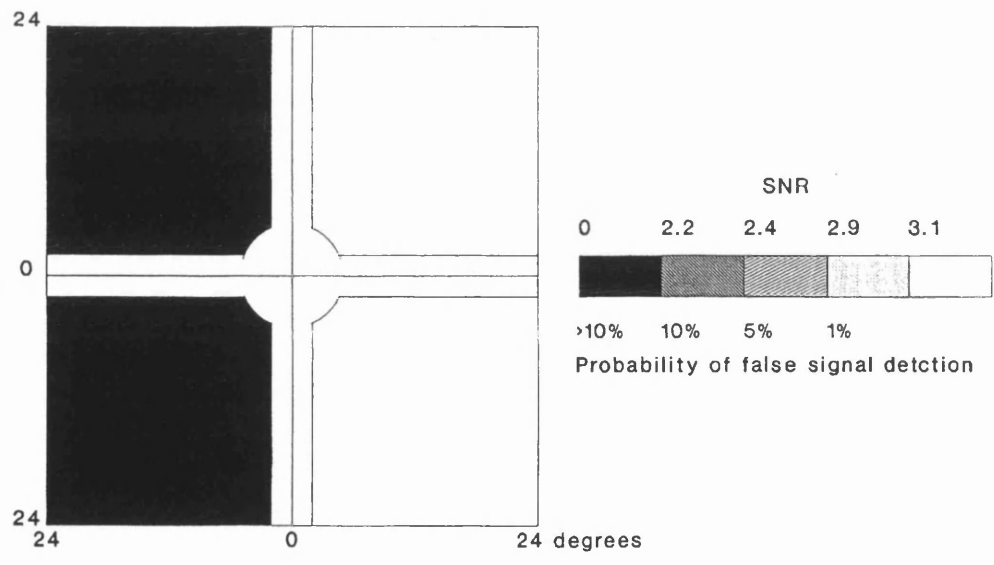
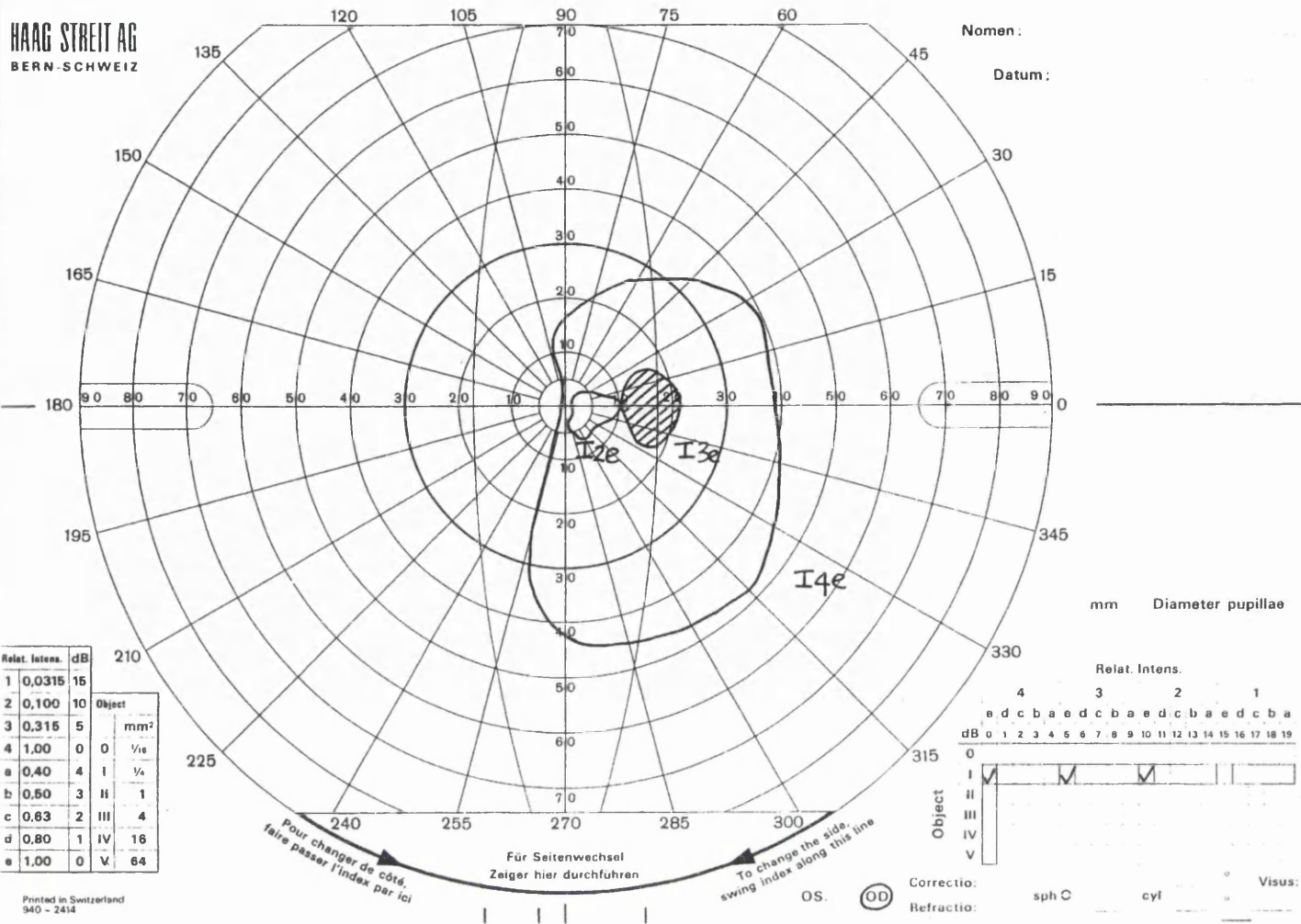


Figure 6.12 Subject 5 - field chart and result of electroperimetry for right eye

HAAG STREIT AG  
BERN · SCHWEIZ

Nomen : \_\_\_\_\_  
Datum : \_\_\_\_\_

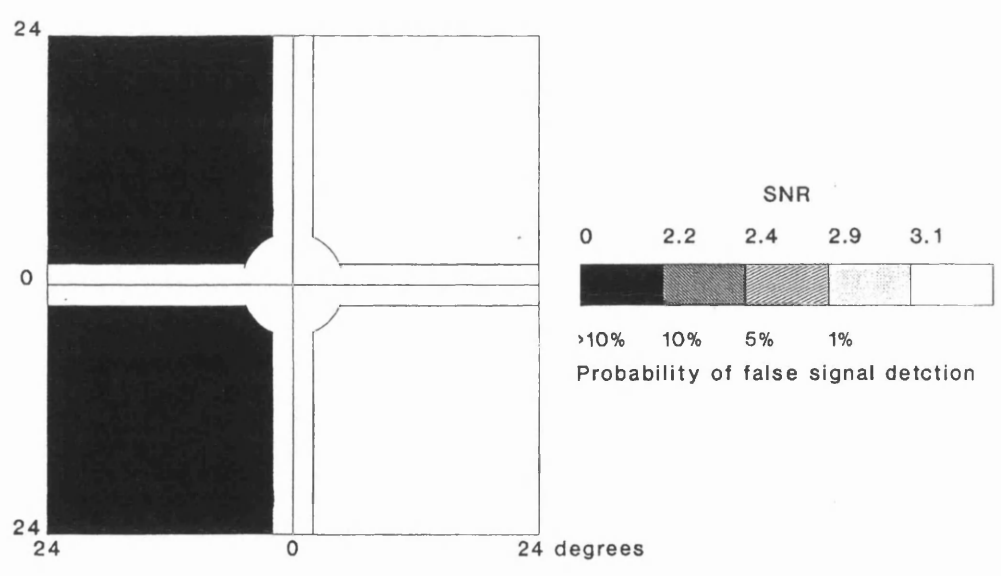
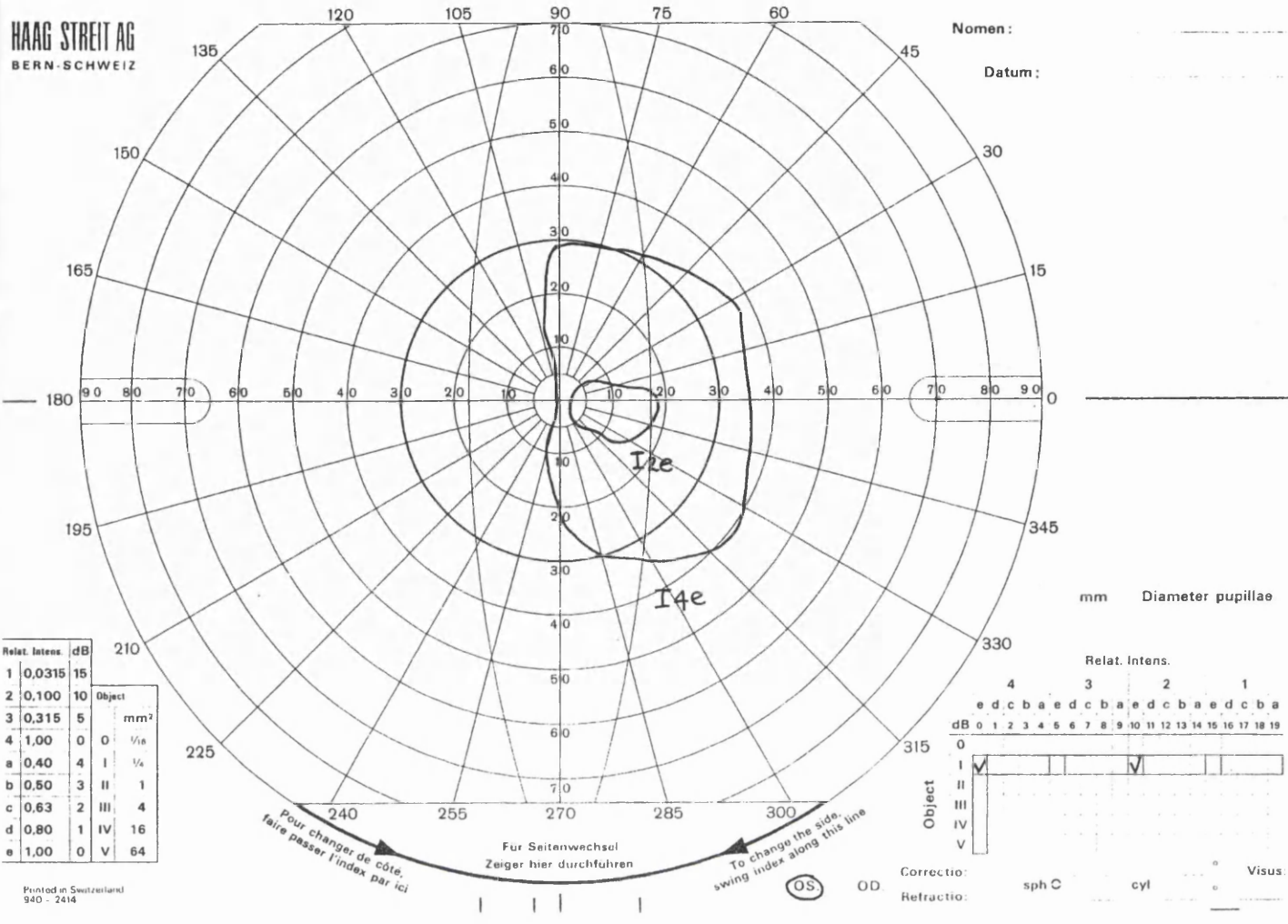


Figure 6.13 Subject 5 - field chart and result of electroperimetry for left eye

**Subject 6** - A 23 year old lady developed occipitoparietal ischaemia which produced a left homonymous hemianopia. The field charts and results are presented in Figures 6.14 and 6.15. A significant signal was recorded from all four 'seeing' quadrants. No significant signal was recorded from the four affected quadrants.

HAAG STREIT AG  
BERN-SCHWEIZ

Nomen: \_\_\_\_\_  
Datum: \_\_\_\_\_

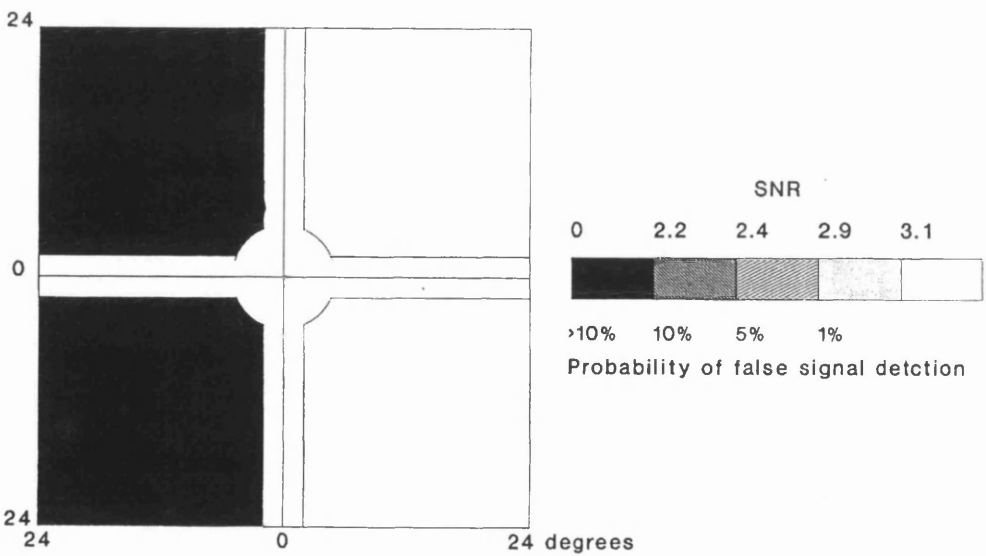
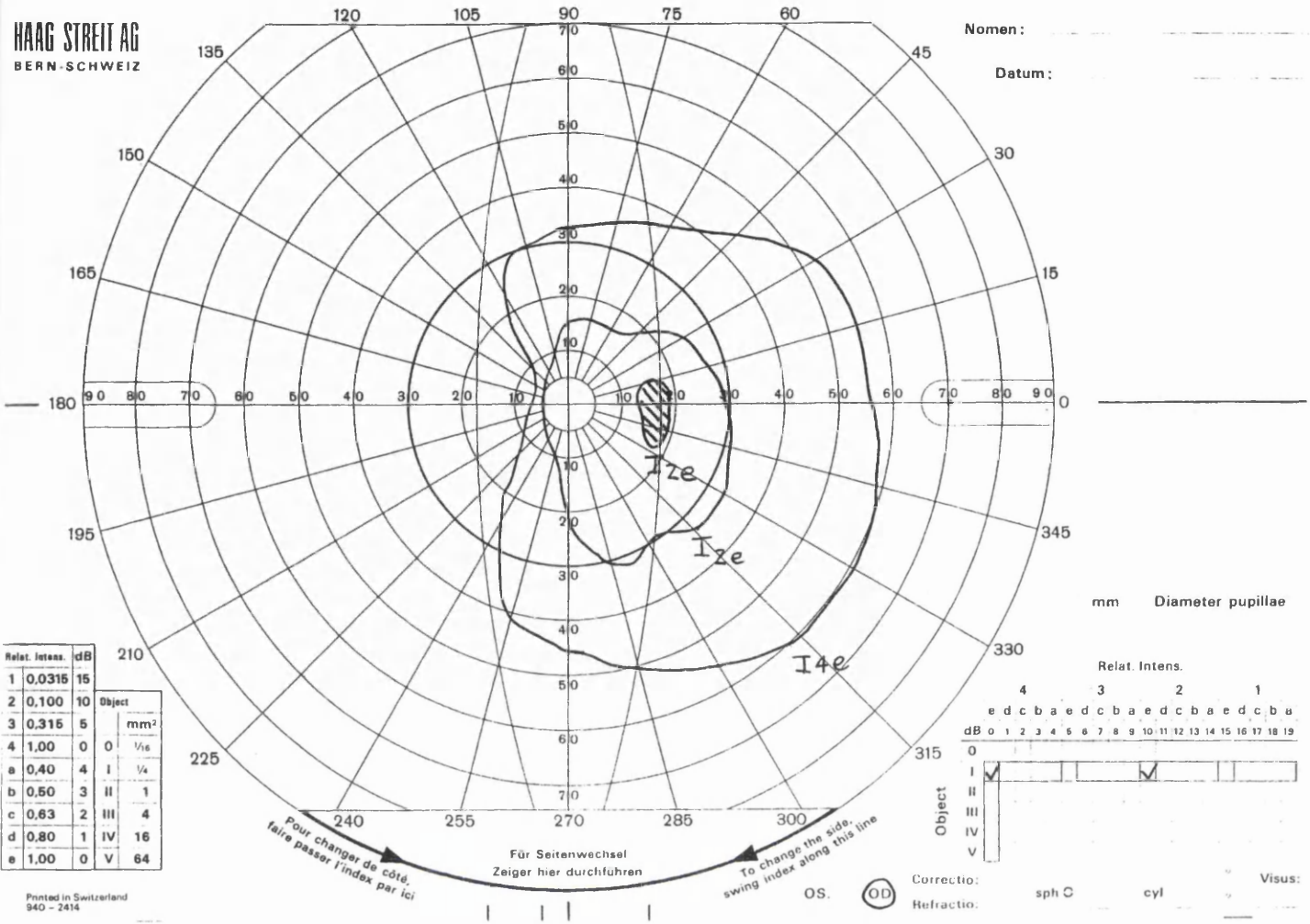


Figure 6.14 Subject 6 - field chart and result of electroperimetry for right eye

HAAG STREIT AG  
BERN - SCHWEIZ

Nomen: \_\_\_\_\_  
Datum: \_\_\_\_\_

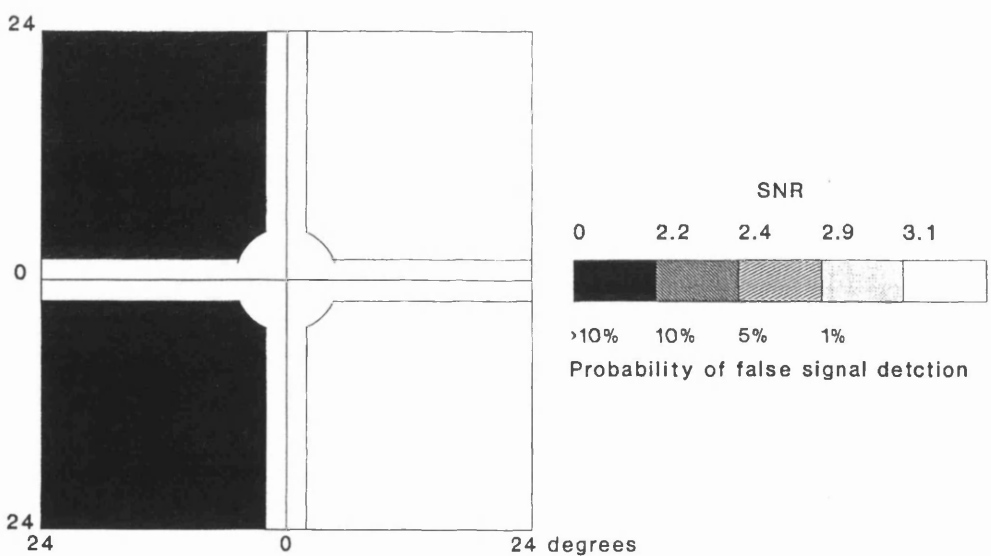
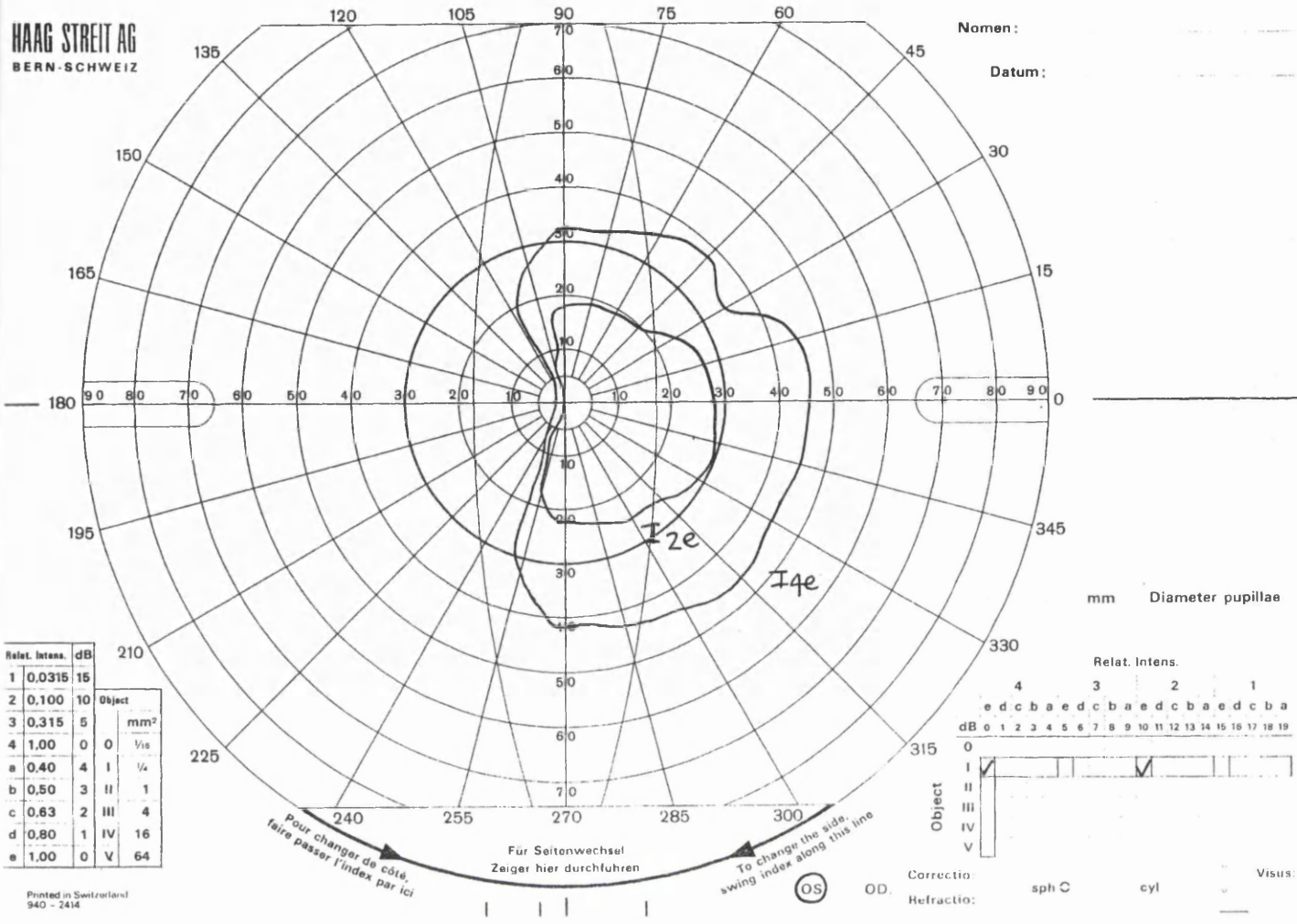


Figure 6.15 Subject 6 - field chart and result of electroperimetry for left eye

**Subject 7** - A 69 year old lady developed an occipital infarct which produced a left homonymous hemianopia. The field charts and results of electroperimetry are presented in Figures 6.16 and 6.17. A significant signal was recorded from the four 'seeing' quadrants. A small, yet significant, signal was recorded from the affected inferior quadrants.



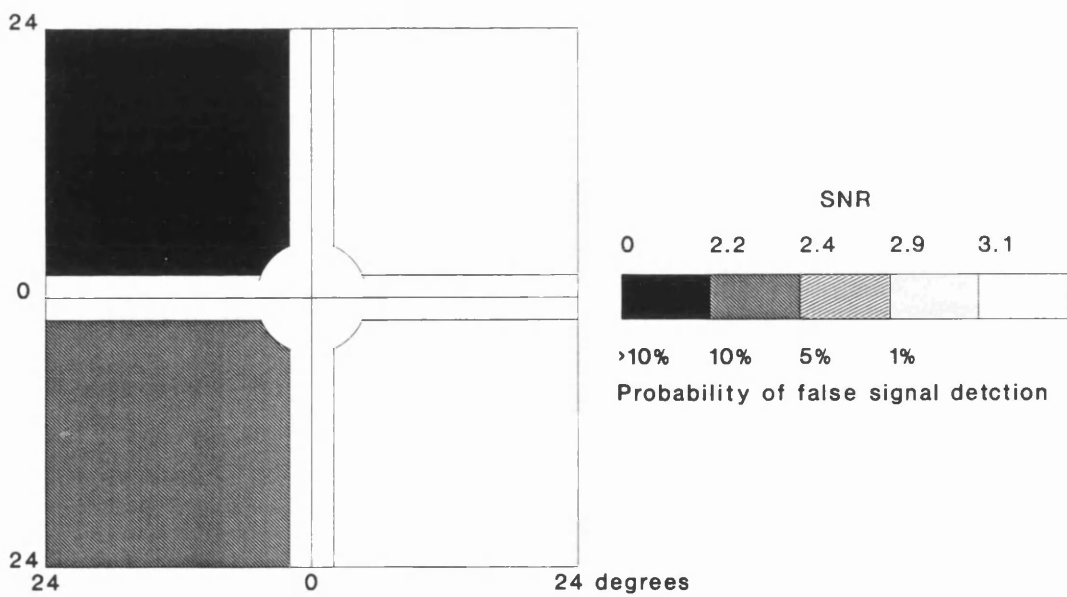
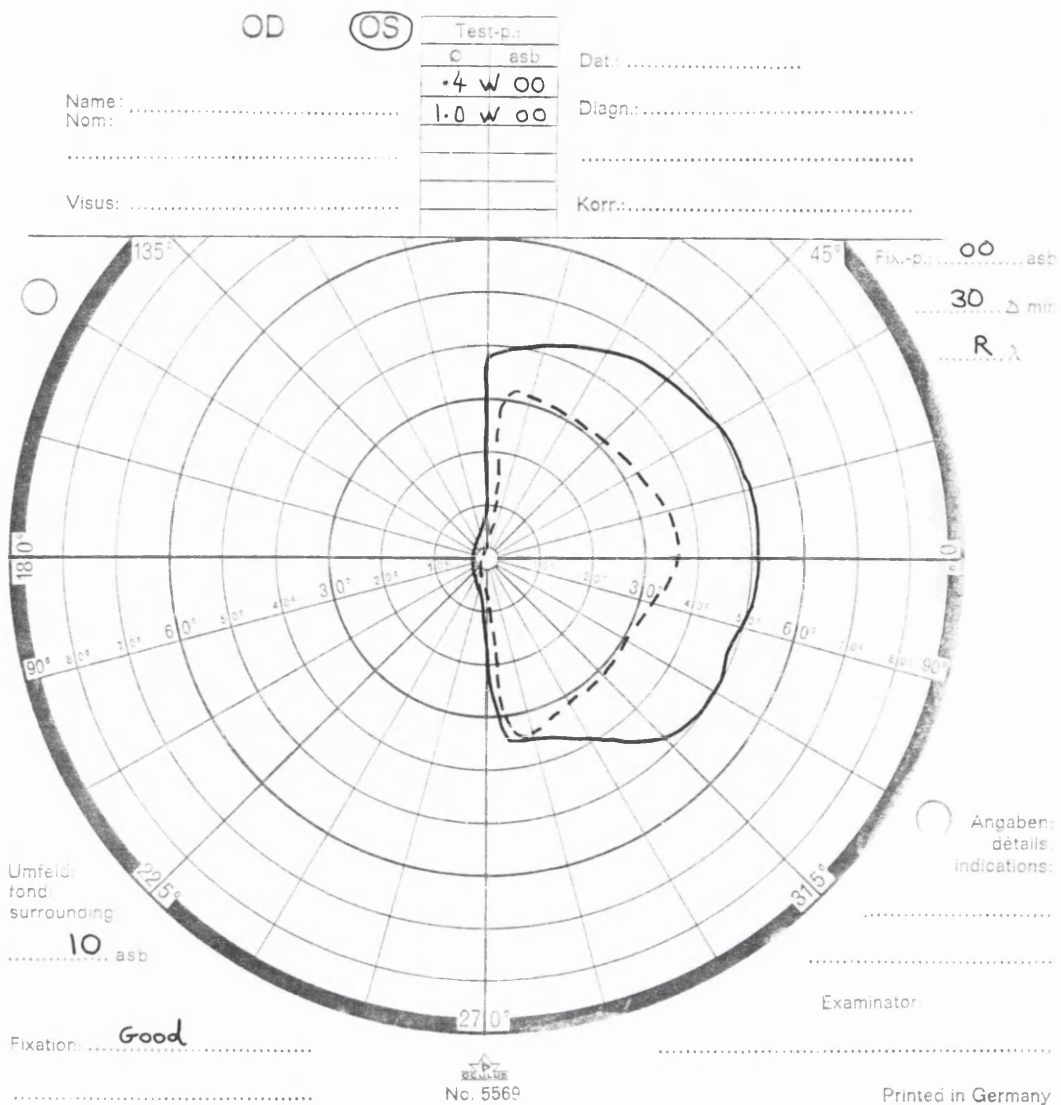


Figure 6.17 Subject 7 - field chart and result of electroperimetry for left eye

**Subject 8** - A 62 year old lady developed bilateral occipital infarcts following embolisation of a basilar aneurysm and this produced a left homonymous hemianopia and a right inferior homonymous quadrantanopia. There were islands of residual vision in the affected quadrants. The field charts and results of electroperimetry are presented in Figures 6.18 and 6.19. A significant signal was recorded from the two 'seeing' quadrants. In the right eye a reduced amplitude signal was also recorded from the affected left superior and right inferior quadrants. In the left eye a reduced amplitude signal was also recorded from the affected right inferior quadrant.

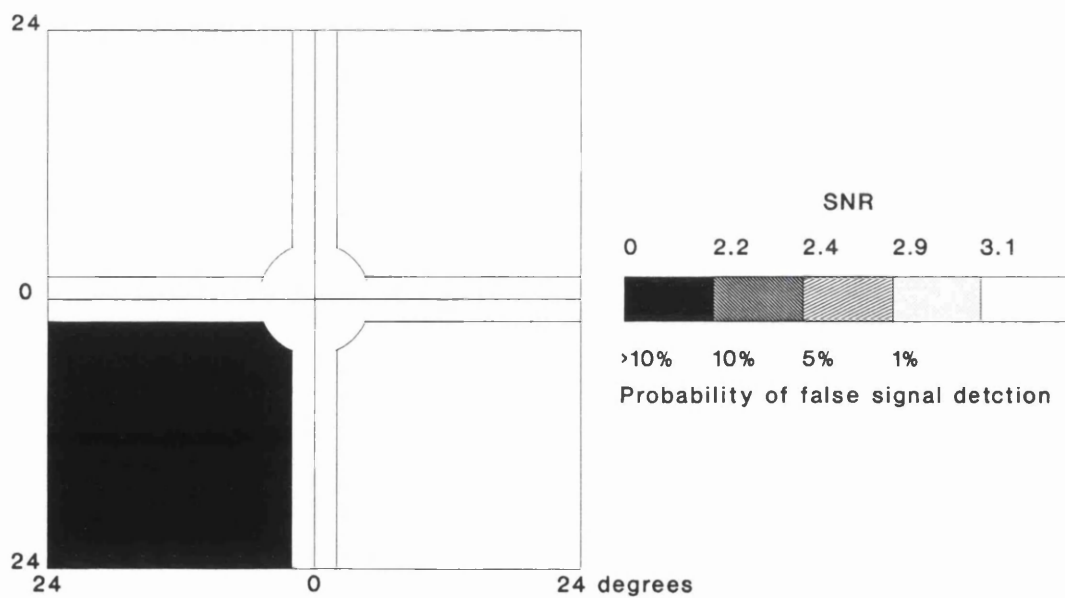


Figure 6.18 Subject 8 - field chart and result of electroperimetry for right eye

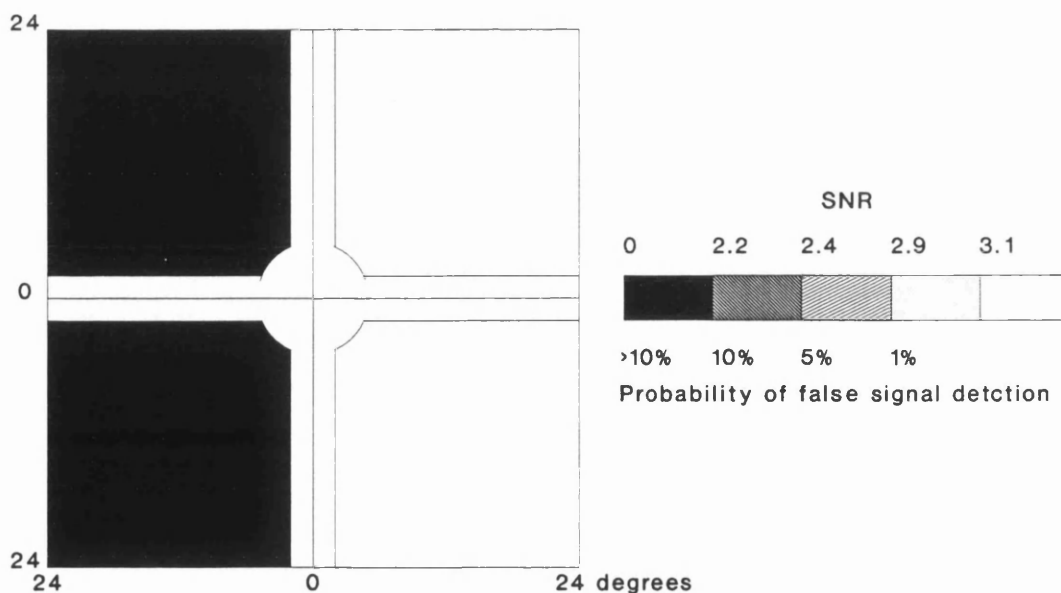
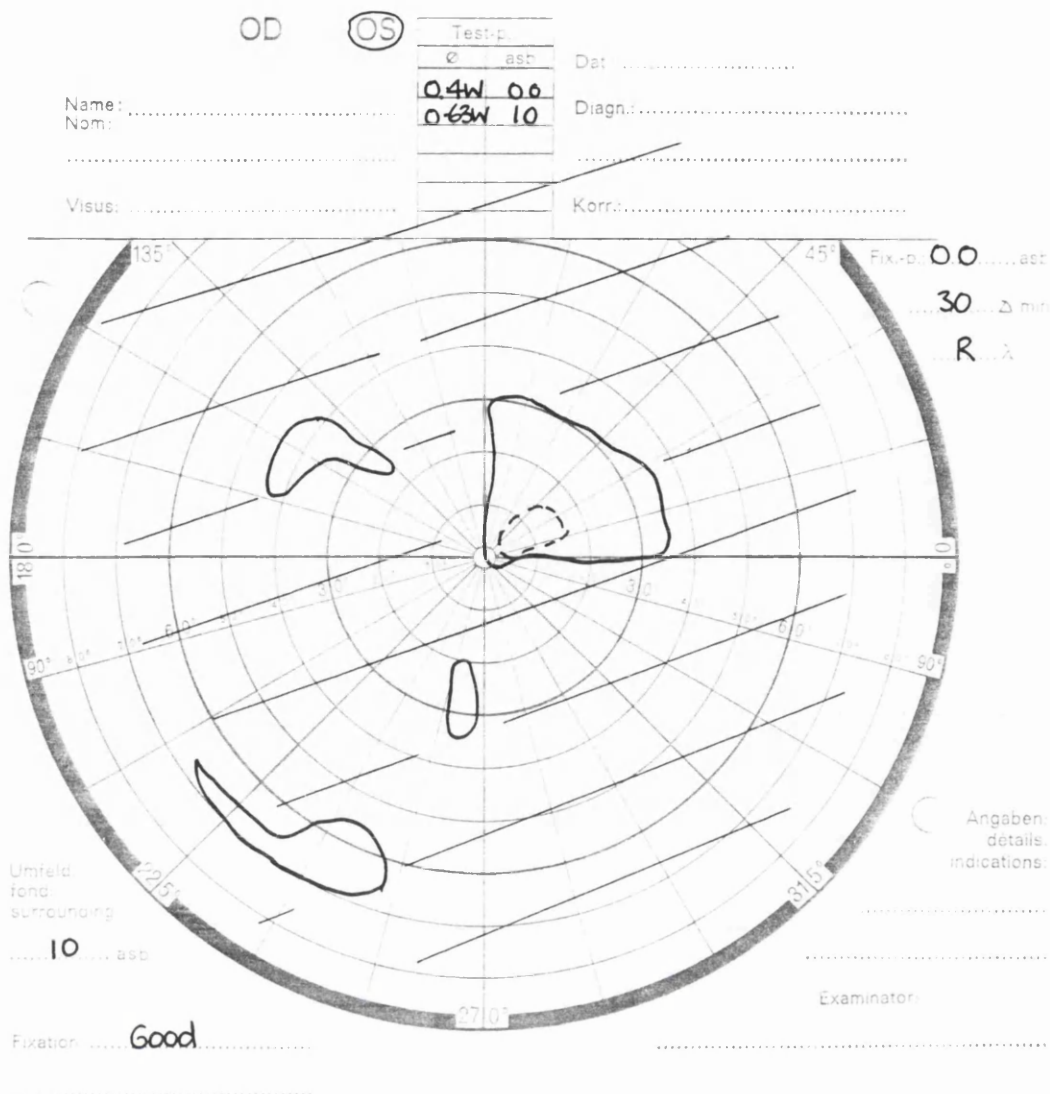


Figure 6.19 Subject 8 - field chart and result of electroperimetry for left eye

**Subject 9** - A 17 year old girl with long standing hydrocephalus as a result of aqueduct stenosis had a right homonymous hemianopia. The field charts and results of electroperimetry are presented in Figures 6.20 and 6.21. A significant signal was recorded from only one of four 'seeing' quadrants. A signal was recorded from the other three 'seeing' quadrants but the SNR was not significant because the signal amplitude was too small. The full-field VECF amplitude from this patient was also small. A significant signal was detected from the affected right inferior quadrant of the right eye and it is possible that this was due to a loss of fixation because the fixation monitor was not used during this study.

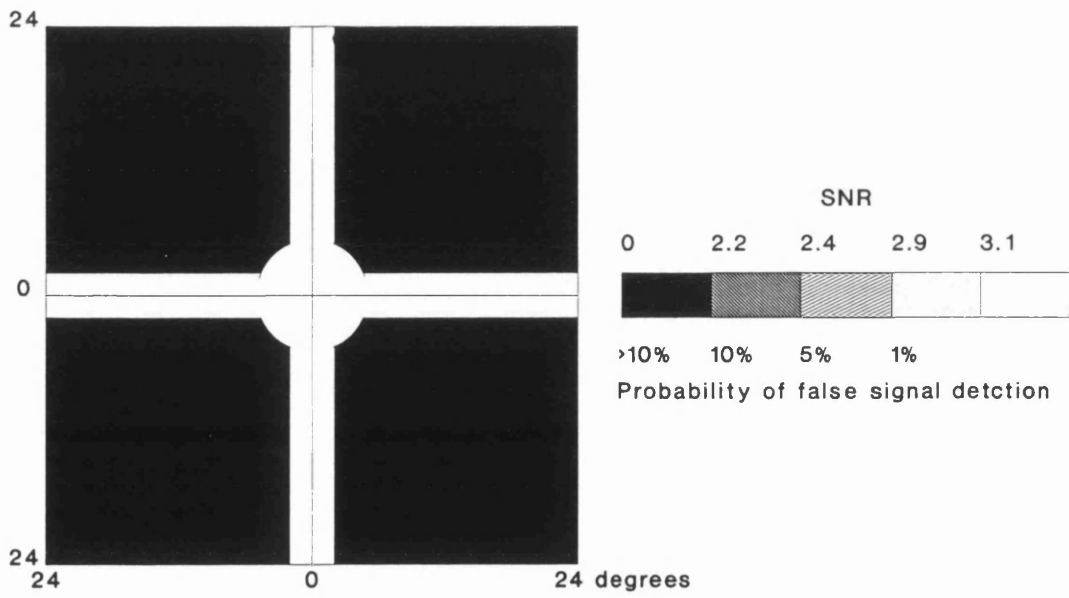


Figure 6.20 Subject 9 - field chart and result of electroperimetry for right eye

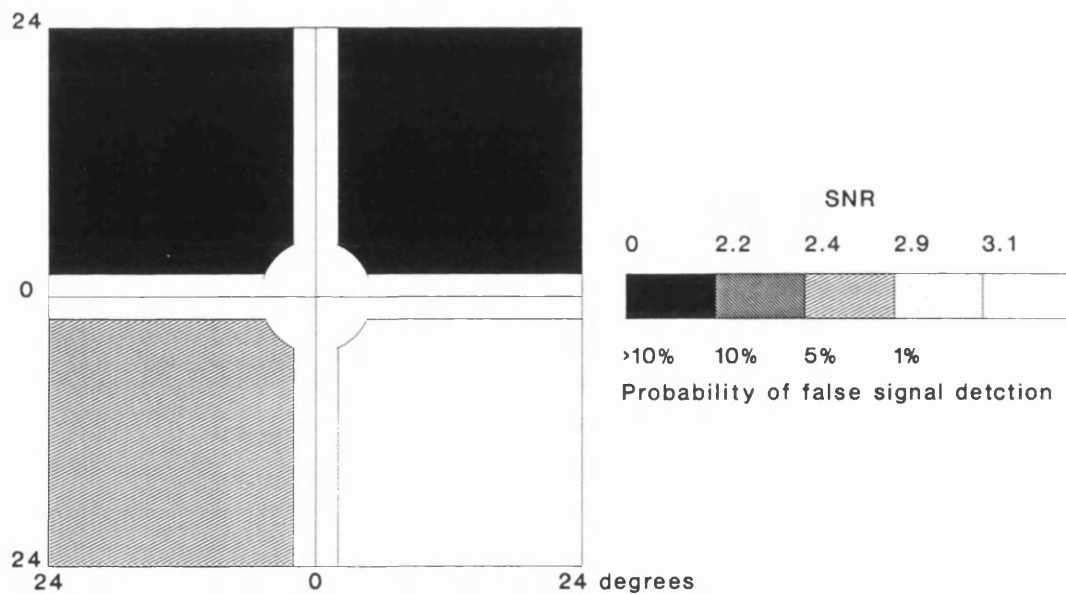
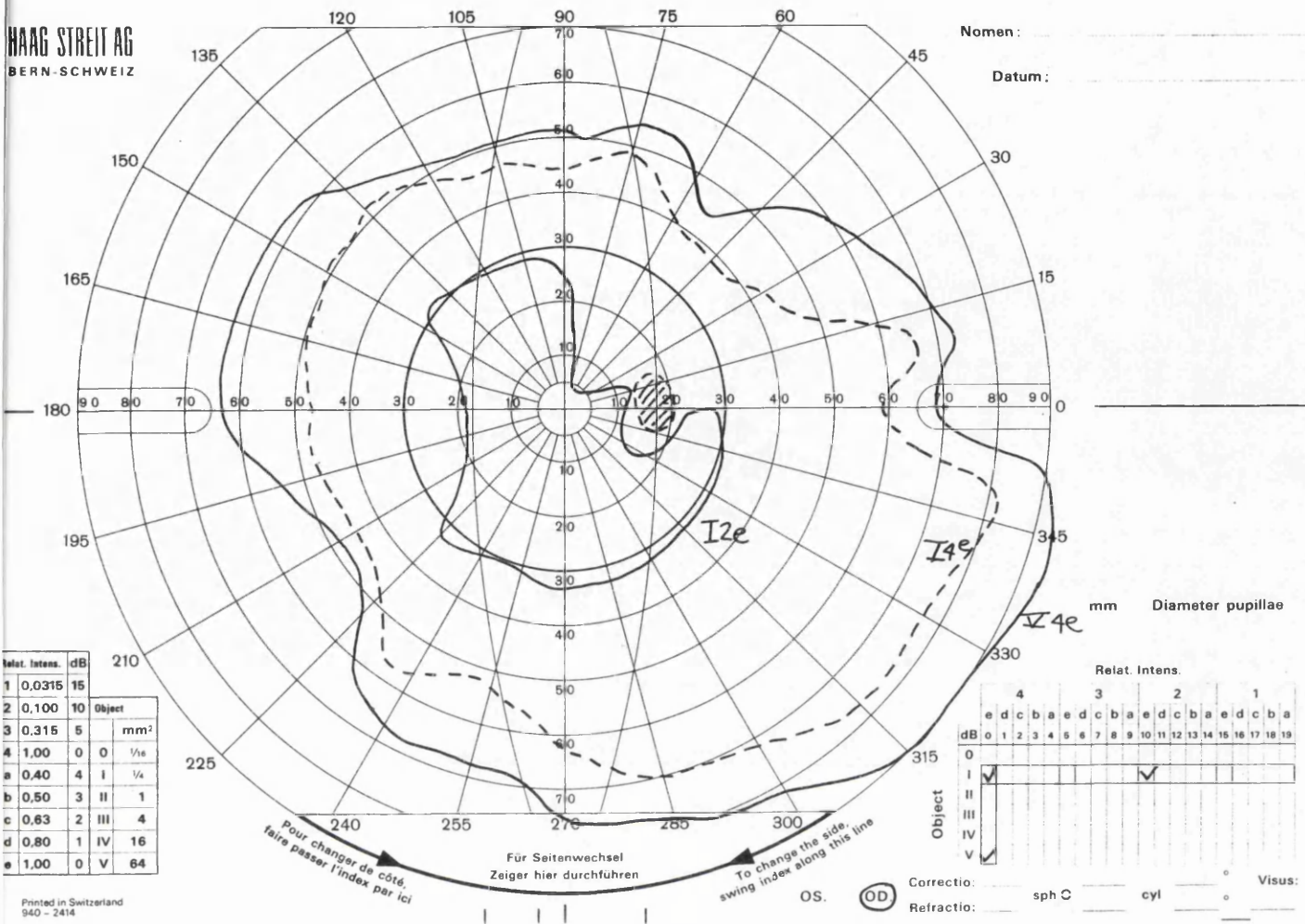


Figure 6.21 Subject 9 - field chart and result of electroperimetry for left eye

**Subject 10** - A 43 year old lady developed a left temporal epidermoid cyst which produced a relative right superior homonymous quadrantanopia. The field charts and results of electroperimetry are presented in Figures 6.22 and 6.23. A significant signal was recorded from the six 'seeing' quadrants. A significant but reduced signal was recorded from the two affected quadrants.

HAG STREIT AG  
BERN - SCHWEIZ



Printed in Switzerland  
940 - 2414

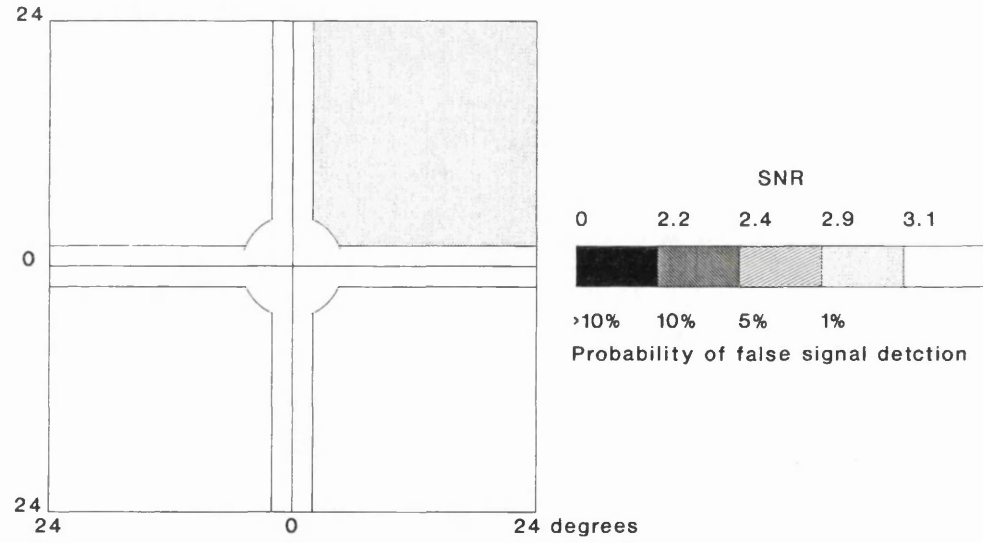


Figure 6.22 Subject 10 -field chart and result of electroperimetry for right eye

HAAG STREIT AG  
BERN-SCHWEIZ

Nomen: \_\_\_\_\_  
Datum: \_\_\_\_\_

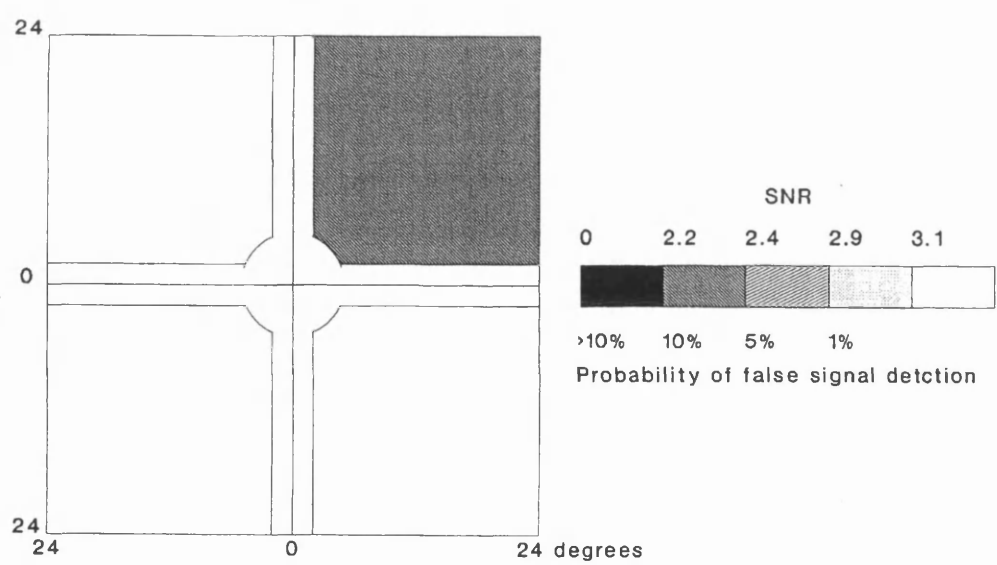
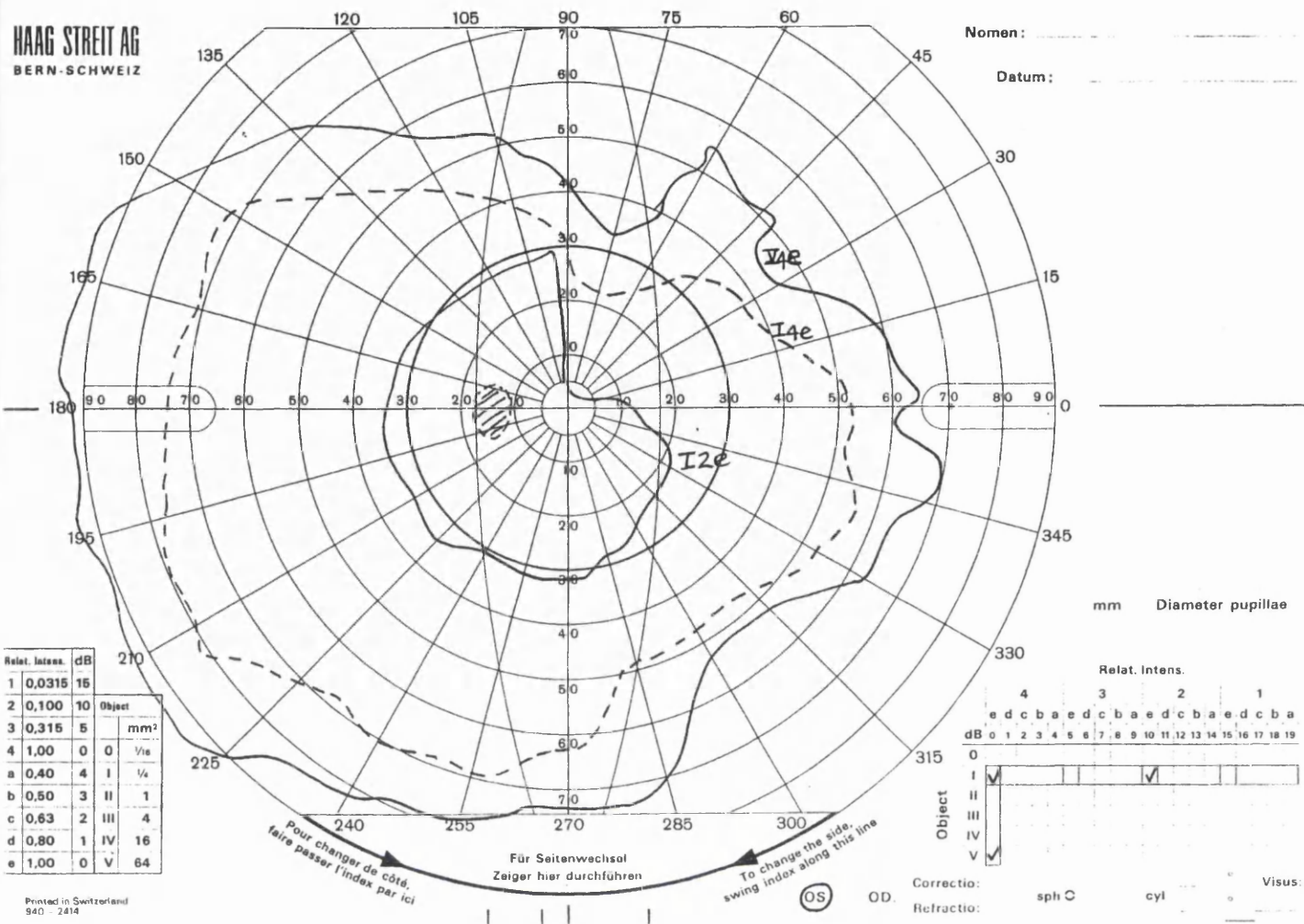


Figure 6.23 Subject 10 -field chart and result of electroperimetry for left eye

### Hotelling's $t^2$ statistic

Hotelling's  $t^2$  statistic uses the time variation in the measured signal to determine the significance of the signal detection. Using the ANC and Hotelling's  $t^2$  statistic a signal was objectively detected in all 40 'seeing' quadrants, with a probability greater than 90 %. Like the measurements made using the FFT, the mean signal amplitude was  $3.7 \mu\text{V}$  and the range was 1.1 to  $10.1 \mu\text{V}$ . The mean difference in the signal amplitude measured via the FFT and the ANC was only  $0.1 \mu\text{V}$ ; the lower quartile difference was  $-0.05 \mu\text{V}$ , the upper quartile was  $0.2 \mu\text{V}$  and the range was  $-0.5$  to  $1.6 \mu\text{V}$ . With the exception of just one case, the maximum signal was detected on the same recording channel irrespective of the measurement technique that was used.

A signal was detected in 16 out of 34 'non-seeing' quadrants, with a probability greater than 90 %. The mean signal amplitude was  $1.5 \mu\text{V}$  and the range was 0.2 to  $3.4 \mu\text{V}$ . In 13 of these 16 cases the signal amplitude was reduced compared to that obtained from the corresponding 'seeing' quadrant on the opposite side of the vertical meridian. In five of the 16 cases, the field defects were incomplete. In a further two cases, the field defects were not absolute but relative.

In general, the probability of signal detection was greater in the 'seeing' quadrants than in the 'non-seeing' quadrants. ROC curves were generated to determine the optimum signal detection threshold. An ROC curve is a plot of true positive fraction versus false positive fraction (Metz 1978). The true positive fraction is equal to the test sensitivity and the false positive fraction is equal to  $(1 - \text{the test specificity})$ . In this study, the true positive fraction was the number of 'non-seeing' quadrants correctly identified divided by the total number of 'non-seeing' quadrants. The false positive fraction was the number of 'seeing' quadrants in which a signal was not detected divided by the total number of 'seeing' quadrants. The true positive and false positive fractions vary according to the probability of signal detection that is used as the threshold for signal detection. The true positive and false positive fractions were calculated for a 90 %, 95 %, 97.5 %, 99 % and 99.9 % probability of signal detection and the ROC curve is plotted in Figure 6.24. Assuming that test sensitivity and specificity are equally important, the best decision performance is indicated by the point on the curve that is closest to the top left corner of the ROC space. In Figure 6.24 two points are equally close to the top left corner, one is for a 99 % probability of signal detection and one is for a 97.5 % probability. The sensitivity and specificity were 85 % and 80 % respectively for a 99 % probability of signal detection and were

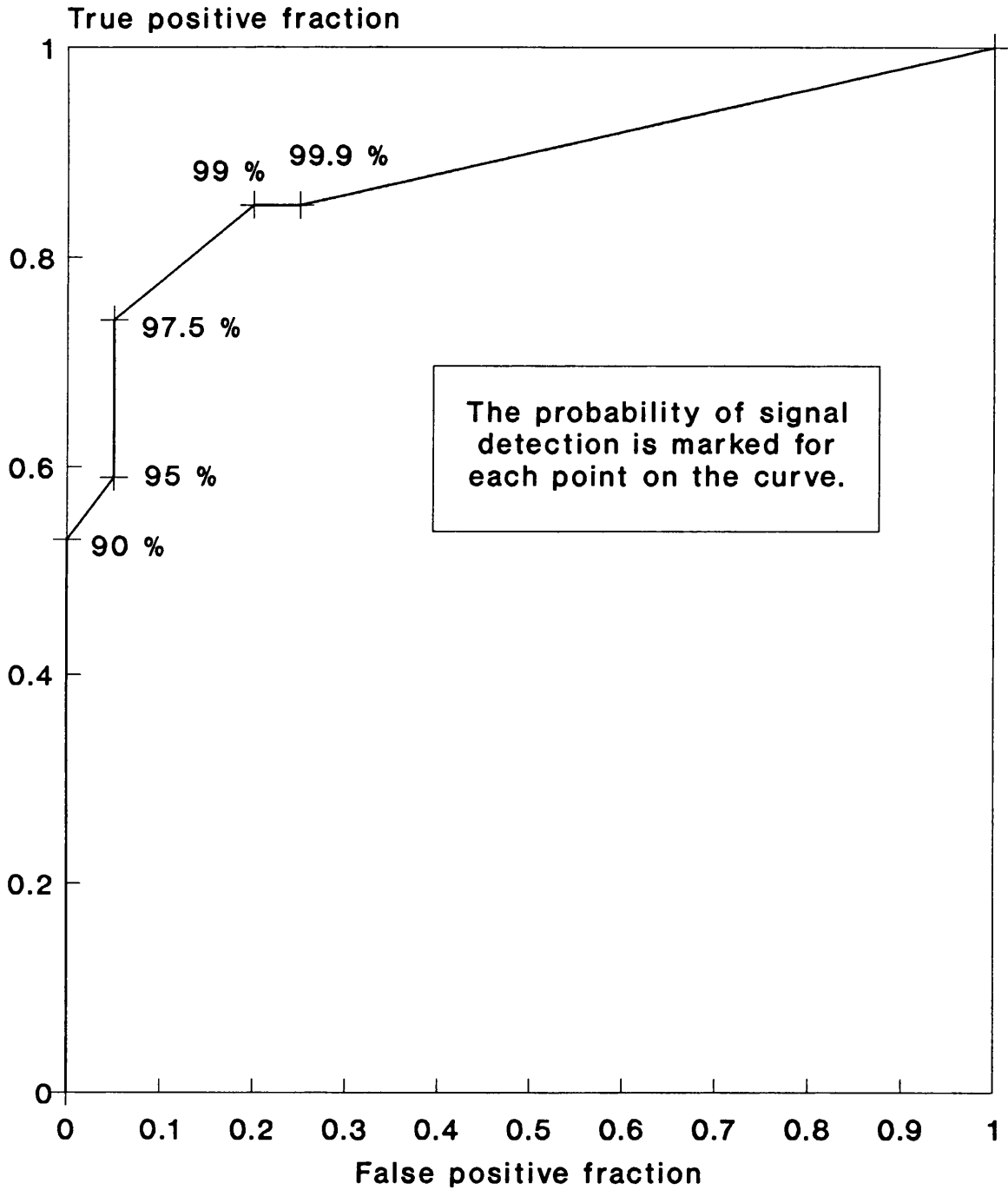


Figure 6.24 Receiver operating characteristic (ROC) curve for various probabilities of signal detection.

74 % and 95 % respectively for a 97.5% probability of signal detection. If the relative and incomplete field defects were ignored the curve would be shifted towards the top left corner and have an improved decision performance.

### 6.3.3 Discussion

This study has demonstrated that the stimulus and recording system developed in this laboratory can be used to detect complete and absolute hemi-field and quadrantic field defects. The objective results obtained from the study corresponded well with the patterns of field loss mapped using conventional subjective perimetry.

The operation of the novel ANC signal measurement technique has been validated in a total of 40 clinical recordings. These recordings were obtained from 'seeing' quadrants in 10 subjects. The estimates of signal amplitude and phase obtained using the ANC were comparable to those values obtained using a Fourier transform. In some cases there were small differences in the values and this was probably due to the fact that the ANC included an artefact rejection mechanism.

A greater number of recordings were statistically significant ( $p > 0.9$ ) when Hotelling's  $t^2$  statistic was applied to the ANC output than when the SNR was measured in the frequency domain. There were three contributory factors to this:

1. When the performance of the ANC and the FFT were compared using simulated signals (Section 3.4.4), slightly smaller signals were detected using the ANC output.
2. The ANC used in this study included a method of artefact rejection.
3.  $t^2$  statistic has a different statistical basis than measurement of the SNR in the frequency domain. It measures the temporal variation of the signal at the stimulus frequency and is independent of signals or noise at other frequencies.

The improved signal detection provided by the ANC and Hotelling's  $t^2$  statistic also enabled the detection of signals in more 'non-seeing' quadrants than measurement of the SNR in the frequency domain. In most of these quadrants the signal amplitude was reduced relative to that in the corresponding 'seeing' quadrant. Signals were detected from some 'non-seeing' quadrants because some field defects were not

complete and some defects were relative. Unfortunately, the largest stimulus targets were not always used on the Goldmann perimeter, so the number of relative defects is not known precisely. The brightest stimulus was however always used, therefore, the sensitivity of any relative defect not detected using subjective perimetry was very low. Procedures for subjective perimetry are to be improved as a result of this study. The largest stimulus target will always be used to delineate absolute field defects using the Goldmann perimeter.

Undetected losses of fixation may have contributed to the detection of signals from 'non-seeing' areas. To monitor this situation an improved method for continuously checking fixation could be introduced. An infrared camera could possibly be used to detect eye movements or alternatively eye movements could be detected using an electrooculogram (EOG). If fixation was not adequately maintained the recording would be aborted or interpreted accordingly.

Despite the fact that VECF signals were detected from 'non-seeing' areas the probability of false signal detection was generally higher in these areas. ROC curve analysis was used to choose which probability of false signal detection gave the best decision performance for the detection of 'seeing' and 'non-seeing' areas. The generated ROC curve is specific to the recording parameters used in the study. If, for example, the recording time were to be increased, the probability of false signal detection would decrease when a signal was recorded. The best decision performance would then be provided by a lower probability of false signal detection.

There are three clinical VECF studies in the literature in which visual fields were tested using quadrant field stimuli (Cappin and Nissim 1975, Howe and Mitchell 1980, Yanashima 1982). Cappin and Nissim studied field defects in 21 subjects with glaucoma and also tested 11 subjects with raised intraocular pressure. Howe and Mitchell studied 12 subjects with field defects due to cerebrovascular accident and migraine. Yanashima tested subjects with neuro-ophthalmic field defects.

Unlike the studies reported in this chapter, Yanashima only tested field quadrants out to an eccentricity of  $10^\circ$  and Howe and Mitchell only tested  $8.7^\circ \times 6.5^\circ$  quadrant fields. These studies used a maximum check-size of  $40'$  and  $50'$ , respectively, which was optimal for stimulation at a retinal eccentricity of about  $5^\circ$  (Section 4.2). Consequently, due to varying amounts of central sparing, Howe and Mitchell either reported normal or attenuated responses from the affected field quadrants in their patients. Yanashima did not use a foveal mask and this would have compromised his

results. In fact Yanashima (1982) only reported the results from two of his subjects. Cappin and Nissim (1975) stimulated  $24^\circ \times 24^\circ$  quadrants with a 50' check-size and found that the VECF was absent or delayed from stimulation of affected field quadrants.

The main novel aspects of the clinical studies reported in this chapter were the use of objective signal detection methods and the use of a fixation monitor. The stimulus check-size was 90' which was larger than that used in other studies and was optimal for stimulating more peripheral areas of the visual field. Any sparing of the central field was therefore less likely to affect the results of these studies.

Yanashima is the only worker who has previously used frequency domain analysis to analyse visual field defects. Furthermore, Yanashima used five recording channels and as a result recommended that more than two recording channels should be used for electroperimetry. The requirement to use multiple recording channels for optimal signal detection is confirmed by the studies in this chapter. In contrast, Cappin and Nissim and Howe and Mitchell only used one recording channel.

The SNR obtained in the studies reported in this chapter could probably be further improved by using an additional recording electrode, placed 5 cm superior of the mid-occipital location (Section 4.3). This would provide a total of four primary and six derived recording channels. The stimulus could also be further optimised so that it optimally stimulates receptive fields at all retinal eccentricities. This could be achieved by using the dartboard stimulus described in Section 4.3. The improved stimulus and SNR would enable the testing of smaller areas in the visual field and would hopefully enable the detection of incomplete quadrantic and hemi-field field defects.

## 7. CONCLUSION

The work described in this thesis has demonstrated that the recording of VECPs in response to visual stimuli can be used to test areas of the visual field. This technique is an objective form of perimetry and has been termed electroperimetry. The technique has great potential for the assessment of patients who are unable to cooperate adequately with subjective methods of perimetry. Such patients would include the young, the elderly and those with severe learning difficulties.

To date electroperimetry has been a research interest at a few specialised centres. There have been few clinical studies using the technique and little if any routine clinical use. It was concluded by the author that electroperimetry had not become clinically established for the following reasons:

1. The test was very time consuming. It took at least several minutes to make each measurement.
2. The test provided limited resolution of the visual field. To date no studies have been published in which groups of patients with visual field defects have been tested with stimuli which are smaller than visual field quadrants.
3. A practical method for positioning the stimulus on the retina had to be established. In some patients it would be adequate to check their fixation whilst in others it would be necessary for the stimulus to be positioned on the retina.

It was recognised that in order to overcome the first two limitations the SNR of the VECF needed to be improved. By increasing the SNR the VECF signal could be recovered from background EEG activity and muscle noise more rapidly. An improved SNR would also enable signals to be recorded from smaller areas of the visual field. The SNR could be improved in a number of ways:

1. DSP methods could be developed which had a better performance than conventional signal averaging techniques. In addition, objective signal detection techniques could be used to determine the significance of signal detection.
2. Stimuli could be optimised to maximise VECF amplitude.

3. The electrode montage on the scalp could be optimised to maximise the amplitude of the recorded VECP.

Unfortunately, there was no commercial electrophysiology system suitable to pursue the first two of these developments. In commercial equipment slow signal averaging was the only method of signal recovery. Furthermore, the variety of stimuli available in commercial equipment was very limited.

As a result of the current limitations of electroperimetry and the constraints of commercial equipment, six aims were outlined by the author in the introduction to this work (Section 1.6). All of these aims have been successfully achieved and each one is separately addressed in the following six sections (7.1 to 7.6).

## **7.1 RECORDING SYSTEM**

The PC based electrophysiology system (Chapter 2) has proved to be very versatile and has enabled the developments in electroperimetry for which it was designed. A DSP card is used to provide real-time signal processing and a wide range of stimuli are produced by means of computer graphics.

The stimulus monitor was found to be a significant source of electromagnetic interference. The interference was reduced by fitting a mumetal cone over the vertical deflection coils of the monitor and by enclosing the monitor in an earthed steel cabinet (Section 2.5).

A detailed calibration of the monitor luminance was undertaken (Section 2.6) for a range of brightness and contrast settings and this produced significant findings. It was found that the monitor luminance saturates and, furthermore, that the luminance at which saturation occurs is dependent on image size. In order to prevent luminance artefacts in VECP recordings, the monitor was then operated at luminance values that do not saturate and are independent of image size.

The system was first tested with electrical test signals. This was followed by a period of clinical validation in which VECP recordings were collected from a large number of normal subjects in response to standard stimuli (Section 2.11). The results were used to calculate a normal range for signal amplitude and latency and were compared with published data from other systems.

In addition to being used for research and development, the system has also provided wider clinical benefits and has been used to provide a regional clinical visual electrophysiology service performing in excess of 400 patient studies per annum. The system was immediately adopted in the clinical environment due to the thorough commissioning, testing and optimising procedures to which it had been subjected. Attention was paid to making the system software user-friendly (Section 2.4) and this has contributed to its successful implementation.

## **7.2 SIGNAL PROCESSING DEVELOPMENTS**

It was concluded that the steady-state VECP had five significant advantages over the transient VECP for developing techniques in electroperimetry (Section 3.2.2):

1. The steady-state VECP can be recorded more rapidly than the transient VECP.
2. The SNR of the steady-state VECP is enhanced by analysis in the frequency domain.
3. Objective signal detection techniques have already been developed for the steady-state VECP.
4. Temporal information on the VECP can be obtained by sub-dividing the recording into a number of time periods and measuring the signal in each. These measurements can be used to calculate the confidence interval of the signal mean and can also be used to detect temporal trends in the amplitude and the phase of the signal due to reduced attention, sensory adaptation, progressive fatigue or loss of ocular accommodation.
5. The steady-state VECP is represented by discrete frequency components at the stimulus frequency and its harmonics. Therefore, if different parts of the visual field are stimulated at different frequencies it is possible to test them simultaneously, further reducing recording times.

The first four of these advantages have currently been exploited. Two objective methods for determining the significance of VECP signals have been applied to electroperimetry for the first time. One method estimates the SNR in the frequency

domain and the other method uses Hotelling's  $t^2$  statistic to study temporal variation in the signal. Hotelling's  $t^2$  has not previously been applied to VECP measurements.

Several methods are available to measure the steady-state VECP and they can be classified into one of two groups according to whether the detection process is phase insensitive or phase sensitive (Section 3.2.2). A phase insensitive detector is equally sensitive to all signal phases whilst a phase sensitive detector is optimally sensitive to one signal phase. If the phase of a sinusoidal signal is unknown or time varying, a phase insensitive technique is required which measures both signal amplitude and phase. The FFT is an example of a phase insensitive method. If the phase of a sinusoidal signal is known and remains constant, then the optimal measurement technique is a phase sensitive detector. A phase sensitive detector can yield a 3 dB improvement in the SNR when compared with phase insensitive methods.

In this laboratory a major development has been the application of adaptive noise cancelling principles to the measurement of steady-state VECPs (Section 3.4). The ANC has the advantage that it can be implemented as a phase insensitive or a phase sensitive detector (Section 3.2.2). The ANC has a number of operating advantages over the FFT (Section 3.4.5); it is less computationally intensive, it requires less memory, it can be implemented in real-time, it provides continuous temporal information on variation of the VECP signal and artefact rejection can be included. The theoretical performance of the ANC has been verified using simulated and real physiological signals (Section 3.4.4). Following these simulations the ANC was successfully utilised to analyse clinical data (Section 6.3.2).

### **7.3 STIMULUS DEVELOPMENT**

Visual stimuli were developed using computer graphics and presented to the subject on a computer monitor screen (Chapter 4). The use of computer graphics allowed a wide range of stimuli to be produced and so enabled stimuli to be tailored to different pathways of the visual system.

Stimulus development naturally concentrated on steady-state stimuli because of the signal processing advantages. Pattern-reversal checkerboard stimuli were investigated and the optimum check-sizes were determined for testing different size visual field quadrants (Section 4.2). The optimum check-size was found to increase with retinal eccentricity and the results were compatible with the hypothesis that the

optimum check-size is inversely proportional to the cortical magnification factor. As a result of this work, a dartboard stimulus was developed in which the most effective check-size was presented at each location in the visual field (Section 4.3).

The dartboard stimulus enabled the testing of three small areas within each visual field quadrant (Section 4.3). Four recording electrodes were used to maximise the recorded SNR (Section 4.3.2). Together with the reference electrode, there were ten possible electrode pair combinations. The pair of electrodes between which the maximum VECP was recorded varied according to the part of the visual field being tested and was also subject to interindividual variation (Section 4.3.3). All pairs of electrodes were found to be necessary to detect the signals.

A limitation of the pattern-reversal stimulus is that the VECP amplitude is smaller for stimulation of the peripheral visual field than the central field. Some workers have suggested that motion-onset stimuli may produce larger amplitude VECPs than pattern-reversal stimuli when testing the extramacular area of the visual field. Motion-onset stimuli were therefore developed and compared with pattern-reversal stimuli (Section 4.4). In order to maximise the amplitude of the motion-onset VECP, a novel stimulus was developed consisting of circular rings that had pattern elements simultaneously moving in all directions. The theoretical advantage of this stimulus, as compared to traditional stimuli consisting of horizontally moving bars, was that more direction sensitive cortical cells would be stimulated (Section 4.4.1). The stimulus did in fact produce a larger amplitude VECP than a pattern-reversal stimulus when the fovea was masked (Section 4.4.3). Unfortunately, however, it was found that the visual system rapidly adapts to motion. It was therefore necessary to use long interstimulus intervals in order to prevent adaptation to the stimulus and this made the test prohibitively slow for testing small areas of the visual field. Potentially, the motion-onset stimulus may have clinical applications for testing the parts of the visual system that process motion stimuli.

It was concluded that the steady-state dartboard pattern-reversal stimulus was preferable to motion-onset stimuli for electroperimetry.

## 7.4 SUBJECT FIXATION

Accurate positioning of the stimulus on the retina is essential for electroperimetry. A fixation monitor was developed in which subjects reported momentary changes in a fixation letter at varying time intervals (Section 4.3.2). This simple task also helped the subjects to concentrate and to reduce fatigue. A disadvantage of the technique was that it did not continuously monitor fixation. Additional techniques could be developed to enable continuous monitoring of fixation (Section 4.3.4). An infra-red camera could possibly be used to detect eye movements. Alternatively, eye movements could be detected by recording the EOG. The problem with using the EOG is that in addition to the time and discomfort of placing an additional two electrodes on the patient, an additional amplifier channel is also required.

## 7.5 STIMULUS PROJECTION

The ideal method for accurately stimulating particular parts of the visual field is for the stimulus pattern to be positioned on the retina under the view of an operator. A system employing a miniature LCD display and an indirect ophthalmoscope has been successfully developed to meet this objective (Chapter 5). The response time of the LCD fluid was, however, slow when compared to a computer monitor screen and steady-state stimuli could not be produced. Consequently, it was necessary to use transient stimuli. Reproducible VECPs were successfully recorded from full-field and quadrant field stimuli so demonstrating the feasibility of this technique (Sections 5.4 and 5.6).

The potential hazard to patients from excessive blue light exposure during ophthalmic procedures is well recognised (Section 5.5.1). Radiometric measurements were therefore made to ensure that the system complied with guidelines on safe exposure limits (Section 5.5.4).

An important finding was that the blue light hazard was significantly reduced when a yellow coated lens was used in the indirect ophthalmoscope (Section 5.5.5). Nevertheless, intense light remains a potential hazard, especially as the tolerance of diseased eyes may be lower than that of healthy eyes. Retinal exposure must therefore be limited by keeping the recording time to a minimum (Section 5.5.6).

Potentially, the system has wider applications in electrophysiology (Section 5.6.4). It would be useful for testing subjects suspected of hysteria or malingering, as correct fixation and focusing of the stimulus on the retina could be ensured. The system could also be used to record PERGs which would be especially valuable in the study of maculopathy.

Outside the field of electrophysiology the system has the potential to be used for making fundus measurements and assessing fixation prior to laser photocoagulation (Section 5.6.4).

It would be possible to construct a similar projection system using an SLO (Sections 5.2 and 5.6.4). The SLO has the advantages that it uses lower levels of retinal illumination, does not require dilation of the pupil and can already be used to present steady-state stimuli. The LCD system, however, has the advantages that it is compact, portable and inexpensive when compared with the SLO.

## **7.6 CLINICAL EVALUATION**

The stimulus and signal analysis techniques which have been developed were clinically validated by assessing patients with complete and absolute hemifield and quadrantic field defects (Chapter 6). The subjects had a variety of field defects due to pathology affecting the optic nerve, optic chiasm, optic radiation and occipital cortex.

Quadrant field stimuli were used and they were presented on the monitor screen. A steady-state stimulation rate was used to maximise the SNR. A unique aspect of the study was the use of objective signal detection techniques to determine the significance of signal measurements. Two tests were used, one measured the SNR in the frequency domain (Sections 3.2.2, 6.2.1 and 6.3.1) the other used Hotelling's  $t^2$  statistic (Section 3.2.2 and 6.3.1). The results confirmed patterns of subjective field loss (Sections 6.2.2 and 6.3.2). The results also enabled the sensitivity and specificity of the system to be determined for the detection of abnormal, 'non-seeing', quadrants in the visual field (Section 6.3.2).

## 7.7 FUTURE WORK

The steady-state pattern-reversal dartboard stimulus (Sections 4.3 and 7.3) is now being assessed in a clinical trial of 20 subjects with absolute visual field defects. Three areas are being tested in each visual field quadrant, outside the fovea and within 30° of fixation. The object of this stimulus is to be able to detect visual field defects that are smaller than a visual field quadrant (Section 4.3.1). Subjects have been recruited with a variety of field defects due to retinal and cortical pathology. The experimental protocol is the same as that presented in Section 4.3.2 and each of the twelve areas is being tested separately. Software will shortly be developed to test the three areas in each quadrant simultaneously (Yanashima 1982) and so reduce the duration of the test by a factor of three. Assuming that each recording takes 2 minutes, the total recording time for testing both eyes would only be 16 minutes.

The system has been duplicated for assessing vision in multi-handicapped children at the Royal Hospital for Sick Children in Glasgow (Section 2.8) and this work will be developed. In addition to assessing visual fields, the system is being used to assess visual acuity by means of VECF recording (Section 1.4.3), preferential looking and optokinetic nystagmus. By means of computer graphics it has been possible to perform all three acuity tests with the same monitor screen, so enabling a direct comparison of results. In order to determine the VECF acuity threshold as rapidly as possible, the objective signal detection techniques presented in Chapter 3 will be applied in real-time to detect the presence of VECF signals in EEG noise. Steady-state stimuli will be used in preference to transient stimuli because of the advantages given in Section 3.2.2. Furthermore, the signal amplitude and phase will be measured by means of the ANC in preference to the FFT, due to its computational advantages (Section 3.4.5). Hotelling's  $t^2$  statistic (Section 3.2.2) will be used to objectively detect any signal present in the recording. EEG recordings from children contain more muscle artefact than adults. So, various artefact rejection techniques will be evaluated to optimise the performance of the ANC (Section 3.4.5). If the phase of the VECF can be accurately predicted it may be possible to use the ANC as a phase sensitive detector and improve the SNR by 3 dB (Section 3.2.2). For some subjects steady-state stimuli may not be appropriate as the visual system may not be sufficiently well developed to process the stimulus. For these subjects transient stimuli will have to be used. Transient VECF signals will be detected objectively by means of a method based on cross-correlation (Section 3.3.4). By modelling VECF signals in EEG noise it will be possible to empirically determine what value of cross-correlation relates to what probability of signal detection.

The indirect ophthalmoscope stimulus delivery system (Chapter 5) is a useful device for positioning stimulus patterns on the retina under direct view of an observer. Unfortunately, because the LCD fluid does not respond sufficiently fast to permit the use of steady-state stimuli, it has not been possible to exploit the advantages of the steady-state DSP techniques developed in this work. Current developments in LCD technology should permit the use of steady-state stimuli on small chip-on-glass displays in the near future (Section 5.5.6). If, however, such LCDs do not become commercially available, an alternative route for future development may be to produce a compact, inexpensive SLO delivery system. In the mean time, the current indirect ophthalmoscope system is being used to collect data from more normal subjects and will be used to assess subjects with absolute field defects.

## GLOSSARY

- ADC** - Analogue-to-digital converter. An electronic circuit that converts an analogue signal into a digital signal (Section 2.3.3).
- Ametropia** - A condition of the eye in which the image fails to come to a proper focus on the retina. Ametropic, adj.
- ANC** - Adaptive noise canceller (Sections 3.2.2 and 3.4). A method for estimating a signal corrupted with uncorrelated noise. In this laboratory, a novel implementation of the ANC has been developed to estimate visual evoked cortical potentials (VECPs) corrupted with electroencephalographic activity and muscle noise. An adaptive filter is used to cancel the noise and provide an estimate of the VECP signal.
- APWF** - A posteriori 'Wiener' filtering (Section 3.4.2).
- Card** - A printed circuit board.
- CT** - Computed tomography, as in x-ray CT.
- DAC** - Digital-to-analogue converter. An electronic circuit that converts a digital signal into an analogue signal (Section 2.4.3).
- Digital signal** - A signal that is sampled and represented by digital numbers.
- DSP** - Digital signal processing. The mathematical processing of digital signals (Chapter 3).
- EEG** - Electroencephalogram.
- Electroperimetry** - An objective form of perimetry in which the visual field is assessed by recording the cortical potentials evoked in response to visual stimuli (Section 1.5).

- Emmetropia - The ideal condition of the eye, with no refractive error. Parallel light rays come to a focus on the retina. Emmetropic, adj.
- EOG - Electrooculogram.
- ERG - Electroretinogram (Section 1.4.2).
- FFT - Fast Fourier Transform. An efficient algorithm for performing a Fourier Transform (Section 3.2.2).
- Hypermetropia - Long sightedness; ametropia in which parallel light rays come to a focus behind the retina. Hypermetropic, adj.
- LCD - Liquid crystal display.
- LGN - Lateral geniculate nucleus (Section 1.1.4).
- LMS - Least mean square. (See Section 3.4.2 for the LMS adaptive algorithm.)
- MRI - Magnetic resonance imaging.
- Myopia - Short sightedness; ametropia in which parallel light rays come to a focus in front of the retina. Myopic, adj.
- OD - *Oculus dexter*, right eye.
- OS - *Oculus sinister*, left eye.
- PC - Personal computer.
- PERG - An ERG recorded in response to a pattern stimulus (Section 1.4.2).
- Perimetry - A technique for measuring the extent of the visual field (Section 1.3).

- PET - Positron emission tomography.
- PRBS - Pseudo random binary stimulation (Section 3.2.3).
- SLO - Scanning laser ophthalmoscope. A type of ophthalmoscope in which the retina is examined using a raster scanning laser beam (Section 5.2).
- SNR - Signal-to-noise ratio. The ratio of the signal amplitude being measured relative to the amplitude of the background noise. The SNR is sometimes quoted in decibels.
- TFT - Thin film transistor (Section 5.5.6).
- VECP - Visual evoked cortical potential. A cortical potential evoked in response to a visual stimulus (Section 1.4.3).
- VGA - Video Graphics Adapter (Section 2.3.5).
- Visual field - The part of space in which objects are simultaneously visible to the steadily fixating eye (Section 1.2).

## REFERENCES

Adachi-Usami E, Misago M and Kanayama N (1978).

Electro-perimetry by means of the scotopic VECF.

Doc Ophthalmol Proc Series 15, 179-187.

Airas K and Petersen J (1985).

Objective determination of dark adaptation: accuracy of the evoked potential method.

Graefe's Arch Clin Exp Ophthalmol 223, 63-65.

Albright TD, Desimone R and Gross CG (1984).

Columnar organization of directionally selective cells in visual area MT of the macaque.

J Neurophysiol 51, 16-31.

American Conference of Governmental Industrial Hygienists (ACGIH) (1983).

Threshold limit values for chemical substances and physical agents in the workroom environment.

ACGIH, Cincinnati.

Anderson TW (1958).

The generalised  $T^2$  statistic.

An introduction to multivariate statistical analysis. John Wiley and sons, New York, 101-125.

Aulhorn E and Karmeyer H (1977).

Frequency distribution in early glaucomatous visual field defects.

Doc Ophthalmol 14, 75-83.

Bach M and Speidel-Fiaux A (1989).

Pattern electroretinogram in glaucoma and ocular hypertension.

Doc Ophthalmol 73, 173-181.

Barber C (1981).

Inherent characteristics of visual stimulus systems and their effect on the visual evoked potential.

Clin Phys Physiol Meas 2, 135-146.

Barber C and Galloway NR (1976).

A pattern stimulus for optimal response from the retina.  
Doc Ophthalmol 10, 77-86.

Bedwell CH (1982).

Visual fields: a basis for efficient investigation.  
Butterworths, London.

Beers APA, Rienslag FCC and Spekrijse H (1992).

Visual evoked potential estimation of visual acuity with a Laplacian derivation.  
Doc Ophthalmol 79, 383-389.

Beinhocker GD, Brooks PR, Anfenger E and Copenhaver RM (1966).

Electroperimetry.  
IEEE Trans Bio-Med Eng BME 13, 11-18.

Bergland GD (1969).

A guided tour of the fast Fourier transform.  
IEEE Spectrum 6, 41-52.

Berninger TA and Arden GB (1988).

The pattern electroretinogram.  
Eye 2 (Suppl), S257-S283.

Blumhardt LD, Barrett G and Halliday AM (1977).

The asymmetrical visual evoked potential to pattern reversal in one half field and its significance for the analysis of visual field defects.  
Br J Ophthalmol 61, 454-461.

British Standards Institution (1989).

BS 5724 part 1. Medical electrical equipment: general requirements for safety.  
BSI, Milton Keynes.

Bradnam MS, Keating D, Montgomery DMI, Evans AL, Damato BE and Cluckie A (1992).

Steady-state visual evoked cortical potentials from stimulation of visual field quadrants: optimizing pattern variables for the size of the field to be investigated.  
Docum Ophthalmol 79, 151-160.

Bradnam MS, Evans AL, Montgomery DMI, Keating D, Damato BE, Cluckie A and Allan D (1993).

A personal computer based visual evoked potential stimulus and recording system.  
Docum Ophthalmol (in press).

Brodmann K (1909).

Vergleichende lokalisationslehre der grosshirnrinde.  
Johann Ambrosius Barth, Leipzig.

Bunt AH and Minckler DS (1977).

Foveal sparing: new anatomical evidence for bilateral representation of the central retina.

Arch Ophthalmol 95, 1445-1447.

Calkins JL and Hochheimer BF (1980).

Retinal light exposure from ophthalmoscopes, slit lamps, and overhead surgical lamps: an analysis of potential hazards.

Invest Ophthalmol Vis Sci 19, 1009-1015.

Calkins JL, Hochheimer BF and D'Anna SA (1980).

Potential hazards from specific ophthalmic devices.

Vis Res 20, 1039-1053.

Cameron JR and Skofronick JG (1978).

Medical physics.

John Wiley and sons, New York.

Campbell FW and Maffei L (1970).

Electrophysiological evidence for the existence of orientation and size detectors in the human visual system.

J Physiol Lond 207, 635-652.

Cappin JM and Nissim S (1975).

Visual evoked responses in the assessment of field defects in glaucoma.

Arch Ophthalmol 93, 9-18.

Carlton EH and Katz S (1980).

Is Wiener filtering an effective method of improving evoked potential estimation?  
IEEE Trans Bio-Med Eng BME 27, 187-192.

Carr RE and Siegel IM (1990).

Electrodiagnostic testing of the visual system: a clinical guide.  
FA Davis Company, Philadelphia.

Celesia G G (1991).

Visual evoked potentials.

In: Evoked potentials review no.4. Barber C and Taylor MJ (Eds.),  
IEPS Publications, Nottingham. 45-56.

Cerutti S, Bersani V, Carrara A and Liberati D (1987a).

Analysis of visual evoked potentials through Wiener filtering applied to a small  
number of sweeps.

J Biomed Eng, 9, 3-12.

Cerutti S, Baselli G, Liberati D and Pavesi G (1987b).

Single sweep analysis of visual evoked potentials through a model of parametric  
identification.

Bio Cybern 56, 111-120.

Chiappa KH (1991).

Perspectives in evoked potentials.

In: Evoked potentials review no. 4. Barber C and Taylor MJ (Eds),  
IEPS Publications, Nottingham. 93-96.

Ciganek L (1961).

The EEG response (evoked potential) to light stimulus in man.

Electroencephal Clin Neurophysiol 13, 165-172.

Clarke PGH (1973).

Visual evoked potentials to changes in the motion of a patterned field.

Exp Brain Res 18, 145-155.

Cobb WA and Dawson GD (1960).

The latency and form in man of the occipital potentials evoked by bright flashes.  
J Physiol Lond 152, 108-152.

Collins AD and Sawhney BB (1993).

Pseudorandom binary sequence stimulation applied to the visual evoked response:  
normative data and a comparative study with pattern and flash stimulation.  
Docum Ophthalmol 83, 163-173.

Collins DWK, Black JL and Mastaglia FL (1978).

Pattern-reversal visual evoked potential.  
J Neurol Sci 36, 83-95.

Cookman EM (1990).

Fact or fiction - another alternative to glue?  
J Electrophysiol Technol 16, 15-21.

Cooley JW and Tukey JW (1965).

An algorithm for the machine calculation of complex Fourier series.  
Math Comput 19, 297-301.

Copenhaver RM, Beinhocker GD (1963).

Evoked occipital potentials recorded from scalp electrodes in response to focal visual  
illumination.  
Invest Ophthalmol 2, 393-406.

Crook JM, Lange-Malecki B and Valberg A (1988).

Visual resolution of macaque retinal ganglion cells.  
J Physiol 396, 205-224.

Curcio CA and Allen KA (1990).

Topography of ganglion cells in human retina.  
J Comp Neurol 300, 5-25.

Curcio CA, Sloan KR, Kalina RE and Hendrickson AE (1990).

Human photoreceptor topography.  
J Comp Neurol 292, 497-523.

Daniel PM and Whitteridge D (1961).

The representation of the visual field on the cerebral cortex in monkeys.

J Physiol 159, 203-221.

Dawson GD (1954).

A summation technique for the detection of small evoked potentials.

Electroenceph Clin Neurophysiol 6, 65-84.

Dawson WW and Herron WL (1970).

Retinal illumination during indirect ophthalmoscopy: subsequent dark adaptation.

Invest Ophthalmol 9,89-96.

de Mott DW and Boynton RM (1958a).

Retinal distribution of entopic stray light.

J Opt Soc Am 48,13-22.

de Mott DW and Boynton RM (1958b).

Sources of entopic stray light.

J Opt Soc Am 48,120-125.

de Waal BJ, Reits D, Spekreijse H, Grimbergen CA (1983).

Implementation of a portable pattern stimulator and VEP/ERG recording system based on an Apple microcomputer.

Doc Ophthalmol Proc Series 37, 209-216.

de Weerd JPC and Martens WLJ (1978).

Theory and practice of a posteriori 'Wiener' filtering of averaged evoked potentials.

Biol Cybern 30, 81-94.

de Weerd JPC (1981).

A posteriori time-varying filtering of averaged evoked potentials.

I. Introduction and conceptual basis.

Biol Cybern 41, 211-222.

de Weerd JPC and Kap JI (1981).

A posteriori time-varying filtering of averaged evoked potentials.

II. Mathematical and computational aspects.

Biol Cybern 41, 223-234.

Dow BM, Vautin RG and Bauer R (1985).

The mapping of visual space onto foveal striate cortex in the macaque monkey.  
J Neurosci 5, 890-902.

Doyle DJ (1975).

Some comments on the use of Wiener filtering for the estimation of evoked potentials.

Electroenceph Clin Neurophysiol 38, 533-534.

Drasdo N (1983).

Electrophysiology of the human visual system.

Ophthal Physiol Opt 3, 321-329.

Duke-Elder S and Wybar KC (1961).

The anatomy of the visual system.

In: System of ophthalmology: Volume II. Duke-Elder S (Ed), Kimpton, London.  
264 -269.

Eisenberg MF and Copenhaver RM (1967).

A fiberoptic ophthalmoscope for focal retinal stimulation.

Med Res Eng 6, 23-25.

Eizenman M, Skarf B, McCulloch DL and Katz L (1993).

New system for objective measurements of cortical binocularity in human infants.

In press.

Elberger AJ and Spydell JD (1985).

Visual field perimetry analysis using evoked potentials in normal and corpus callosum sectioned cats.

Electroenceph Clin Neurophysiol 60, 249-257.

Elberling C and Don M (1984).

Quality estimation of averaged auditory brainstem responses.

Scand Audiol 8, 187-197.

Elkington AR and Frank HJ (1984).

Clinical optics.

Blackwell Scientific, Oxford.

Epstein CM, Gammon JA, Gemmill M, Till J (1983).

Visual evoked potential pattern generation, recording, and data analysis with a single microcomputer.

Electroenceph Clin Neurophysiol 56, 691-693.

Fender DH (1964).

Control mechanisms of the eye.

Sci Amer 211, 24-33.

Fox PT, Miezin FM, Allman JM, Van Essen DC and Raichle ME (1987).

Retinotopic organization of human visual cortex mapped with positron-emission tomography.

J Neuroscience, 7, 913-922.

Fricker SJ and Kuperwaser M (1982).

Advantages of a cross-correlation technique for ERG measurement in children.

J Pediatr Ophthalmol Strabismus 19, 26-32.

Fricker SJ and Sanders JJ (1974).

Clinical studies of the evoked response to rapid random flash.

Electroenceph Clin Neurophysiol 36, 525-532.

Fricker SJ and Sanders JJ (1975).

A new method of cone electroretinography: the rapid random flash response.

Invest Ophthalmol Vis Sci 14, 131-137.

Fujimoto N and Adachi-Usami E (1988).

Comparison of automated perimetry and pattern visually evoked cortical potentials in optic neuritis.

Doc Ophthalmol 69, 263-269.

Fukuda Y, Sawai H, Watanabe M, Wakakuwa K and Morigiwa K (1989).

Nasotemporal overlap of crossed and uncrossed retinal ganglion cell projections in the Japanese monkey (*macaca fuscata*).

J Neurosci 9, 2353-2373.

Galloway NR (1981).

Ophthalmic electrodiagnosis 2nd edition.

Lloyd-Luke, London.

Galloway NR (1986).

Review article : evoked responses and the eye.

Trans Ophthalmol Soc UK. 105, 273-286.

Galloway NR (1988).

Electrophysiological testing of eyes with opaque media.

Eye 2, 615-624.

Gattass R and Gross CG (1981).

Visual topography of striate projection zone (MT) in posterior superior temporal sulcus of the macaque.

J Neurophysiol 46, 621-638.

Gevins AS (1984).

Analysis of the electromagnetic signals of the human brain: milestones, obstacles, and goals.

IEEE Trans Bio-Med Eng, BME 31, 833-850.

Halliday AM (1972).

Evoked responses in organic and functional sensory loss.

In: *Activités évoquées et leur conditionnement chez l'homme normal et en pathologie mentale.* Fessard A and Lelord G (Eds), Editions Inserm, Paris, 189-212.

Halliday AM (1982).

Evoked potentials in clinical testing.

Churchill Livingstone, Edinburgh.

Halliday AM, Barrett G, Halliday E and Michael WF (1977).

The topography of the pattern-evoked potential.

In: *Visual evoked potentials in man.* Desmedt JE (Ed), Clarendon, Oxford, 121-133.

Halliday AM, McDonald WI and Mushin J (1972).

Delayed visual evoked response in optic neuritis.

Lancet 1, 982-985.

Harrington DO and Drake MV (1990).

The visual fields: Text and atlas of clinical perimetry (sixth edition).

CV Mosby, St Louis.

Harter MR (1970).

Evoked cortical responses to checkerboard patterns: effect of check-size as a function of retinal eccentricity.

Vision Res 10, 1365-1376.

Hartwell JW and Erwin CW (1976).

Evoked potential analysis: on-line signal optimization using a mini-computer.

Electroenceph Clin Neurophysiol 41, 416-421.

Hays WL (1963).

Statistics.

Holt, Rinehart and Winston, New York.

Hayward M, Mills IM (1980).

Design effects of video pattern generators on the visual evoked potential.

In: Evoked potentials. Barber C (Ed), MTP Press, Lancaster.

Heckenlively JR and Arden GB (Eds).(1991).

Principles and practice of clinical electrophysiology of vision.

Mosby Year Book, Saint Louis, MO.

Henkes HE and Van Lith GHM (1973).

Electroperimetry.

Doc Ophthalmol Proc Ser 2, 245-251.

Hess RF and Pointer JS (1988).

The contrast sensitivity gradient along the horizontal visual field in man.

J Physiol 396, 136P.

Hirose T, Miyake Y and Hara A (1977).

Simultaneous recording of electroretinogram and visual evoked response. Focal stimulation under direct observation.

Arch Ophthalmol 95, 1205-1208.

Holden AL and Fitzke FW (1988).

Image size in the fundus: structural evidence for wide-field retinal magnification factor.

Br J Ophthalmol 72, 228-230.

Holder GE (1987).

Significance of abnormal pattern electroretinography in anterior visual pathway dysfunction.

Br J Ophthalmol 71, 166-171.

Holmes G (1918).

Disturbance of vision by cerebral lesions.

Br J Ophthalmol 2, 353-383.

Holmes G (1945).

The organisation of the visual cortex in man.

Proc R Soc Lond Series B (Biol) 1945, 132, 348-361.

Holmes G and Lister WT (1916).

Disturbances of vision from cerebral lesions, with special reference to the cortical representation of the macula.

Brain 39, 34-73.

Horton JC and Hoyt WF (1991).

The representation of the visual field in the human striate cortex: a revision of the classic Holmes map.

Arch Ophthalmol 109, 816-824.

Hotelling H (1931).

The generalisation of Student's ratio.

Ann Math Stat 2, 360-378.

Howe JW and Mitchell KW (1980).

Visual evoked potentials from quadrantic field stimulation in the investigation of homonymous field defects.

In: Evoked potentials. Barber C (Ed), MTP Press, Lancaster, 279-283.

Howe JW and Mitchell KW (1986).

Visual evoked cortical potential to paracentral retinal stimulation in chronic glaucoma, ocular hypertension, and an age-matched group of normals.

Doc Ophthalmol 63, 37-44.

Hoyt WF and Luis O (1963).

The primate chiasm: details of visual fibre organisation studied by silver impregnation techniques.

Arch Ophthalmol 70, 69-85.

Hoyt WF and Tudor RC (1963).

The course of the parapapillary temporal retinal axons through the anterior optic nerve.

Arch Ophthalmol 69, 503-507.

Hubel DH (1988).

Eye, Brain and Vision.

Scientific American, New York.

Hubel DH and Freeman DC (1977).

Projection into the visual field of ocular dominance columns in macaque monkey.

Brain Res 122, 336-343.

Hyvarinen L. (1991).

Visual acuity testing principles.

In: Principles and practice of clinical electrophysiology of vision. Heckenlively JR and Arden GB (Eds), Mosby Year Book, Saint Louis, MO. 459-464.

Inoue J, Takei K and Akibe T (1973).

The visual evoked potentials to focal illumination of the retina by direct view ophthalmoscopy.

Acta Soc Ophthalmol Jap 77, 1149-1160.

Inouye T (1909).

Die sehstörungen bei schussverletzungen der kortikalen sehshpere.

Engelmann, Leipzig.

Cited by Holmes and Lister (1916).

International Electrotechnical Commission (IEC) (1988).

IEC 601 part 1. Medical electrical equipment: general requirements for safety.  
IEC, Geneva.

Jasper HH (1958).

The ten twenty electrode system of the international society.  
Electroenceph Clin Neurophysiol 10, 371-375.

Johnston SC, Damato BE, Evans AL and Allan D (1989).

Computerised visual field test for children using multiple moving fixation targets.  
Med Biol Eng Comput 27, 612-616.

Jonas JB, Gusek GC, Guggenmoos-Holzmann I and Naumann GOH (1988).

Variability of the real dimensions of normal human optic discs.  
Graefes Arch Clin Exp Ophthalmol 226, 332-336.

Jonas JB, Schmidt AM, Muller-Bergh JA, Schlotzer-Schrehardt UM and Naumann GOH (1992).

Human optic nerve fiber count and optic disc size.  
Invest Ophthalmol Vis Sci 33, 2012-2018.

Katsumi O, Hirose T, Tsukada T (1988).

Effect of number of pattern elements and size of stimulus field on recordability of pattern reversal visual evoked response.  
Invest Ophthalmol Vis Sci 29, 922-927.

Katsumi O, Timberlake GT, Hirose T, Van de Velde FJ and Sakaue H (1989).

Recording pattern reversal visual evoked response with the scanning laser ophthalmoscope.  
Acta Ophthalmol 67, 243-248.

Katsumi O, van de Velde FJ, Mehta MC and Hirose T (1991).

Topographical analysis of peripheral vs. central retina with pattern reversal visual evoked response and the scanning laser ophthalmoscope.  
Acta Ophthalmol 69, 596-602.

Katz J and Sommer A (1990).

Screening for glaucomatous visual field loss: the effect of patient reliability.  
Ophthalmol 97, 1032-1037.

Keating D and Mutlukan E (1993).

A versatile multiple stimulus computerised perimeter.  
Submitted for publication.

Keltner JL, Johnson CA, Calif D (1986).

Current status of automated perimetry: is the ideal automated perimeter available.  
Arch Ophthalmol 104,347-349.

Kojima M and Zrenner E (1980).

Determination of local thresholds in the visual field by recording the scotopic visually evoked cortical potential in man.  
Ophthalmic Res 12, 1-8.

Kossol J, Cole C and Dayhaw-Barker P (1983).

Spectral irradiances of and maximal permissible exposures to two indirect ophthalmoscopes.  
Am J Optom Physiol Opt 60, 616-621.

Kuba M and Kubova Z (1992).

Visual evoked potentials specific for motion-onset.  
Doc Ophthalmol 80, 83-89.

Kubova Z and Kuba M (1992).

Clinical application of motion-onset visual evoked cortical potentials.  
Doc Ophthalmol 81, 209-218.

Kubova Z, Kuba M, Hubacek J and Vit F (1990).

Properties of visual evoked potentials to onset of movement on a television screen.  
Doc Ophthalmol 75, 67-72.

Kuo FF (1966).

Network analysis and synthesis, second edition.  
Wiley, New York. 368-372.

le Gargasson JF, Lamare M, Rigaudiere F, Corno F, Grall Y, Charlier J and Simon J (1989).

Ophthalmoscope laser à balayage et potentiels évoqués visuels.  
J Med Nucl Biophys 13, 343-354.

Leske MC (1983).

The epidemiology of open-angled glaucoma: a review.  
Am J Epidemiol 118, 166-191.

Le Vay S, Connolly M, Houde J and Van Essen DC (1985).

The complete pattern of ocular dominance stripes in the striate cortex and visual field of the macaque monkey.  
J Neurosci 5, 486-501.

Leventhal AG, Ault SJ and Vitek DJ (1988).

The nasotemporal division in primate retina: the neural basis of macular sparing and splitting.  
Science 240, 66-67.

Liberati D (1988).

Single-sweep evoked potential brain monitoring in neurosurgery.  
J Clin Monitoring 4, 147-148.

Liberati D, Cerutti S, Di Ponzio E, Ventimiglia V and Zaninelli L (1989).

The implementation of an autoregressive model with exogenous input in a single sweep evoked potential analysis.  
J Biomed Eng 11, 285-292.

Liu S and Wong-Riley M (1990).

Quantitative light- and electron-microscopic analysis of cytochrome-oxidase distribution in neurons of the lateral geniculate nucleus of the adult monkey.  
Visual Neurosci 4, 269-287.

Lynn PA (1989).

An introduction to the analysis and processing of signals, third edition.  
MacMillan, Basingstoke.

McFadzean R, Brosnahan D, Hadley D and Mutlukan E (1993).  
The representation of the visual field in the occipital striate cortex.  
Submitted for publication.

Maffei L and Fiorentini A (1981).  
Electroretinographic responses to alternating gratings before and after section of the optic nerve.  
*Science* 211, 953-955.

Maier J, Dagnelie G, Spekreijse H and van Dijk BW (1987).  
Principal components analysis for source localization of VEPs in man.  
*Vision Res* 27, 165-177.

Mainster MA, Ham WT and Delori FC (1983).  
Potential retinal hazards. Instrument and environmental light sources.  
*Ophthalmology* 90, 927-32.

Marmor MF, Arden GB, Nilsson SEG, Zrenner E (1989).  
International standardisation committee. Standard for clinical electroretinography.  
*Arch Ophthalmol* 107, 816-819.

Marozas DS and May DC (1985).  
Effects of figure-ground reversal on the visual-perceptual and visuo-motor performances of cerebral palsied and normal children.  
*Percept Mot Skills*, 60, 591-598.

Marshall J (1991).  
The macula, ageing and age-related macular degeneration.  
In: *Vision and visual dysfunction: Volume 16*. Cronly-Dillon J (Ed), Macmillan, Basingstoke. 79-80.

Maunsell JHR and Van Essen DC (1983).  
Functional properties of neurons in middle temporal visual area of the macaque monkey. I. Selectivity for stimulus direction, speed and orientation.  
*J Neurophysiol* 49, 1127-1147.

May DC (1978).

Effects of color reversal of figure and ground drawing materials on drawing performance.

Except Child 44, 254-260.

Metz CE (1978).

Basic principles of ROC analysis.

Seminars in nuclear medicine, 8, 283-298.

Missotten L (1974).

Estimation of the ratio of cones to neurons in the fovea of the human retina.

Invest Ophthalmol 13, 1045-1049.

Montgomery DMI (1991).

Measurement of optic disc and neuroretinal rim areas in normal and glaucomatous eyes: a new clinical method.

Ophthalmol 98, 50-59.

Morrison DF (1976).

Multivariate statistical methods.

McGraw-Hill, New York, 128-133.

Moskowitz A and Sokol S (1985).

Effect of stimulus orientation on the latency and amplitude of the VEP.

Invest Ophthalmol Vis Sci 26, 246-248.

Muller R, Gopfert E, Schlykova L and Anke D (1990).

The human motion VEP as a function of size and eccentricity of the stimulation field.

Doc Ophthalmol 76, 81-90.

Mutlukan E and Damato BE (1992).

The dark perimetric stimulus.

Br J Ophthalmol 76, 264-267.

Mutlukan E, Bradnam MS, Keating D and Damato BE (1992).

Visual evoked cortical potentials from transient dark and bright stimuli: selective 'on' and 'off-pathway' testing?

Doc Ophthalmol 80, 171-181.

Nakayama K (1985).

Biological image motion processing: a review.

Vision Res 25, 625-660.

Nelson JJ, Seiple WH, Kupersmith MJ and Carr RE (1984).

Lock-in techniques for the swept stimulus evoked potential.

J Clin Neurophysiol 1, 409-436.

New Scientist (1991).

Desktop test catches glaucoma early.

16 March, 27.

Newsome WT and Pare EB (1988).

A selective impairment of motion perception following lesions of the middle temporal visual area (MT).

J Neurosci 8, 2201-2211.

Newsome WT, Wurtz RH, Dursteler MR and Mikami A (1985).

Deficits in visual motion processing following ibotenic acid lesions of the middle temporal visual area of the macaque monkey.

J Neurosci 5, 825-840.

Norcia AM, Clarke M and Tyler CW (1985).

Digital filtering and robust regression techniques for estimating sensory thresholds from the evoked potential.

IEEE Eng Med Biol Magazine, December, 26-32.

Norcia AM, Tyler CW, Hamer RD and Wesemann W (1989).

Measurement of spatial contrast sensitivity with the swept contrast VEP.

Vision Res 29, 627-637.

Nunez PL, Pilgreen KL and Law SK (1991).

Mapping of evoked potentials.

In: Evoked potentials review no. 4. C Barber (Ed), IPES, Nottingham. 57-64.

Osterberg GA (1935).

Topography of the layer of rods and cones in the human retina.

Acta Ophthalmol (Suppl 6), 13, 1-97.

Perry VH and Cowey A (1981).

The morphological correlates of X- and Y-like retinal ganglion cells in the retina of monkeys.

Exp Brain Res 43, 226-228.

Petersen J and Airas K (1985).

Testing of concentric visual field constriction by means of scotopic visually evoked potentials.

Graefe's Arch Clin Exp Ophthalmol 223, 66-68.

Picton TW (1987a).

Human auditory steady state responses.

In: Evoked potentials III. Barber C and Blum T (Eds), Butterworths, Boston, 117-124.

Picton TW (1987b).

The recording and measurement of evoked potentials.

In: A textbook of clinical neurophysiology. Halliday AM, Butler SR and Paul R (Eds), John Wiley and sons, Chichester, 23-40.

Quigley HA, Dunkelberger GR and Green WR (1989).

Retinal ganglion cell atrophy correlated with automated perimetry in human eyes with glaucoma.

Am J Ophthalmol 107, 453-464.

Quigley HA, Sanchez RM, Dunkelberger GR, L'Hernault NL and Baginski TA (1987).

Chronic glaucoma selectively damages large optic nerve fibers.

Invest Ophthalmol Vis Sci 28, 913-920.

Regan D (1966).

Some characteristics of average steady-state and transient responses evoked by modulated light.

Electroenceph Clin Neurophysiol 20, 238-248.

Regan D (1972).

Evoked potentials in psychology, sensory physiology and clinical medicine.

Chapman and Hall, London.

Regan D (1977).

Steady-state evoked potentials.

J Opt Soc Am, 67, 1475-1489.

Regan D (1989).

Human brain electrophysiology: evoked potentials and evoked magnetic fields in science and medicine.

Elsevier, New York.

Regan D and Milner BA (1978).

Objective perimetry by evoked potential recording: limitations.

Electroenceph Clin Neurophysiol 44, 393-397.

Regan D and Spekreijse H (1986).

Evoked potentials in vision research 1961-1986.

Vision Res 26, 1461-1480.

Robertson DM and Erickson GJ (1979).

The effect of prolonged indirect ophthalmoscopy on the human eye.

Am J Ophthalmol 87, 652-661.

Rovamo J and Virsu V (1979).

An estimation and application of the human cortical magnification factor.

Exp Brain Res 37, 495-510.

Sandberg MA and Ariel MA (1977).

A hand-held, two-channel stimulator-ophthalmoscope.

Arch Ophthalmol 95, 1881-1882.

Sandini G, Romano P, Scotto A and Traverso G (1983).

Topography of brain electrical activity: a bioengineering approach.

Medical Progress through Technology 10, 5-19.

Schacham SE and Pratt H (1985).

Detection and measurement of steady-state evoked potentials in real-time using a lock-in amplifier.

J Neurosurg., 62, 935-938.

Schein SJ and de Monasterio FM (1987).

Mapping of retinal and geniculate neurons onto striate cortex of the macaque.  
J Neurosci 7, 996-1009.

Schiller PH (1986).

The central visual system.  
Vision Res 26, 1351-86.

Schiller PH, Sandell JH and Maunsell JHR (1986).

Functions of the ON and OFF channels of the visual system.  
Nature 322, 824-5.

Schreinemachers HP and Henkes HE (1968).

Relation between localized retinal stimuli and the visual evoked response in man.  
Ophthalmol 155, 2-27.

Seiple WH, Kupersmith MJ, Nelson JJ, and Carr RE (1984).

The assessment of evoked potential contrast thresholds using real-time retrieval.  
Invest Ophthalmol Vis Sci, 25, 627-630.

Shapley R and Perry VH (1986).

Cat and monkey retinal ganglion cells and their visual functional roles.  
Trends Neurosci 9, 229-235.

Shipley T (1969).

The visually evoked occipitogram in strabismic amblyopia under direct view  
ophthalmoscopy.  
J Pediatr Ophthalmol 6, 97-112.

Sliney DH (1983).

Standards for use of visible and nonvisible radiation on the eye.  
Am J Optom Physiol Opt 60, 278-86.

Smith CG and Richardson WFG (1966).

The course and distribution of the arteries supplying the visual (striate) cortex.  
Am J Ophthalmol 61, 1391-1396.

Sokol S, Hansen VC, Moskowitz A, Greenfield P and Towle VL (1983).  
Evoked potential and preferential looking estimates of visual acuity in paediatric patients.  
*Ophthalmol* 90, 552-562.

Spector RH, Glaser JS, David NJ and Vining DQ (1981).  
Occipital lobe infarctions: perimetry and computed tomography.  
*Neurology*, 31, 1098-1106.

Spehlmann R (1965).  
The averaged electrical responses to diffuse and to patterned light in the human.  
*Electroenceph Clin Neurophysiol* 19, 560-569.

Spehlmann R (1985).  
Evoked potential primer: visual, auditory and somatosensory evoked potentials in clinical diagnosis.  
Butterworth, Boston.

Spekreijse H (1980).  
Pattern evoked potentials: principles, methodology and phenomenology.  
In: *Evoked potentials*. Barber C (Ed), MTP, Lancaster. 55-74.

Stanziano G, Kaplan H, Koblasz A, Davey K (1988).  
Microcomputer analyses of clinical ERG, EOG and other tests of retinal function.  
*Med Instrum* 22, 12-19.

Stone J, Leicester J, Sherman SM (1973).  
The naso-temporal division of the monkey's retina.  
*J Comp Neurol* 150, 333-348.

Strasburger H (1987).  
The analysis of steady state evoked potentials revisited.  
*Clin Vision Sci*, 1, 245-256.

Sutter EE and Duong T (1992).  
The field topography of ERG components in man -  
I. The Photopic Luminance Response.  
*Vision Research* 32, 433-446.

Talbot SA and Marshall WH (1941).

Physiological studies on neural mechanisms of visual localization and discrimination.  
Am J Ophthalmol 24, 1255-1264.

Taylor MJ and McCulloch DL (1992).

Visual evoked potentials in infants and children.  
J Clin Neurophysiol 9, 357-372.

Teping C, Wolf S, Schippers V, Plesch A and Silny J (1989).

Anwendung des scanning laser-ophthalmoskops zur registrierung des muster-ERG und VECP.

Klin Mbl Augenheilk 195, 203-206.

Tootell RBH, Switkes E, Silverman MS and Hamilton SL (1988).

Functional anatomy of macaque striate cortex, II retinotopic organization.

J Neurosci 8, 1531-1568.

Torok B (1990).

Microcomputer-based recording system for clinical electrophysiology.

Doc Ophthalmol 75, 189-197.

Towle VL, Moskowitz A, Sokol S and Schwartz B (1983).

The visual evoked potential in glaucoma and ocular hypertension: effects of check size, field size, and stimulation rate.

Invest Ophthalmol Vis Sci 24, 175-183.

Townsend JC, Selvin GJ, Griffin JR and Comer GW (1991).

Visual fields: clinical case presentations.

Butterworth-Heinemann, Boston.

Traquair HM (1927).

An introduction to clinical perimetry.

Kimpton, London.

Trick GL (1985).

Retinal potentials in patients with primary open-angle glaucoma: physiological evidence for temporal frequency tuning deficits.

Invest Ophthalmol Vis Sci 26, 1750-1758.

Ts'o MOM, Wallow IHL, Powell JO and Zimmerman LE (1972).

Recovery of the rod and cone cells after photic injury.

Trans Am Acad Ophthalmol Otolaryngol 76, 1247.

Tyler CW (1991).

Visual acuity estimation in infants by visual evoked cortical potentials.

In: Principles and practice of clinical electrophysiology of vision. Heckenlively JR and Arden GB (Eds), Mosby Year Book, Saint Louis, MO. 408-416.

Uhlin DM and Dickson JD (1970).

The effect of figure-ground reversal in H-T-P drawings by spastic cerebral palsied children.

J Clin Psychol 26, 87-88.

Ungan P and Basar B (1976).

Comparison of Wiener filtering and selective averaging of evoked potentials.

Electroenceph Clin Neurophysiol 40, 516-520.

van den Berg TJTP, Boltjes B, Spekreijse H (1988).

Pattern electroretinogram can be more than the sum of local luminance responses.

Doc Ophthalmol 69, 307-314.

van der Tweel LH and Estevez O (1991).

Analytical techniques.

In: Principles and practice of clinical electrophysiology of vision. Heckenlively JR and Arden GB (Eds), Mosby Year Book, St Louis, 231-253.

Van Essen DC, Newsome WT and Maunsell (1984).

The visual field representation in striate cortex of the macaque monkey: asymmetries, anisotropies, and individual variability.

Vision Res 24, 429-448.

van Lith GHM, van Marle GW, van Dok-Mak GTM (1978).

Variation in latency times of visual evoked cortical potentials.

Br J Ophthalmol 62, 220-222.

van Lith GHM, van Marle GW, Vijfvinkel-Bbruinenga S (1979).

Interference of 50 Hz electrical cortical potentials produced by TV systems.

Br J Ophthalmol 63, 779-781.

Virsu V and Rovamo J (1979).

Visual resolution, contrast sensitivity, and the cortical magnification factor.

Exp Brain Res 37, 475-494.

Walter DO (1969).

A posteriori 'Wiener filtering' of average evoked responses.

Electroenceph Clin Neurophysiol Supp 27, 61-70.

Wassle H and Boycott BB (1991).

Functional architecture of the mammalian retina.

Physiological Reviews 71, 447-80.

Weber H and Dobek K (1986).

What is the most suitable grid for computer perimetry in glaucoma patients?

Ophthalmol 192, 88-96.

Werner EB (1991).

Manual of visual fields.

Churchill Livingstone, New York.

Wicke JD, Donchin E, Lindsley DB (1964).

Visual evoked potentials as a function of flash luminance and duration.

Science 146, 83-85.

Widrow B, Glover JR, McCool JM, Kaunitz J, Williams CS, Hearn RH, Zeidler JR, Dong E and Goodlin RC (1975).

Adaptive noise cancelling: principles and applications.

Proc IEEE 63, 1692-1716.

Widrow B, McCool JM, Larimore MG and Johnson CR (1976).

Stationary and nonstationary learning characteristics of the LMS adaptive filter.

Proc IEEE 64, 1151-1163.

Widrow B and Stearns SD (1985).

Adaptive signal processing.

Prentice-Hall, Englewood Cliffs, New Jersey.

Wilton R (1987).

Programmer's guide to PC and PS/2 video systems.

Microsoft, Redmond.

World Health Organisation (1982).

Environmental Health Criteria 23. Lasers and optical radiation.

Geneva.

Yanashima K (1982).

Determination of visual field defects by the visually evoked cortical potential (VECP) decoded by fast Fourier transform (FFT).

Doc Ophthalmol Proc Series 31, 427-435.

Zeki SM (1980).

The response properties of cells in the middle temporal area (area MT) of owl monkey visual cortex.

Proc R Soc London Ser B 207, 239-248.

Zeki S (1992).

The visual image in mind and brain.

Sci Am, September, 68-76.

Zeki S, Watson JDG, Lueck CJ, Friston KJ, Kennard C and Frackowiak RSJ (1991).

A direct demonstration of functional specialization in human visual cortex.

J Neurosci 11, 641-649.